



This electronic thesis or dissertation has been downloaded from Explore Bristol Research, <http://research-information.bristol.ac.uk>

Author:

Shi, Gongyu

Title:

Investigating the action of genes and compounds that modify mitophagy and pro-survival pathways in cellular models of Parkinson's disease

General rights

Access to the thesis is subject to the Creative Commons Attribution - NonCommercial-No Derivatives 4.0 International Public License. A copy of this may be found at <https://creativecommons.org/licenses/by-nc-nd/4.0/legalcode>. This license sets out your rights and the restrictions that apply to your access to the thesis so it is important you read this before proceeding.

Take down policy

Some pages of this thesis may have been removed for copyright restrictions prior to having it been deposited in Explore Bristol Research. However, if you have discovered material within the thesis that you consider to be unlawful e.g. breaches of copyright (either yours or that of a third party) or any other law, including but not limited to those relating to patent, trademark, confidentiality, data protection, obscenity, defamation, libel, then please contact collections-metadata@bristol.ac.uk and include the following information in your message:

- Your contact details
- Bibliographic details for the item, including a URL
- An outline nature of the complaint

Your claim will be investigated and, where appropriate, the item in question will be removed from public view as soon as possible.

Investigating the action of genes and compounds that modify mitophagy and pro-survival pathways in cellular models of Parkinson's disease

Gongyu Shi

A dissertation submitted to the University of Bristol in accordance with the requirements for award of the degree of Doctor of Philosophy in the Faculty of

Health Sciences, Bristol Medical School.

July 2022

Word count: 46600

Abstract

Parkinson's disease (PD) is a neurodegenerative condition characterised by a loss of dopaminergic nigrostriatal nerve cells. Emerging evidence shows ageing, altered mitochondrial function, genetic factors and exposure to environmental toxins targeting mitochondria are major risk factors for idiopathic Parkinson's disease. Dopaminergic neurons have uniquely complex dendritic networks and are therefore vulnerable to disruptions in energy homeostasis caused by mitochondrial dysfunction. Therefore, identifying drugs that improve mitochondrial function could be used to treat or prevent PD. This study focused on investigating whether GSK3 α/β and CDK inhibitors improved mitochondrial function and neuronal health and had the potential to treat PD. Kenpauillone, a GSK3 α/β and CDK inhibitor, was previously reported to improve the mitochondrial network and was shown to protect mitochondria following a PD-stressor (MPP+). This evidence suggested that studying drugs that target GSK3 α/β and CDKs may give an insight into the mechanism governing mitochondrial quality control pathways and may lead to the discovery of drugs useful in treating Parkinson's disease. This study investigated drugs with similar targets to kenpauillone, namely AZD5438, AT7519, alsterpauillone and 1-azakenapauillone and mitochondrial protective drugs, dexpramipexole and olesoxime, that target mitochondria in a similar manner to kenpauillone. The findings showed that AZD5438, a potent GSK3 α/β and CDK inhibitor, restores mitochondrial membrane potential and inhibits Parkin recruitment and fragmentation of the mitochondrial network following treatment with CCCP. Furthermore, AZD5438 was shown to improve mitochondrial networks and prevent the death of neurons (derived from human iPSC) following the treatment with the mitochondrial complex I inhibitor, rotenone. AZD5438 was also shown to inhibit mitochondrial ROS and neuronal apoptosis while it upregulated glycolysis and improved the electrophysiological function of neurons. Based on these novel findings, AZD5438 is suggested to have potential as a therapeutic drug for neurodegenerative diseases such as Parkinson's disease.

Dedication

This thesis is dedicated to my Mother and Father,

Mrs Liping Weng and Mr Zhigang Shi.

Thank you for your unconditional and continuing love. I was, am and will always
be grateful for your invaluable support

Acknowledgements

I would like to thank Professor James Uney for supervising my PhD. Your continued support inspired and encouraged me to step forward during the journey. I am sincerely grateful for the opportunity that I could learn from you. I thank Dr Liang-Fong Wong for your support and advice. I want to extend a special thank you to Dr Helen Scott for your support and for being a role model in all aspects of the lab, providing me all the training I need. Thank you to Dr Oscar Cordero-Llana for your support, you are brilliant to turn to. Thank you to Gavin Welsh for your guidance on the progress of my work. Thank you to Dr Becky Foster for your attentive support during my hard days. I would like to thank Dr Daniel Whitcomb for offering the opportunity to study the electrophysiology of neurons in your lab.

I have been lucky to work with a wonderful group of colleagues within both the UWOK research labs and the PhD offices in the Biomedical Science Building and Dorothy Hodgkin Building. I would like to thank my colleagues Dr Nicola Buckner, Dr Sian Baker, Dr Renata Raele-Rolfe, Dr Mahmoud Khazim, Dr Mamdouh Allahyani, Dr Jenny Hurcombe, Ms Andriana Gialedi, Ms Izzah Farhana Mohamad Azhar, Mr Ben Exley, Mr Yiming Zhang, Mr Keng Siang Lee, Mr Ben Clennell and Mr Tom Steward. Nikki, thank you for your collaboration from the start of my project, you are always brilliant to learn from. Mahmoud, thank you for teaching me the art of iPSCs. Mamdouh and Renata, thank you for your warm faces and heater when we were in the basement office. Andriana, thank you for your help in immunostaining and for working so hard in maintaining the lab. Sian, thank you for your valued words, both on Weston blot and advice on PhD. Thank you to Ben E and Yiming for your help with primary neuron culture. Thank you to Ben C and Tom for your expert help with the electrophysiology experiments. Thank you to Izzah for your contribution to the *Zombie* staining experiments and

to Keng for your help with generating human dopaminergic neurons. Thank you to Jenny for the collaboration on the podocyte project.

Thank you to my wonderful parents for your love and generous support. I also thank my cat Daodao. His company has been necessary for me to wake up every morning of those challenging days, occasionally at midnights. I wish to thank my partner, Shujie, for your constant company. Even thousands of miles apart, I can still embrace your care. I must thank all my friends who supported me, especially Bob, Yulong, Zoe, Xiaoyang and Chris, you are all stars in the night sky, lightening my path.

Thanks to the covid19-extension funding from the University of Bristol, I could concentrate and finish this work.

I could not have done this without you.

Author's declaration

I declare that the work in this dissertation was carried out in accordance with the requirements of the University's Regulations and Code of Practice for Research Degree Programmes and that it has not been submitted for any other academic award. Except where indicated by specific reference in the text, the work is the candidate's own work. Work done in collaboration with, or with the assistance of, others, is indicated as such. Any views expressed in the dissertation are those of the author.

SIGNED:Gongyu Shi..... DATE: 30th June 2022

Publication statement

Some of the data presented in Chapter 3 has been published in the Journal of Biological Chemistry (295 (10): 3285-3300), "A dual druggable genome-wide siRNA and compound library screening approach identifies modulators of parkin recruitment to mitochondria" by Scott et al. 2020.

The work in this thesis (chapter 3) directly contributed to Figure 5, Figure 6, in the above publication.

Signed by Professor James Uney


Signature..... Date....1st July

TABLE OF CONTENT

CHAPTER1	INTRODUCTION	1
	PARKINSON'S DISEASE.....	1
	MITOCHONDRIAL FUNCTION -OXIDATIVE PHOSPHORYLATION	5
	MITOCHONDRIAL BIOGENESIS.....	7
	MITOCHONDRIAL DYNAMICS	8
	MITOCHONDRIAL TURNOVER.....	9
	MITOPHAGY	10
	MITOCHONDRIAL ROS AND APOPTOSIS.....	12
	MITOCHONDRIA IN NEURONS	14
	TARGETING MITOCHONDRIA TO TREAT NEURODEGENERATIVE DISEASES.....	16
	CHALLENGES IN NEURODEGENERATIVE RESEARCH	18
	PREVIOUS SCREEN.....	20
	NEURONAL DEVELOPMENT AND KINASE ACTIVITIES	23
	GSK-B AND ITS INVOLVEMENT IN NEURODEGENERATIVE DISEASES.....	24
	CDKS AND THEIR INVOLVEMENT IN NEURODEGENERATIVE DISEASES	27
	FOCUSED COMPOUND TEST.....	31
	SUMMARY AND OVERALL AIMS	32
CHAPTER2	MATERIAL AND METHODS	34
	EVALUATION OF POTENTIAL GENES BY FORMER SCREEN AND LITERATURE	34

HUMAN CELL LINES AND CULTURE	34
E18 RAT PRIMARY NEURONAL CULTURE	35
HUMAN iPSC CULTURE	36
DIFFERENTIATION OF hiPSCs INTO MIDBRAIN DOPAMINERGIC NEURONS	38
COMPOUND TEST.....	40
SIRNA TRANSFECTION	41
PARKIN RECRUITMENT ASSAY	42
MITOCHONDRIAL NETWORK ASSAY	42
MITOCHONDRIAL MEMBRANE POTENTIAL ASSAYS	43
MITOCHONDRIAL ROS ASSAY	43
IMMUNOFLUORESCENCE STAINING	44
HIGH CONTENT IMAGING AND ANALYSIS	45
SEAHORSE EXPERIMENT	46
MTT CELL VIABILITY ASSAY	48
DNA EXTRACTION AND PURIFICATION FROM CELLS	49
RNA EXTRACTION AND cDNA GENERATION	49
QUANTITATIVE PCR (qPCR)	50
PROTEIN EXTRACTION, PURIFICATION, AND QUANTIFICATION.....	51
WESTERN BLOTTING	51
GENE CLONING.....	52
HEK293T CELL CULTURE AND LENTIVIRAL PRODUCTION	53

FLOW CYTOMETRY FOR CELL VIABILITY AND APOPTOSIS	55
ELECTROPHYSIOLOGY	55
<i>Preparation of recording solution</i>	<i>55</i>
<i>Preparation for microelectrodes and inner solution</i>	<i>56</i>
<i>Electrophysiology recording</i>	<i>56</i>
STATISTICAL ANALYSIS	58
EXPERIMENTAL REPLICATES AND DATA NORMALISATION	58
FIGURES	59
ANTIBODIES	59
SOLUTION CONCENTRATION	60
CHAPTER3 EVALUATING KENPAULLONE AS A REGULATOR OF PARKIN RECRUITMENT AND	
ITS EFFECT ON MITOCHONDRIAL ACTIVITIES	61
INTRODUCTION	61
RESULTS	64
<i>Optimisation of the Parkin recruitment assay</i>	<i>64</i>
<i>Cu-ASTM potentially regulates Parkin recruitment in H4 cells</i>	<i>66</i>
<i>Kenpaullone is a negative regulator of Parkin recruitment in H4 cells</i>	<i>69</i>
<i>Parkin recruitment assay established in SH-SY5Y cells</i>	<i>72</i>
<i>Cu-ASTM potentially alters Parkin recruitment in SH-SY5Y cells</i>	<i>74</i>
<i>Kenpaullone is a negative regulator of Parkin recruitment in SH-SY5Y cells</i>	<i>77</i>

<i>Mitochondrial network assay optimisation</i>	83
<i>Kenpaullone protects the mitochondrial network against CCCP</i>	86
<i>Mitochondrial respiration assay optimisation in H4 and SY5Y cells</i>	89
<i>Kenpaullone regulates the metabolic activities in live cells</i>	91
SUMMARY AND DISCUSSION.....	94
<i>Summary of the results</i>	94
<i>Evaluating Parkin recruitment assays in H4 and SH-SY5Y cells, limitations and concerns</i>	94
<i>Evaluating the effects of Cu-ATSM on cell viability and Parkin recruitment</i>	97
<i>Evaluating the effects of kenpaullone on Parkin recruitment and the mitochondrial network</i>	99
<i>Evaluating the effects of kenpaullone on cellular metabolism</i>	102
<i>Pharmacological mechanisms underlying the effects of kenpaullone on mitochondrial activity</i> <i>and cellular metabolism</i>	107
GSK-3 β	107
CDK1 and CDK2.....	110
CDK5	111
<i>Summary</i>	113
CHAPTER4 ASSESSING THE MECHANISM OF ACTION AND THERAPEUTIC POTENTIAL OF SELECTED GSK3A/B AND CDK INHIBITORS THAT TARGET MITOCHONDRIAL FUNCTION	114
INTRODUCTION	114
RESULTS.....	117

Primary validation: investigating the actions of the selected GSK3 α / β and CDK inhibitors on

Parkin recruitment and the mitochondrial network 117

Selected GSK/CDKs inhibitors have the similar effects on Parkin recruitment following the CCCP challenge
as kenpaullone 117

Selected GSK/CDKs inhibitors have similar effects on the mitochondrial network following the CCCP
challenge as kenpaullone 123

AZD5438 prevents mitochondrial membrane potential loss induced by CCCP 126

AZD5438 prevents the mitochondrial DNA loss induced by CCCP 128

Investigating the protective actions of AZD5438 against the mitochondrial toxin rotenone 130

AZD5438 protects the cell viability in the cellular PD model 130

AZD5438 prevents the mitochondrial network damage associated with rotenone, a cellular model of PD 134

Rotenone has no effect on relative mtDNA content in eGFP-Parkin H4 cells 137

AZD5438 inhibits cell death and apoptosis 138

AZD5438 prevents the formation of ROS in the cellular PD model 141

AZD5438 inhibits the activation of caspase-3 and prevents the downregulation of mitochondrial proteins in
the cellular PD model 143

Measuring AZD5438's action on cell metabolism using the Seahorse analyser 145

AZD5438's protective effects against stressors are dependent on glucose 149

Investigating whether AZD5438 acts via a specific CDK 152

CDK9 knockdown reproduced the regulation of Parkin recruitment by AZD5438 152

CDK9 knockdown reproduces the regulation of mitochondrial activities by AZD5438 156

Inhibition of GSK-3 β alone does not alter Parkin recruitment.....	158
<i>Validating the protective effects of AZD5438 in SH-SY5Y cells.....</i>	<i>161</i>
AZD5438 inhibits rotenone toxicity in SHSY-5Y cells.....	161
AZD5438 inhibits Parkin recruitment in eGFP-Parkin SH-SY5Y cells.....	163
AZD5438 regulates the mitochondrial network in eGFP-Parkin SH-SY5Y cells.....	165
Alpha-Synuclein affects the cell viability protection by AZD5438.....	168
DISCUSSION.....	172
CHAPTER5 INVESTIGATING THE EFFECTS OF AZD5438 IN RODENT PRIMARY NEURONS AND	
HUMAN IPSC DERIVED MIDBRAIN NEURONS.	182
INTRODUCTION	182
RESULTS.....	183
<i>Evaluation of AZD5438's action in rat primary cortical neurons</i>	<i>183</i>
AZD5438 protects rat primary cortical neurons from rotenone-induced toxicity.....	183
AZD5438 protects the neuronal network of primary cortical neurons	185
AZD5438 regulates the mitochondrial network of primary cortical neurons	188
AZD5438 prevents the induction of ROS by rotenone in primary cortical neurons	190
<i>Assessing AZD5438's protective effects in hiPSC derived midbrain neuronal cells</i>	<i>192</i>
Midbrain neuronal cultures were generated from hiPSCs	192
AZD5438 protects human midbrain neurons from rotenone-induced stress	194
AZD5438 protects the neuronal network formed by human midbrain cells from rotenone-induced stress	198

AZD5438 regulates the mitochondrial network of human midbrain cells	203
AZD5438 potentially stabilises PGC-1 α in human midbrain cells following rotenone-induced stress	210
AZD5438 prevents ROS formation and Caspase-3 mediated apoptosis in human midbrain cells following rotenone-induced stress	214
Investigating the mechanism of AZD5438 actions using an electrophysiology approach.....	218
SUMMARY AND DISCUSSION.....	226
<i>Study on primary neurons</i>	226
AZD5438 had similar protective effects on primary neurons as on cell lines	226
MTT cell viability assay in neurons	226
AZD5438 protected primary neurons from rotenone toxicity	227
AZD5438 protected the neuronal network of primary neurons	228
AZD5438 protected the mitochondria of primary neurons	228
AZD5438 protected the primary neurons by preventing ROS formation.....	229
<i>Study on hiPSC derived midbrain neurons</i>	230
AZD5438 had similar protective effects on human midbrain neurons as on rat primary neurons	230
AZD5438 protected the human midbrain neurons against rotenone	231
AZD5438 protected the mitochondria network in human midbrain neurons against rotenone	233
AZD5438 and the electrophysiological measurement of neuronal function	235
Limitations and concerns	240
<i>Chapter summary</i>	244

CHAPTER6	STUDY OF GENES THAT REGULATE PARKIN-MEDIATED MITOPHAGY	245
INTRODUCTION		245
RESULT		251
<i>Validation: UBE2N is a positive modular of Parkin-mediated mitophagy in SH-SY5Y cells</i>		251
<i>UBE2N is a potent modular of Parkin-mediated mitophagy</i>		254
<i>UBE2N lentiviral construction</i>		256
<i>Overexpression of UBE2N upregulates Parkin recruitment activity</i>		262
<i>Overexpression of UBE2N alters PGC-1αactivity</i>		264
<i>Overexpression of UBE2N does not protect cells in a cellular model of PD</i>		265
<i>Actions of UBR5, GBP2 and HECTD2 knockdown on Parkin recruitment</i>		266
SUMMARY AND DISCUSSION		270
<i>Results summary</i>		270
<i>Discussion</i>		271
UBE2N and Parkin recruitment study		271
UBE2N and the mitochondria-related proteins		273
UBE2N overexpression and rotenone-induced damage		278
UBR5, GBP2 and HECTD2		279
CHAPTER7	GENERAL DISCUSSION	280
<i>Thesis results summary and broader context</i>		280
<i>Mitophagy alteration for PD treatment: Upregulation or downregulation?</i>		282

*The cellular metabolic balance and PD treatment: Mitochondrial activity and glycolysis.....*284

*Recommendations for future work*285

REFERENCE.....287

LIST OF FIGURES AND TABLES

FIGURE 1-1 PATHOPHYSIOLOGY OF A MULTISYSTEM NEURODEGENERATIVE PROCESS FROM EARLY TO LATE STAGE OF PD.	2
FIGURE 1-2 GRAPHIC ILLUSTRATION OF MITOCHONDRIAL ELECTRON TRANSPORT CHAIN.	6
FIGURE 1-3 MITOCHONDRIAL DYNAMIC.	8
FIGURE 1-4 GRAPHIC ILLUSTRATION OF MITOCHONDRIAL ROS-MEDIATED APOPTOSIS	13
FIGURE 1-5 NEURON CELL DEATH RELATED TO DAMAGED MITOCHONDRIA.	15
FIGURE 1-6 AN EXAMPLE OF HOW TARGETING MITOCHONDRIAL QUALITY CONTROL PATHWAYS MAY PREVENT MITOCHONDRIAL DYSFUNCTION MEDIATED AGEING AND NEURODEGENERATION.	17
FIGURE 1-7 THE WORKFLOW OF THE iPSC STUDY.....	19
FIGURE 1-8 SCREENING OF THE DRUGGABLE GENOME LIBRARY.	21
FIGURE 1-9 COMBINED siRNA KNOCKDOWN OF UBE ENZYMES IDENTIFIED IN SCOTT ET AL MODULATES PRKN RECRUITMENT.....	21
FIGURE 1-10 CDK1 MEDIATES MITOCHONDRIAL ATP PRODUCTION AND USES THE ATP FOR G2 TO M PHASE TRANSITION AND DNA DAMAGE REPAIR.....	30
FIGURE 2-1 DIFFERENTIATING iPSCs INTO MDANs AND THEIR FATE FOLLOWS THIS SIMPLE MEDIA CHANGE SCHEDULE.	40
FIGURE 2-2 PROCESS OF MITOCHONDRIA STRESS TEST.....	48
FIGURE 2-3 PARAMETERS AND FORMULA FOR SEAHORSE EXPERIMENT	48
FIGURE 3-1 PARKIN RECRUITMENT ASSAY OPTIMISATION.	65
FIGURE 3-2 THE EFFECTS OF CU-ASTM ON CELL VIABILITY AND PARKIN RECRUITMENT IN EGFP-PARKIN H4 CELLS....	68

FIGURE 3-3 THE EFFECTS OF KENPAULLONE ON CELL VIABILITY AND PARKIN RECRUITMENT IN EGFP-PARKIN H4	
CELLS.....	71
FIGURE 3-4 PARKIN RECRUITMENT IN SH-SY5Y CELL.....	73
FIGURE 3-5 THE EFFECTS OF CU-ASTM ON CELL VIABILITY AND PARKIN RECRUITMENT IN EGFP-PARKIN SHSY-5Y	
CELLS.....	76
FIGURE 3-6 THE EFFECTS OF KENPAULLONE ON CELL VIABILITY AND PARKIN RECRUITMENT IN EGFP-PARKIN SHSY-5Y CELLS.....	79
FIGURE 3-7 THE EFFECTS OF KENPAULLONE ON CELL VIABILITY AND PARKIN RECRUITMENT IN EGFP-PARKIN SHSY-5Y CELLS WITH HIGH CELL DENSITY.....	82
FIGURE 3-8 PARKIN RECRUITMENT ASSAY OPTIMISATION.....	85
FIGURE 3-9 KENPAULLONE PROTECTS THE MITOCHONDRIA NETWORK FROM CCCP CHALLENGE.....	87
FIGURE 3-10 KENPAULLONE PROTECTS THE MITOCHONDRIA NETWORK IN SHSY-5Y CELLSFROM CCCP CHALLENGE ...	88
FIGURE 3-11 OPTIMISATION OF CONDITIONS FOR MITOCHONDRIAL STRESS TEST USING AGILENT SEAHORSE BIOANALYZER.....	90
FIGURE 3-12 THE EFFECT OF KENPAULLONE ON MITOCHONDRIAL RESPIRATION.....	92
FIGURE 3-13 THE EFFECT OF KENPAULLONE TREATMENT ON MITOCHONDRIAL RESPIRATION IN SH-SY5Y CELLS.....	93
FIGURE 4-1 OVERVIEW OF COMPOUNDS CHOSEN TO STUDY IN TWO CATEGORIES AND THEIR DESCRIPTION.....	115
FIGURE 4-2 AT7519 INHIBITS CCCP-INDUCED PARKIN RECRUITMENT.....	118
FIGURE 4-3 AZD5438 INHIBITS CCCP-INDUCED PARKIN RECRUITMENT.....	119
FIGURE 4-4 TRO19622 DOES NOT REGULATE CCCP-INDUCED PARKIN RECRUITMENT.....	119
FIGURE 4-5 DEXPRAMIPEXOLE DOES NOT REGULATE CCCP-INDUCED PARKIN RECRUITMENT.....	120

FIGURE 4-6 1-AZAKENPAULLONE INHIBITS CCCP-INDUCED PARKIN RECRUITMENT	121
FIGURE 4-7 ALSTERPAULLONE INHIBITS CCCP-INDUCED PARKIN RECRUITMENT	122
FIGURE 4-8 MITOCHONDRIAL NETWORK FOLLOWING PRE-TREATMENT WITH SELECTED GSK/CDKS INHIBITORS IN EGFP-PARKIN H4 CELLS	124
FIGURE 4-9 IMAGES AND ANALYSIS RESULTS OF COMPOUNDS INVESTIGATED FOR MITOCHONDRIAL MEMBRANE POTENTIAL CHANGE USING TMRM DYE.	127
FIGURE 4-10 RELATIVE MTDNA CONTENT FOLLOWING PRE-TREATMENTS OF GSK3/CDKS INHIBITORS	129
FIGURE 4-11 ASSESSING THE PROTECTIVE EFFECTS OF SELECTED GSK/CDK INHIBITORY COMPOUNDS FOLLOWING TREATMENTS WITH MITOCHONDRIAL TOXINS ASSOCIATED WITH PD	132
FIGURE 4-12 ASSESSING THE PROTECTIVE EFFECT OF AZD5438 ON MITOCHONDRIAL MORPHOLOGY AND NETWORK FOLLOWING TREATMENTS WITH ROTENONE.....	135
FIGURE 4-13 THE RELATIVE MTDNA CONTENT FOLLOWING TREATMENT WITH 250NM AZD5438 AND 500NM ROTENONE FOR 24H ASSESSED VIA QPCR MTDNA ASSAY	137
FIGURE 4-14 FLOW CYTOMETRY ASSESSED THE RATIO OF THE LIVE CELL FOLLOWING TREATMENTS WITH 250NM AZD5438 AND 500NM ROTENONE FOR 24H.	139
FIGURE 4-15 THE APOPTOTIC CELL RATIO FOLLOWING TREATMENT WITH 250NM AZD5438 AND 500NM ROTENONE FOR 24H WAS ASSESSED BY FLOW CYTOMETRY.	140
FIGURE 4-16 MITOCHONDRIAL REACTIVE OXYGEN SPECIES (ROS) LEVELS FOLLOWING TREATMENTS WITH 250NM AZD5438 AND A SERIES OF CONCENTRATIONS OF ROTENONE FOR 24H ASSESSED BY ROS ASSAY.	142
FIGURE 4-17 CLEAVED-CASPASE 3, TOMM20 AND PGC1-A PROTEIN LEVELS CHANGE FOLLOWING TREATMENTS WITH 250NM AZD5438 AND 500NM ROTENONE FOR 24H ASSESSED BY WESTON BLOTS.	144

FIGURE 4-18 ASSESSING THE ACTION OF AZD5438 ON CELLULAR ENERGY METABOLISM USING THE SEAHORSE	
ANALYSER.	147
FIGURE 4-19 EFFECT OF GLUCOSE CONCENTRATION ON THE ACTIONS OF AZD5438	150
FIGURE 4-20 COMBINATIONS OF SIRNA-MEDIATED KNOCKDOWN OF CDKs REPRODUCE AZD5438'S EFFECT ON	
PARKIN RECRUITMENT.....	154
FIGURE 4-21 KNOCKDOWN OF CDK9 REPRODUCES AZD5438'S EFFECT ON PARKIN RECRUITMENT.....	155
FIGURE 4-22 CDK9 KNOCKDOWN REPRODUCES AZD5438'S EFFECT ON MITOCHONDRIAL ACTIVITY	157
FIGURE 4-23 GSK3B DOES NOT REGULATE PARKIN RECRUITMENT.....	158
FIGURE 4-24 GSK3B KNOCKOUT DID NOT ALTER PARKIN RECRUITMENT	160
FIGURE 4-25 AZD5438 PREVENTS ROTENONE INDUCED TOXICITY IN SH-SY5Y CELLS	162
FIGURE 4-26 AZD5438 PREVENTS PARKIN RECRUITMENT IN EGFP-PARKIN SHSY-5Y CELLS	164
FIGURE 4-27 AZD5438 PROTECTS EGFP-PARKIN SH-SY5Y CELLS FROM ROTENONE.....	166
FIGURE 4-28 AZD5438 REGULATES RELATIVE MITOCHONDRIAL DNA CONTENT IN EGFP-PARKIN SH-SY5Y	167
FIGURE 4-29 ALPHA-SYNUCLEIN MIGHT HELP AZD5438 PROTECT CELLS IN THE CELLULAR PD MODEL	171
FIGURE 4-30 A GRAPHIC SUMMARY OF THE PROTECTION EFFECTS OF AZD5438.....	172
FIGURE 5-1 AZD5438 PROTECTS RAT PRIMARY CORTICAL NEURONS FROM ROTENONE TOXICITY.....	184
FIGURE 5-2 AZD5438 PROTECTS THE NEURONAL NETWORK OF PRIMARY CORTICAL NEURONS FROM ROTENONE	
TOXICITY	186
FIGURE 5-3 AZD5438 REGULATES THE MITOCHONDRIAL NETWORK OF PRIMARY CORTICAL NEURONS	189
FIGURE 5-4 AZD5438 PREVENTS ROS INDUCION BY ROTENONE IN PRIMARY CORTICAL NEURONS.....	191
FIGURE 5-5 MIDBRAIN NEURONAL CELL CULTURE WAS GENERATED FROM HIPSCs	193

FIGURE 5-6 DOSE-RESPONSE OF ROTENONE AND AZD5438 ASSESSED BY MTT ASSAY.....	195
FIGURE 5-7 AZD5438 PROTECTS HUMAN MIDBRAIN CELLS AGAINST ROTENONE-INDUCED STRESS.....	197
FIGURE 5-8 AZD5438 PROTECTS THE NEURONAL NETWORK OF HUMAN MIDBRAIN NEURONS.	201
FIGURE 5-9 AZD5438 POTENTIALLY PROTECTS THE HUMAN DOPAMINERGIC NEURONAL NETWORK	202
FIGURE 5-10 MITOCHONDRIAL VISUALISATION IN HIPSC DERIVED MIDBRAIN NEURONAL CULTURES.	205
FIGURE 5-11 MITOCHONDRIAL NETWORK IN HIPSC DERIVED MIDBRAIN NEURON CULTURES FOLLOWING TREATMENT WITH ROTENONE AND AZD5438	207
FIGURE 5-12 MITOCHONDRIA IN HIPSC DERIVED MIDBRAIN NEURONAL CULTURES STAINED FOR TOMM20 FOLLOWING TREATMENT WITH ROTENONE AND AZD5438.	208
FIGURE 5-13 PGC-1A EXPRESSION IN HUMAN MIDBRAIN CELLS FOLLOWING ROTENONE-INDUCED STRESS.....	211
FIGURE 5-14 AZD5438 MEDIATES A NON-SIGNIFICANT PROTECTIVE TREND AGAINST CHANGES IN PGC-1A EXPRESSION FOLLOWING ROTENONE TREATMENT IN HUMAN MIDBRAIN CELLS	213
FIGURE 5-15 AZD5438 PREVENTS ROS FORMATION IN HUMAN MIDBRAIN CELLS FOLLOWING ROTENONE-INDUCED STRESS	215
FIGURE 5-16 AZD5438 PREVENTS CASPASE-3 ACTIVATION IN HUMAN MIDBRAIN CELLS FOLLOWING ROTENONE- INDUCED STRESS.....	216
FIGURE 5-17 PATCH CLAMPING OF MIDBRAIN NEURONS WITH TREATMENTS.....	220
FIGURE 5-18. RESTING MEMBRANE POTENTIAL OF MIDBRAIN NEURONS FOLLOWING TREATMENT WITH ROTENONE AND AZD5438.	221
FIGURE 5-19 ACTION POTENTIAL PROPERTIES OF MIDBRAIN NEURONS FOLLOWING TREATMENT WITH AZD5438 AND ROTENONE	223

FIGURE 5-20 MEMBRANE POTENTIAL PROPERTIES OF MIDBRAIN NEURONS FOLLOWING TREATMENT WITH AZD5438 AND ROTENONE	225
FIGURE 6-1 UBE2N IS A POSITIVE MODULATOR OF PARKIN-RECRUITMENT IN SH-SY5Y CELLS	253
FIGURE 6-2 UBE2N IS A POTENT MODULATOR OF PARKIN RECRUITMENT	255
FIGURE 6-3 THE MAP OF PCR PRODUCT WITH XBAI AND SALI SITES.	257
FIGURE 6-4 THE MAP OF PRRL.SIN.CPPT.CMV.EGFP.WPRE PLASMID, SHOWING THE TWO AIM DIGESTION SITES(SALI AND XBAL) MARKED BY BLUE BOXES.....	257
FIGURE 6-5 VIRTUAL CUT RESULT OF XBA I +SAL I ON PRRL.SIN.CPPT.CMV.EGFP.WPRE PLASMID, SHOWING TWO FRAGMENTS GENERATED.	258
FIGURE 6-6 FIGURE 22. GEL RUNNING IMAGE SHOWING PPL PLASMID IN THE LEFT WAS CUT INTO 2 PIECES AND THE DIGESTED PCR PRODUCT WAS IN THE RIGHT.	258
FIGURE 6-7 THE MAP OF VIRTUAL LIGATION RESULTS OF INSERT A GENE OF INTEREST INTO THE BACKBONE.	259
FIGURE 6-8 VIRTUAL CUT RESULTS FOR RESTRICTION DIGESTION CHECK. ACC65I, KPN I AND STU I CUT THE BACKBONE AND THE CLONED PRODUCT, RESPECTIVELY, SHOWING A SINGLE BAND FOR THE BACKBONE AND DOUBLE BANDS FOR THE CLONED PRODUCT.....	260
FIGURE 6-9 THE X SAMPLE SHOWED TWO BANDS WITH THE CORRECT POSITION, INDICATING THE INSERT WAS CORRECTLY CLONED INTO THE BACKBONE.....	260
FIGURE 6-10 RESTRICTION DIGESTION CHECK RESULTS AFTER MAXIPREP OF THE CLONED DNA, CUT BY KPN I, ACC65 RESPECTIVELY. KPN I AND ACC65 RESULTS SHOWED CORRECT BANDS.	261
FIGURE 6-11. OVEREXPRESSION OF UBE2N UPREGULATES PARKIN RECRUITMENT ACTIVITY.....	263
FIGURE 6-12 OVEREXPRESSION OF UBE2N ALTERS PGC-1A GENE EXPRESSION.....	264

FIGURE 6-13 OVEREXPRESSION OF UBE2N DOES NOT PROTECT CELLS AGAINST ROTENONE.....	265
FIGURE 6-14 VALIDATION OF TARGET KNOCKDOWN BY SIRNAS.	266
FIGURE 6-15 EFFECT OF SIRNA KNOCKDOWN OF UBR5, GBP2 AND HECTD2 ON PARKIN RECRUITMENT IN H4 CELLS	268
FIGURE 6-16 EFFECT OF SIRNA KNOCKDOWN OF UBR5, GBP2 AND HECTD2 ON PARKIN RECRUITMENT IN SH- SY5Y CELLS.....	269
TABLE 1-1 OVERVIEW OF PARKINSON'S DISEASE (PD)-RELATED GENES. GENES RELATED TO PD AND THEIR DESCRIPTION ARE SHOWN.	3
TABLE 1-2 PD-RELATED GENES WHICH AFFECT MITOCHONDRIAL ACTIVITY.	4
TABLE 1-3 FULL LIST OF THE SELECTED PHARMACOLOGICAL COMPOUNDS SCREENED BY SCOTT ET AL.....	22
TABLE 1-4 SUMMARY OF NATURAL COMPOUNDS AND THEIR REGULATION ON MITOCHONDRIAL ACTIVITY THROUGH GSK-3B	26
TABLE 1-5 SUMMARY OF CDKS/CYCLINS AND THEIR FUNCTIONS IN THE CELL.....	30
TABLE 2-1 MEDIA COMPOSITION FOR FEEDING PRIMARY CORTICAL NEURONAL CULTURE.....	36
TABLE 2-2 THE LIST OF MEDIA IN USE FOR MDANS DIFFERENTIATION AND THEIR COMPOSITION	39
TABLE 2-3 COMPOUND LIST.....	41
TABLE 2-4 FINAL SIRNA AND RNAIMAX CONCENTRATION AND VALUE, RESPECTIVELY, PER WELL FOR 96-WELL PLATE AND 12 WELL PLATE.	41
TABLE 2-5 LIST OF MAIN CHANNELS USED FOR INCELL IMAGING.....	46
TABLE 2-6 GENES AND PRIMERS SEQUENCE FOR DETECTION IN QPCR.	50

TABLE 2-7 RECIPE FOR MEDIA, BUFFER AND DNA MIXTURE IN USE FOR LENTIVIRAL PRODUCTION	54
TABLE 2-8 ANTIBODIES LIST.	60
TABLE 6-1. GENES WERE FOUND TO SIGNIFICANTLY AFFECT PARKIN RECRUITMENT, AS INDICATED BY THE STRICTLY STANDARDISED MEAN DIFFERENCE (SSMD) SCORE. THE COMPLETE LIST SHOULD REFER TO THE PUBLICATION[108].....	247

Chapter1 Introduction

Parkinson's disease

Parkinson's disease (PD) is a heterogeneous neurodegenerative disease affecting 7 million people worldwide [1]. The main symptoms of PD are classified as motor symptoms such as rigidity and slowness and non-motor neuropsychiatric symptoms such as depression. A recent study suggested that the neurodegenerative process not only affects the dopaminergic neurons in the substantia nigra but also occurs in multiple areas, which is evident in the early and late stages of the disease (**Figure 1-1**) [2]. The cause of the disease is not clear yet, but both genetic (Table 1-1) and environmental factors are suggested to be involved[3] [4]. Hallmarks of PD are the death of dopaminergic neurons in the midbrain area[5] and the abnormal accumulation of the protein alpha-synuclein, which forms potentially toxic inclusions called Lewy bodies in neurons[6]. Lysosomal and mitochondrial dysfunction have been suggested as possible mechanisms that contribute to cell death in PD.

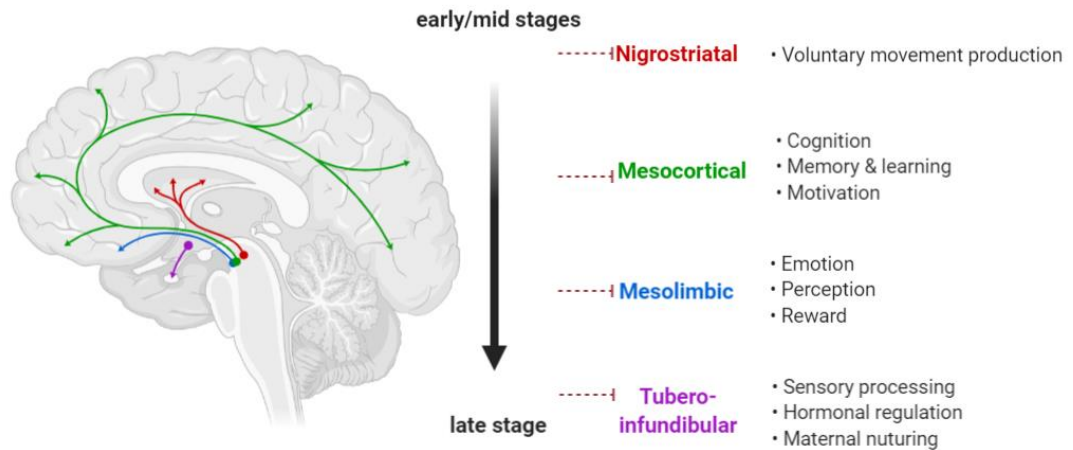


Figure 1-1 Pathophysiology of a multisystem neurodegenerative process from early to late stage of PD.

Loci	Gene	Protein
PARK1	SNCA	Alpha-synuclein
PARK2	PRKN	Parkin
PARK3	Unknown	Unknown
PARK5	UCHL1	Ubiquitin C-Terminal Hydrolase L1
PARK6	PINK1	PTEN-induced putative kinase 1
PARK7	DJ-1	Protein DJ-1
PARK8	LRRK2	Leucine-rich repeat kinase 2
PARK9	ATP13A2	ATPase 13A2
PARK10	Unknown	Unknown
PARK11	GIGYF2	GRB10 interacting GYF protein 2
PARK12	Unknown	Unknown
PARK13	HTRA2	Serine peptidase 2
PARK14	PLA2G6	Phospholipase A2 Group VI
PARK15	FBX07	F-Box protein 7
PARK17	VPS35	Vacuolar protein sorting 35
PARK18	EIF4G1	Eukaryotic translation initiation factor 4 gamma, 1
PARK19	DNAJC6	DNAJ subfamily C member 6

PARK20	SYNJ1	Synaptojanin-1
PARK21	DNAJC13	DNAJ subfamily C member 13
PARK22	CHCHD2	Coiled coil-helix-coiled coil-helix domain 2
PARK23	VPS13C	Vacuolar protein sorting 13 homolog C
-	GBA	Glucocerebrosidase

Table 1-1 Overview of Parkinson's disease (PD)-related genes. Genes related to PD and their description are shown.

Relatively recent research has found that mutations in coding genes, including PTEN-induced putative kinase 1 (PINK1), Parkin (PRKN), alpha-synuclein (SNCA), leucine-rich repeat kinase 2 (LRRK2), ATPase 13A2 (ATP13A2), VPS35 (PARK17) and PARK7/DJ-1 [7] [8] [9] are associated with early onset PD (EOPD). A number of these genes have been found to have functions associated with mitochondrial quality control, ubiquitin-proteasome system and lysosomal degradation pathways [10]. The list of PD-related genes and their function in mitochondrial activity is summarised in **Table 1-2**.

The treatment of PD patients with L-dopa is based on improving dopamine levels in the brain. However, extrapyramidal side-effects are associated with tolerance and the need for treatment with increasingly high doses. In the past few decades, surgery for PD has advanced, and motor symptoms are treated with deep brain stimulation [11]. Other therapies currently being developed include gene therapy and neural transplantation both of which are based on compensating for the loss of dopaminergic neurons/neurotransmission [12].

Experiments described in this thesis have focused on investigating mechanisms by which the function of mitochondria can be improved. In particular, modulators that positively regulate mitochondrial function and cell survival have been investigated as potential treatments for PD.

Loci	Gene	Mitochondrial related function
PARK1	SNCA	Aggregated protein inhibits complex I
PARK2	PRKN	Mitophagy signalling
PARK6	PINK1	Mitophagy signalling, mitochondrial unfolded protein response
PARK7	DJ-1	Maintains mitochondrial function against oxidative stress
PARK8	LRRK2	Regulates endolysosomal for the downstream activity of mitophagy
PARK9	ATP13A2	Lysosomal transmembrane protein, supports mitochondrial function
PARK14	PLA2G6	Supports mitochondrial function
PARK17	VPS35	Endosomal and lysosomal trafficking, supports mitochondrial function
-	GBA	Autophagy and lysosomal degradation

Table 1-2 PD-related genes which affect mitochondrial activity.

Mitochondrial function -Oxidative phosphorylation

Mitochondria play an important role in cell function and survival. They facilitate oxidative phosphorylation, control reactive oxygen species (ROS), mediate apoptosis and buffer cytosolic calcium.

The protein complexes of the electron transport chain (ETC) located at the inner mitochondrial membrane (IMM) generate ATP following electrons transport through the ETC and protons transport across the IMM. ETC complexes I, III, and IV use the electrons energy when transporting them to pump protons across the inner mitochondrial membrane to the mitochondrial intermembrane space to produce an electrochemical gradient. Protons return across the electrochemical gradient and this provides the energy for complex V to phosphorylate ADP to ATP[13]. The above processes are shown in **Figure 1-2**.

If mitochondria are dysfunctional, the consequences would be: a cessation of ATP production; the generation of ROS; the activation of caspase signalling and apoptosis. In addition, a disrupted mitochondrial membrane potential, either due to ECT dysfunction-associated proton gradient failure or the opening of mitochondrial permeability transition pore (mPTP) (by destabilising the mPTP proteins) would result in disrupted calcium homeostasis. Depending on the cell type, this compromised calcium homeostasis could contribute to different

pathological conditions [14]. For neurons, it eventually leads to the loss of function and apoptotic cell death.

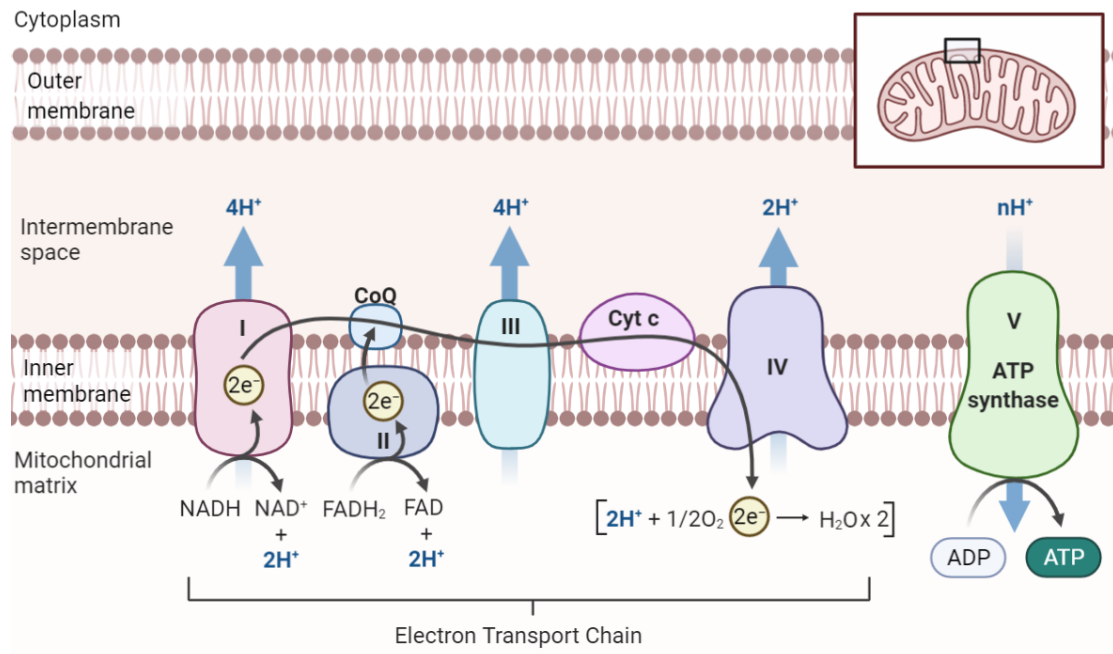


Figure 1-2 Graphic illustration of mitochondrial electron transport chain.

ECT locates at IMM. Electron and proton transportation in the ECT mediate ATP generation.

Mitochondrial biogenesis

The mitochondrial population is critical to maintaining the cell's energy demands. Thus, the generation of new mitochondria and removal of old is crucial to supporting a healthy mitochondrial population. Unlike other organelles, mitochondria have their DNA that encodes for a number of protein-coding genes. However, mitochondrial biogenesis and function depend on genes transcribed from mitochondria and cell nuclei[15]. Peroxisome proliferator-activated receptor γ (PPAR γ) coactivator 1 α (PGC-1 α) is a master regulator of mitochondrial biogenesis [16]. PGC-1 α and its downstream cofactors, nuclear respiratory factors (NRF1, 2), regulate the transcription of all nuclear-encoded mitochondrial respiration chain proteins, which are essential for mitochondrial function. Decreased PGC-1 α expression levels have been associated with a loss of dopaminergic neurons in animal models of PD and with PD patients [17] [18]. Thus, mitochondrial biogenesis is hypothesised to be reduced in PD neurons, consequently leading to damaged mitochondria accumulation and neurodegeneration.

Mitochondrial dynamics

Mitochondria are dynamic organelles. Through continuous fusion, fission, and biogenesis activities, they keep an appropriate population in the cell fitting its metabolic demands[19]. The graphic illustration of the processes is presented in **Figure 1-3**. An accurate balance between fusion and fission is critical in maintaining mitochondrial dynamics regarding different cellular functions [20] [21]. Mitochondrial fusion is regulated by a mitochondrial transmembrane GTPase, Mitofusin (Mfn) [22], whereas mitochondrial fission is mediated by dynamin-related protein 1 (DRP1) [23]. DRP1 translocates from the cytosol to the mitochondrial outer membrane (MOM), where the activated DRP1 punctuates marks to proceed with membrane constriction and fission directed by Fis1[21]. A deficiency of active DRP1 causes mitochondria elongation, leads to mitochondrial dysfunction, and causes a decrease in cellular ATP generation, eventually leading to cell death [24]. Fusion and fission also help eliminate the general stress level in the mitochondrial network.

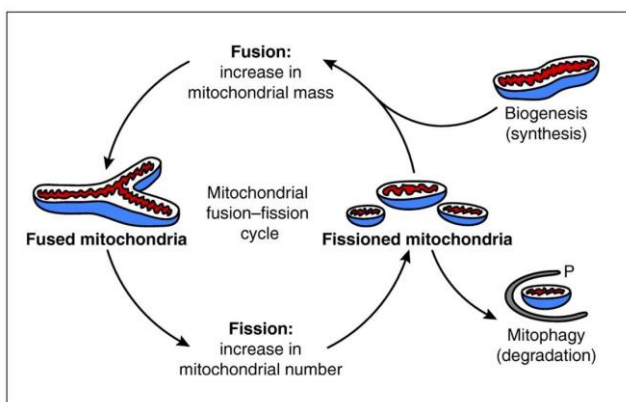


Figure 1-3 Mitochondrial dynamic.

Figure reproduced from Seo et al. 2010, with permission from Company of Biologists.

Mitochondrial turnover

There are four main processes responsible for mitochondrial turnover. First, the mitochondrial ATP-dependent proteases identify misfolded or damaged polypeptides and initiate proteolysis, and the ubiquitin-proteasome system (UPS) targets OMM proteins for degradation[25]. In addition, the mitochondrial unfolded protein response (UPR_{mt}) activates a retrograde signalling cascade in the nucleus to upregulate the expression of mitochondrial genes[26]. Furthermore, the mitigation of mitochondrial damage is aided by continual fission and fusion processes. When these quality control mechanisms fail, mitophagy pathways are activated, eventually clearing the damaged mitochondria[25]. The most prominent mechanism of mitochondrial clearance is autophagy. Autophagy helps recycle necessary metabolites and also protects cells from toxicity caused by abnormal organelles or protein aggregation.

Mitophagy

The key point in the mitochondrial lifecycle is the selective clearance of damaged mitochondria by an autophagic process, mitophagy[27]. This process is required for maintaining cellular energy homeostasis and mitochondrial function [28].

Parkin-mediated mitophagy is the dominant mitophagy type of neuronal cell [29]. PINK1 and PRKN encode PTEN-induced kinase 1 and an E3 ubiquitin ligase Parkin, respectively. Mutations in the genes encoding these proteins are associated with early-onset forms of PD [30]. PINK1 targets mitochondria via a mitochondrial localisation signal in its amino terminal. Under normal conditions, it is rapidly transported across the outer mitochondrial membrane through translocase of the outer membrane (TOM) to the interspace, where it is cleaved by proteases, including matrix processing peptidases and presenilin-associated rhomboid-like (PARL). The cleavage products translocate from mitochondria to the cytosol and are rapidly degraded by the proteasome. Under stress conditions, depolarisation of the mitochondrial membrane reduces the cleavage of PINK1; thus, PINK1 starts to accumulate on the outer membrane and is activated through autophosphorylation. Phosphorylated ubiquitin-substrates interact with OPTN or NDP52 to recruit Parkin, which is then activated by PINK1 for polyubiquitination. Polyubiquitinated substrates are then recognised by microtubule-associated protein 1 light chain 3 beta (LC3) adapters, which form the connection of the

damaged mitochondria to an autophagosome.

In addition to PINK1/PRKN-mediated mitophagy described above, other types of receptors that mediate mitophagy have been discovered recently. In mammalian cells, the FUN14 domain containing 1 (FUNDC1) is an outer mitochondrial membrane protein, and it was discovered to mediate hypoxia-induced mitophagy [31]. FUNDC1 contains a conserved LC3-interacting region (LIR), which binds to LC3, mediating clearance. PGC-1 α and NRF1 regulate FUNDC1 to promote mitophagy [32]. Moreover, BCL2 interacting protein 3 (BNIP3) and NIX are hypoxia-inducible genes that play an essential role in hypoxia-induced macrophage and mitophagy [33]. In yeast, the mitophagy protein Atg32 (Atg32) was reported to mediate mitophagy[34].

Mitochondrial ROS and apoptosis

Mitochondria are major generators of reactive oxygen species (ROS), and they produce ROS primarily by monoelectron reduction of oxygen at the ETC. ROS can be harmful, resulting in oxidative damage to cellular lipids, proteins, or DNA, and can contribute to apoptosis. Nicotinamide adenine dinucleotide (NAD⁺)/reduced NAD⁺ (NADH) and NADP⁺/reduced NADP⁺ (NADPH) redox couples are involved in reducing ROS levels and thus protects cells from damage and apoptotic cell death. Oxidative stress to mitochondrial components, such as mitochondrial DNA, may result from an imbalance between ROS production and the effectiveness of the antioxidant defence systems. Very high levels of ROS may lead to intrinsic mitochondria-mediated apoptosis. During the initiation of intrinsic apoptosis, mitochondrial ROS pushes mitochondrial apoptogenic factors like cytochrome c to be released into the cytosol. Apoptosome is formed when cytochrome c binds to cytosolic protein Apaf-1. Caspase-9 is activated following the apoptosome formation and activates downstream caspases and BID (a BH3 domain-containing proapoptotic Bcl2 family member) to trigger the mitochondria to release more apoptotic factors. Caspase-3, the major executor of apoptotic death, is produced following the cleavage of pro-caspase by Caspase-9, effectively leading the cells to apoptosis. [35] [36, 37] [38] [39] [40] The process of mitochondrial ROS-mediated apoptosis is shown in **Figure 1-4**.

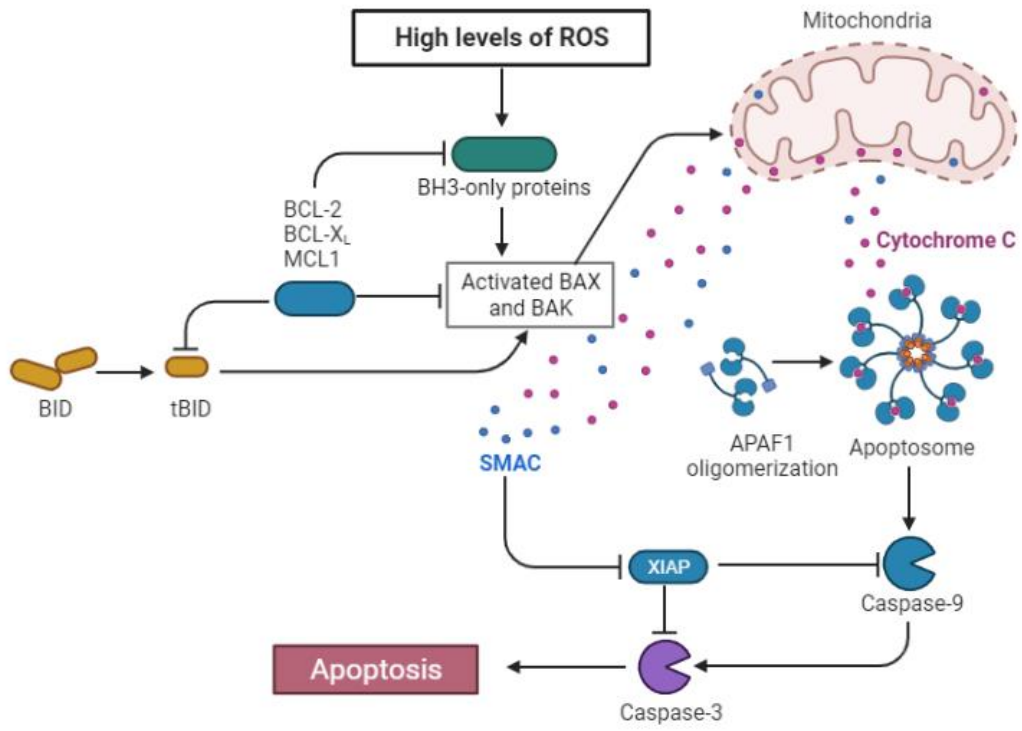


Figure 1-4 Graphic illustration of mitochondrial ROS-mediated apoptosis

Mitochondria in neurons

Neuronal activity is highly energy-dependent, and the brain consumes at least 20 per cent of the body's energy generation, most of which is used for synaptic transmission[41] [42]. In addition, neurons possess a complex and large mitochondrial network that produces energy primarily by oxidative phosphorylation [43] [44]. Neurons are the most complicated structure of all cells in the human body, and their axons and dendritic projections need efficient transport and healthy maintenance of mitochondrial networks[45]. In addition, mature neurons are differentiated and non-dividing cells. Therefore, they must sustain function throughout life, which requires careful regulation of a healthy mitochondrial population via biogenesis, fission/fusion dynamic, and clearance system [46].

Recent studies have offered vital insights into mitochondria's function and spatial positioning in neurons. In hippocampal neurons, dendritic mitochondria rapidly apply fission and congregate in the region of dendritic spines and synapses in response to neuronal activity, showing that mitochondria dynamically respond to neuronal activity[47]. Moreover, the presence of mitochondria at synapses is responsible for their critical physiological roles in providing energy for synaptic vesicle release and recycling and buffering calcium during synaptic transmission [48].

Research evidence suggests that mitochondria play a crucial role in age-related neurodegenerative disorder[49]. It is believed that alongside aging, the efficiency of mitochondrial quality control decreases, leading to the accumulation of damaged mitochondria which reduces ATP genesis, releases pro-apoptotic factors and increases ROS level, resulting in axon degeneration of neurons and neuronal apoptosis, and eventually, neurodegenerative diseases[50] [51] [52] [53, 54]. This mitochondrial related neuron death is illustrated in **Figure 1-5**.

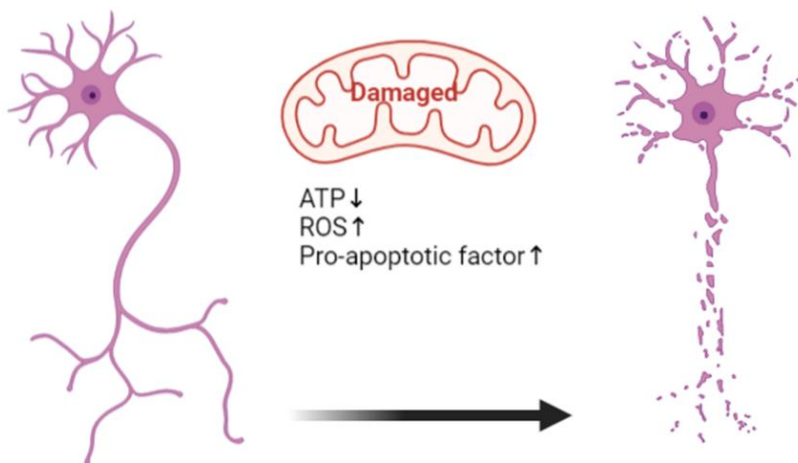


Figure 1-5 Neuron cell death related to damaged mitochondria.

Targeting Mitochondria to treat neurodegenerative diseases

Mitochondrial dysfunction is a hallmark of ageing and is widely observed in numerous neurodegenerative diseases[55]. Dysfunctional mitophagy is closely associated with Parkinson's disease (PD). Reduced mitochondrial membrane potential and dysfunctional respiration are also linked to Huntington's disease (HD) [56]. Mitochondrial dysfunction is also linked to beta-amyloid induced Alzheimer's disease (AD) pathology [57]. Therefore, further systematic studies of mitochondrial quality control may not only improve the understanding of the mechanisms of neurodegenerative diseases but also point out therapeutic strategies for them.

It may be possible to facilitate fission, fusion and mitophagy by increasing the expression of autophagic proteins, regulating the activity of mitophagy-related receptors and the action pathways [58]. However, just targeting one of these processes alone would clearly be detrimental to the cell. Hence, therapies targeted at mitochondria should stimulate the removal of unhealthy mitochondria while promoting the production of new or even increased numbers of mitochondria.

The central hypothesis in this thesis is that neurodegenerative pathologies may be delayed, prevented, or restored by improving mitochondrial quality control

through genetic modification and/or via the targeting of quality control processes (Figure 1-6). For example, improved mitophagy with increased healthy mitochondrial population could improve energy metabolism and inhibit apoptosis in the aged brain and thus delay or prevent the cellular damage associated with neurodegenerative diseases.

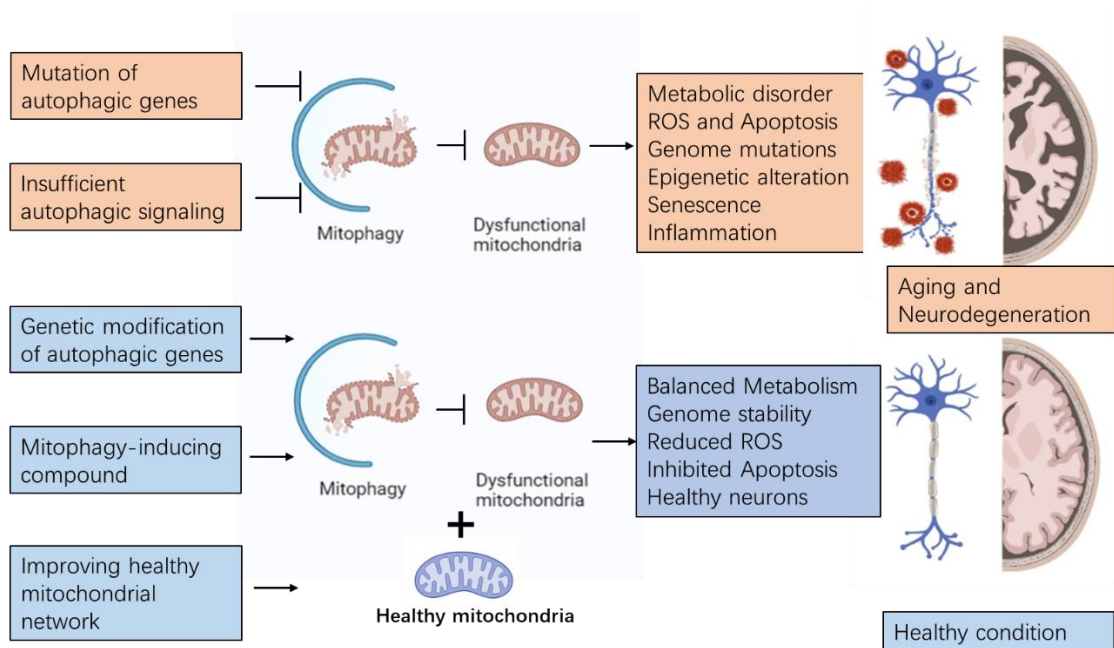


Figure 1-6 An example of how targeting mitochondrial quality control pathways may prevent mitochondrial dysfunction mediated ageing and neurodegeneration.

Challenges in neurodegenerative research

One of the main challenges in human neurodegenerative diseases research has been accessing human diseased tissue or other samples for study. Even if tissue is available, terminally differentiated cells like neurons can neither be maintained nor expanded in the lab, which affects the reproducibility and scalability of a strictly designed experiment. Accessible tissues, such as neonatal umbilical cord samples, do not contain the genes and molecular pathways involved in diseases. Therefore, alternative approaches, such as transgenic animals and immortalised cell lines, with overexpression or knockdown of specific disease transgenes have been used. These methods have shown advantages through pre-clinical efficacy and safety as they point out the relationship between the gene, protein, and disease phenotype. However, such methods have not translated well and have often led to high-cost failed clinical trials in humans [59].

The reprogramming of human cells to iPSCs reported in 2007 offered an alternative tool for studying physiologically relevant human cell types and proteins without altering heterologous genes. Somatic cells from patients with the genes of interest can be reprogrammed into iPSC. Neurons can be differentiated into 2D and 3D cultures from patient iPSCs to investigate cellular microenvironments further, the so-called 'brain in a dish' [60]. The workflow of iPSC from patient to in vitro experiment is shown in **Figure 1-7**.

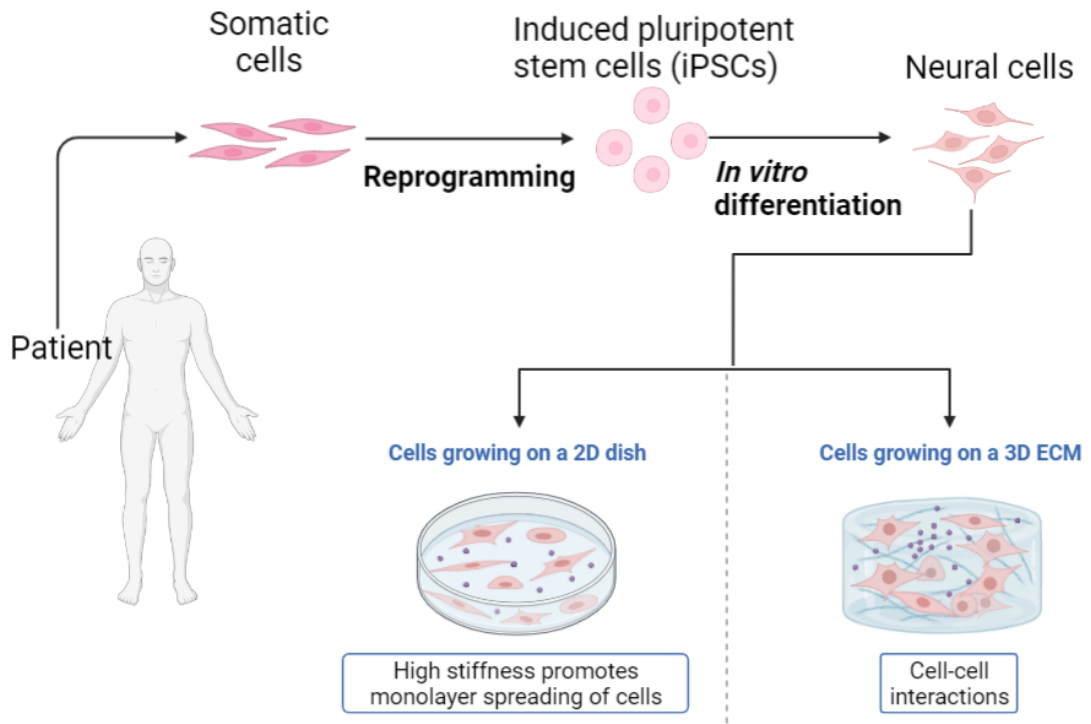


Figure 1-7 The workflow of the iPSC study.

Somatic cells are collected from the patient with the gene of interest and reprogrammed into iPSCs. iPSCs are then differentiated into the objective types of neurons, which could be cultured in 2D or 3D. 2D culture has the advantage of monolayer for imaging assay. 3D culture has the advantage of investigating cell-cell interaction.

Previous screen

Previous research by the group in the regenerative medicine laboratory at the University of Bristol [34] used an in vitro phenotypic model based on measuring parkin recruitment following mitochondrial membrane depolarisation to carry out a high-throughput screen of 7500 genes. Genes of interest were chosen from the druggable gene library focusing on disease-relevant targets. The primary screen was evaluated by principal components analysis (PCA) and a parameter-agnostic machine-learning approach. The screen processes are shown in **Figure 1-8**. The genes identified fell into three broad classes, those that regulate: (i) protein degradation pathways; (ii) free radical levels, DNA repair; (iii) transcription. The results identified that a group of genes targeting ubiquitin-proteasome pathways (such as UBE2N) significantly altered Parkin recruitment activity (**Figure 1-9**). In chapter 6, the follow-up investigation of the effects of genetic modification of UBE2N on Parkin recruitment and the potential of protection for PD was performed.

Additional to the siRNA screen, a small pharmacological compound library containing modulators of neurodegenerative pathways was also screened (**Table 1-3**). After the compounds screen, kenpaullone was identified as a potential negative modulator of mitophagy, and Cu-ATSM was identified as the potential positive modulator. Kenpaullone is GSK3-beta and CDKs inhibitor, and plenty of

evidence suggests it is neuron protective by decreasing oxidative stress. Cu-ATSM is identified as a copper delivery compound, and copper deficiency is known to relate to mitochondrial morphology.

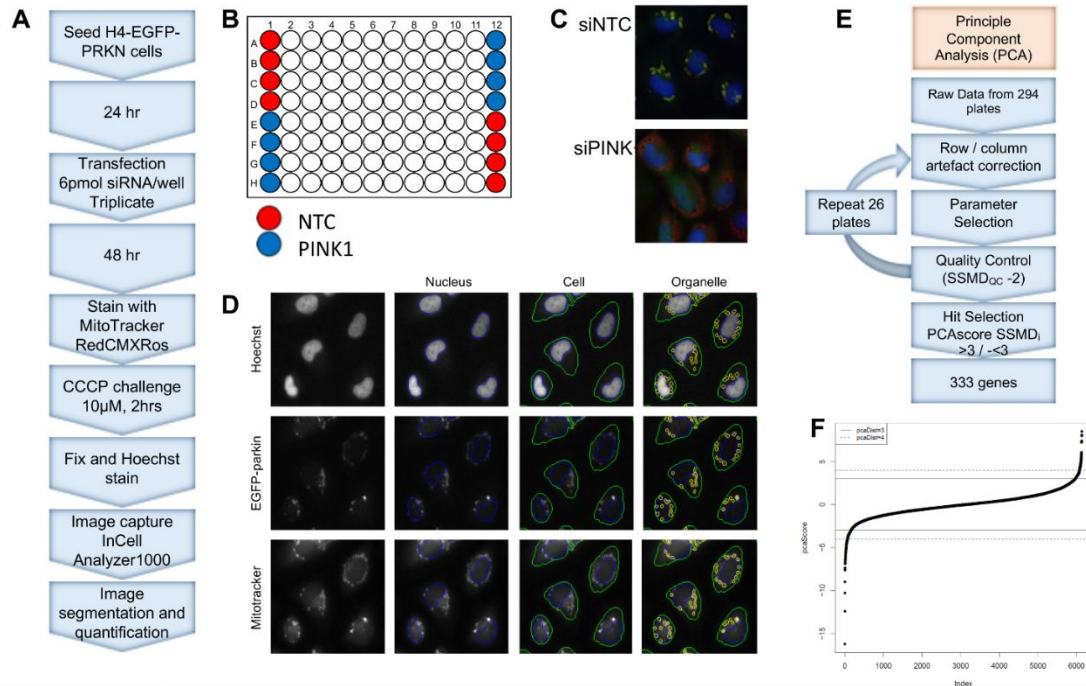


Figure 1-8 Screening of the druggable genome library.

(A) Screen process workflow. (B) Plate map. (C) Overlay of Hoechst and e-GFP PRKN with siPINK and NTC. (D) Images captured by InCell Analyser, and the segmentation. (E) PCA analysis pipeline. (F) PCA score showing >3 and <-3 . Figure taken from Scott et al.

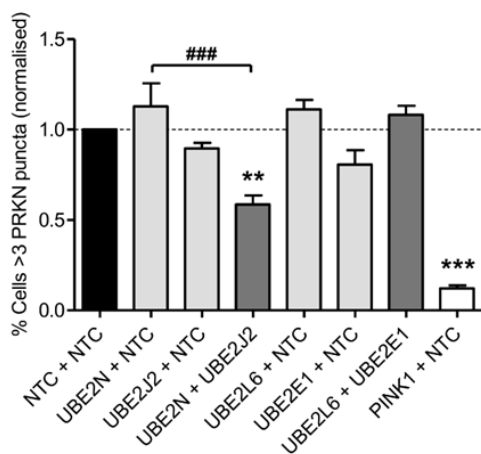


Figure 1-9 Combined siRNA knockdown of UBE enzymes identified in Scott et al modulates PRKN recruitment.

Compound	Description
GSK2606414	Potent and selective PERK inhibitor
N-Acetylcysteine amide	Cell permeable antioxidant
cu-ASTM (Sigma)	Antioxidant, acts on peroxynitrite
Rapamycin	mTOR inhibitor, immunosuppressant
trans-ISRIB	Integrated stress response (ISR) inhibitor
Resveratrol	Cyclooxygenase inhibitor
AR-A 014418	Selective GSK-3 inhibitor
Sodium 4- Phenylbutyrate	HDAC inhibitor; ER stress blocker
Dimethylfumarate	Nrf2 pathway activator; neuroprotective
TRC 051384	Inducer of heat shock protein Hsp70
Edaravone	Anti-ischaemic and antioxidant
BIX	BiP (Hsp70-5) ER chaperone inducer
DMSO	Vehicle
Z-VAD-FMK	Cell-permeable, irreversible caspase inhibitor
SP600125	Selective JNK inhibitor
Kenpaullone	GSK-3 inhibitor. Also inhibits CDKs
Olesoxime	Binds VDAC
Azoramide	Unfolded protein response (UPR) modulator
Riluzole	Glutamate release inhibitor/GABA uptake inhibitor
Dantrolene	Ca ²⁺ release inhibitor
LOE 908 hydrochloride	Broad spectrum cation channel blocker; neuroprotective
SKF 85536	Potent and selective D1-like dopamine receptor antagonist
B2	Promotes inclusion formation in HD and PD
Memantine	NMDA antagonist; acts at ion channel site
PD-150606	Calpain inhibitor

Table 1-3 Full list of the selected pharmacological compounds screened by Scott et al.

Neuronal development and kinase activities

Neurons differentiate, migrate, grow neurites, and eventually build connections within their network. The neurites' development and degradation are crucially responsible for neuronal function. Neurodegenerative diseases such as spinal cord injury, stroke, multiple sclerosis, Alzheimer's disease and Parkinson's disease are often identified with losing functional neuronal networks. Thus, treatment could be mediated by therapies targeting neuronal network protection and regeneration. Apart from the cellular metabolism that mediates ATP generation for neuronal development, multiple kinases and phosphatases also influence neuronal morphology and function by regulating the signalling pathways that directly and indirectly regulate energy metabolism and control neurite formation [61]. Some individual kinases and phosphatases affect neurite development. For instance, the non-receptor tyrosine kinase Src is essential for cell adhesion-dependent neurite outgrowth, and the phosphatase Calcineurin is necessary for transiently blocking the expansion of spinal neurons.

Besides the individual kinases and phosphatases, signalling pathways dependent on kinases activities, including the mitogen-activated protein kinases (MAPKs), cytoskeletal, growth factor signalling and calcium-dependent pathways, have been found to affect neuronal function and energy metabolism [62] [63] [64] [65] [66]. Recent studies showed that glycogen synthase kinase-3 (GSK3) and Cyclin-

dependent kinases (CDKs) regulate mitochondrial function and neuronal development, function, and death[67, 68].

GSK- β and its involvement in neurodegenerative diseases

GSK3 was first identified as the kinase phosphorylating glycogen synthase in a skeletal muscle [69] and has since been shown to be critical in multiple signalling pathways [70]. GSK3 activity is a key developmental component in inflammation and tumorigenesis, as either active or inhibited GSK3 is suggested to regulate cell fate via the Wnt-mediated pathway [71]. Research also showed that GSK3 β plays an important role in neuronal apoptosis and contributes to certain pathogenesis of neurodegenerative diseases such as AD and PD. ([72].

1-methyl-4-phenyl-1,2,3,6-tetrahydropyridine (MPTP) is widely used to selectively damage dopaminergic neurons in substantia nigra to model PD[73]. Research showed that the GSK-3 β -dependent pathway mediates the MPTP-induced apoptosis of dopaminergic neurons, while inhibition of GSK-3 β reduces the damage induced by MPTP, indicating the association of GSK-3 β with PD. MPTP is also a complex I inhibitor of the mitochondrial respiratory chain. Inhibition of complex I by MPTP via GSK-3 β increases the production of reactive oxygen species (ROS) and contributes to cellular oxidative stress and, eventually, neuron cell death, [74] suggesting mitochondrial dysfunction involving GSK-3 β is involved in the pathogenesis of PD.

Evidence suggests that commonly used drugs regulate mitochondrial activity and cell apoptosis via an action on GSK-3 β (**Table 1-4**)[75]. This evidence suggests a strong link between the therapeutic potential of GSK-3 β with mitochondrial dysfunction-related disease pathogenesis.

Accumulating evidence points out that GSK-3 β interacts with mitochondrial proteins, such as components of the respiratory chain and subunits of mPTP. Inactivation of GSK-3 β has been shown to promote biogenesis and dynamics of mitochondria, reduce mitochondrial membrane permeability and inhibit mitochondria-mediated apoptosis. Through altering the opening of the mPTP, GSK-3 β participates in the mitochondrial apoptosis pathway mediated by the disruption of the mitochondrial membrane and the release of pro-apoptosis factors[76] [77]. Inhibition of GSK-3 β also suppresses pathogenic pathways in PD and supports neuron survival [78]. GSK-3 β inhibition was shown to decrease α -synuclein protein levels and promote cell survival in a cellular model of PD, suggesting that inactivation of GSK-3 β may promote dopaminergic neuron survival by reducing the toxicity of abnormal α -synuclein aggregation[79].

Compounds	upregulation	downregulation
Curcumin	mitochondrial functions, Akt/GSK-3 β signalling	oxidative stress, cell apoptosis
Resveratrol	Akt/GSK3 β signalling	mitochondrial dysfunctions
Asiatic acid	mitochondrial functions, Akt/GSK-3 β signalling	I/R injury
Triptolide	desensitisation of mPTP	mitochondrial apoptosis, CyP-D phosphorylation
Formononetin	Akt/GSK-3 β signaling, phosphor-Ser9-GSK-3 β -ANT	CyP-D-ANT, mPTP opening, ROS generation
Hesperidin	activities of mitochondrial complex	GSK3 β activity
liquiritin	ERK and Akt-GSK-3 β signaling \uparrow	mitochondrial apoptosis
Sulfuretin		apoptotic cascade, GSK-3 β signaling, NF- κ B signaling
Baicalein	phosphorylation of Akt-Thr308 and GSK-3 β -Ser9	cytochrome c release

Table 1-4 Summary of natural compounds and their regulation on mitochondrial activity through GSK-3 β

CDKs and their involvement in neurodegenerative diseases

CDKs are serine/threonine kinases acting on the cyclins and are responsible for promoting transitions through the cell cycle[80]. The effects of CDK inhibitors on the cell cycle and their anti-cancer potential have been widely studied [32]. In addition to the well-known cell cycle regulation by CDK1 and CDK2, CDKs also regulate apoptosis, transcription, differentiation in the nervous system.

CDK1, CDK4 and CDK6 play key roles in neuronal cell death, and CDK5 and CDK11 also participate in apoptosis. CDK7, CDK8, CDK9 and CDK11 are well known for their transcription mediating roles. CDK5 has multiple functions in the neuronal network, affecting neurite growth and glutamate receptor and dopamine signalling pathways(**Table 1-5**) [81] [82] [83] [84].

Recent studies reported mitochondria are the primary cellular organelle targeted by CDKs during cell cycle regulation [85] [86]. Cyclin B1/CDK1 has been shown to regulate mitochondrial fission and mitotic mitochondrial fragmentation via phosphorylating and activating DRP1 [87]. In addition, CDK1 is also involved in regulating mitochondrial bioenergetics [88] and mitochondria-associated apoptosis [89]. CDK1 bind to cyclin B1 and relocates to mitochondria during G2 to M phase. It then phosphorylates and activates multiple subunits of the

mitochondrial respiration chain to drive ATP production. This CDK1 mediates ATP output from mitochondria, enters nuclei and further drives the G2 to M phase transition, which is energy sensitive[90]. Moreover, CDK1-cyclin B1 binding unit activates p53, MnSOD, and SIRT3 to eliminate mitochondrial ROS and prevent the further ROS induced apoptosis of the cell [91]. In addition, CDK1 has been reported to mediate the maintenance of the DNA-damage repair system following radiotherapy [92] [93]. DNA damage enhances the translocation of cyclin CDK1/cyclin B1 to mitochondria. It then causes phosphorylation and activation of OXPHOS, leading to enhanced ATP output. This ATP serves as emergency energy to repair DNA damage and promotes cell survival. A graphic illustration of the above processes is presented in **Figure 1-10**.

CDK inhibitors have protective roles in non-proliferating neurons facing chemical stressors. CDK1 has been reported to phosphorylate β -amyloid, and inhibitors of CDK1 have been reported to reduce β -amyloid-induced cytotoxicity by preventing β -amyloid phosphorylation[94]. CDK5 is widely expressed in the neural system and phosphorylates many substrates[81]. CDK5 phosphorylates dopamine- and cAMP-regulated phosphoprotein 32 kDa (DARPP-32) on Thr75, inhibiting cAMP-dependent kinase, thus affecting the DARPP-32-dependent activities of neurons[95]. CDK5 dysregulation was observed in several neurodegenerative disorders (AD [83], ALS [96]), suggesting that CDK5 regulators might have clinical potential. A study showed that Cdk5-dependent disruption of microtubules

could prevent the aggregation formation in the pathophysiology of poly(Q) disorders[97], and another study suggested that CDK5 phosphorylation of huntingtin (htt) mediates its cleavage and protects cells from mutant htt toxicity [98]. CDKs and GSK-3 activity within neuronal cells was analysed [99], and it was suggested that using dual pharmacological inhibitors of CDKs and GSK-3 could prevent cell death. Thus, the study on CDKs and GSK-3 inhibitors might be a promising strategy for clinical drug development for mitochondria-associated neuronal degenerative diseases, especially PD.

CDK	cyclin	functions
CDK1	cyclin B; RINGO	prophase to metaphase transition, regulation of topoisomerase 2
CDK2	cyclin A; cyclin E	G1/S transition, S phase and G2 phase, centrosome duplication, regulation of Sp1-mediated transcription
CDK3	cyclin E	G1/S transition
CDK4	cyclin D	G1 phase, Excitotoxin-induced neuron death
CDK5	p35,p25; p39,p29	Apoptosis, neurite growth, neuronal migration, dopamine and glutamate signalling, Phototransduction, neurotransmitter release
CDK6	cyclin D	G1 phase, neuron death
CDK7	cyclin H	CDK1, CDK2 activation, basal transcription (TFIIH)

CDK8	cyclin C	CDK7-cyclin H regulation
		signal transduction,
	cyclin K;	RNA transcription (P-TEFb),
CDK9	cyclin T	HIV-Tat-dependent transcription
		RNA transcription,
		apoptosis,
CDK11	cyclin L	dopamine and glutamate signalling

Table 1-5 Summary of CDKs/cyclins and their functions in the cell.

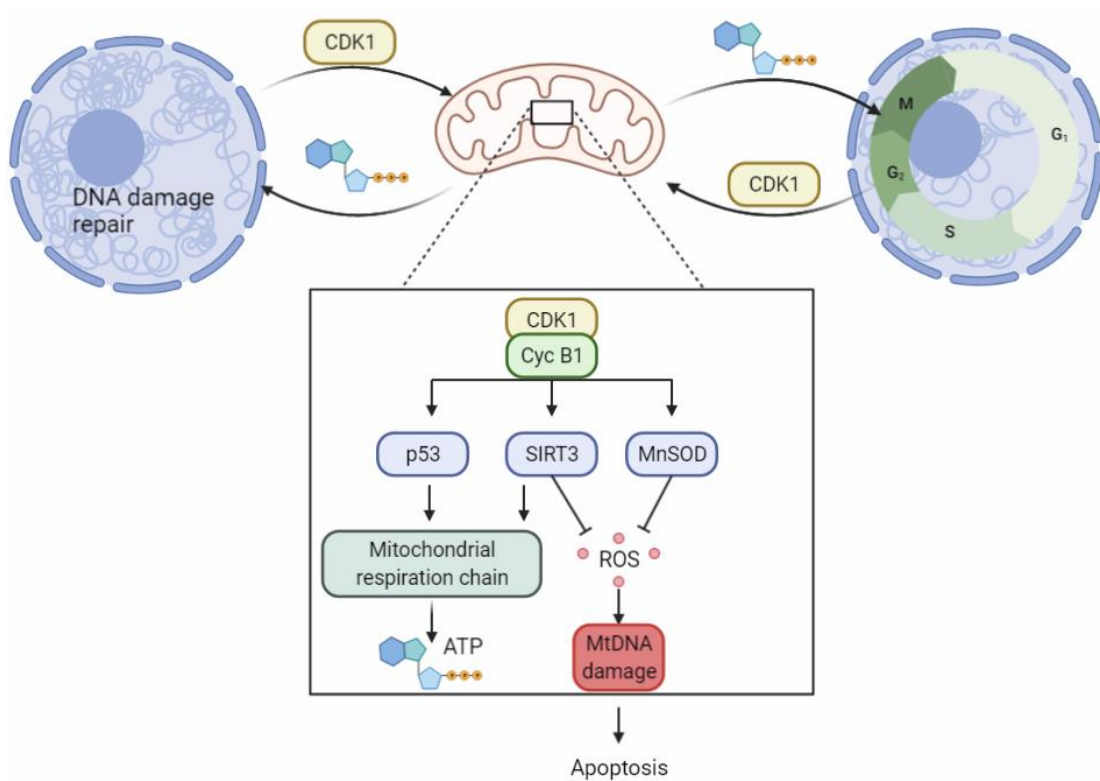


Figure 1-10 CDK1 mediates mitochondrial ATP production and uses the ATP for G2 to M phase transition and DNA damage repair.

Focused compound test

The precious findings suggest drugs acting in a similar manner to kenpaullone would have potential as a therapy for Parkinson's. This study therefore identified compounds that acted in a similar manner to kenpaullone and were being used in preclinical/clinical studies. Those new compounds were analogues of kenpaullone, inhibitors of CDKS/GSK3 and compounds known to act on the mitochondrial transition pore.

Dexpramipexole (KNS-760704) and TR019622 (olesoxime) are compounds known to target the mitochondrial permeability transition pore (mPTP) and have been investigated as potential treatments for ASL in clinical trials [100]. AT7519 and AZD5438 were identified following a screen of CDK2 inhibitors the purpose of which was to identify protective agents against cisplatin cytotoxicity[101]. AT7519 and AZD5438 have similar inhibitory targets (GSK3/CDKs) as kenpaullone and its derivatives alsterpaullone and 1-azakenapaullone. The paullones are highly effective at protecting podocytes by preventing apoptosis following activation of GSK3 and p38 mitogen-activated protein kinase pathways[102].

Summary and overall aims

The removal of mitochondrial from the cell can occur by mitophagy and this important quality control pathway is dependent on signalling via Parkin and PINK1. In response to mitochondrial membrane depolarisation parkin is recruited to mitochondria in a PINK1 dependent manner and this initiates the processes governing mitophagy and mitochondria quality control. My research group previously used a high-content assay of parkin recruitment to identify siRNAs and small molecules that modulate mitochondrial function. A screen of 7500 siRNAs identified genes that positively and negatively regulated parkin recruitment and a screen of a neuroactive compound library identified Kenpaullone (an inhibitor of GSK3 α/β and CDKs) as the most significant non-toxic hit/modulator of parkin recruitment. Kenpaullone was also found to augment the mitochondrial network and reverse the CCCP-induced perinuclear clustering and fragmentation of mitochondria, maintaining a healthy network throughout the cytoplasm. Additionally, kenpaullone was shown to reverse the loss of mitochondrial membrane potential (Ψ_m) caused by treatment of cells with the complex I inhibitor MPP⁺. These observations suggest that drugs that target GSK3 α/β and CDKs and/or mediate an effect on mitochondrial quality control pathways may have potential as therapies for Parkinson's disease.

The overall aim of the experiments described in this thesis was to identify

compounds that could be used to treat Parkinson's disease. To achieve this drugs that act in a similar manner to kenpaullone were identified and their efficacy in screens of mitochondrial function was assessed. The drug with the most promising actions was then assessed further, and its neuroprotective effects and mechanism of action were assessed in cell lines, rodent primary neurons and human neurons derived from induced pluripotent stem cells.

Chapter2 Material and Methods

Evaluation of potential genes by former screen and literature

Firstly, genes of interest were picked as the results got from the 3 steps previous screen. The first step was to carry out a huge siRNA library screen of 7500 genes. The next step was to choose the top hits of 300 genes to a more detailed screen. The third step was to pick further 58 genes based on a statistic combination of primary and secondary results to investigate. Thus, the genes of interest in this project were obtained.

Separately, based on the primary screen, effect values (SSMD.new) were considered to evaluate the genes. It is suggested that the gene that may greatly impact the PINK1/PRKN pathway should be located close to PINK1 in the effect value list as they may have similar downstream effects in the mitophagy pathway as PINK1 does. In contrast, those locate the opposite direction to PINK1 may have the opposite effect, which is also interesting to investigate. An additional literature search was carried out to evaluate those genes' function, based on the criteria that the genes have general links to mitochondrial function or neurodegeneration.

Human cell lines and culture

Human neuroglioma H4 cell line and human neuroblastoma SY5H-5Y cells are

used to test chosen genes' function. Both cell lines were stably expressing PRKN with eGFP tag and were previously made by lab members. They were made by cloning eGFP-PRKN into a lentiviral backbone which was then made into viral to transduce target cells. A further sorting process was then applied to get the cells consistent expressing eGFP-PRKN. Both cell lines were maintained in the incubator with 5% CO₂ at 37 °C. eGFP-PRKN H4 cells were maintained in DMEM (Sigma) supplemented with 10% FBS, 1% L-Glutamine (Sigma) and 1% Penicillin Streptomycin (Sigma). eGFP-PRKN SYSH-5Y cells were maintained in DMEMF₁₂ (Sigma) supplemented with 10% FBS, 1% L-Glutamine (Sigma) and 1% Penicillin Streptomycin (Sigma). The passages of both cell lines were conducted twice a week to keep them in a good population. The cells were disposed of when they became high passage with ageing-related morphology. The passage was done by firstly disassociating the cells with 0.5% trypsin-EDTA and splitting with a ratio of 1:8. The cell counting was carried out usually when passage and seed of the cells through a standard haemocytometer under a microscope.

E18 rat primary neuronal culture

Plates/coverlips were prepared with coating by 0.1 mg/mL Poly-D-Lysin (Gibco™, A3890401) at first. The mother rat was killed by an inhalation anaesthetic (isoflurane) overdose and sterilised with 70% Ethanol. The foetuses were taken, and their brains were dissected to collect cortex region tissue fast on

ice-cold HBSS in dishes. Trituration of the tissue was performed using 1X Trypsin-EDTA (Sigma, T417) at 37 °C for 30 mins, then pipetting it to the cell suspension. The desired density of cells was then determined and seeded, and the cells were growing in plates. Media was changed every four days until day 14 or when the cells were in the desired confluence without apparent stress conditions.

Experimental treatments were started then.

		Stock Concentration	Final concentration	Volume to add for 50mL
Neurobasal	Gibco 21103-049	-	-	49 mL
B27	Gibco 17504-044	50x	1x	1 mL
Pen / Strep	Sigma P-4458	5 mg/mL	25 mg/mL	250 mL
L- Glutamine	Sigma G7513	200 mM	500 mM	125 mL

Table 2-1 Media composition for feeding primary cortical neuronal culture.

Human iPSC culture

The normal SNCA2 (NAS2) human induced pluripotent stem cells (hiPSC) line was a gift from Dr Tilo Kunath, the Centre for Regenerative Medicine, University of Edinburgh. Following the guideline from the recently published protocols by Stathkos [103], the NAS2 lines were maintained and passaged as required to keep their morphology and population to meet the requirement before the differentiation

attempt. Researchers suggested that the quality of iPSC used could affect the successful differentiation rate, so it is important that the cell has been monitored carefully before the next step can be started [103]. There are two main factors to be considered the most critical objects to monitoring the iPSC culture. One is cell morphology, and the other is cell proliferation [104]. For the cell morphology, it is important to check under a microscope for these characteristics, including a high ratio of nucleus/cytoplasm, scant cytoplasm, prominent nucleoli, and compact colonies with smooth edges [105]. For the other factor, cell proliferation, it is suggested to keep a close monitor and allow space for their fast-dividing activity, which supports pluripotency [106]. According to the research on cell cycles in hESCs, it is highly suggested that a change of pace in proliferation is associated with spontaneous differentiation, which damages stem cell renewability [107].

Given the reasons explained above, the hiPSCs were carefully grown as below. To grow, cells were seeded onto Vitronectin-coated plates containing complete Essential 8 (E8) feeder-free media at a density of 5×10^4 cells/cm² and incubated in a humidified cell cultural incubator 37°C with 5% CO₂. Premade complete E8 media was pre-warmed in room temperature 2h before being carefully changed with the one feeding the cells daily, with about ten percent of media left in the well between taking out the old and adding the new one.

Passage of cells was needed when either the cells population reached about 75% confluency or when cells were seeded on to plate for 4-5 days or a small amount

of spontaneous differentiation had been spotted. For dissociation, 0.5 mM EDTA solution was applied for 3-5 minutes at 37°C while the cells' morphology was under carefully evaluated to decide when to stop.

Differentiation of hiPSCs into midbrain dopaminergic neurons

NAS2 hiPSCs derived midbrain dopaminergic neural culture were differentiated and maintained mainly following Stathakos' protocol as it optimised the culture for monolayer imaging study [103].

Healthy and functioning NAS2 hiPSCs were used for mDAN differentiation by first exchanging complete E8 media with neuron differentiation media 1 (NDM1). NDM1 contained N2B27 supplemented with neural fate-inducing factors (100 nM LDN193189 and 10 μ M SB431542) and patterning factors (400 ng/mL SHH C24II and 1.0 μ M CHIR99021). On day 9, media was completely exchanged with N2B27 without any other factors. At day 11, media was replaced by neuron differentiation media 2 (NDM2), which was N2B27 supplemented with neurotrophic factors (20 ng/mL BDNF, 20 ng/mL GDNF) and 0.2 mM ascorbic acid. After day 16, cells were passaged and plated onto Polyornithine/Laminin coated coverslips or plates as required. Cells were maintained and matured with neuron feeding media (NFM), incubator-stored at 20% O₂, 5% CO₂, 37 °C. NFM contained NDM2 plus 500 μ M db-cAMP and 10 μ M DAPT. Frequently later

passages were avoided to keep healthy culture growing. Throughout the process, from day 1 to day 16, cells were passaged four times, on day 3, day 7, day 12 and day 16 in a 1:2-3 ratio according to the confluency by dissociating with Accutase to ensure single-cell suspensions. A summary of the whole process is shown in **Figure 2-1**. After each passage, 10 μ M ROCK inhibitor (Y-27632) was used in the media to enhance the survival of cells, while every media exchanged contained no further Y-27632. N2B27, NDM1, NDM2 and NFM composition are shown in

Table 2-2.

Medium	Composition				
N2B27	48% DMEM/F-12	48% Neurobasal	1% Glutamax	1% NEAA	1% PenStrep
	0.5% N2	1% B27	5 μ g/mL Insulin	75 μ M β -mercaptoethanol	
NDM1	N2B27	100 nM LDN193189	10 μ M SB431542	400 ng/mL LSH	1.0 μ M CHIR99021
NDM2	N2B27	20 ng/mL BDNF	10 ng/mL GDNF	0.2mM Ascorbic Acid	
NFM	NDM2	500 μ M db-cAMP	10 μ M DAPT		

Table 2-2 The list of media in use for mDANs differentiation and their composition

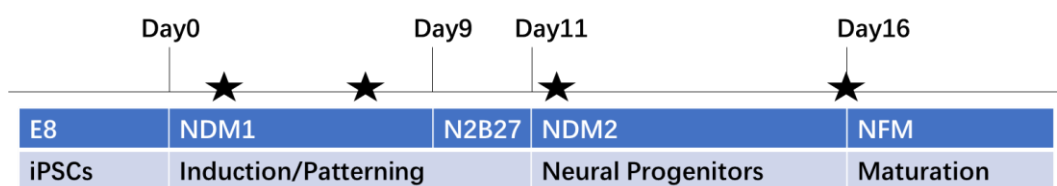


Figure 2-1 Differentiating hiPSCs into mDANs and their fate follows this simple media change schedule.

Neutralisation begins at day 0 using NDM1. Media is exchanged to N2B27 only on day9. At day11, NDM2 is used to replace old media to maintain neural progenitor. From day 16 on, NFM is used to keep neurons growing and reach maturation. Stars indicate the critical passage days, which are days 3, 7,12 and 16.

Compound test

The compound (**Table 2-3**) was purchased and dissolved in DMSO as stock. The working concentration of 0.1µM-50µM was then diluted in corresponding media before operating the treatment. The desired pre-treatment duration was optimised, and then the following assay was performed as designed. The same value DMSO that compound contained was used as vehicle control across the experiments; when there were muti doses, the value DMSO control used was same as the highest dose of compound contained.

Compound Name	Cas No.	Product No.
AT7519	902135-91-5	A5719-APE
TRO (Olesoxime)	19622 22033-87-0	Bio-Techne- 2906
AZD5438 5438	602306-29-6	Bio-Techne- 3968

Dexpramipexole	104632-27-1	Sigma-SML0392
1-Azakenpaullone	676596-65-9	Sigma-A3734
Alsterpaullone	237430-03-4	Sigma-A4847
Kenpaullone	142273-20-9	Sigma-K3888
Cu-ASTM	68341-09-3	Sigma-SML0769

Table 2-3 Compound list

siRNA transfection

siRNA transfection was carried out in 96-well plates for imaging assay and 12-well plates for expression tests. Transfection was performed after cells were seeded for 24h. Lipofectamine RNAiMAX reagent (Fisher) and siRNAs were diluted in Opti-MED media (Fisher) separately, mixed together with a 1:1 ratio, and 5 mins incubation at room temperature waited. The siRNA-lipid complex was added to cells and left overnight before replacing it with normal cell cultural media. The visualisation or extraction was then performed 48 hours after transfection.

	96-well	12-well
Final siRNA per well	1 pmol	10 pmol
Final Lipofectamine RNAiMAX per well	0.3 μ L	3 μ L

Table 2-4 Final siRNA and RNAiMAX concentration and value, respectively, per well for 96-well plate and 12 well plate.

Parkin recruitment assay

Cells were seeded into 96-well black bottom tissue culture plates (Corning, 3904) at an optimised density with 100ul media. After 24h of settling down, the treatment (compound, siRNA) can be loaded for the desired duration. Optimised duration and dose of CCCP treatment were then used before the cells were taken to be fixed with 4% PFA for 10min at 37 °C and stained with 0.05mg/ml Hoechst at RT for 30 min. The plates were then covered with 100 µl PBS per well and protected from light with foil warped and stored at 4 °C or taken to be imaged immediately. DMSO was used as vehicle control. Cell type-specific optimised Parkin recruitment protocol was used to analyse the desired parameters.

Mitochondrial network assay

MitoTracker™ Red CMXRos (Invitrogen™, M7512) was used for mitochondrial visualisation following the user guide supplied by Invitrogen. Briefly, 1:10000 dilution for a working concentration of 100nM in cultural media from premade 1mM stock was applied on live cells for 30 mins at 37°C in an incubator before washing off. For CCCP used assays, a mitotracker was applied before CCCP treatment. Live cells can then be incubated with Hoechst and taken images directly or be fixed with 4% PFA and then stained with Hoechst. Cells can be stored at 4 °C with warped by foil or taken to be imaged. Cell type-specific optimised

mitochondrial network protocol was used to analyse the desired parameters. Total mitochondrial area per cell and mitochondrial elongation factor were chosen to be presented as they best reflect the information on the mitochondrial network, the population content, and morphology. Notably, data collected from mitochondrial segmentation in neuron studies were based on total mitochondrial data in the fields detected rather than it within single cell body in cell lines studies

Mitochondrial membrane potential assays

Tetramethylrhodamine (TMRM) (Invitrogen™, I34361) with 1:1000 dilution was used in live cells after designed experiment processes for 30min at 37°C before being imaged. Approximate fluorescence excitation and emission: 548/574 nm.

JC-1 Dye (Invitrogen™, T3168) was made into 5mg/ml stock solutions in DMSO and used 1:1000 dilution in cell culture media. 15min incubation time was required. Approximate fluorescence excitation and emission for J-aggregate alone:535/ 590 nm

Mitochondrial ROS assay

MitoSOX™ Red reagent (Invitrogen™, M36008) was used to detect superoxide in mitochondria of live cells following a manual supplied by Invitrogen. Briefly,

after the designed experiment performed, 1:1000 dilution for 5 μ M working solution in PBS from premade 5mM stock was used in live cells for 15min at 37°C in an incubator, before taking to image lively.

Immunofluorescence staining

Conventional immunostaining was used to observe the cells' specific gene expression level alterations, followed by the experimental treatment. Generally, plated cells at the desired stage or after treatment were fixed and permeabilised with ice-cold methanol in a freezer for 20 mins and simultaneously blocked with 10% normal goat serum (NGS) and 1% bovine serum albumin (BSA) for 1 hour at room temperature (RT). After blocking, cells were covered with the primary antibodies diluted in 10% NGS with 1% BSA PBS solution at 4°C overnight. The cells were washed three times with PBS at RT, and then the matched secondary antibodies diluted in 10% NGS and 1% BSA PBS solution were applied for 1 hour at RT, covered to avoid light exposure. After secondary antibodies incubation, samples were washed carefully and gently with PBS three times. Each time, samples were immersed within PBS for 10mins, avoiding direct light. After all the above procedures, Hoechst was used to stain nuclei with a dilution of 1:200 for 30mins and then replaced by PBS. For coverslips, they were mounted onto a microscope slide (mowiol mount optional), and stored at 4°C until taken to be imaged. For plates, they were covered with PBS and store 4°C until taken to be

imaged.

Quantification analysis methods were chosen depending on where the samples were attached to 1) INCell Workstation software was applied for the samples from the 96-well plate used for INCell imaging. 2) Fiji, ImageJ, was applied when the samples were on coverslips and imaged by Leitz DMRD fluorescent microscope and the Leica Application Suite 3.3.1.

High content imaging and analysis

The images of 96-well plates were captured using the INCell Analyzer 2200 with high speed and autofocus fluorescent imaging advantages. The 10X objective lens was used for ROS assay or cell population test in neurons, 20X objective lens was used for Parkin recruitment assay while the 40X was used to image mitochondrial network or protein staining change in neurons. 4 randomly positioned fields (avoided edges) of view were used for 20X and 10X, while 2 for 40X objective lens. The analysis was conducted within the corresponding software named INCell Analyzer workstation. Protocols of the software were edited and optimised separately for segmenting Parkin puncta, mitochondria and other objectives in different types of cells following the images taken by the set channel settings (**Table 2-5**). Notably, data collected and presented in neuron studies using INCell Analyzer reflect the data collected in fields detected rather than in single cell, showing as (total) neuronal population and (total) neurites length. The data

acquired by the Analyser was then taken for combination and arrangement using excel and prism to calculate the mean and SEM and output the statistically analysed final data by bar graphs.

Objective	Fluorophore	Channel name	Excitation filter	Emission filter
Nuclei	Blue	DAPI	390/18	432.5/48
eGFP-Cell, Parkin, Neuron	Green	FITC1	475/28	511.5/23
Cellular components (Mitochondria, Protein, ROS)	Red	Cy3	542/27	597/45

Table 2-5 List of main channels used for INCell imaging.

Seahorse experiment

Oxygen consumption rate (OCR) and extracellular acidification rate (ECAR) in live cells were measured using a Seahorse XFp analyser (Agilent). The machine works by conducting measurements of OCR and ECAR by isolating an extremely small volume of the medium above of cells with its sensor. Briefly, the sensor probes residing 200 um above the cell monolayer detect the rapid and measurable changes to the concentrations of dissolved oxygen and free protons resulting from the activities of cellular oxygen consumption and proton excretion. Cells were seeded into Seahorse XFp microplates at an optimised density (40% of which in the 96-well plate). 24 hours later, cells were washed and kept with prepared

Seahorse XF Cell Energy Phenotype Assay Media with a final well volume of 180 μL and incubated without CO_2 for 1 hour at 37°C . FCCP titration assay was performed following Agilent's FCCP Titration protocol to determine the optimised chemical concentration for Mito Stress Test use.

The performance of mitochondria affected by the compound tested in live cells was carried out using the Seahorse XFp Cell Mito Stress Test kit (Agilent). Cells were washed and kept with prepared assay media and incubated without CO_2 for 45 mins at 37°C . The standard Cell Mito Stress Test protocol (**Figure 2-2**) was performed without further modification to allow OCR and ECAR detection and calculation after chemical injection. Data were normalised to protein level or cell count. The formula calculated key metabolic parameters from OCR and ECAR data are shown in **Figure 2-3**.

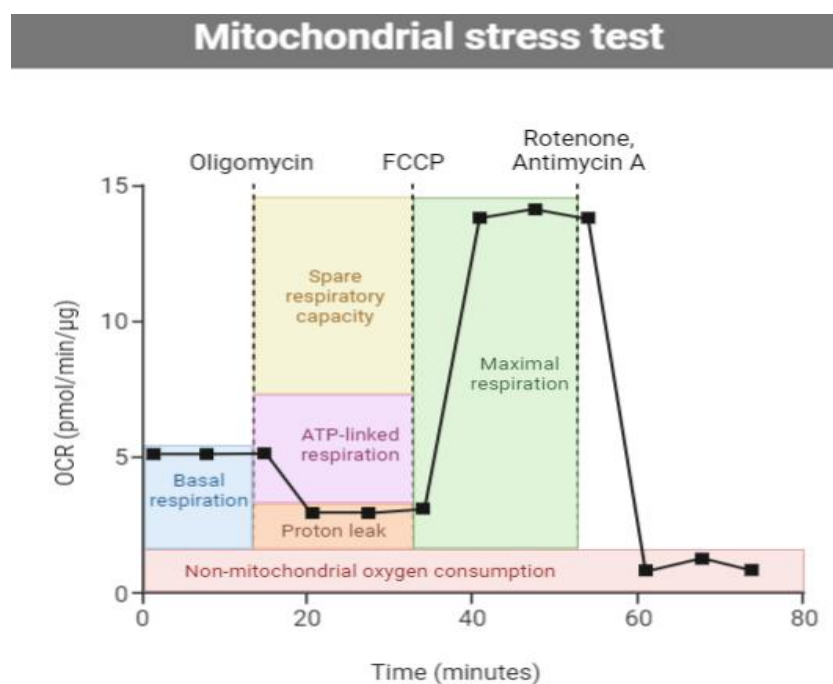


Figure 2-2 Process of mitochondria stress test

	Parameter	Formula
OCR	Basal Respiration	(Last rate measurement before first injection) – (Non-mitochondrial respiration rate)
	Maximal Respiration	(Maximum rate measurement after FCCP injection) – (Non-mitochondrial respiration)
	ATP Production	(Last rate measurement before oligomycin injection) – (Minimum rate measurement after oligomycin injection)
	Non-Mito Oxygen Consumption	Minimum rate measurement after ROT/AA injection
ECAR	Respiratory Reserve	Maximal Respiration- Basal Respiration
	Basal Glycolysis	Last rate measurement before first injection
	Maximal Glycolysis	Maximum rate measurement after FCCP injection
	Extra Glycolysis	(Maximum rate measurement after ROT/AA injection) – Maximal Glycolysis
	Glycolytic Reserve	Maximal Glycolysis– Basal Glycolysis

Figure 2-3 Parameters and formula for Seahorse experiment

MTT Cell Viability Assay

Cell viability was measured by MTT assay. MTT powder was purchased from Sigma(M2128). Before experiments, MTT solution was premade to the stock concentration of 5mg/mL in PBS, filtered and kept at -20°C before use. In each experiment, 10 µl media was taken out of the wells to test in a 96-well plate and replaced by 10 µl MTT stock solution to reach a working concentration of 0.5mg/mL. Plates were then incubated for 2 hours at 37°C in an incubator before all the liquid was carefully removed and replaced by 100µl freshly made solvent (Isopropanol: ethanol: DMSO: = 2:4:1). 10 mins of gentle rocking at RT were

required to dissolve the MTT formazan, after which the absorbance value was read at OD=570 nm by the plate reader immediately. The actual value was corrected by deducting the value of wells without cells as the background.

DNA extraction and purification from cells

DNA was extracted from cells and purified using a Wizard Genomic DNA Purification Kit (Promega), following the standard protocol for Tissue Culture Cells. A combination of wells was performed when a high concentration of DNA was needed. Measurement of DNA concentration was done by a nano-drop spectrophotometer (ThermoFisher Scientific). Samples were used immediately or stored at -20°C until use.

RNA extraction and cDNA generation

RNA was extracted from the cell after the protein lysates were carefully prepared. ReliaPrep RNA cell miniprep kit (Promega) was used following the manufacturer's instructions. RNA concentration was measured by nano-drop, used immediately or stored at -80°C

The cDNA was generated with the GoScript Reverse Transcription System kit (Promega) using random or Oligo(dT) primers for reverse transcription. cDNA was used immediately or stored at -20°C.

Quantitative PCR (qPCR)

A qPCR was carried out using a StepOnePlus™ Real-Time PCR system (ThermoFisher Scientific) using modified 2-hour PCR protocols according to each primer's requirement. A mastermix was made with Power SYBR Green (ThermoFisher Scientific) following the standard recipe and the required pairs of primers were added into the plate for the qPCR process. Primers used for qPCR are listed below.

Target	Forward primer sequence	Reverse primer sequence
UBE2E1	TCCGTGTATGAGGGTGG TGTA	CGAAATGTAACCTTTG GAGGCTT
UBE2J2	GGACTTCACGAAAAGA CAACTGG	TCCTCCACGACTTCAG GAAATAA
UBE2L6	TGGACGAGAACGGACA GATTT	GGCTCCCTGATATTCGG TCTATT
UBE2N	CCAGAAGAATACCCAAT GGCAG	GCTGGGGACCACTTAT CTTTCA
UBR5	ACCATGACGTCCATCCA TTT	ATTTGGTCCCACCCACAC ACT
GBP2	AAAGCAGTGCAGCCAA ACTC	CACCAGCTGCCCTTTA GTGT
HECDT2	GCTGTTAGCCCGAAGAA AGA	CAGTTTTGGGCTGGATA GGA
RNA- Leu(UU R)	CAC CCA AGA ACA GGG TTT GT	TGG CCA TGG GTA TGT TGT TA
B2- microglo bulin	TGCTGTCTCCATGTTTG ATGTATC T	TCTCTGCTCCCACCTCT AAGT

Table 2-6 Genes and primers sequence for detection in qPCR.

Protein extraction, purification, and quantification

Cell lysis buffer (typically RIPA buffer) was added to lyse the cells on ice, and then protein supernatant was taken out into tubes after centrifuging. The protein concentration was calculated by standard BSA assay following protocol using Pierce BCA protein assay kit (Thermo Scientific) and the protein could be used immediately or stored at -80°C.

Western blotting

20µg of protein per sample was added 1:1 to 2x SDS sample buffer and heat-denatured at 95°C for 5 minutes. Samples were loaded onto a pre-cast linear gradient gel (Bio-rad 161-1123EDU), and electrophoresis at 100V for 20 min and 150V for the rest of the time required was carried out in a running buffer. Proteins were then transferred onto a PVDF membrane (Bio-rad 1704156EDU) using a Trans-Blot Turbo transfer system (Bio-Rad). After transfer, membranes were blocked in 5% milk powder in PBS (w/v) for 1 hour at RT and then probed with primary antibody diluted in 1% milk powder in PBS overnight at 4°C. After thoroughly washed with PBS-T, the proteins were incubated with the species-paired secondary antibody (peroxidase-linked anti-rabbit IgG (NA934, GE Healthcare) or anti-mouse IgG (NA931, GE Healthcare)) diluted in 1% skimmed

milk powder for 1 hour at RT. After washed with PBS-T, enhanced chemiluminescence (ECL) reagent was used to visualise the antibody-bound protein and G:Box F3 (Syngene) was used to image the light signal for the protein bands.

Gene cloning

pcDNA3.0--HA-UbcH13 was purchased from Addgene (plasmid # 12461). Miniprep kit (Promega) was used to extract and purify DNA, and sequencing was conducted through Source Bioscience. PCR primers with extra restriction digestion sites were designed to allow the insert to be cloned into pRRL backbone. PCR amplification reaction was done using KAPA HiFi Taq Polymerase. The sample then ran in 1% agarose gel, and the right band was cut and purified using a gel purification kit. The DNA eluted was taken to restriction digestion with enzyme Sall and XbaI. The same digestion was carried out for the pRRL.CMV.EGPF.WPRE plasmid in the meantime. Gel running and purification steps were performed before the qualified insert and backbone were taken to dephosphorylation and ligation using the rAPid dephosphorylation kit (Roche). Different ligation reactions were set up with molar ratios, for instance, 1:1, 3:1 and 5:1 of the insert to the backbone. The DH5 α cells were used as competent cells, put on ice, gently mixed with 5 μ l ligation product, left on ice for 5 minutes before 30 seconds of heat shock and put back on the ice for 2 minutes. Then 200 μ l LB

was added, and the cells were put into an incubator for 1 hour. The product was then spread at proper volume (20uL or 200uL) onto LB ampicillin plates, and the plates were incubated at 37°C overnight. 8 colonies in every plate were picked into LB ampicillin and incubated with shaking overnight. The miniprep and restriction digestion check were conducted the next day, and positive ones were sent for sequencing. Once the sequencing was confirmed, a maxiprep using GeneJET Plasmid Maxiprep Kit (Thermo Scientific™, K0491) was carried out to harvest a higher concentration of cloned DNA.

HEK293T cell culture and lentiviral production

HEK293T cells were maintained in DMEM supplemented with 10% FBS, 1% Glutamax and 1% Non-Essential Amino Acids (NEAA) (Gibco) in a standard 5% CO₂ incubator at 37°C.

On day 1, cells in low passages (< p25) were seeded onto 15cm² dishes for lentiviral production. On day 2, co-transfection of lentiviral backbone plasmid DNA, Gag/Pol plasmid DNA, Rev plasmid DNA and VSVG were mixed and added with 2M CaCl₂ and H₂O as listed in Table 2-7. HEPES-buffered saline (HBS) was added in dropwise and mixed whilst bubbling. The mixture was added to HEK293T cells when was shown cloudy in RT for 30mins and incubated overnight at a standard incubator. On day 3, the media was changed in the morning, and the first harvest was done in the afternoon. On day 4, media was further

collected, centrifuged, sterilise-filtered and centrifuged overnight at 4°C. On day 5, the viral pellet was carefully washed with cold PBS and ultracentrifuged at 20,000rpm for 90 mins at 4°C (Beckman ultracentrifuge, SW40 rotor). The supernatant was carefully poured off, and the pellet was covered with 100µl TSSM buffer for 2h on ice. Last, 192µL (2000 fold concentrate of harvested media) total volume was made up, the virus was aliquot and stored at -80°C.

The titre of the GFP expressing lentivirus was measured using flow cytometry cell sorting using the equation:

$$\text{Transducing units/ ml} = (\text{total cell count} * \% \text{GFP positive}) / \text{dilution}$$

The titre of the non-GFP expressing lentivirus was measured by a Taqman (ThermoFisher) qPCR-based approach following protocol.

Mixture	Recipe
Media	DMEM containing: FBS 10%, Pen/Strep (50U/50ug / mL), L-Glutamine (2mM), 1X MEM-Non essential amino acids (Sigma M7145)
TSSM buffer	20mM Tromethamine, 100mM NaCl, 10mg/mL sucrose, 10mg/mL mannito
2xHBS buffer	50 mM Hepes, 280 mM NaCl, 1.5 mM Na ₂ HPO ₄
1x DNA	10µg vector DNA, 10µg pMDLg-pRRe, 2µg pRSV-Rev, 3.4µg pMD2-VSVG, 140µl CaCl ₂

Table 2-7 Recipe for media, buffer and DNA mixture in use for lentiviral production

Flow cytometry for cell viability and apoptosis

Cells after treatment was harvest using Trypsin/EDTA, washed and centrifuged. Zombie NIR™ (Biolegend) (pre-dissolved in DMSO, 1 vial into 100µL) was using in dilution of 1:500 in PBS to resuspend the cells and incubated for 15mins at 37°C. Followed by 4% PFA fixation and Hoechst staining and resuspended in 100µL in PBS for flow cytometry experiment using Flow Cytometer (Novocyte). Experiment stop condition was set at 20000 single cell detected or 80µL of sample was used. The results were further analysed from the compatible software NovoExpress. Traditional gating strategy based on forward and side scatter properties of the samples in the control (FSC and SSC) was applied to determine the cell population in each group for investigated. The square gate, 'Live', was set based on the low red intensity of the Zombie NIR™ dye staining (APC-Cy7-H) to reflect the rest population from dead cells. The quadrant gate was set to sort apoptotic cells based on extremely high intensity of the Hoescht staining (Pacific Blue-H). All the gates were set in the control and applied unchanged on the other groups.

Electrophysiology

Preparation of recording solution

1L of HEPES-buffered saline (HBS) was made containing 119 mM NaCl, 5 mM

KCl, 25 mM HEPES, 33 mM glucose, 2 mM CaCl₂, 2 mM MgCl₂, 1 μM glycine, 100 μM picrotoxin, pH 7.4 adjusted with NaOH pellets.

Preparation for microelectrodes and inner solution

Transparent glass microelectrodes were pulled by a micropipette puller P1000 (Sutter Instrument, Novato, California, USA) from the lab's protocol with resistances ranging from 6 to 8 MΩ after filling with a complete inner solution containing: 135 mM K-gluconate, 10 mM HEPES, 0.5 mM EGTA, 2 mM Mg-ATP, 0.3 mM Na-GTP, 8 mM NaCl, pH 7.2 adjusted with KOH, osmolarity 285 mOsm.

Electrophysiology recording

Conventional whole-cell patch-clamp recording was performed in Whitcomb's Electrophysiology Laboratory. In brief, hiPSC derived midbrain neurons at day 58-65 after differentiating were patched, and their membrane potentials change was recorded in response to the certain input as designed. Coverslips with neurons were treated with an experimental compound for 24h before being transferred into a recording chamber submerged in HBS, flowing at 2 ml/min. One coverslip was in recording solution for up to 30mins for the electrophysiology experiment to maintain the quality of the data collected. Cells' size, morphology, and patching

availability were evaluated by experience to reach a high success rate for the experiment. In addition to the stability, access resistance, capacitance and membrane resistance were continuously monitored during the recording. Between each experiment, the chamber was thoroughly washed with HBS.

Recordings were made using an Axon Axopatch 200 B Microelectrode Amplifier (Axon Instruments, Molecular Devices, California, USA). Resting membrane potentials were recorded once the cells entered whole-cell mode successfully with current adjusted to 0 A. The cells were then held at -60mV to maintain the depolarisation status before triggering their electrophysiological activity by current puls. Evoked action potentials were recorded in response to sequential stepwise current injections ranging from -50 pA to +400 pA (20pA per step), single voltage trace at 100pa was chosen to represent the result. Passive membrane properties were recorded and calculated as below. Membrane input resistance (R_m) was derived by dividing the steady-state membrane voltage by the injected current amplitude (-10pA). The time constant of the membrane voltage (τ_{m}) was obtained by fitting a single exponential during the first 10 ms time window of the current injection. The membrane capacitance (C_m) was calculated using the formula $C_m = \tau_{m}/R_m$ with these variables obtained.

Action potential and passive membrane properties were monitored and reanalysed using the WinLTP and Clampfit 10.7 (Molecular Devices, USA) software. Trace

graphs were redrawn by exporting trace data into GraphPad Prism 8.

Statistical analysis

Statistical analysis was carried out on experiments with a minimum of 3 biological replicates (n=3). All statistical analyses were performed and presented using GraphPad Prism software. The student's t-test (unpaired, two-tailed) was used to compare the two groups. The one-way ANOVA with the appropriate post-hoc tests was used for multiple groups with a single variable. The two-way ANOVA with the suitable post-hoc tests was used for multiple groups with two variables. In all cases, p-values of <0.05 were considered statistically significant. P-value significance levels when displayed in figures are denoted as follows: ns not significant, * p<0.05, ** p<0.01, *** p<0.001 and ****<0.0001. Further statistical details will be described for the relevant data where it is presented.

Experimental replicates and data normalisation

Biological replicates in cell-based assays were defined as individual plates of cells, which could be different passages of the same cells, prepared at different times following the same experimental protocol. In each biological replicate, a minimum of three technical replicates were set in plate-based assays as different wells of the same experimental condition.

For electrophysiology, one recording on a different cell contributes to one biological replicate.

Data normalisation to the control was conducted in most cases throughout this thesis to reach a standardised presentation to illustrate the effects of treatment compared to the control (except the control value presented with the figures are not 1 or 100). Notably, in the parkin recruitment experiments, data were normalized to the positive control (CCCP) to reflect the effectiveness of treatments in reducing parkin puncta formation.

Figures

Figures in this thesis work contain components created using Biorender.

Antibodies

Antibodies	species	Source
Anti-TH	Rabbit	Millipore, AB152
Alexa Fluor® 488 anti-TUJ1	Mouse	Biolegend,A488-435L
Anti-Cleaved-caspase3	Rabbit	Abcam,ab186734
Anti-PGC1 α	Rabbit	Invitrogen
Anti-TOMM20	Rabbit	Abcam,ab186734
Anti- α synuclein	Mouse	BDBioscience; 610787
Anti- α tublin	Mouse	Sigma,T5168
Anti- β actin	Mouse	Abcam,ab8226

Alexa Fluor® 594	Goat anti-rabbit	Abcam,ab150080
Peroxidase-linked IgG	Donkey anti-mouse	GE Healthcare, NA931
Peroxidase-linked IgG	Donkey anti-rabbit	GE Healthcare, NA934

Table 2-8 Antibodies list.

Solution concentration

All the concentration presented in this thesis with % indicates the volume ratio of solute to its solvent unless otherwise stated.

Chapter3 Evaluating kenpaullone as a regulator of Parkin recruitment and its effect on mitochondrial activities

Introduction

Cells respond to changes in their metabolic needs by directing mitochondrial processes such as biogenesis, fusion, fission, and mitophagy. Together these mitochondrial quality control processes maintain the appropriate number of mitochondria in the cell, enabling it to cope with varying metabolic demands[19]. A key point in this lifecycle is the selective clearance of damaged mitochondria by an autophagic process termed mitophagy [27]. PINK1 and PRKN encode PTEN-induced kinase one and an E3 ubiquitin ligase Parkin, respectively. These two proteins are critical initiators of the mitochondrial quality control pathway, which clears damaged mitochondria [30].

Previous research by the lab members in the regenerative medicine laboratory at the University of Bristol (Uney's group) established an *in vitro* phenotypic model that measures Parkin recruitment to mitochondria following their destabilisation [108]. EGFP-PRKN was stably overexpressed in H4 cells, and CCCP was used to trigger Parkin translocation to mitochondria to establish this assay. The formation and number of EGFP-staining Parkin puncta in response to the altered expression

of genes or due to pharmacological manipulation was then monitored using the INCell Analyser 2200. This Parkin recruitment assay was first developed using H4 neuroglioma cells as they are easily grown, efficiently transfected, and firmly attached to plates with a microscopy-friendly flat morphology. These characteristics are needed for high content and high throughput assays. Dr Helen Scott used this phenotypic assay to screen a (7500) siRNA druggable library, and Dr Nicola Buckner used it to screen a small pharmacological library of neuroactive drugs.

Following the drug screen, kenpaullone was identified as the potentially negative modulator of mitophagy, and Cu-ATSM was identified as a potentially positive modulator. There is evidence that both compounds have neuroprotective properties. Kenpaullone is a potent GSK3- α/β and multi CDKs inhibitor, and evidence suggests it may mediate neuroprotection by decreasing oxidative stress [109] [110] [111] [112]. Cu-ATSM is a copper delivery compound that improves motor neuron survival in the central nervous system[113]. The profiles of these compounds suggest they may have potential as treatments for Parkinson's disease, and this study, therefore, carried out experiments to verify these results and investigate the effect of these drugs in a second cell line, the SH-SY5Y cell line. The SH-SY5Y cell line is derived from the SK-N-SH neuroblastoma line; they can be easily expanded and express human-specific proteins and protein isoforms like H4 cells. Importantly, SHSY-5Y cells express dopaminergic neuronal markers, TH,

dopamine transporter (DAT) and dopamine receptor subtypes 2 and 3 (D2R and D3R) [1], making them an excellent line for PD-related studies. Thus, the Parkin recruitment assay was established and optimised in SH-SY5Y cells to validate the previous findings.

The primary aim of the experiments described in this chapter was to validate the previous findings implicating kenpauillone and Cu-ASTM as regulators of Parkin recruitment. To achieve this aim, Parkin recruitment assays were carried out in H4 and SH-SY5Y cells. After the drugs' effect on Parkin recruitment was confirmed, the action on mitochondrial morphology and function was also investigated.

Results

Optimisation of the Parkin recruitment assay

In the previously established assay, an H4 cell line stably expressing eGFP- Parkin was produced by Dr Helen Scott. CCCP, which disrupts the mitochondrial membrane potential, was used to induce Parkin recruitment to mitochondria. The INCell Analyser 2200 was used to measure Parkin recruitment (and other indices of mitochondrial function), and only cells having three or more Parkin puncta were recorded [108]. The first experiments carried out in this study aimed to optimise the assay. The 'Corning' 96-well plate was used to replace the 'Greiner' plate as they had a higher clarity of resolution, and the INCell Analyser, therefore, obtained higher resolution images and yielded better results. Based on this improvement, a modified protocol was set up, and it allowed a greater number of smaller Parkin puncta to be visualised and captured by the INCell. The protocol entailed calculating the total area of the Parkin puncta per cell instead of the previously used '% of cells with >3 Parkin puncta', and it had the advantage of higher accuracy and lower variation than the previous method.

Figure 3-1 A shows representative images obtained using the optimised assay of Parkin recruitment. It shows that the treatment of cells with CCCP induced the recruitment of Parkin puncta to mitochondria. **Figure 3-1 B** shows high magnification images (x40 objective lens) used for segmentation for analysis by

the INCell Analyser applied to the optimised protocol. The analysis allows cell count and total Parkin puncta area per cell to be calculated simultaneously. Treatment with CCCP mediated a significant increase in the total area of Parkin puncta per cell but did not change the cell count (indicating no cell death has occurred) (**Figure 3-1 C**).

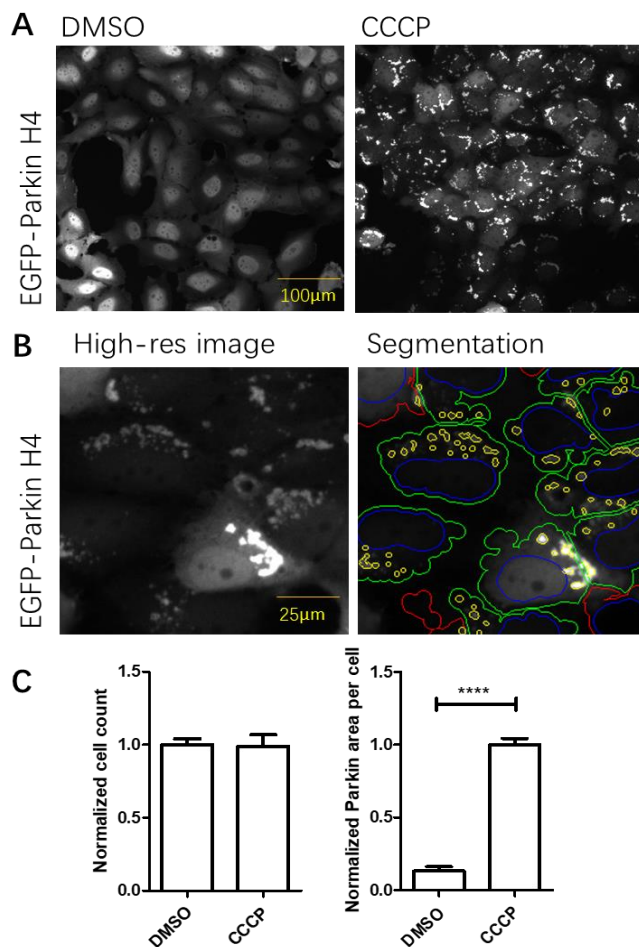


Figure 3-1 Parkin recruitment assay optimisation.

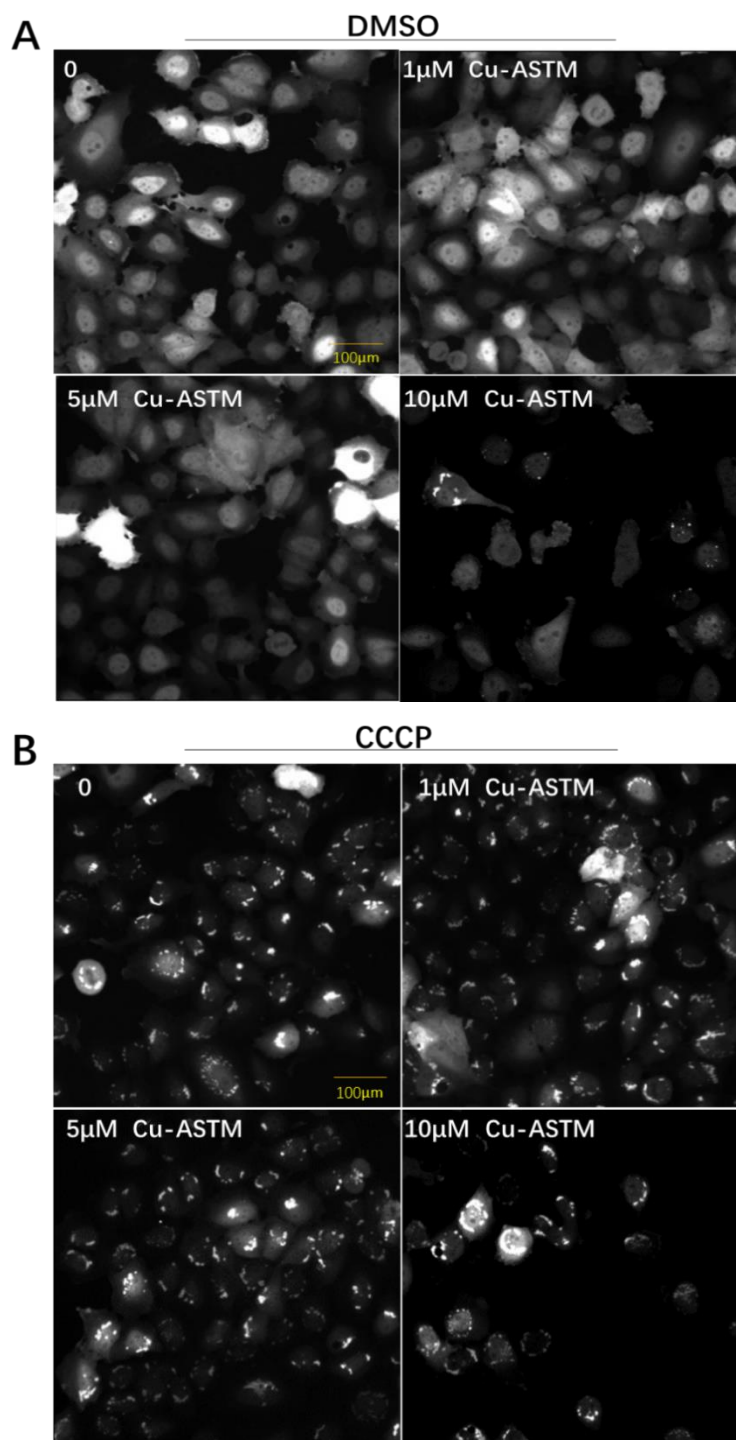
A) Images taken with the INCell 2200 show Parkin puncta formation following 10 μ M CCCP treatment for 2.5h. Only GFP channel images are shown. B) 4X zoomed-in images show details of the Parkin puncta induced by CCCP and its segmentation. C) The results were analysed using the optimised protocol from INCell Workstation, showing that treatment with CCCP significantly increased the Parkin puncta total area per cell but did not affect cell count. Statistical analysis was conducted by unpaired t-test. N=3; data is displayed as mean \pm SEM, and significance is displayed as **** p<0.0001.

Cu-ASTM potentially regulates Parkin recruitment in H4 cells

The pilot drug screen conducted by Dr Nicola Buckner suggested Cu-ASTM was a positive regulator of Parkin recruitment, but this result may have been influenced by Cu-ASTM toxicity at the selected dose of 10 μ M. This study, therefore, evaluated the effects of Cu-ASTM at a lower dose range using the optimised Parkin recruitment assay.

H4 cells were incubated with Cu-ATSM at doses of 1, 5 and 10 μ M for 24h before 2.5h 10 μ M CCCP was applied to trigger Parkin recruitment. Cells were then fixed and stained with Hoechst. Images were taken and analysed using the INCell 2200 workstation program.

The results shown in **Figure 3-2** confirmed that at a dose of 10 μ M but not lower doses, there was significant cell loss compared to the no compound control. There was a trend toward Cu-ASTM mediating an increase in Parkin puncta total area per cell (and a decrease in cell counts) though this did not reach significance. Parkin puncta formation following treatment with 10 μ M Cu-ASTM alone (but not with lower doses) can be observed in **Figure 3-2 A**. However, the unhealthy cell morphology with rough edges and collapsed cell bodies were also observed when cells were treated with 10 μ M Cu-ASTM.



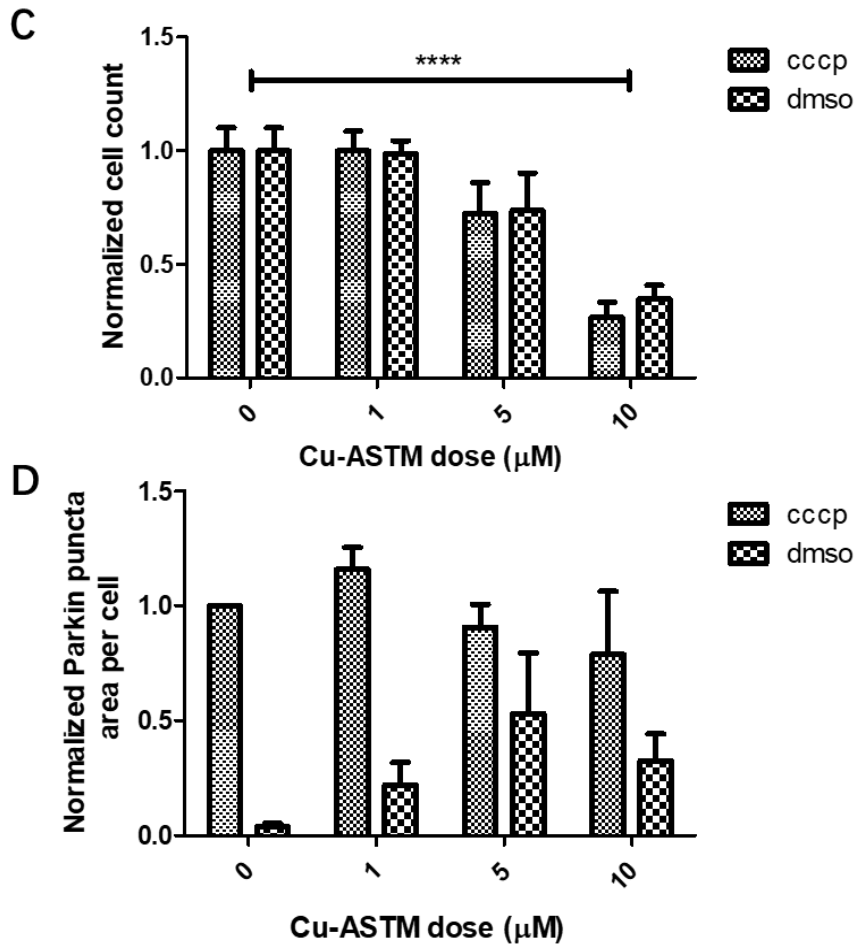


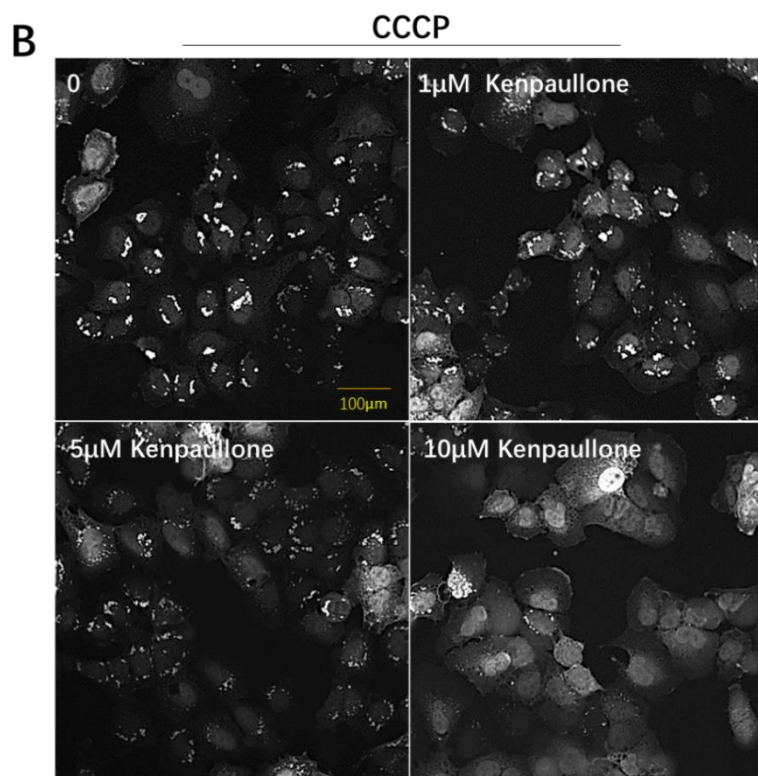
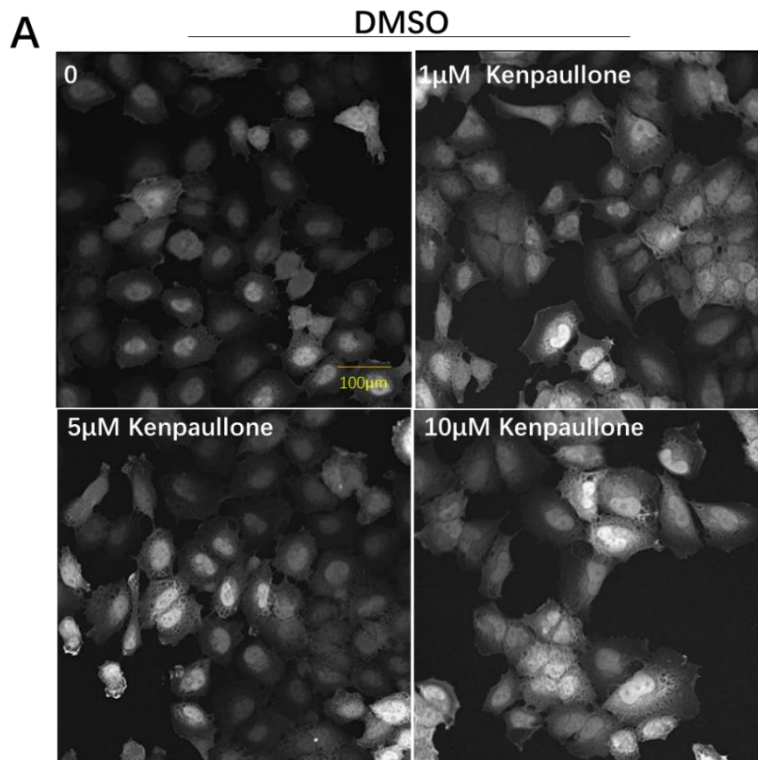
Figure 3-2 The effects of Cu-ASTM on cell viability and Parkin recruitment in eGFP-Parkin H4 cells.

A) Images taken by INCell 2200 show the cells' morphology in DMSO groups (vehicle control to CCCP) with Cu-ASTM of 0, 1, 5 and 10 μM . Only GFP channel images were shown. B) Images show the cells' morphology and Parkin puncta formation in CCCP groups with compound doses of 0, 1, 5 and 10 μM . Cell amount was less with 10 μM Cu-ASTM compared to no compound control in both A and B. C) Bar graph shows analysis results of cell viability by cell count. 10 μM compound significantly decreased the cell count in both DMSO and CCCP groups. D) Bar graph shows Parkin recruitment activity analysis results by Parkin puncta area per cell. There was no evident change with CCCP groups, while an increasing trend appeared in DMSO groups with the compound dose increased. Statistical analysis was carried out by two-way ANOVA test with Tukey's multiple comparisons test. N=3; data is displayed as mean \pm SEM, and significance is displayed as **** $p < 0.0001$.

Kenpaullone is a negative regulator of Parkin recruitment in H4 cells

The drug screen conducted by Dr Nicola Buckner suggested that kenpaullone was a negative regulator of Parkin recruitment as it decreased Parkin puncta formation significantly following the CCCP challenge. Kenpaullone is GSK3(α and β) and multi CDKs inhibitor. Evidence suggests that kenpaullone may mediate cell protection by lowering oxidative stress [114], and it was identified as a promising candidate therapeutic for ALS [111]. However, no previous studies have linked kenpaullone to modulating mitochondrial activity. Hence, this study investigated the link between kenpaullone, mitochondria and cell protection. In this study, the dose-response of kenpaullone in eGFP-Parkin H4 cells was studied, and its effect on Parkin recruitment was assessed following the compound treatment protocol and Parkin recruitment assay for H4 cells.

The results in **Figure 3-3** show that kenpaullone significantly reduced the cell viability and Parkin recruitment of H4 cells at a high dose (10 μ m). However, at a lower dose of 5 μ M that did not affect cell viability, there was a significant reduction in Parkin recruitment. In addition, no dramatic cell morphology change was observed between cells treated with kenpaullone (even at the dose of 10 μ m) and vehicle control, indicating kenpaullone was not toxic.



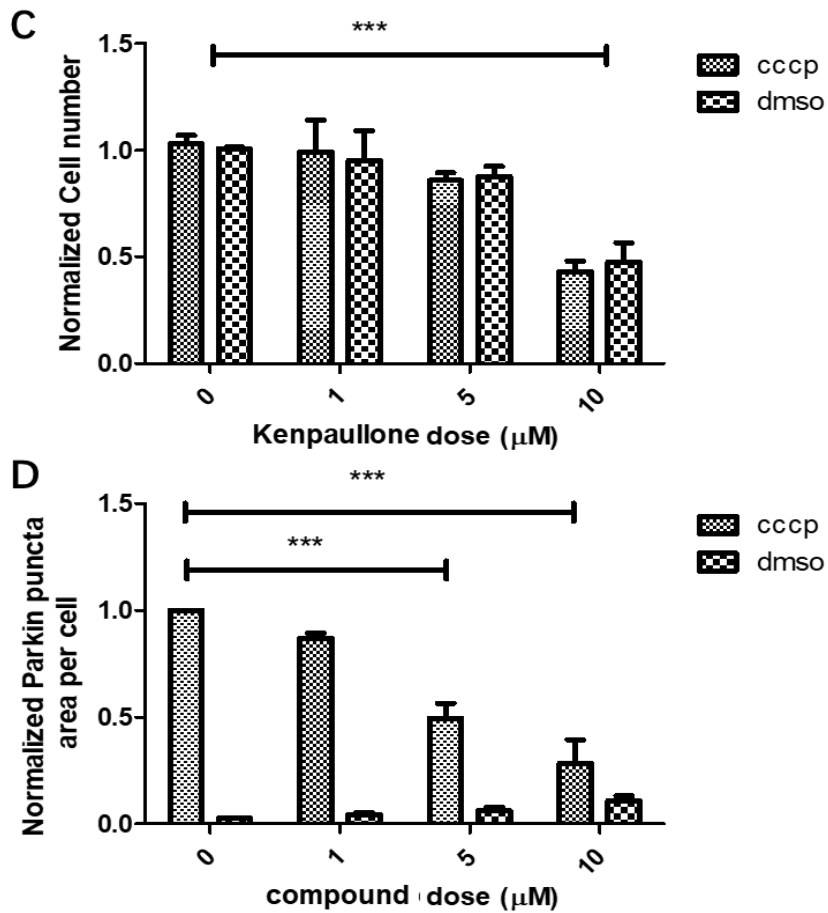


Figure 3-3 The effects of kenpaullone on cell viability and Parkin recruitment in eGFP-Parkin H4 cells.

A) Images taken by the INCell 2200 show the cells' morphology in DMSO groups (vehicle control to CCCP) and with kenpaullone 0, 1, 5 and 10 μ M. Only GFP channel images were shown. B) Images show the cells' morphology and Parkin puncta formation in CCCP groups with compound doses of 0, 1, 5 and 10 μ M. Parkin puncta formation was inhibited by 5 μ M kenpaullone compared to no compound control. C) Bar graph shows analysis results of cell viability by cell count. 5 μ M kenpaullone did not alter the cell count in the DMSO or CCCP groups. D) Bar graph shows the results of Parkin recruitment activity by Parkin puncta area per cell. In CCCP groups, 5 μ M ($p=0.0005$) and 10 μ M ($p=0.0004$) kenpaullone significantly decreased the Parkin puncta area per cell compared to 0 compound control. Statistical analysis was carried out by two-way ANOVA test with Tukey's multiple comparisons test. $N=3$; data is displayed as mean \pm SEM, and significance is displayed as *** $p<0.001$.

Parkin recruitment assay established in SH-SY5Y cells

SHSY-5Y cells stably expressing eGFP-Parkin were also used to conduct parkin recruitment assays and confirm that the results were not specific to the H4 neuroglioma cell line. SHSY-5Y cells stably expressing eGFP-Parkin were created by Dr Fella Hammachi. The establishment and optimisation of the Parkin recruitment assay in SHSY-5Y cells were performed in this study. Unlike H4 cells, SH-SY5Y cells are semi-adherent [115], and this may result in them being more easily washed off during the compound treatment and assay processes where media changing and washing between steps are required. This cell loss can potentially interfere with the interpretation of the tested compound's effect on cell viability. Thus, Poly-D-Lysine (PDL) pre-coated plates were used to enhance the attachment of SHSY-5Y cells to the plate.

EGFP-Parkin SHSY-5Y cells were treated with CCCP at doses of 10 μ M and 15 μ M for 2h, 4h and 6h, respectively. DMSO was used as vehicle control for CCCP. **Figure 3-4** showed that both 10 μ M and 15 μ M CCCP triggered significant Parkin recruitment activity in SHSY-5Y cells from 4h treatment onwards and compared to the DMSO control. The 4h incubation with 15 μ M CCCP treatment was chosen as the default setting as this mediated maximal Parkin recruitment in SHSY-5Y cells and was highly reproducible.

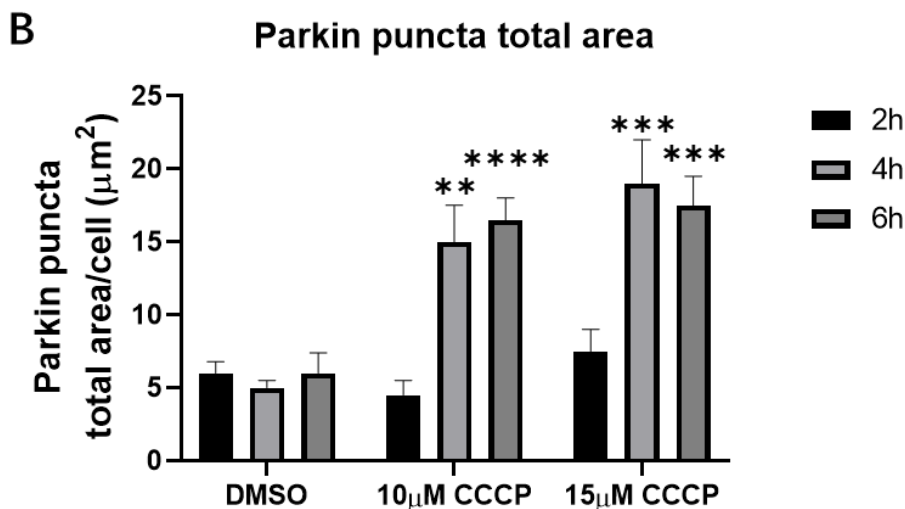
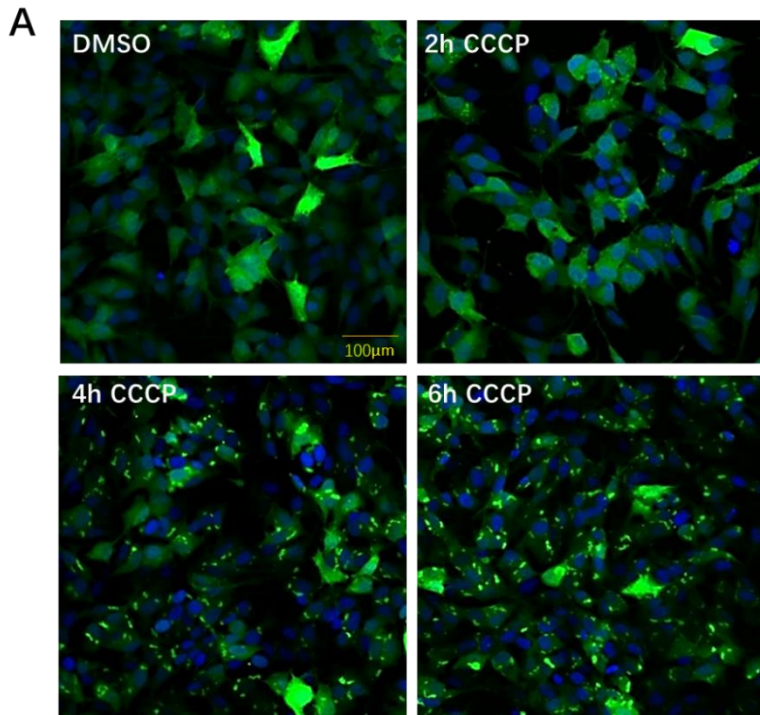


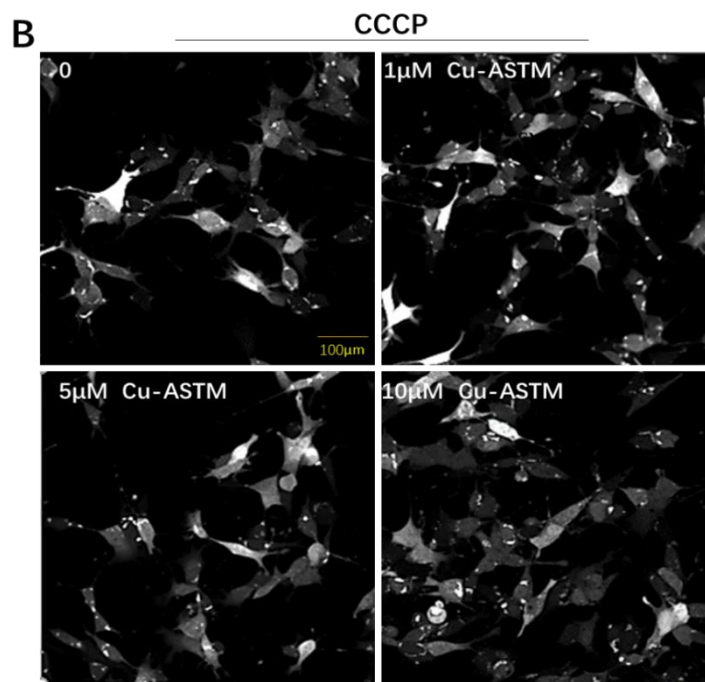
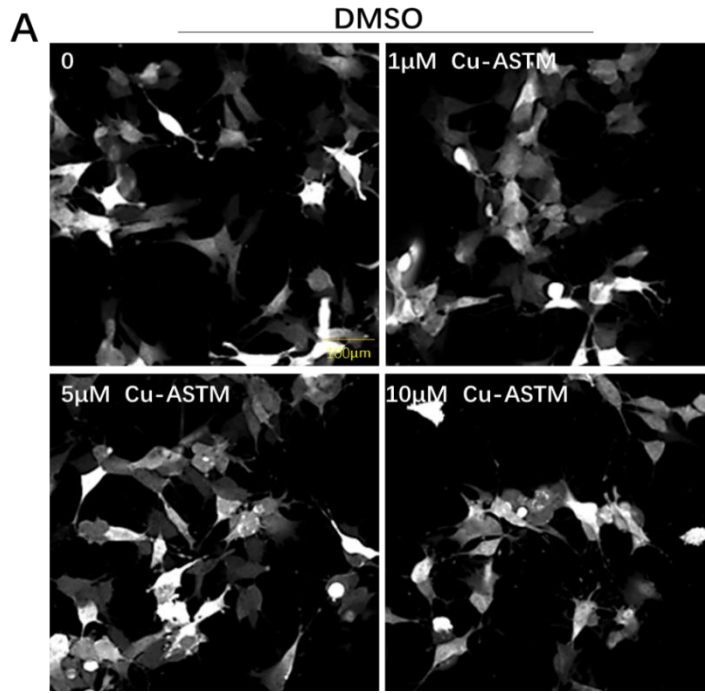
Figure 3-4 Parkin recruitment in SH-SY5Y cell.

A) The merged images from INCell 2200 show the Parkin recruitment condition of SH-SY5Y cells with eGFP labelled Parkin (green) and Hoechst-stained nuclei (blue). Cells were treated with 10µM (not shown in images) and 15µM CCCP(DMSO) for 2h, 4h and 6h. 4h CCCP (15µM) induced Parkin puncta formation in SH-SY5Y cells compared to DMSO, and 6h CCCP increased the Parkin puncta observed. B) Bar graph shows the analysis results of the Parkin puncta total area per cell after each treatment. 10µM and 15µM of CCCP significantly increased the Parkin puncta area per cell when treated for 4h and 6h. Significant differences were marked between no CCCP and CCCP within each treatment duration. Statistical analysis was carried out by two-way ANOVA test with Tukey's multiple comparisons test. N=3; data is displayed as mean ± SEM, significance is displayed as * p<0.05, ** p<0.01, ***p<0.001, **** p<0.0001.

Cu-ASTM potentially alters Parkin recruitment in SH-SY5Y cells

The effects of Cu-ASTM on cell viability and Parkin recruitment activity were also evaluated in SHSY-5Y cells. Following the same compound treatment protocol for H4 cells, SHSY-5Y cells were incubated with Cu-ATSM at doses of 1, 5 and 10 μ M for 24h. 15 μ M CCCP treatment for 4h was applied to trigger Parkin recruitment in SH-SY5Y cells. Cells were then fixed and stained as previously; then, images were taken and analysed using the INCell 2200 workstation program following the segmentation protocol for SH-SY5Y cells.

The results in **Figure 3-5** show that treatment with Cu-ASTM did not affect the cell viability of SH-SY5Y cells. There was a trend towards Cu-ASTM (at the 10 μ M dose) mediating an increase in Parkin puncta total area per cell without the presence of CCCP, though this did not reach significance. In addition, no dramatic cell morphology change was observed between cells treated with Cu-ASTM and vehicle control, indicating the compound, when applied to SHSY-5Y cells, was not toxic.



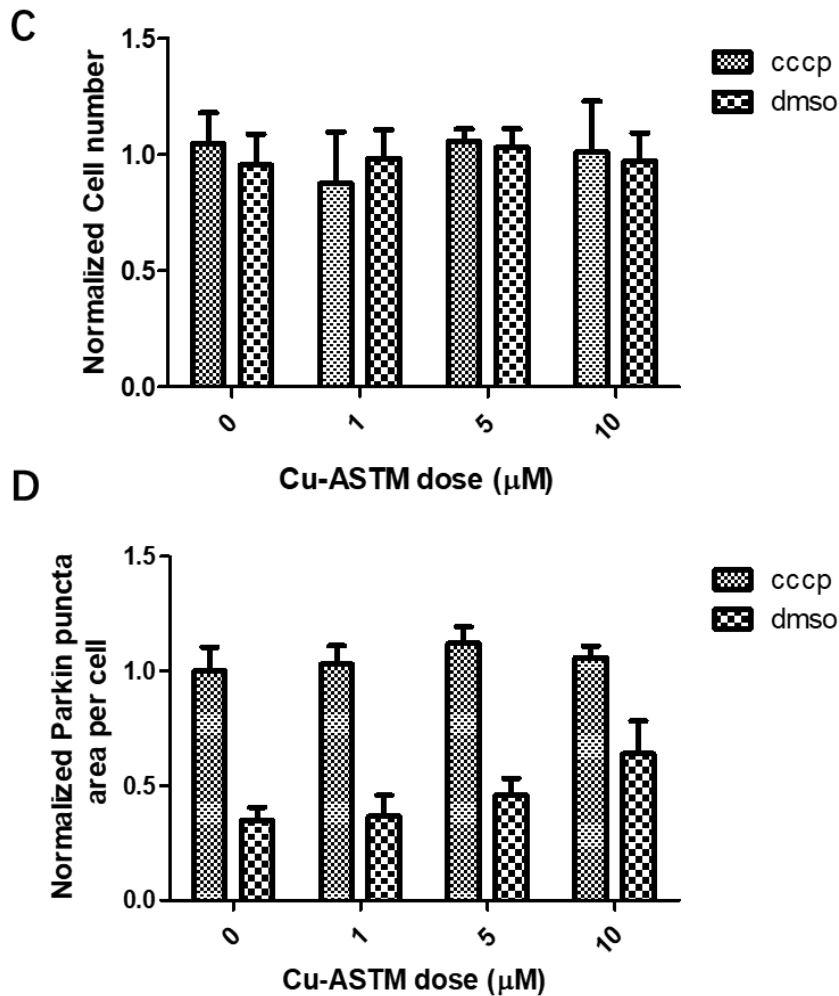


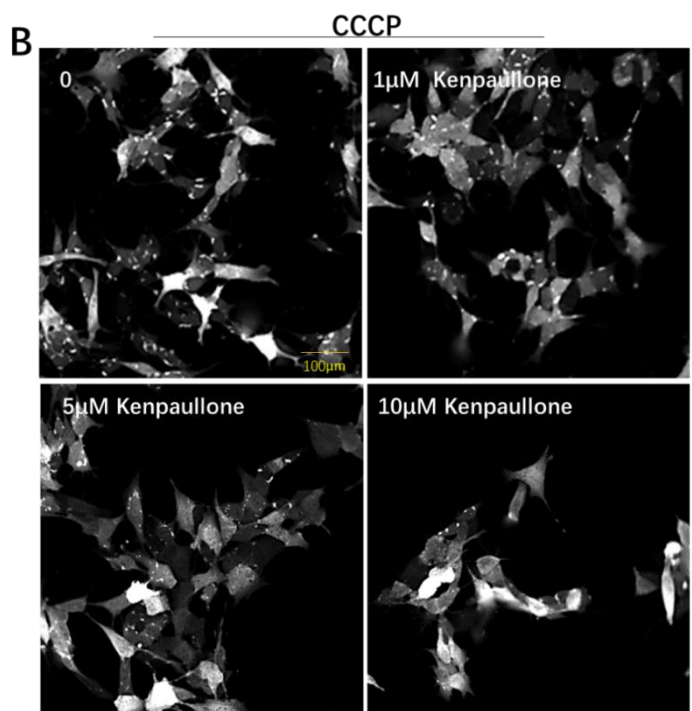
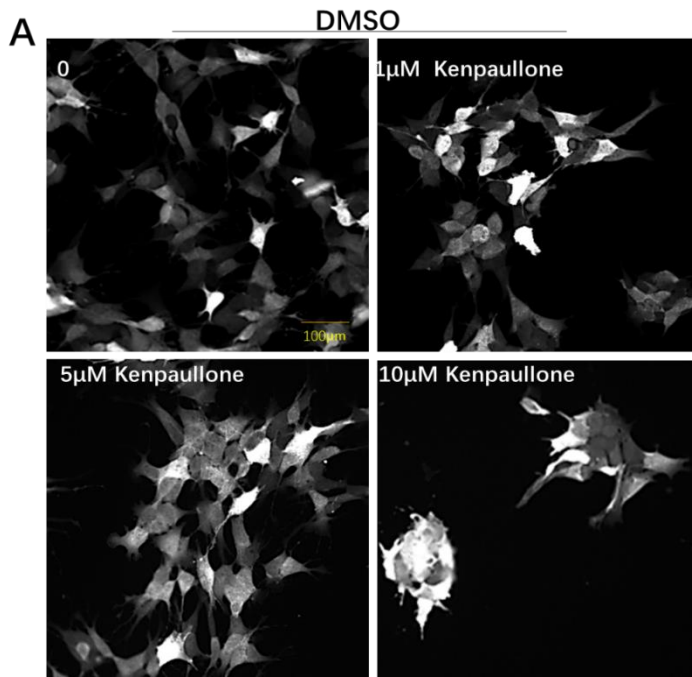
Figure 3-5 The effects of Cu-ASTM on cell viability and Parkin recruitment in eGFP-Parkin SHSY-5Y cells

A) Images taken by INCell 2200 show the cells' morphology in DMSO groups with Cu-ASTM of 0, 1, 5 and 10 μM . B) Images show the cells' morphology and Parkin puncta formation in CCCP groups with compound doses of 0, 1, 5 and 10 μM . Compared to the compound treatment groups with no compound groups, no noticeable change was found. C) Bar graph shows analysis results of cell viability by cell count—no significant change across the groups. D) Bar graph shows Parkin recruitment activity analysis results by Parkin puncta area per cell. There was no evident change with CCCP groups, while an increasing trend appeared in DMSO groups with the compound dose increased. Statistical analysis was carried out by two-way ANOVA test with Tukey's multiple comparisons test. N=3; data is displayed as mean \pm SEM. No significance was marked.

Kenpaullone is a negative regulator of Parkin recruitment in SH-SY5Y cells

The effects of kenpaullone on cell viability and Parkin recruitment activity were investigated in SHSY-5Y cells to validate the previous finding that kenpaullone negatively regulated Parkin recruitment in H4 cells.

Experiments were conducted following the compound treatment and Parkin recruitment assay protocols for SH-SY5Y cells. The results in **Figure 3-6** show that kenpaullone significantly reduced Parkin puncta total area per cell from the treatment dose of 1 μ M, and there was no alteration in cell viability. However, the cell count decreased significantly when SHSY-5Y cells were treated with the higher doses of kenpaullone (5 μ M, 10 μ M).



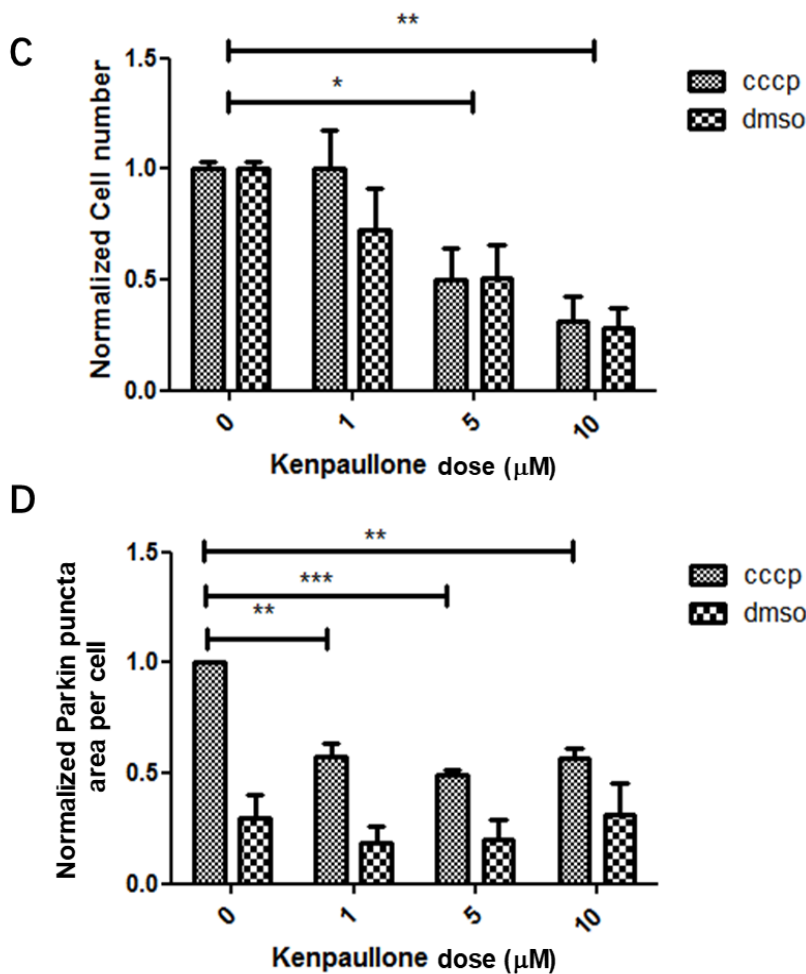


Figure 3-6 The effects of kenpaullone on cell viability and Parkin recruitment in eGFP-Parkin SHSY-5Y cells.

A) Images taken by the INCell 2200 show the cells' morphology in DMSO groups with kenpaullone of 0, 1, 5 and 10μM. B) Images show the cells' morphology and Parkin puncta formation in CCCP groups with compound doses of 0, 1, 5 and 10μM. Parkin puncta and cell counts were decreased following treatment with 10μM kenpaullone. C) Bar graphs show cell count was reduced with 5μM ($p=0.0252$), and 10μM ($p=0.0060$) compounds significantly decreased the cell count in both DMSO and CCCP groups. D) Bar graph shows Parkin recruitment activity analysis results by Parkin puncta area per cell. In CCCP groups, 1μM($p=0.0094$), 5μM ($p=0.0008$) and 10μM ($p=0.0046$) kenpaullone significantly decreased the Parkin puncta area per cell compared to 0 compound control. Statistical analysis was conducted by two-way ANOVA test with Tukey's multiple comparisons test. $N=3$; data is displayed as mean \pm SEM, significance is displayed as * $p<0.05$, ** $p<0.01$, *** $p<0.001$, **** $p<0.0001$.

The cell viability loss is usually due to cell death from toxicity, detachment of cells and reduced cell proliferation. Evidence suggests kenpaullone is potentially cell-protective, and the attachment of cells in the experiment was enhanced with PDL coating; thus, there was a high possibility that kenpaullone might affect cells proliferation as it inhibits cell cycle regulators CDK1/2.

It is known that when the cells maximal occupy the available substrate, they enter the stationary phase, where the proliferation is significantly reduced (also known as contact inhibition) [116]. In addition, cells seeded at high density produce trophic factors that support cell survival and better reflect normal physiological conditions. Therefore, the cells were seeded at a high density to reduce cell proliferation (of the rapidly dividing cancer) cells before compound treatment so that the effect of kenpaullone on cells dividing was weakened. In this way, the effect of kenpaullone on Parkin recruitment can be evaluated while minimising interference from its inhibitory action on cell proliferation. Following the compound treatment and Parkin recruitment assay protocols, experiments were performed on SH-SY5Y cells with high cell density.

Results in **Figure 3-7** show that all doses of kenpaullone significantly decreased the total Parkin puncta area, and there was no change in cell viability detected. This result further confirms that kenpaullone had a strong negatively regulative effect on Parkin recruitment, which did not depend on its acting on inhibiting the

cells' proliferation.

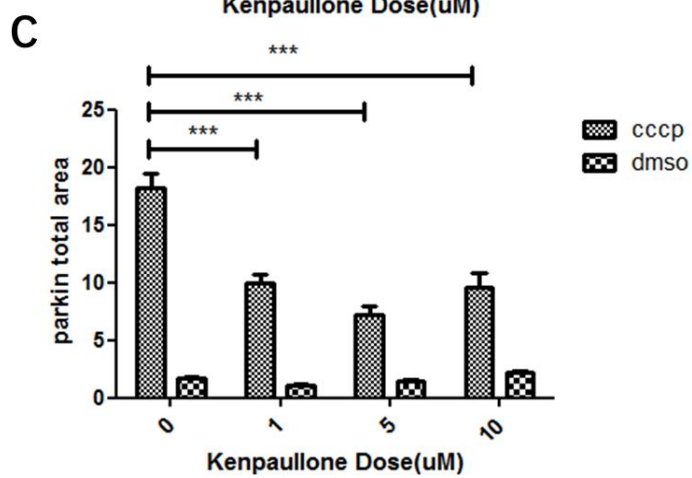
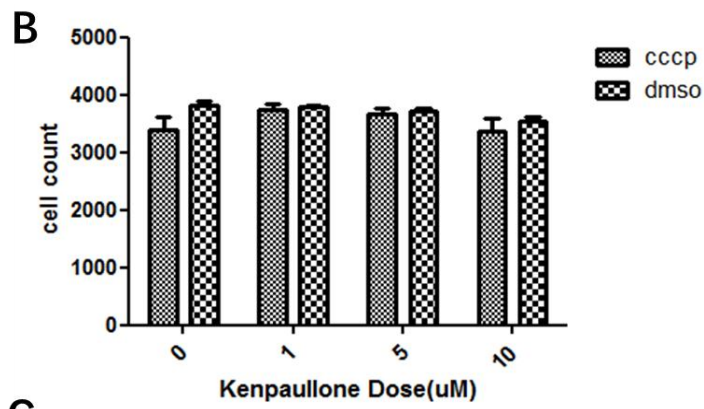
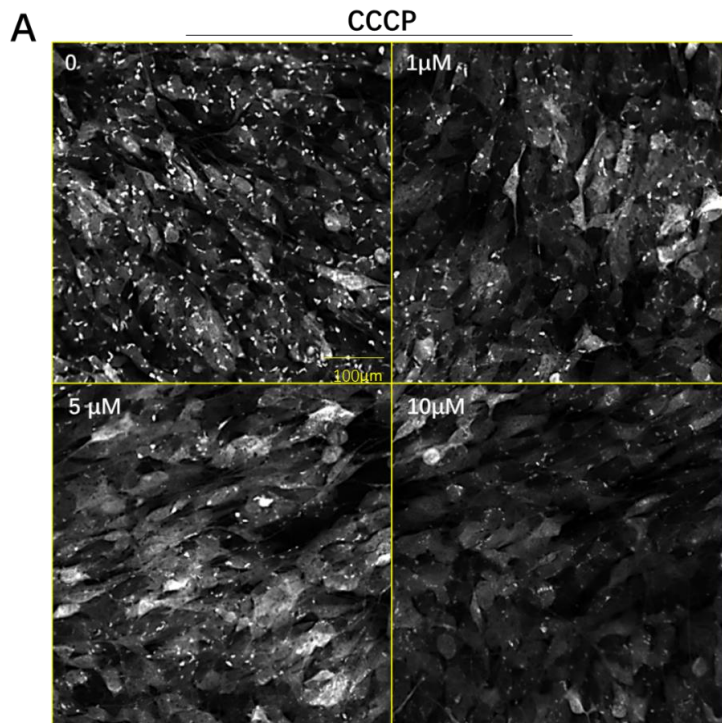


Figure 3-7 The effects of kenpaullone on cell viability and Parkin recruitment in eGFP-Parkin SHSY-5Y cells with high cell density.

A) Images taken by INCell 2200 show the cells' morphology and Parkin puncta formation in CCCP groups with kenpaullone of 0, 1, 5 and 10 μ M. Cells were seeded by 15000 per well in 96-well plates. No cell population change was observed, but Parkin puncta were observed to be decreasing along with the dose of kenpaullone increased. B) Bar graph shows analysis results of cell viability by cell count. No significant difference was marked. C) Bar graph shows Parkin recruitment activity analysis results by Parkin puncta area per cell. In CCCP groups, 1 μ M($p=0.0004$), 5 μ M ($p=0.0002$) and 10 μ M ($p=0.0006$) kenpaullone significantly decreased the Parkin puncta area per cell compared to 0 compound control. Statistical analysis was carried out by two-way ANOVA test with Tukey's multiple comparisons test. N=4; data is displayed as mean \pm SEM; significance is displayed as *** $p<0.001$.

Mitochondrial network assay optimisation

To analyse and quantitate changes in mitochondrial form, automated image analysis assays were performed using the INCell system. MitoTracker Red was used to visualise mitochondria as its take-up is dependent on an intact mitochondrial membrane potential being present (live mitochondria), and it remains in mitochondria after fixation. CCCP was used to disrupt the mitochondrial membrane potential before loading MitoTracker so that a change of MitoTracker staining would indicate the effect of candidates tested against CCCP challenge on the mitochondrial network.

Mitochondria stained with MitoTracker Red were imaged using the INCell Analyser 2200 at 40X magnification in high-definition quality; the results showed CCCP dramatically disrupted the mitochondrial network (**Figure 3-8 A**). The analysis protocol of INCell Workstation was optimised to better segment the staining areas. Visual inspection by comparing the high-rez image and segmentation confirmed that the software could detect mitochondria of different sizes and shapes to reflect the observation (**Figure 3-8 B**). To determine whether the analysis protocol effectively worked for the assay, CCCP-induced changes to the mitochondrial network were compared to control. The analysis showed that CCCP treatment significantly reduced total mitochondrial area per cell and increased mitochondrial elongation (**Figure 3-8 c**). As MitoTracker only enters

live mitochondria, the mitochondrial total area per cell values obtained represent mitochondria with healthy membrane potentials. The mitochondrial elongation indicated the average shape of mitochondria in one cell; a more elongation value stood for a more circular mitochondrial shape, indicating more fragmented mitochondria are present in cells. Thus, the analysis protocol successfully detected CCCP-induced mitochondrial network damage and less healthy mitochondria and more damaged mitochondria showing fragmented shapes.

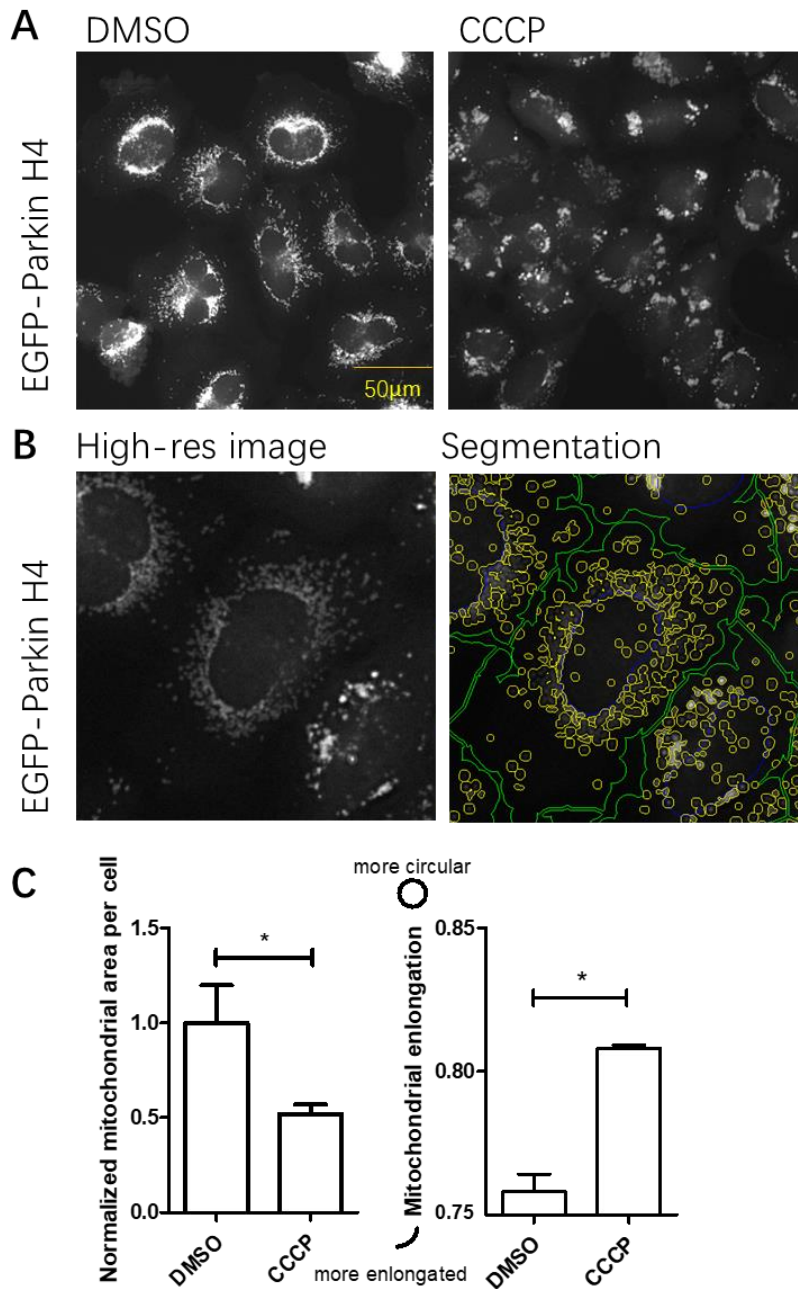


Figure 3-8 Parkin recruitment assay optimisation.

A) Images taken by INCell 2200 show mitochondrial network change with 10µM CCCP treatment for 2.5h. Only CY3 channel images were shown. B) 4X zoomed-in images show details of the mitochondrial network and the segmentation of each mitochondrion. C) Analysis results by the optimised protocol from INCell Workstation show CCCP significantly decreased the mitochondrial area per cell and increased the mitochondrial elongation value. Statistical analysis was carried out by unpaired t-test. N=3; data is displayed as mean ± SEM, and significance is displayed as * p<0.05.

Kenpaullone protects the mitochondrial network against CCCP

EGFP-Parkin H4 cells were pre-treated with 0 (vehicle control), 5 μ M, and 10 μ M kenpaullone for 24 hours, then challenged with 10 μ M CCCP or DMSO (vehicle control) for 2.5 hours and stained with MitoTracker Red. Images were taken and analysed by INCell Analyzer and INCell Workstation after the cells were fixed and stained with Hoechst.

The results shown in **Figure 3-9 A** show CCCP induced Parkin puncta formation, triggered damage to the mitochondrial network and reduced the mitochondrial population as characterised by a decrease in mitochondrial total area per cell and the fragmentation of mitochondria. This damage to the mitochondrial network was prevented by pre-treatment with kenpaullone for 24h. In the presence of CCCP, kenpaullone treatment significantly increased the total mitochondrial area per cell in H4 cells and significantly decreased the mitochondrial elongation compared to the vehicle control without kenpaullone treatment (**Figure 3-9 B and C**). Similarly, kenpaullone prevented Parkin puncta formation and mitochondrial network damage following treatment with CCCP in SHSY-5Y cells (**Figure 3-10 A**). The results in **Figure 3-10 B** show mitochondrial total area is increased when cells are pre-treated with kenpaullone compared to no kenpaullone with CCCP present.

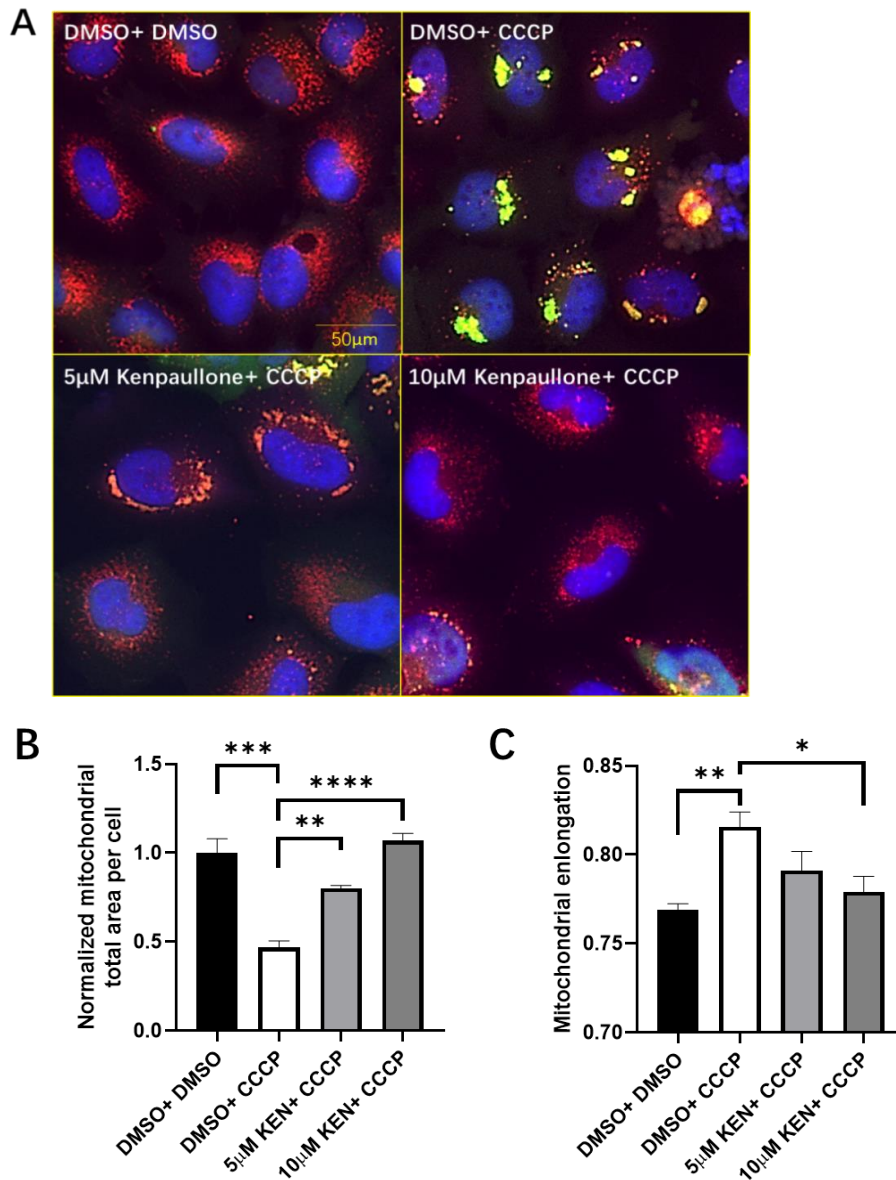


Figure 3-9 Kenpaullone protects the mitochondria network from CCCP challenge.

A) The merged images from INCell 2200 show Mitotracker-stained mitochondrial network (red) in H4 cells with eGFP-labeled Parkin (green) and Hoechst-stained nuclei (blue). 10 μ M CCCP treatment for 2.5h induced the Parkin puncta formation and caused the mitochondrial network to shrink. Pre-treatment with kenpaullone prevented this change, and healthier mitochondrial are observed. B) CCCP significantly ($p=0.002$) decreased the mitochondrial area per cell compared to no CCCP. 5 μ M ($p=0.0041$) and 10 μ M ($p<0.0001$) kenpaullone significantly increased the mitochondrial area per cell compared to no kenpaullone with the presence of CCCP. C) CCCP significantly ($p=0.0096$) increased the mitochondrial elongation, and it was significantly ($p=0.0338$) decreased by 10 μ M kenpaullone treatment. Statistical analysis was carried out by one-way ANOVA test with Tukey's multiple comparisons test. N=3; data is displayed as mean \pm SEM, significance is displayed as * $p<0.05$, ** $p<0.01$, *** $p<0.001$, **** $p<0.0001$.

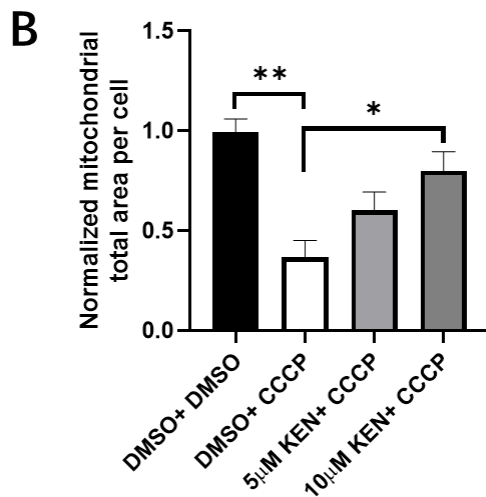
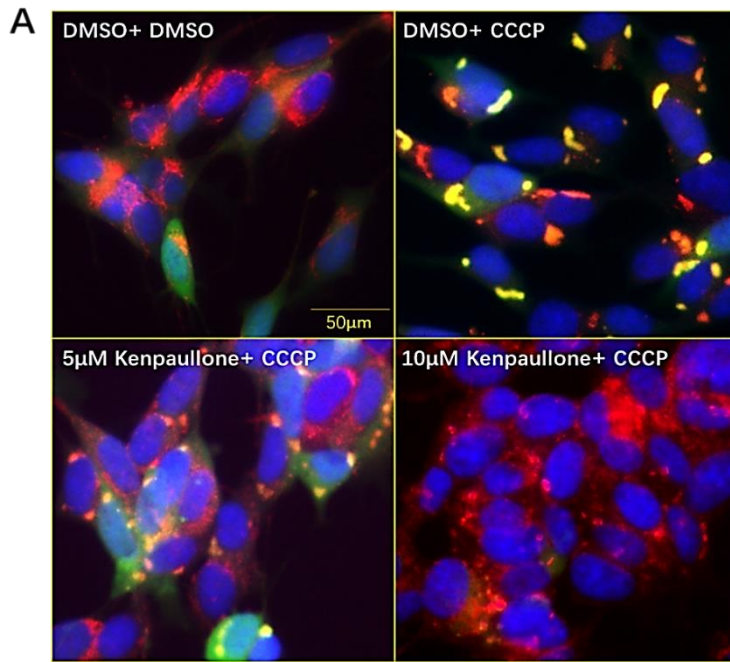


Figure 3-10 Kenpaullone protects the mitochondria network in SHSY-5Y cells from CCCP challenge

A) The merged representative images taken with the INCell 2200 show the Mitotracker-stained mitochondrial network (red) condition in SH-SY5Y cells with eGFP-labeled Parkin (green) and Hoechst-stained nuclei (blue). 15µM CCCP treatment for 4h induced Parkin puncta formation and collapsed the mitochondrial network. Pre-treatment with kenpaullone prevented these changes. B) CCCP significantly ($p=0.0023$) decreased the mitochondrial area per cell compared to no CCCP. 10µM kenpaullone significantly ($p<0.0191$) increased the mitochondrial area per cell compared to no kenpaullone with CCCP presence. Statistical analysis was carried out by one-way ANOVA test with Tukey's multiple comparisons test. $N=3$; data is displayed as mean \pm SEM, significance is displayed as * $p<0.05$, ** $p<0.01$.

Mitochondrial respiration assay optimisation in H4 and SY5Y cells

Mitochondrial respiration activity is one of the most critical activities directly linked to cells' healthy condition. The Seahorse Bioanalyzer XFp (Agilent) was used to investigate the effect of the candidate compound on mitochondrial respiration activity in live cells. The Mito Stress Test protocol was used, and this involves the sequential injection of drugs that disrupt the specific electron transport chain (ETC) complexes. This allows oxygen consumption rate (OCR) and extracellular acidification rate (ECAR) to be recorded under conditions that alter mitochondrial respiration. Mitochondrial respiration and glycolytic activity were analysed based on changes in the OCR and ECAR values at different experiment stages and are fully described in the method chapter. This study was coordinated with Dr Nicola Buckner, and practical suggestions were given by Dr Virginie Betin.

Before applying the Mito Stress Test, dose optimisation was performed in both H4 and SH-SY5Y cells as per the manufacturer's instructions. The OCR data following sequential chemical injection in the titration experiments in H4 and SH-SY5Y cells are shown in **Figure 3-11 A** and **C**, respectively. The maximal OCR in each experiment was plotted against the dose of FCCP. In H4 cells, the maximal OCR was observed with 2 μ M FCCP (**Figure 3-11 B**). In SHSY-5Y cells, the

maximal OCR was observed at 0.5 μ M FCCP, and increasing the dose did not dramatically increase the OCR (**Figure 3-11 D**).

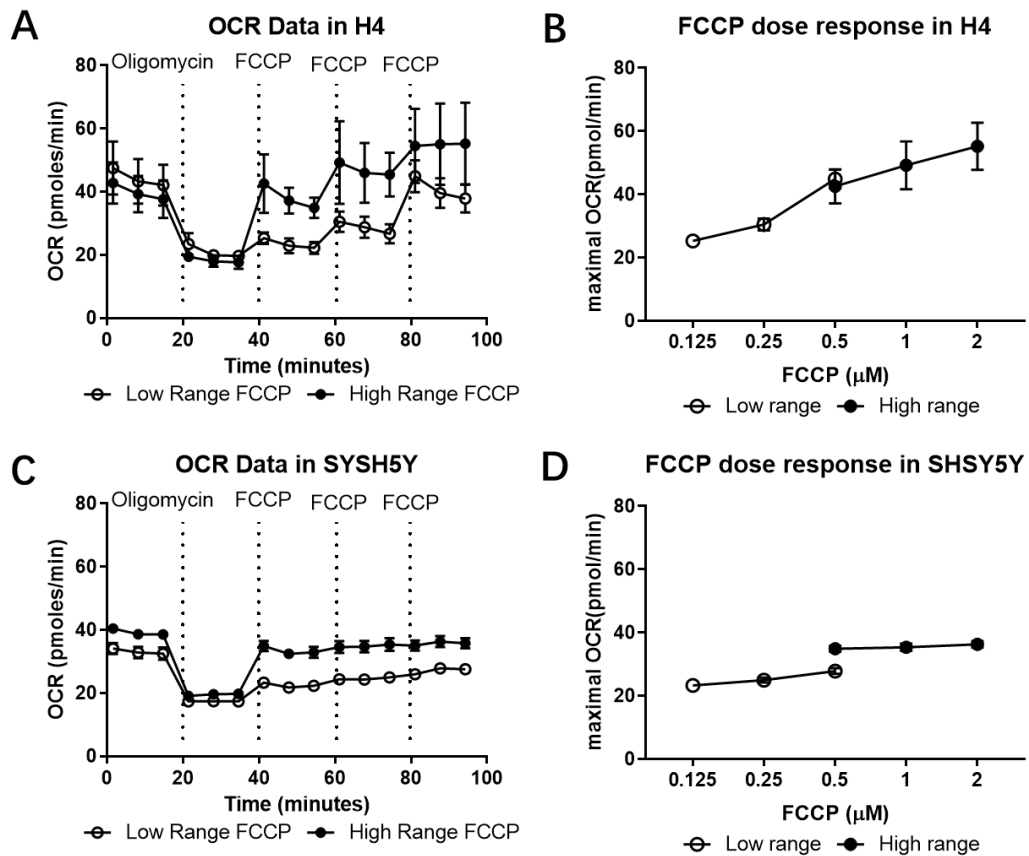


Figure 3-11 Optimisation of conditions for Mitochondrial Stress Test using Agilent Seahorse Bioanalyzer

- A) Graph shows the OCR data in the titration experiment along time in H4 cells.
- B) Graph shows the maximal OCR plotted against the FCCP dose in H4 cells.
- C) Graph shows the OCR data in the titration experiment along time in SH-SY5Y cells.
- D) Graph shows the maximal OCR plotted against the FCCP dose in SH-SY5Y cells.

Kenpaullone regulates the metabolic activities in live cells

Both H4 and SH-SY5Y cells were pre-treated with kenpaullone or DMSO vehicle control for 24h, and The Mito Stress Test was then performed. Oxygen consumption rate was normalised to total protein after each experiment as stipulated in the experimental protocol. This normalisation reduces errors due to differences in population of cells, and allows the effect kenpaullone on the cells' metabolic activities to be more accurately recorded.

The curves of OCR and ECAR from the experiment in H4 cells are shown in **Figure 3-12 A and B**, respectively. Kenpaullone-treated cells showed relatively lower OCR and higher ECAR curves than vehicle control at the majority stages of the experiment. After the features of cells' metabolism were analysed, kenpaullone was pointed out to significantly decrease the ATP production of the mitochondria (**Figure 3-12 C**) and significantly increase the extra glycolysis in H4 cells (**Figure 3-12 D**). The curves of OCR and ECAR from the experiment in SH-SY5Y cells are shown in **Figure 3-13 A and B**, respectively. Kenpaullone-treated cells showed relatively higher OCR and ECAR curves than DMSO control in the experiment. Moreover, unlike the results in H4 cells, no significant change in mitochondrial respiration activity was recorded in SH-SY5Y cells (**Figure 3-13 C**). Nevertheless, same with the results in H4 cells, kenpaullone significantly increased the extra glycolysis in SH-SY5Y cells (**Figure 3-13 D**).

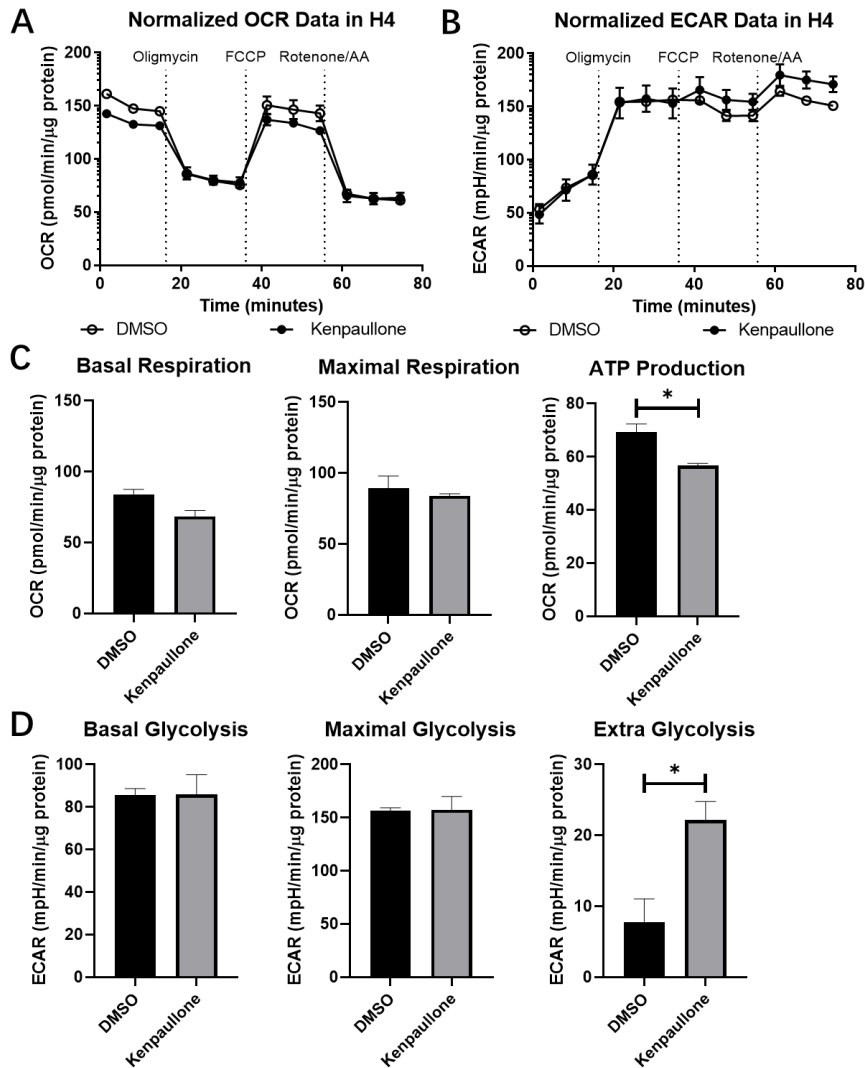


Figure 3-12 The effect of kenpauillone on mitochondrial respiration

EGFP-Parkin H4 cells were treated with 5μM kenpauillone/DMSO for 24h before undergoing Mito Stress Test experiments. A) Graph shows the OCR data in the Mito Stress Test experiment with time. B) Graph shows the ECAR data in the Mito Stress Test experiment with time. C) Graphs show the selected mitochondrial respiration measurements from OCR data: basal respiration, maximal respiration, and ATP production. Kenpauillone treatment significantly decreased ATP production ($p=0.0139$) compared to the vehicle control in H4 cells. D) Graphs show the selected measurements of glycolysis from ECAR data; they are basal glycolysis, maximal glycolysis, and extra glycolysis. Kenpauillone treatment significantly increased the extra glycolysis ($p=0.0265$) compared to the vehicle control in H4 cells. Statistical analysis was carried out by unpaired t-test. $N=3$; data is displayed as mean \pm SEM, and significance is displayed as * $p<0.05$.

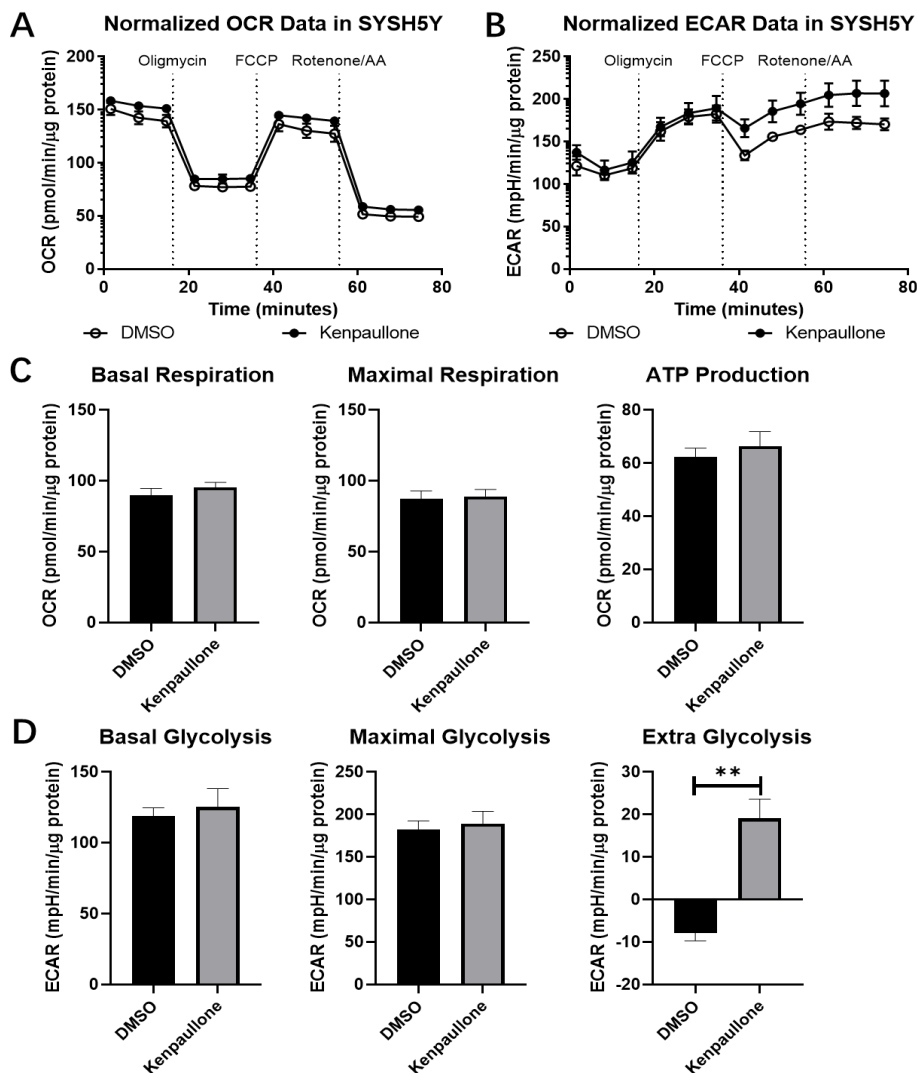


Figure 3-13 The effect of kenpaullone treatment on mitochondrial respiration in SH-SY5Y cells. EGFP-Parkin SH-SY5Y cells were treated with 5μM kenpaullone/DMSO for 24h before undergoing Mito Stress Test experiments. A) Graph shows the OCR data in the Mito Stress Test experiment along time. B) Graph shows the ECAR data in the Mito Stress Test experiment along time. C) Graphs show the selected mitochondrial respiration measurements from OCR data: basal respiration, maximal respiration, and ATP production. No significant difference between the kenpaullone and DMSO groups in these measurements. D) Graphs show the selected measurements of glycolysis from ECAR data; they are basal glycolysis, maximal glycolysis, and extra glycolysis. Kenpaullone treatment significantly increased the extra glycolysis ($p=0.0054$) compared to the vehicle control in H4 cells. Statistical analysis was carried out by unpaired t-test. $N=3$; data is displayed as mean \pm SEM, and significance is displayed as ** $p<0.01$.

Summary and discussion

Summary of the results

Mitochondrial dysfunction contributes to the death of neurons in human neurodegenerative diseases, especially in PD. Thus, drugs that positively regulate mitochondrial activity may have therapeutic potential for PD. The experiments described in this chapter aimed to evaluate Cu-ATSM and kenpaullone as potential mitochondrial modulators in H4 and SHSY-5Y cell lines. The phenotypic assay of Parkin recruitment confirmed kenpaullone as the negative regulator of Parkin recruitment (downregulation of Parkin puncta total area against CCCP-induced rise) in the two human neurological cell lines. A follow-up mitochondrial network study identified the protective effect of kenpaullone against morphological damage to mitochondria (decreased mitochondrial total area) induced by CCCP. Moreover, kenpaullone altered mitochondrial respiratory activity (down-regulation of ATP in H4 cells) and cell metabolic activity (up-regulation of extra glycolysis in both H4 and SH-SY5Y cells). This study identified that kenpaullone acts as a negative modulator for Parkin-recruitment and protects cells from mitochondrial stress-induced damage.

Evaluating Parkin recruitment assays in H4 and SH-SY5Y cells, limitations and concerns

In this study, the Parkin recruitment assay was established in the undifferentiated

SH-SY5Y cells for the following reasons. Firstly, the morphology and specific neuronal enzyme activities have been well-evaluated in the undifferentiated SH-SY5Y cell line, making it a standard cell line for PD research [117] [118]. Secondly, they are efficient (both time and cost) and are morphologically suitable for high-content imaging studies. The Parkin recruitment established in SH-SY5Y cells also allows the evaluation of previous findings from H4 cells, adding more evidence to the current understanding from a view relatively closer to dopaminergic neurons through comparison and contrast analysis.

There was a difference in the average treatment time that the CCCP was required for Parkin puncta formation between H4 cells (2h) and SYSH5Y cells (4.5h). As EGFP- Parkin was stably overexpressed at approximately the same level in each cell line, it is likely that the differing availability of cofactors in the cell lines results in altered Parkin signalling dynamics. For example, the various expression level of regulators of PINK1 such as Foxo3a[119], nuclear factor κ B(NF κ B) [120], p53 [121] and ATF3 [121] could differentially affect the availability of PINK1 signalling that recruits Parkin. Similarly, regulators that bind Parkin could affect Parkin recruitment efficiency.

Unexpected signals were seen from nuclear in images of H4-EGFP-PRKN cells where only EGFP channel was visualized, though this does not affect this study. It could be due to that nuclear-targeted Parkin was detected. Parkin, a cytosolic

ubiquitin E3 enzyme, has been reported to recruit to the nucleus and mediate gene transcription [122]. It is possible to investigate the change of nuclear parkin intensity to reach other research purposes, however, the segmentation protocol in this study was optimized to selectively identify the cytoplasmic parkin puncta, specifically focusing on the parkin-mitochondrial activities.

After optimising the assay, the results showed that Parkin recruitment in SH-SY5Y were similar to those obtained in H4 cells. As SHSY-5Y cells have some dopaminergic neuronal features, it also suggests that inhibitors of GSK3 and CDKs may have promise as treatments for PD.

Notably, Parkin recruitment suggests that stress to mitochondria has instigated changes to the quality control pathways but does not show an obligate link with mitophagy. To study how CCCP and our drugs of interest regulate mitophagy, the removal of damaged mitochondria would need to be measured. For example, some research groups investigate the mitochondrial localisation to autophagosomes and lysosomal degradation to determine the complete process of mitophagy [123] [124]. Moreover, The alteration effects from candidates detected by these assays might rely on the overexpression of Parkin. Therefore, further validation studies of the modulators detected by these assays using non-PINK1/Parkin modified cells, especially neuronal cells, and in vivo approaches are encouraged.

Evaluating the effects of Cu-ATSM on cell viability and Parkin recruitment

The results from Parkin recruitment assays in both H4 and SH-SY5Y cells suggest that Cu-ATSM potentially upregulates Parkin recruitment. Cu-ATSM was developed as an agent for hypoxia-sensitive positron emission tomography [125], but recent reports highlighted the neuroprotective properties of this compound, both in a PD study (MPTP toxicity) [126] and in an ALS study [125]. MPTP is a neurotoxin whose derivative MPP⁺ is toxic to dopaminergic neurons [73] by causing oxidative and nitrosative stress [127]. Furthermore, when delivered *in vivo*, it causes PD-like symptoms and is used to model PD. There are a number of mechanisms by which altered mitochondrial quality control could protect against oxidative and nitrosative stress. The consequences of the stress could be minimised by clearing the damaged mitochondria via mitophagy [128]. This suggests that the protective effect from Cu-ATSM against MPTP [126] might rely on the upregulation of mitophagy. Paradoxically, the supposed positive alteration in Parkin recruitment required for Parkin-mediated mitophagy by Cu-ATSM treatment was not observed in cells challenged by CCCP. This suggests that Cu-ATSM does not affect CCCP-induced mitophagy. Moreover, the trend of increased Parkin puncta total area in SYSH-5Y without the presence of CCCP further implies that Cu-ATSM upregulates the Parkin recruitment independent of mitochondrial membrane depolarisation.

Moreover, MPTP toxicity is suggested to be specifically mediated by nitrated α -synuclein oligomers aggregation as either inhibition of α -synuclein or nitric oxide synthase is resistant to MPTP-induced damage [129] [130]. Plentiful nitrated α -synuclein was presented in the Lewy bodies [131], a hallmark of PD. Then it is suggested that Cu-ATSM protects against MPTP toxicity by inhibiting the nitrated α -synuclein oligomers aggregation. This assumption is evidenced by inhibition of the actions of ONOO^- by Cu-ATSM prevented reaction of ONOO^- with α -synuclein, thereby reducing the nitrated α -synuclein formation [126]. Therefore, it is suggested that Cu-ATSM may protect against PD via its anti-stress action.

Parkin puncta were observed following high doses of Cu-ATSM treatment without CCCP, though this did not reach significance. These Parkin puncta may be stress-induced as high doses of Cu-ATSM treatment triggered significant viability loss and observed apoptotic morphology (collapsed nuclei) of the cells. Interestingly, Cu-ATSM was shown to upregulate Cu retention more in the tissue of human PD subjects, which was suggested to be driven by the impairment of the mitochondrial electron transport chain (ETC) with more advanced disease pathogenesis [132]. More Cu retention might also indicate the more severe disruption of mitochondrial membrane function, which might be related to mPTP opening. A recent study showed that Cu exposure could cause Parkin-mediated mitophagy in chicken livers and that mitophagy might attenuate Cu-induced mitochondrial apoptosis in

turn [133]. The above findings suggest that Cu-ATSM could induce Parkin-mediated mitophagy with high available doses and apoptosis in PD-stressed cells containing advanced mitochondrial damage, which is consistent with the results that a high dose of Cu-ATSM triggered both Parkin recruitment and cell loss of H4 cells in this study. Together, it is suggested that the dose of this compound is crucial to determine whether inducing mitophagy or apoptosis, protecting or eliminating the stressed cells.

This study suggests that Cu-ATSM potentially alter Parkin recruitment in a positive direction to protect the cells. Besides altering the Parkin recruitment, under its effective dose, the anti-stress and anti-apoptosis effects of Cu-ATSM against α -synuclein oligomers aggregation could make it a potential candidate for PD treatment.

Evaluating the effects of kenpaullone on Parkin recruitment and the mitochondrial network

Based on the results of Parkin recruitment in H4 and SH-SY5Y cells, kenpaullone was suggested to be the modulator that negatively regulates Parkin puncta formation. The Parkin puncta formation in eGFP-Parkin cells is mainly due to the disrupted mitochondrial membrane potential by CCCP, which stops PINK1 translocation from the outer membrane into the inner side of mitochondria and starts to recruit Parkin [134]. As PINK1 recruits Parkin in a positive feedback

manner, more and more Parkin gathers outside the mitochondria, and eventually, they are shown as clusters with eGFP labels in those eGFP-Parkin cell lines. The reduction of the Parkin puncta induced by CCCP shown with kenpaullone pretreatment suggests effects upon the step-by-step processes: the first one is the disruption of mitochondrial membrane potential by CCCP, and the second one is PINK1/Parkin signalling for Parkin recruitment.

The image-based mitochondrial network investigation added credible evidence to support the assumption that kenpaullone prevents the disruption of the mitochondrial membrane potential. Mitochondria with a depolarised membrane potential do not take up MitoTracker dye uptake, showing less fluorescent intensity, and therefore would not be detected. The proton ionophore CCCP is an oxidative phosphorylation uncoupler that opens the permeability transition pore (PTP) on the mitochondrial membrane (mPTP), allowing proton flux to disrupt the functional-maintained chemical gradient resulting in the mitochondrial membrane potential loss [111]. Kenpaullone may work by stabilising the mPTP against CCCP-induced change (no evidence of proton binding or releasing effect from kenpaullone). The mPTP is suggested to be important not only for affecting mitochondrial function (ATP genesis [135]) but also for altering cell survival (Ca²⁺ and ROS-induced apoptosis [136] [137]). Moreover, the formation of mPTP has been reported to be closely associated with various neurodegenerative diseases, including Alzheimer's disease (AD) [138], PD [139] and Huntington's disease (HD)

[140]; and drugs that inhibit mPTP formation are being sought [141] [142]. Theoretically, inhibiting the formation of the mPTP for Ca^{2+} would prevent Ca^{2+} overload and prevent apoptosis, while inhibiting mPTP formation for H^{+} could encourage ATP production. Thus, inhibition of mPTP opening for H^{+} and Ca^{2+} would potentially benefit the treatment for PD. Research showed that when blocking mPTP by Cyclosporin A (CsA), both autoxidises induced Ca^{2+} -related stress [143] and CCCP [144] induced damage were prevented.

Kenpaullone could act by stabilising the mPTP, maintaining ATP generation, and preventing the Ca^{2+} homeostasis disruption induced oxidative stress and apoptosis. These proposed protective effects might contribute to the previous finding that kenpaullone protects against oxidative stress [110].

Kenpaullone prevented the CCCP-induced mitochondrial fragmentation. This observation could be due to kenpaullone inhibiting the fission-dependent fragmentation of mitochondria induced by CCCP [145]. Given the evidence that enhanced mitochondrial fragmentation was accompanied by increased mitochondrial ROS production [146], kenpaullone might be beneficial in reducing the mitochondria ROS level, avoiding apoptosis of the cells. Additionally, evidence shows that abolished PINK1/Parkin mitophagy results from fission inhibition [146], while PINK1/Parkin signalling promotes mitochondrial fission [147]. Taking this evidence together with the results of Parkin recruitment, they

suggest that kenpaullone might inhibit PINK1/Parkin signalling through the mitochondrial fission-preventing manor.

Evaluating the effects of kenpaullone on cellular metabolism

Mitochondrial respiration is one of the most critical activities directly linked to cells' health. To investigate the effects of kenpaullone on mitochondrial respiration, Mito Stress Tests were performed using the Seahorse Bioanalyzer XFp system, the gold-standard assay for quantifying mitochondrial oxygen consumption[148]. The oxygen consumption rate (OCR) results, which represents mitochondrial respiration, differed slightly in H4 cells compared to SH-SY5Y cells. In H4 cells, the lower position of the general OCR curve suggested the downregulation of mitochondrial respiration by kenpaullone treatment compared to the vehicle control. The ATP production-related mitochondrial respiration was significantly downregulated by kenpaullone treatment, suggesting kenpaullone reduces mitochondrial ATP generation of H4 cells.

In contrast, the general OCR curve and ATP-related OCR remained unchanged in SH-SY5Y cells following kenpaullone treatment compared to the vehicle control, suggesting kenpaullone did not alter mitochondrial respiration in SH-SY5Y cells.

This inconsistency might be because these two cancer cell lines have different

metabolic activities. This assumption could be supported by comparing the extracellular acidification rate (ECAR) and OCR at the basal level between the two cell lines, where the OCR are relatively close, but SH-SY5Y had obvious higher ECAR compared to H4. The SH-SY5Y cells with higher ECAR might suggest they require more energy given the similar basal OCR compared to H4.

No enhancement of mitochondrial respiration by kenpaullone was recorded, suggesting other mechanisms may mediate its protective effects. Kenpaullone may act by preventing stress-induced respiratory failure and thus protect mitochondrial function. Additionally, the changes in mitochondrial respiration due to kenpaullone may not be evident for the following reasons. First, it is well accepted that mitochondria energy production responds to the energy demand of the cells [149]. Given the unchanged energy demand by cells at the basal level, mitochondrial activity in cells treated with kenpaullone might not need to change, shown as the unaltered basal OCR. Second, the maximal mitochondrial respiration was supposed to be induced by acute FCCP injection, delivering protons to drive maximal OCR. However, the FCCP mediated pH change (ECAR) may be rapidly attenuated in kenpaullone treated cells, resulting in the real 'maximal OCR' being undetected; thus, an inaccurate 'maximal OCR' was detected. Third, the ATP-related OCR drop observed in H4 treated with kenpaullone might reflect its protective profile. Oligomycin was injected to block ATP synthase, reflecting the OCR for ATP production. It is possible that the dropped ATP-OCR recorded with

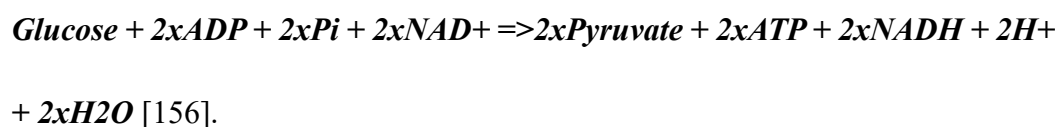
kenpaullone was due to protected mitochondria not being fully inhibited by oligomycin. However, these effects were not seen in SHSY-5Y cells as they are more sensitive to oligomycin, as a study showed the blocking effect of oligomycin was stronger on SH-SY5Y than on other cancer cells (H1299, A549, Calu-3, SkBr3, MCF7) [150].

The extracellular acidification rate (ECAR) from the experiments showed that kenpaullone helped upregulate glycolysis. Intact mitochondria cycle protons, drive electron transport and facilitate ATP generation. This occurs at the intermembrane space and in the mitochondrial matrix, and overall, there is no significant change in extrusion of protons into the cytosol or medium. However, the extrusion of protons into the medium by rapid glycolysis causes an increase in ECAR. Thus, the ECAR indicated the level of rapid glycolytic activity. The ECAR curves in both H4 and SHSY-5Y cells show the same trend, suggesting: (i) kenpaullone does not affect the cells' basal glycolytic rate, which helps maintain the stable cellular metabolism when there is no extra demand for energy; (ii) oligomycin might not entirely block the mitochondrial oxygen consumption when the mitochondria are protected by kenpaullone, which fails to drive the maximal glycolysis. Thus, the real maximal glycolysis from kenpaullone-treated cells might be higher than it was detected in the experiment; (iii) when mitochondrial respiration was further blocked by the other mitochondrial ETC inhibitors, rotenone (complexes I) and antimycin (complexes III), there were significant increases in ECAR, indicating

extra glycolysis happened in kenpaullone treated cells. The extra glycolysis that occurs after 'maximum glycolysis' has been induced might further suggest that mitochondrial respiration was not entirely blocked by oligomycin. Furthermore, the extra glycolysis mediated by kenpaullone might serve the energy demand by cells, thus protecting the cells against mitochondrial stress-induced energy disruption and mitochondrial dysfunction induced apoptosis.

Moreover, kenpaullone might help cells resist intracellular acidification through the upregulation of aerobic glycolysis. The intracellular pH is stably maintained by balanced cellular metabolism and general ion exchange with the extracellular environment within a health range [151]. Rapid intracellular acidification causes a series of disruptions to cellular activities, including those of mitochondria and lysosomes, which are crucial for cell health[152] [153] [154]. For mitochondria, Intracellular acidification induces mPTP opening, which helps mediate mitochondrial ROS-dependent cell death[155]. Thus, a well-maintained intracellular pH is essential for cell health.

Generally, rapid glycolysis is linked to decreasing the cellular pH by producing protons following the equation:

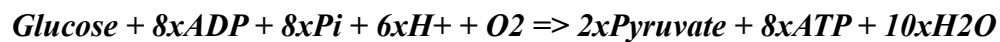


However, cancer cells like to employ a relatively slow aerobic glycolysis for their

proliferation and survival in the long term. With the oxygen present, aerobic glycolysis further consumes eight net protons, as NADH is further oxidated in mitochondrial (independent of ETC) following the equation:



Thus, the final net equation of the aerobic glycolysis is:



The upregulation of glycolysis by kenpaullone might lead to the upregulation of aerobic glycolysis in H4 and SH-SY5Y cells, reducing the concentration of protons in the cytosol, thus protecting against intracellular acidification related stress. Furthermore, researchers from UCL recently raised the point that it is the intracellular pH drop but not the mitochondrial membrane depolarisation inducing the PINK1/Parkin-mediated mitophagy [158]. Their conclusion adds a critical link to the findings in this study. Specifically, that the pH protecting effect mediated by the upregulation of aerobic glycolysis (by kenpaullone) prevents Parkin recruitment.

The interplay of glycolysis and mitochondrial respiration is complicated and crucial for cell survival[159]. This study proposes that when cells face severe mitochondrial stress, the extra upregulated glycolysis by kenpaullone may work to produce the excess energy for the emergent demand of cells to help overcome the situation and avoid mitochondria-related stress, as well as against cellular acidification related damage.

Pharmacological mechanisms underlying the effects of kenpaullone on mitochondrial activity and cellular metabolism

Kenpaullone is a potent inhibitor of GSK-3 β and CDK1/cyclin B, with IC₅₀s of 23 nM and 0.4 μ M. It also inhibits CDK2/cyclin A, CDK2/cyclin E, and CDK5/p25 with IC₅₀s of 0.68 μ M, 7.5 μ M, 0.85 μ M, respectively [160]. GSK-3 β and CDKs have been shown to regulate mitochondrial activities, and their disruption or overactivity may also cause neurodegenerative diseases. Thus, the inhibition of the effective targets could be the mechanism underlying the protective effects of kenpaullone reported [109] [110] [111] [112].

GSK-3 β

GSK-3 β might be the target that mediates the effect of kenpaullone from the mPTP point of view. A report suggests that the inhibition of GSK-3 β might mediate the activation of the Wnt signalling pathway and thus prevent mPTP opening [161]. Moreover, GSK-3 β inhibition reduces the binding of two key mPTP components, ANT and cyclophilin D (CyP-D), preventing the opening of mPTP [162]. Furthermore, GSK-3 β inhibition also delays the opening of mPTP through dephosphorylation of voltage-dependent anion channel (VDAC), another mPTP

component, in response to oxidative stress [163]. All the evidence supports the positive roles of GSK3 inhibition in preventing the mPTP opening. Thus, kenpaullone might work to stabilise the mPTP by inhibiting GSK3, reducing the depolarisation of the mitochondrial membrane potential, further preventing Parkin recruitment, and protecting the cell's health.

GSK-3 β could be the target mediating the effect of kenpaullone from the cellular metabolic point of view. GSK3 is suggested to negatively regulate glucose metabolism[164]. GSK3 downregulated by mTOCR1 was shown to inhibit the expression of glycolytic genes[165]. Activation of GSK3 inhibits glucose transport by downregulating GLUT1 expression [166] while silencing GSK3 increases glucose uptake by increasing the expression of hexokinase 2 (HK2) [167]. Both GLUT1 and HK2 [168] are crucial for glucose metabolism by glycolysis. Thus, the inactivation of GSK3 might lead to the upregulation of glycolysis by upregulating GLUT1 and HK2, given the adequate supply of glucose. This assumption is consistent with the effects of kenpaullone showing the potentially upregulated glycolysis. Besides, GLUT1 is responsible for glucose transport across the blood-brain barrier [169]. This advantage further suggests that the inactivation of GSK3 by kenpaullone could promote glucose uptake by the brain, where extra energy supplement could be provided. Moreover, GSK-3 beta is predominantly in the cytosol in most cells but is partially localised to mitochondria in SHSY-5Y cells, and this form of GSK-3 beta has greater activities

than the cytosolic form [170]. This reason might contribute to the observed more significant difference in glycolysis between kenpaullone-treated cells and control in SH-SY5Y cells than in H4 cells.

Furthermore, from the mitochondria-endoplasmic reticulum (ER)- contact (MERC) point of view, GSK-3 inhibition by kenpaullone could protect the cells under stress. MERC is crucial for mitochondrial fission, mitophagy and other activities requiring contact between mitochondria and ER. Mitochondrial fission is driven by dynamin-related protein 1 (DRP1), whose localisation to the mitochondrial outer membrane (OMM) before activation is accurately regulated by MERC [171]. It is known that DRP1-dependent fission is required for PINK1/Parkin-mediated mitophagy [172] [173]. It is also known that PINK1 and Parkin accumulate at the MERC sites to promote mitophagy [174]. It is, therefore, rational to suggest that disruption of MERC could lead to severely dysregulated signalling for mitophagy [175] [176]. Activation of GSK-3 beta disrupts the interaction of VAPB and PTPIP51, the MERC proteins [177], facilitating MERC destabilisation [178] and thus disrupting mitochondrial fission and mitophagy. In this way, inhibition of GSK-3 beta by kenpaullone would help maintain the MERC, facilitating fission or mitophagy when there is a requirement by the cells. This action does not go against the observation that kenpaullone-treated cells were resistant to mitochondrial fragmentation and mitophagy initiation following the CCCP challenge, as the mitochondrial network was maintained in healthy

conditions even facing stress.

CDK1 and CDK2

From the perspective of mitochondrial activity, CDK1 inhibition may contribute to parts of kenpaullone's effects shown in this study. Cyclin B1/CDK1 has been shown to regulate the cell cycle-regulated mitochondrial fission via phosphorylating and activating DRP1 [87]. Thus, the potential fission (shown by mitochondrial fragmentation) resistant effect from kenpaullone might be contributed by CDK1 inhibition. Moreover, CDK1 could chase ATP production from mitochondria to facilitate G2 /M transition[90] and DNA repair[93]. Thus, the mitochondrial ATP-OCR drop from kenpaullone-treated H4 cells observed, if true, could be the result of CDK1 inhibition. However, no ATP drop being apparent in SHSY-5Y cells makes this unlikely, but this could be due to the combined results of ATP upregulation from other pathways in SH-SY5Y cells.

However, from the perspective of glycolysis, CDK1 and CDK2 are unlikely to mediate the effects of kenpaullone shown in this study. Aerobic glycolysis is extensively required for cancer cell proliferation; CDK1 and CDK2 are the primary cell cycle regulators with paired cyclins to mediate cell proliferation. Therefore, CDK1 and CDK2 might be associated with the regulation of glycolysis. Indeed, during the cell cycle progression, CDK1/cyclin B and CDK2/cyclin E are required to activate a series of glycolytic enzymes to drive different cell cycle

phases, especially in the G1 phase as the 'energy boost' required for G1/S transition [179]. For example, the activation of CDK2 is associated with HK2 upregulation in cancer-associated fibroblasts (CAFs) and promotes the aerobic glycolysis for G1/S transition [180]. Moreover, the positive association of CDK1 and glycolysis has also been reported to mediate the protective role of the 6-phosphofructo-2-kinase/fructose-2,6-bisphosphatase (PFKFB3) in neurons [181]. From these points of view, the positive CDK1/CDK2-glycolysis relationship might counter the observed upregulation of glycolysis by kenpaullone's CDK1/2 inhibitory effect. This contradiction points out that the glycolysis up-regulatory effect from inhibition of other targets by kenpaullone is more potent than the down-regulatory effect from inhibition of CDK1/2.

In addition, from the perspective of MERC, CDK1 might not be an effective target mediating kenpaullone's actions seen. Oxidative-stress-induced CDK1/Cyclin B1 activation impairs MERC [182], which could lead to impaired fission and dysfunctional mitophagy, leading to damaged mitochondrial network. Thus, improvement in the mitochondrial network mediated by kenpaullone is unlikely to be due to the inhibition of CDK1.

CDK5

CDK5 might mediate the effects of kenpaullone observed in this study from many

aspects. The first and direct link is that CDK5 phosphorylates and activates Parkin for ubiquitylation [183]. Thus, downregulated phosphorylation of Parkin by inhibition of CDK5 affects its ubiquitylation which directly leads to negatively regulated Parkin recruitment activity as shown with kenpaullone treatment. Furthermore, stress-induced CDK5 activity would enhance autophagy [184]. Autophagy was shown to be mediated by CDK5 phosphorylation of endophilin B1 [185]. Endophilin B1 is required for outer mitochondrial membrane maintenance [186] and mediating the link between the damaged mitochondria and phagophores during Parkin-mediated mitophagy [187]. This positive association of CDK5 and Parkin-mediated mitophagy might suggest that CDK5 inhibition by kenpaullone would lead to negatively regulated Parkin recruitment. Moreover, phosphorylation of DRP1 by p25-activated CDK5 could lead to excessive fission in the MPTP-induced PD model [188], dopaminergic toxicity study [189] and many others [190] [191] [192]. Thus, inhibition of CDK5/p25 by kenpaullone could reduce DRP1 activation, thus preventing DRP1- dependent fission, consistent with the observation.

To sum up, it is suggested that the protective actions of kenpaullone described in this study may be due to it differentially inhibiting GSK3 and CDKs.

Summary

This study suggests that kenpaullone might primarily prevent CCCP-induced mitochondrial membrane depolarisation by inhibiting the opening of the mPTP. It also suggests that kenpaullone might inhibit PINK1/Parkin signalling through the mitochondrial fission-preventing manner. This study highlights the potential that kenpaullone could be cell protective against mitochondria-related oxidative stress, thus serving as a promising candidate for PD treatment. Effects of kenpaullone observed in this study suggest that the drug compound has the potential for mitochondrial protection by mPTP stabilising and fission prevention and cellular acidification prevention by upregulation of glycolytic activities. Given the potentially cell-protective effects identified and analysed, there is a strong possibility that kenpaullone could serve as a promising therapeutic candidate for PD treatment by preventing mitochondrial dysfunction and oxidative stress-related neuronal cell death in the disease pathogenesis. More studies on its protective effects in the PD models and the underlying mechanisms need further investigation to reach a more comprehensive conclusion.

Chapter4 Assessing the mechanism of action and therapeutic potential of selected GSK3 α / β and CDK inhibitors that target mitochondrial function

Introduction

Kenpaullone, a GSK3 α / β and CDK inhibitor, was shown to act as a mitochondrial modulator inhibiting Parkin recruitment following CCCP-induced mitochondrial depolarisation and enhancing the mitochondrial network (detailed in chapter 3). These observations suggest that studying drugs that target GSK3 α / β and CDKs may give an insight into the mechanism governing mitochondrial quality control pathways and may lead to the discovery of drugs useful in treating Parkinson's disease. Compounds that acted similarly to kenpaullone, had better pharmacodynamic properties and were being used in preclinical/clinical studies were therefore identified and studied further.

Drugs that act as GSK3 α / β and CDK inhibitors include AZD5438, AT7519, alsterpaullone and 1-azakenapaullone. AZD5438 and AT7519 were identified in a kinase screen and found to inhibit CDK pathways with stronger potency than kenpaullone, and additional research on cochlear explants showed they both protected against cisplatin-induced ototoxicity[101]. AZD5438 also has a

favourable pharmacologic profile, including more favourable drug absorption, distribution, and penetrance properties [193] [194]. A study of paullone compounds showed that kenpaullone, alsterpaullone and 1-azakenapaullone protected podocytes primarily suppressing GSK3 β and inhibiting apoptosis [114].

In a small-molecule screen to identify drugs for the treatment of ALS, kenpaullone and TRO19622 were found to protect human motor neurons (MNs) from trophic support withdrawal[111]. TRO19622 was shown to target the mitochondrial permeability transition pore (mPTP), an action that kenpaullone is also thought to mediate[100]. Dexamipexole, is the enantiomer of TRO19622 and was found to mediate positive effects on brain mitochondrial conductance and bioenergetic efficiency and was therefore also studied [195, 196]. An overview of compounds and descriptions are shown in **Figure 4-1**.

	Compound	Description
CDKs/GSK Inhibitors	Kenpaullone	Inhibitor---Main: CDK1/cyclin B and GSK-3 β Less : CDK2/cyclin A, CDK2/cyclin E, and CDK5/p25
	AZD5438	Inhibitor---Potent: CDK1/2/9 Less: GSK3 β , CDK5 and CDK6
	AT7519	Inhibitor---Potent: CDK1, CDK2, CDK4 to CDK6, and CDK9 Less:GSK-3 β
	1-azakenapaullone	Inhibitor--GSK-3 β
	Alsterpaullone	Inhibitor---Potent: CDK1/cyclin B, CDK2/cyclin A, CDK2/cyclin E and CDK5/p35 Less: GSK-3alpha/GSK-3beta
Neuro-protective	TRO 19622	Decrease axonal degradation, enhance the rescue of motor nerve conduction in peripheral neuropathy.
	Dexamipexole	A treatment of amyotrophic lateral sclerosis (ALS) based partly on enhanced brain mitochondrial function.

Figure 4-1 Overview of compounds chosen to study in two categories and their description. CDKs/GSK inhibitors shown in green and potential neuroprotective compounds shown in blue.

Aims

Experiments described in this chapter were conducted to investigate the function and therapeutic potential of alsterpaullone, 1-azakenapaullone, AZD5438, AT7519, dextramipexole (KNS-760704) and olesoxime (TR019622). To achieve this, assays to measure, parkin recruitment, mitochondrial morphology and DNA content and neuroprotection assays were conducted. The pathway by which the compounds mediate their effects were also investigated by selectively inhibiting either the GSK3 β or CDK pathways.

Results

Primary validation: investigating the actions of the selected GSK3 α/β and CDK inhibitors on Parkin recruitment and the mitochondrial network

Selected GSK/CDKs inhibitors have the similar effects on Parkin recruitment following the CCCP challenge as kenpaullone

Dose-response curves for the compounds were carried out, and cell viability and Parkin recruitment activity were measured in eGFP-Parkin H4 cells. The dose range used was based on findings from previous experiments and those reported in the literature. Kenpaullone was used at the dose of 5 μ M and acted as a positive control to ensure the assay was working properly and provide a reference point.

AT7518, AZD5438 and alsterpaullone were shown to reduce the cells count at doses above 1 μ M (**Figure 4-2 to Figure 4-7**), while the alsterpaullone, 1-azakenapaullone, TRO19622 and Dexpramipexole did not affect the cell viability within the given dose. The reduction in cell number was most likely associated with the CDK-mediated inhibition of cell division rather than cell death via toxicity, as cell/nuclei morphology was not altered, and there was no cell detachment. A lower dose range was later used to keep the cell number above 75% of the control group, as shown in (**Figure 4-8 B**).

The Parkin recruitment activity triggered by CCCP was inhibited by AZD5438, AT7519, alsterpaullone and 1-azakenapauellone, but not TRO19622 or Dexpramipexole. AZD5438 showed the most potent effect on the change of Parkin total area per cell.

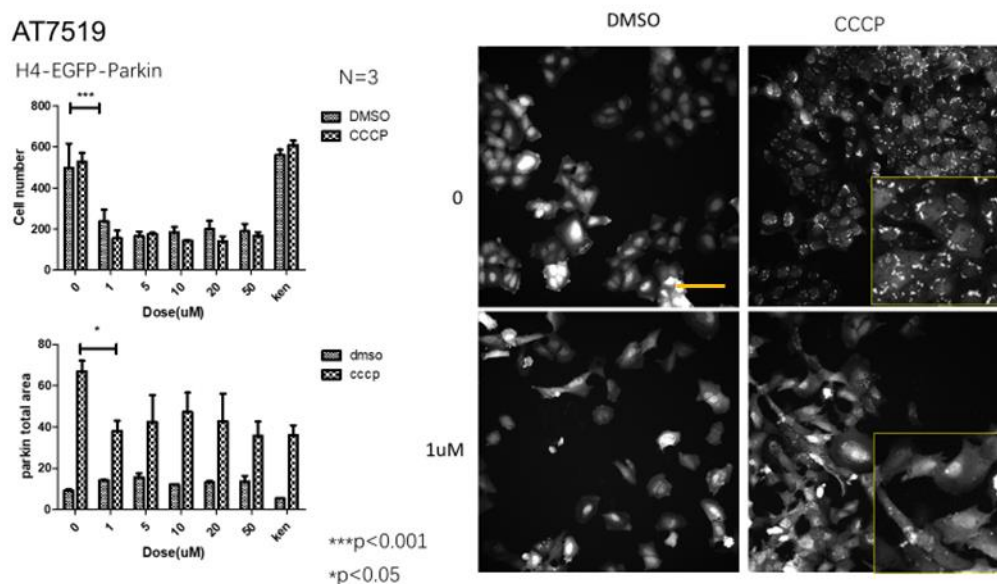


Figure 4-2 AT7519 inhibits CCCP-induced Parkin recruitment

Bar graphs show compound actions on cell count(top) and Parkin total area per cell(bottom) from INCell; representative images captured by INCell following the CCCP challenge after cells were pre-treated with compound for 24h are shown. Cell counts started to decrease significantly from 1 μ M AT7519 treatment, and at that dose, a significant drop in Parkin total area started to appear. The greyscale images show single-channel images for visualising eGFP-Parkin change at the treatment dose image. The compound reduced the Parkin puncta total area induced by CCCP. Statistical analysis was carried out by a two-way ANOVA test. N=3 plates, data is displayed as mean \pm SEM. The significance is displayed for the lowest dose groups. * p<0.05.***p<0.001.

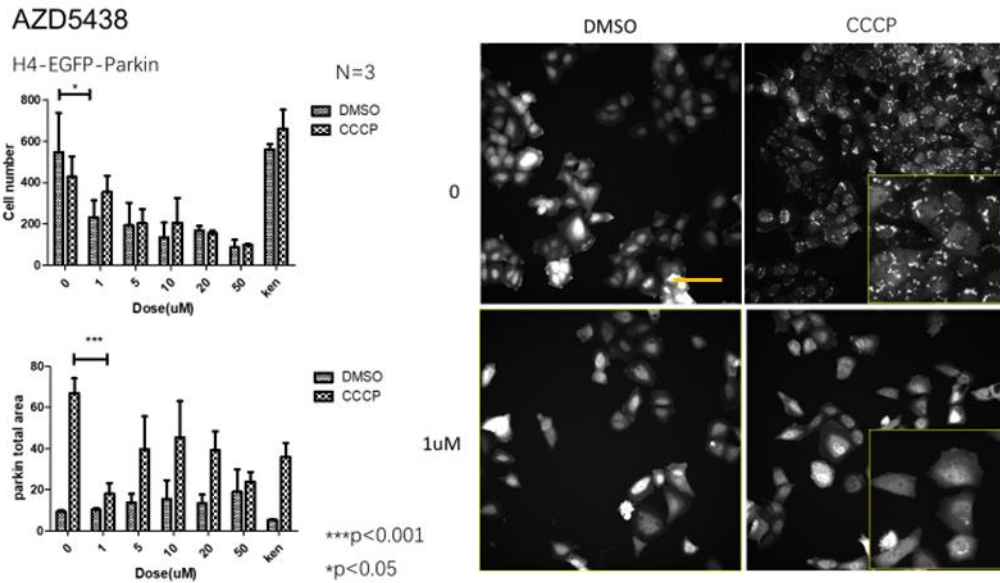


Figure 4-3 AZD5438 inhibits CCCP-induced Parkin recruitment

Bar graphs show compound actions on cell count(top) and Parkin total area per cell(bottom) from INCell; representative images captured by INCell following the CCCP challenge after cells were pre-treated with compound for 24h are shown. Cell counts started to decrease significantly from 1 μ M AZD5438 treatment, and at that dose, a significant drop of Parkin total area started to appear. The greyscale images show single-channel images for visualising eGFP-Parkin change at the treatment dose image. The compound reduced the Parkin puncta total area induced by CCCP. Statistical analysis was carried out by a two-way ANOVA test. N=3 plates, data is displayed as mean \pm SEM. The significance is only displayed for the lowest dose groups. * p<0.05.***p<0.001.

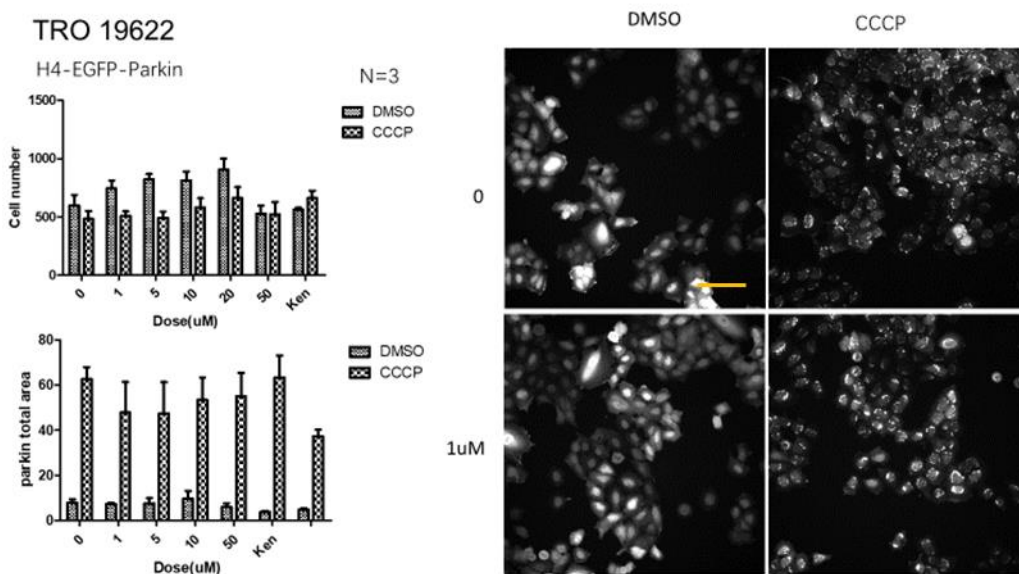


Figure 4-4 TRO19622 does not regulate CCCP-induced Parkin recruitment

Bar graphs show compound actions on cell count(top) and Parkin total area per cell(bottom) from INCell; representative images captured by INCell following the CCCP challenge after cells were pre-treated with compound for 24h are shown. There was no change both regarding cell count and Parkin total area. The greyscale images show single-channel images for visualising eGFP-Parkin change at the treatment dose image. There were no clear differences when treated with TRO19622, no significance based on the two-way ANOVA test. N=3 plates.

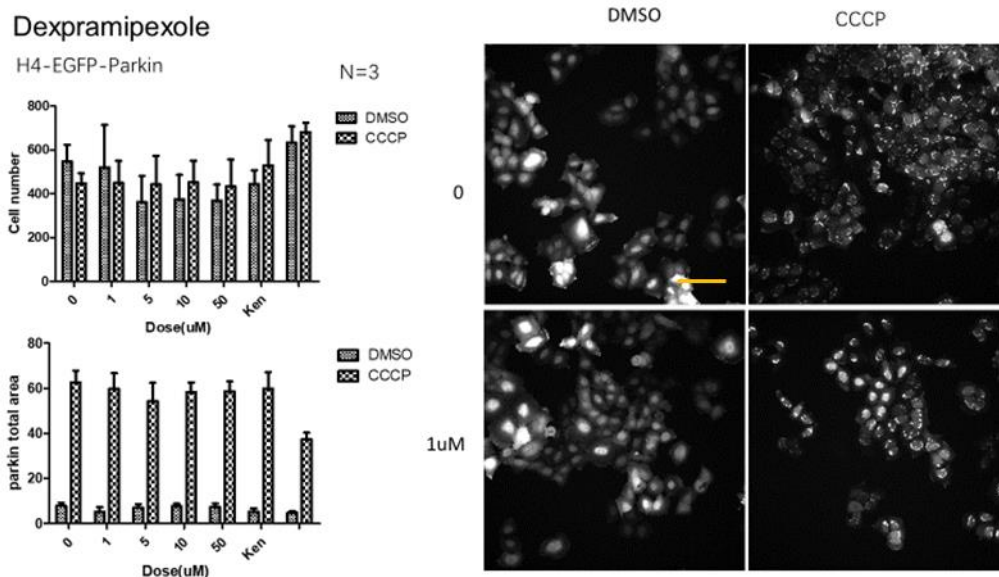


Figure 4-5 Dexpramipexole does not regulate CCCP-induced Parkin recruitment

Bar graphs show compound actions on cell count(top) and Parkin total area per cell(bottom) from INCell; representative images captured by INCell following the CCCP challenge after cells were pre-treated with compound for 24h are shown. There was no change both regarding cell count and Parkin total area. The greyscale images show single-channel images for visualising eGFP-Parkin change at the treatment dose image. There were no clear differences when treated with dexpramipexole, no significance based on the two-way ANOVA test. N=3 plates.

1-azakenpaullone

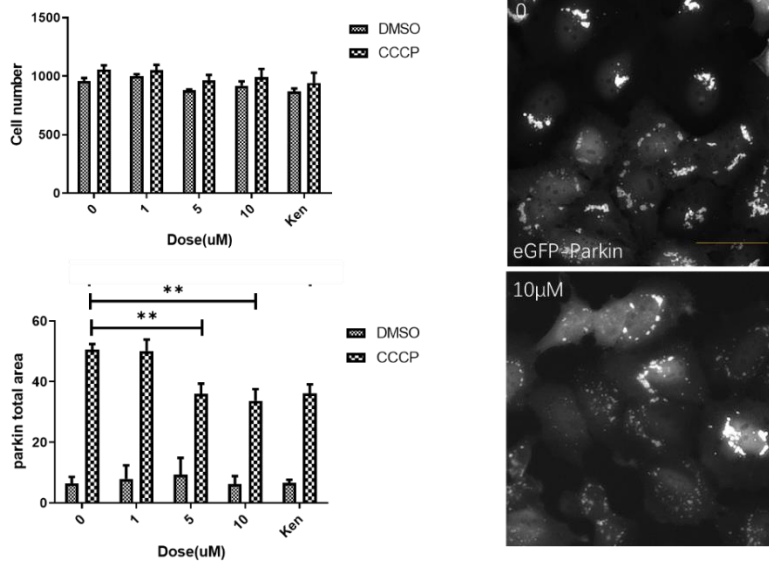


Figure 4-6 1-azakenpaullone inhibits CCCP-induced Parkin recruitment

Bar graphs show compound actions on cell count(top) and Parkin total area per cell(bottom) from INCell; representative images captured by INCell following the CCCP challenge after cells were pre-treated with compound for 24h are shown. No change in cell counts was recorded in the given dose range while the Parkin total area started to decrease significantly from 5µM 1-azakenpaullone treatment. The greyscale images show single-channel images for visualising eGFP-Parkin change compared to CCCP, which was given a 10µM compound treatment. Scale bar=50µm. The compound slightly reduced the Parkin puncta total area induced by CCCP. Statistical analysis was carried out by a two-way ANOVA test. N=3 plates, data is displayed as mean ± SEM, significance is displayed. ** p<0.01.

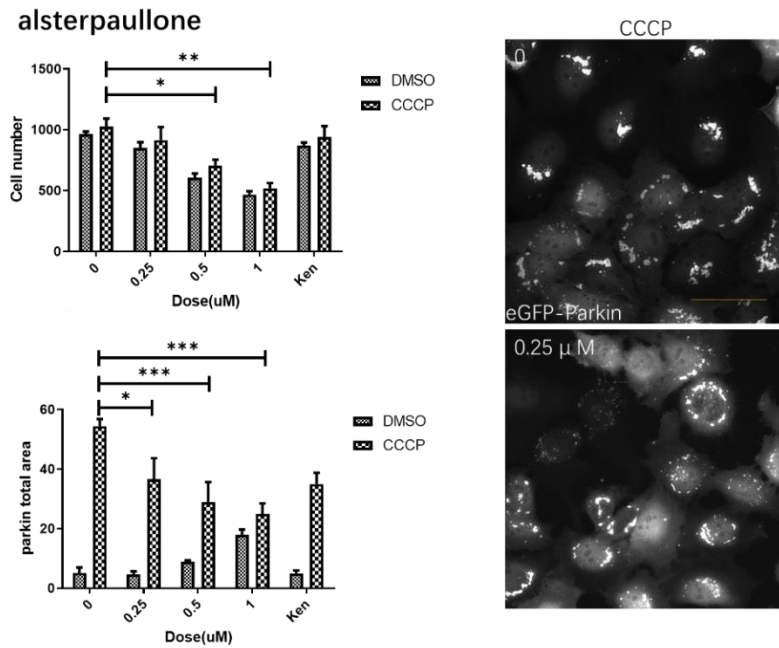


Figure 4-7 Alsterpauellone inhibits CCCP-induced Parkin recruitment

Bar graphs show compound actions on cell count(top) and Parkin total area per cell(bottom) from INCell; representative images captured by INCell following the CCCP challenge after cells were pre-treated with compound for 24h are shown. Cell counts started to decrease significantly from 0.5uM alsterpauellone treatment and 0.25uM dose, and a significant drop in Parkin total area started to appear. The greyscale images show single-channel images for visualising eGFP-Parkin change compared to CCCP given 0.25uM compound treatment. Scale bar=50um. The compound slightly reduced the Parkin puncta total area induced by CCCP. Statistical analysis was carried out by a two-way ANOVA test. N=3 plates, data is displayed as mean ± SEM, significance is displayed. * p<0.05. ** p<0.01, ***p<0.001.

Selected GSK/CDKs inhibitors have similar effects on the mitochondrial network following the CCCP challenge as kenpaullone

The action of alsterpaullone, 1-azakenapauillone, AZD5438, AT7519, dexpramipexole (KNS-760704) and olesoxime (TR019622) on the mitochondrial network and morphology were assessed by INCell imaging and analysis (as described previously in chapter 3).

The results (**Figure 4-8**) show: 1) CCCP triggered the formation of giant mitochondrial clusters close to the nuclei. This caused the mitochondrial network to shrink. Moreover, mitochondria damage was associated with them becoming rounded in shape rather than their normal elongated form. 2) AZD5438, AT7519 and alsterpaullone significantly increased the total mitochondrial area compared to controls, and they prevented the CCCP-induced mitochondria network degradation. 3) AZD5438, AT7519 and 1-azakenapauillone inhibited the change in the mitochondrial shape associated with CCCP induced damage. 4) Treatment with dexpramipexole (KNS-760704) and olesoxime (TR019622). azakenapauillone did not inhibit CCCP-mediated changes to the mitochondrial network.

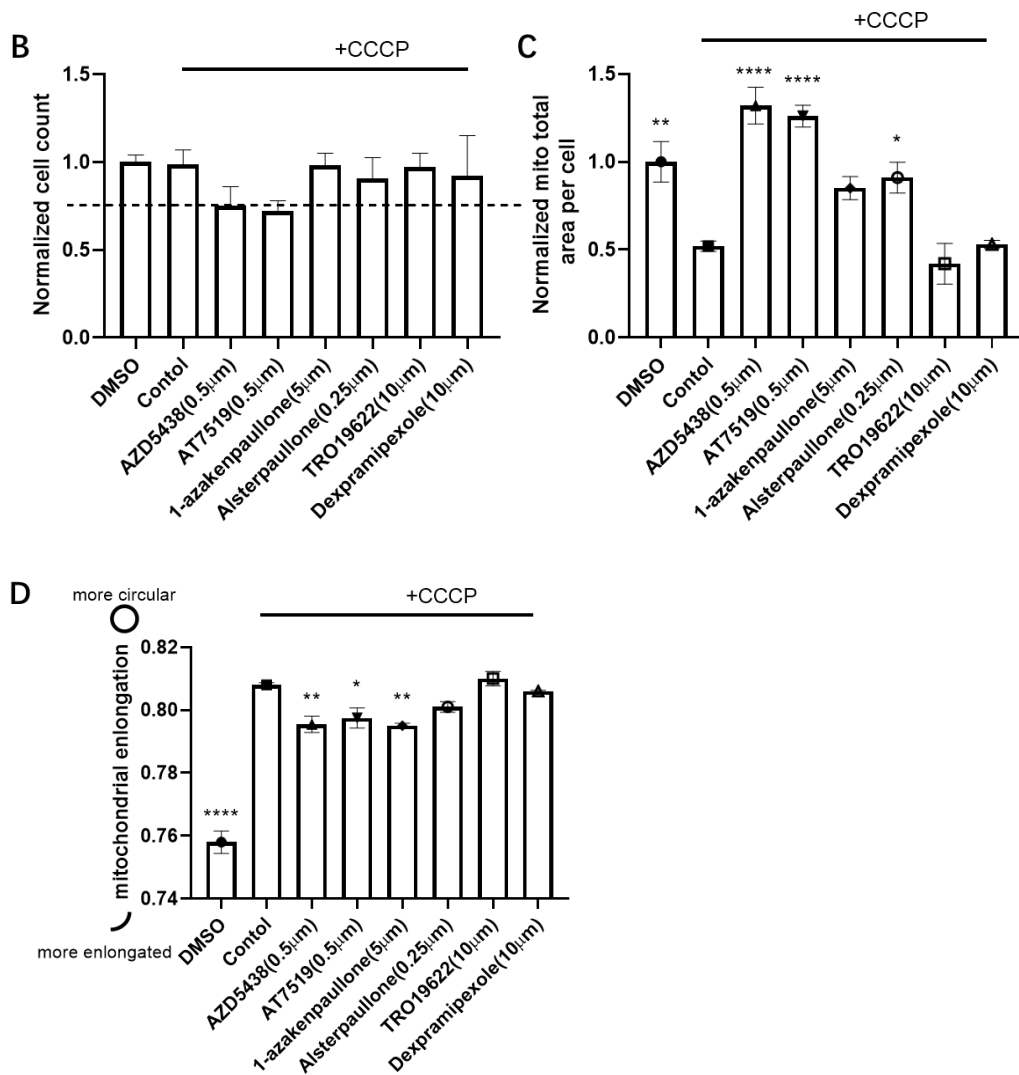
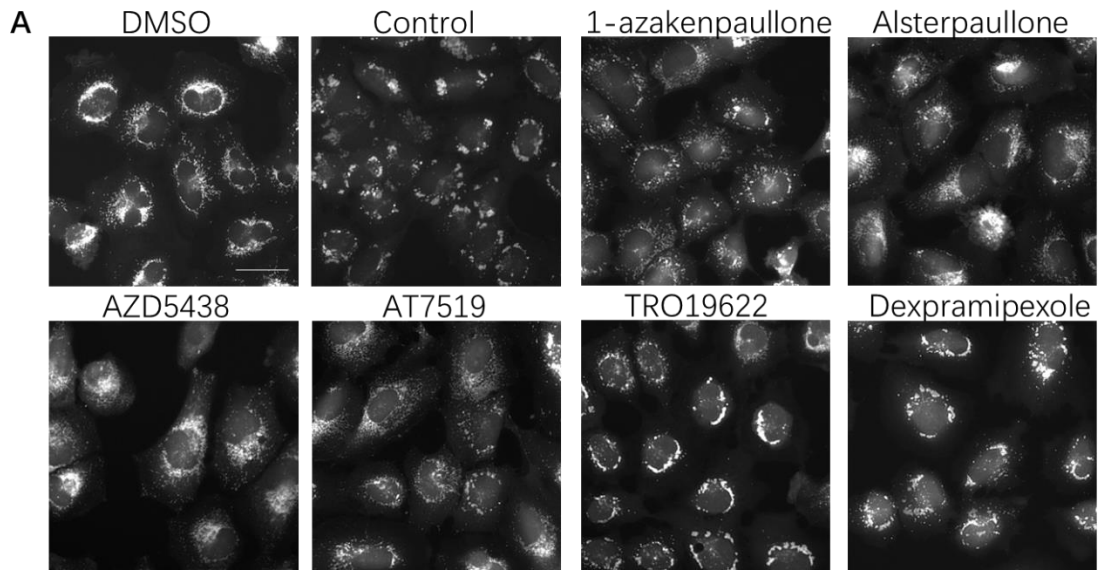


Figure 4-8 Mitochondrial network following pre-treatment with selected GSK/CDKs inhibitors in eGFP-Parkin H4 cells

Images were captured and analysed with INCell 2200, statistical analysis was performed using GraphPad Prism. **A)** Images showing mitochondria in the cells after 2h CCCP were applied following 24h compound pre-treatment, presented as DMSO (negative control without CCCP), control (positive control with CCCP only) and compound (with CCCP). After group one compounds pre-treatment, the mitochondrial network of cells looks more like the no-CCCP control with evenly distributed mitochondrial network and few or no clusters shown, while group two compounds have less spread mitochondrial network following CCCP treatment. Scale bar=50µm. **B)** It shows all cells count above 75% of control with compound treatment at the given doses, the dashed line indicates the value of 0.75. **C)** DMSO was used as the baseline value for the normalisation. AZD5438, AT7519 and alsterpaullone significantly increased the total mitochondrial area compared to non-drug control. **D)** AZD5438, AT7519 and 1-azakenpaullone had a significant effect on decreasing the mitochondrial elongation compared to non-drug control following CCCP treatment. Statistical analysis was carried out by one-way ANOVA test with Sidak's multiple comparisons test to control. n=3, data is displayed as mean ± SEM. *p<0.05, ** p<0.01, **** p<0.0001.

AZD5438 prevents mitochondrial membrane potential loss induced by CCCP

To investigate effects on mitochondrial membrane potential TMRM was used. TMRM is a widely used cell-permeant dye absorbed by active mitochondria, while its accumulation ceases and signal decreases as mitochondria lose membrane potential. Unlike the analysis used to measure Mitotracker, the analysis of TMRM was based on intensity rather than the area of staining, as its intensity with depolarised mitochondria was below the threshold for the established INCell segmentation protocol and the TMRM intensity was assessed in the whole cytoplasm area (green channel). The results using the TMRM dye are shown in **Figure 4-9** and support the previous finding that alsterpaullone, 1-azakenapaullone, AZD5438, AT7519 maintain mitochondrial membrane potential following CCCP disruption.

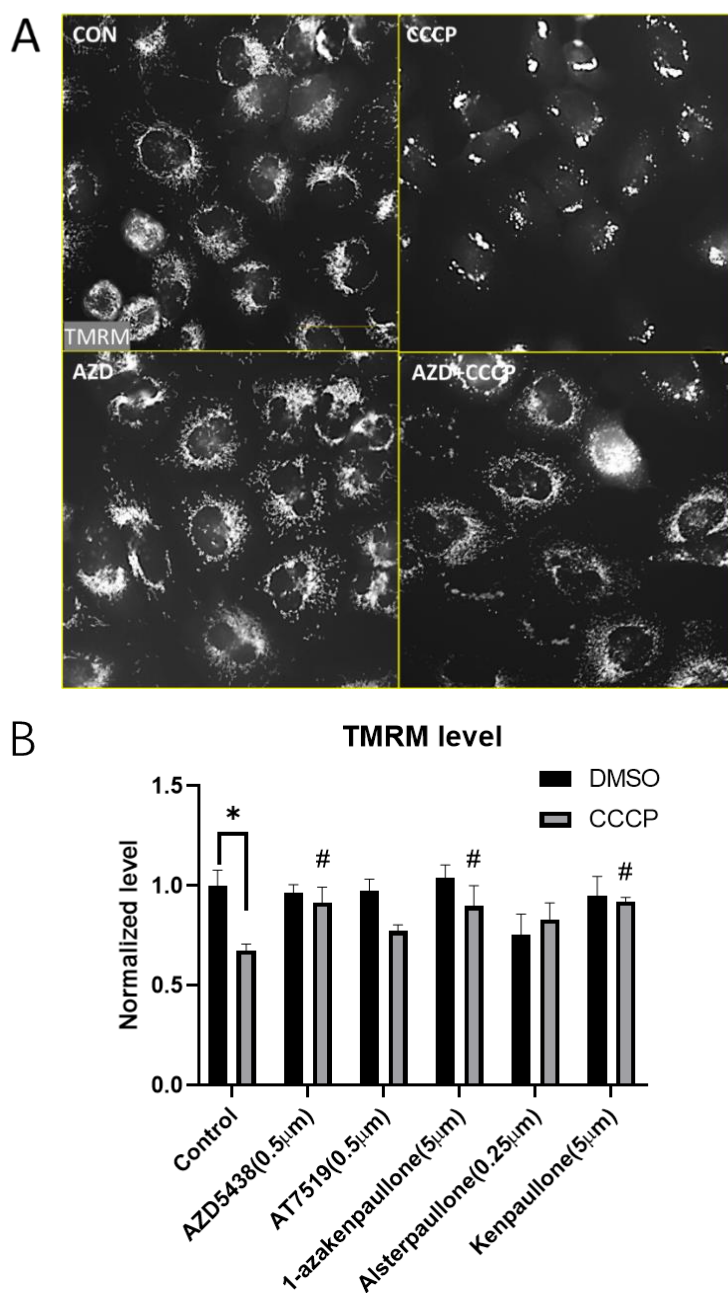


Figure 4-9 Images and analysis results of compounds investigated for mitochondrial membrane potential change using TMRM dye.

A) Representative images from INCell 2200 show 24h AZD5438 pre-treatment prevented the staining loss following 2h CCCP treatment. Scale bar=50µm. B) Bar graph shows the significant ($p=0.0240$) loss in TMRM level were significantly prevented by pre-treatment of AZD5438($p=0.0276$), 1-azakenpauillone($p=0.0415$) and kenpauillone ($p=0.0229$). The data shown have been normalised to DMSO control. Statistical analysis was carried out by two-way ANOVA test with Sidak's multiple comparisons test. $n=3$ plates, data is displayed as mean \pm SEM. * $p<0.05$. Asterisks denote comparisons between negative (DMSO) and positive (CCCP) control, hashes denote comparisons between positive control and experimental group (CCCP).

AZD5438 prevents the mitochondrial DNA loss induced by CCCP

Mitochondrial activity has a direct effect on the distribution and maintenance of their mtDNA [197]. For example, mitochondrial biogenesis may increase the relative mtDNA content while mitochondrial degradation activity will decrease mtDNA levels. To access mtDNA content, a real-time PCR-based mtDNA assay was applied to examine the relative mtDNA change compared to nuclear DNA, as described in the methods chapter [198].

Initially, all the GSK/CDK inhibitors were investigated, and the results are shown in **Figure 4-10 A**. Although no significant effect of drugs was observed, the results showed a trend towards a reduction in mtDNA following 2h CCCP and AZD5438 mediated a trend towards an increase in mtDNA content. AZD5438 was chosen for a more focused study to eliminate the interference from technical issues, such as DNA conditions affected by a relatively long extraction procedure associated with the testing of multi-samples. Following 6h CCCP treatment there was a significant decrease in mtDNA content (**Figure 4-10 B**) associated with the mitochondrial degradation. The data in **Figure 4-10 B** also that pre-treatment with AZD5438 alone mediated a significant increase in the relative mtDNA content.

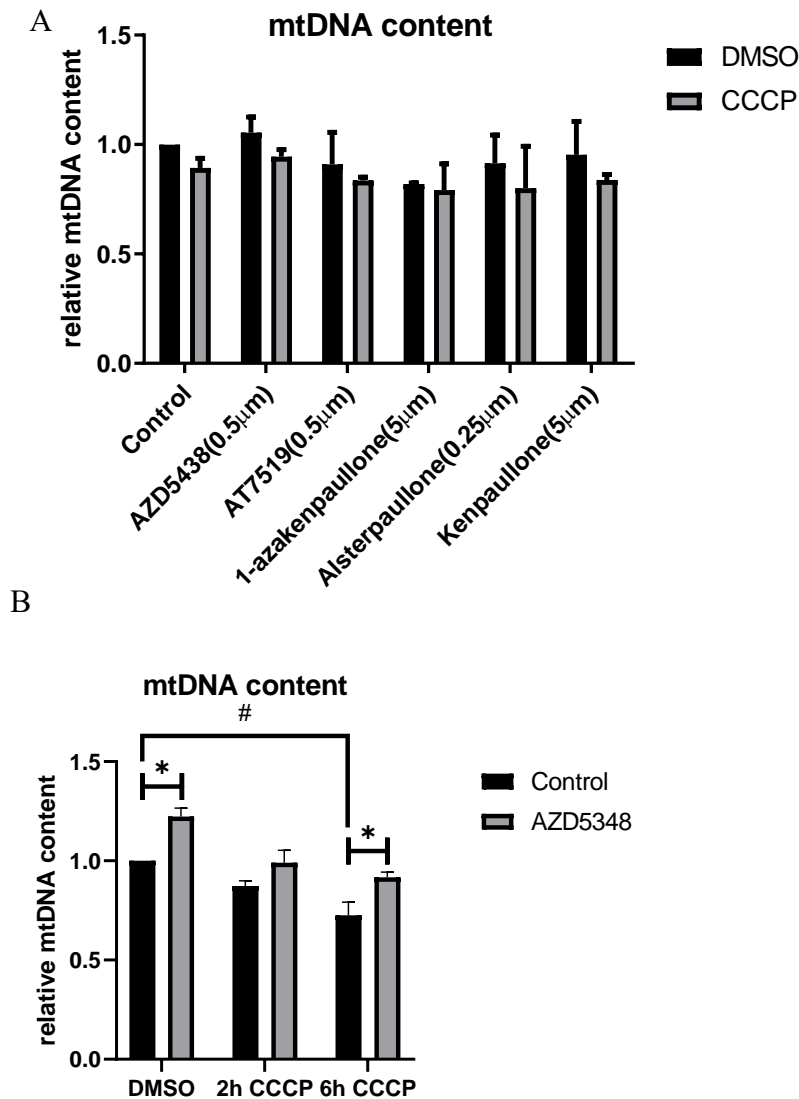


Figure 4-10 Relative mtDNA content following pre-treatments of GSK3/CDKs inhibitors

A) The graph shows relative mtDNA content change when pre-treated with compounds for 24h and followed by 2h CCCP treatment. The trend shows 2h CCCP triggered the mtDNA content reduction; AZD5438 increased the mtDNA content but was insignificant. B) The graph shows relative mtDNA content change when pre-treated with 0.5 μ M AZD5438 for 24h and then maintained for 6h, maintained for 4h then another 2h CCCP and treated with CCCP for 6h before harvest, respectively. It shows AZD5438 treatment increased the relative mtDNA content significantly ($p=0.0115$) after the treatment of 30h(24+6h); 6h CCCP reduced the relative mtDNA content significantly ($p=0.0127$); and which was shown to be significantly ($p=0.0287$) prevented by AZD5438. Statistical analysis was carried out by a two-way ANOVA test with Sidak's multiple comparisons test. $n=3$ (both A and B), data are displayed as mean \pm SEM. * $p<0.05$. Asterisks denote comparisons between no compound control and AZD5438 treatment, hashes denote comparisons between no CCCP control and CCCP treatment.

Investigating the protective actions of AZD5438 against the mitochondrial toxin rotenone

AZD5438 protects the cell viability in the cellular PD model

The primary validation study of compounds showed that AZD5438 had the most potent effects on regulating Parkin recruitment and mitochondrial network. It also revealed that AZD5438 increased mtDNA levels. To evaluate the neuroprotective actions of AZD5438 and the other selected compounds, cells were treated with rotenone, a mitochondrial complex I inhibitor.

Treatment with rotenone reduced the viability of human eGFP-Parkin H4 cells by around 40% at a dose of 500nM, and 500nM AZD5438 inhibited this effect(**Figure 4-11 B**). Moreover, GSK3/CDKs inhibitors, apart from 1-azakenpaullone had positive effects compared to the control following rotenone treatment. As treatment with 500nm AZD5438 slightly reduced the cell number (shown in the previous section), experiments were repeated using a 250nm dose of AZD5438. Additionally, the number of technical repeats was increased from 3 to 6 in each independent experiment to reduce errors further. Results of the MTT assays (**Figure 4-11 A**) show that the darker and more numerous dot-like staining (MTT formazan product) is associated with greater mitochondrial activity. In controls, the formation of the MTT formazan product was similar to the present in AZD5438 treatment. In contrast, significantly decreased levels of MTT formazan product

were observed following rotenone treatment, which was significantly inhibited by treatment with AZD5438. Results in **Figure 4-11 C** confirm the observation that AZD5438 significantly inhibited the toxic action of rotenone. To further assess the neuroprotective effects of AZD5438, a second mitochondrial toxin, 1-methyl-4-phenylpyridinium (MPP⁺), also associated with the aetiology of Parkinson's disease, was used. The results (**Figure 4-11 D**) show that AZD5438 significantly inhibited the toxic action of MPP⁺.

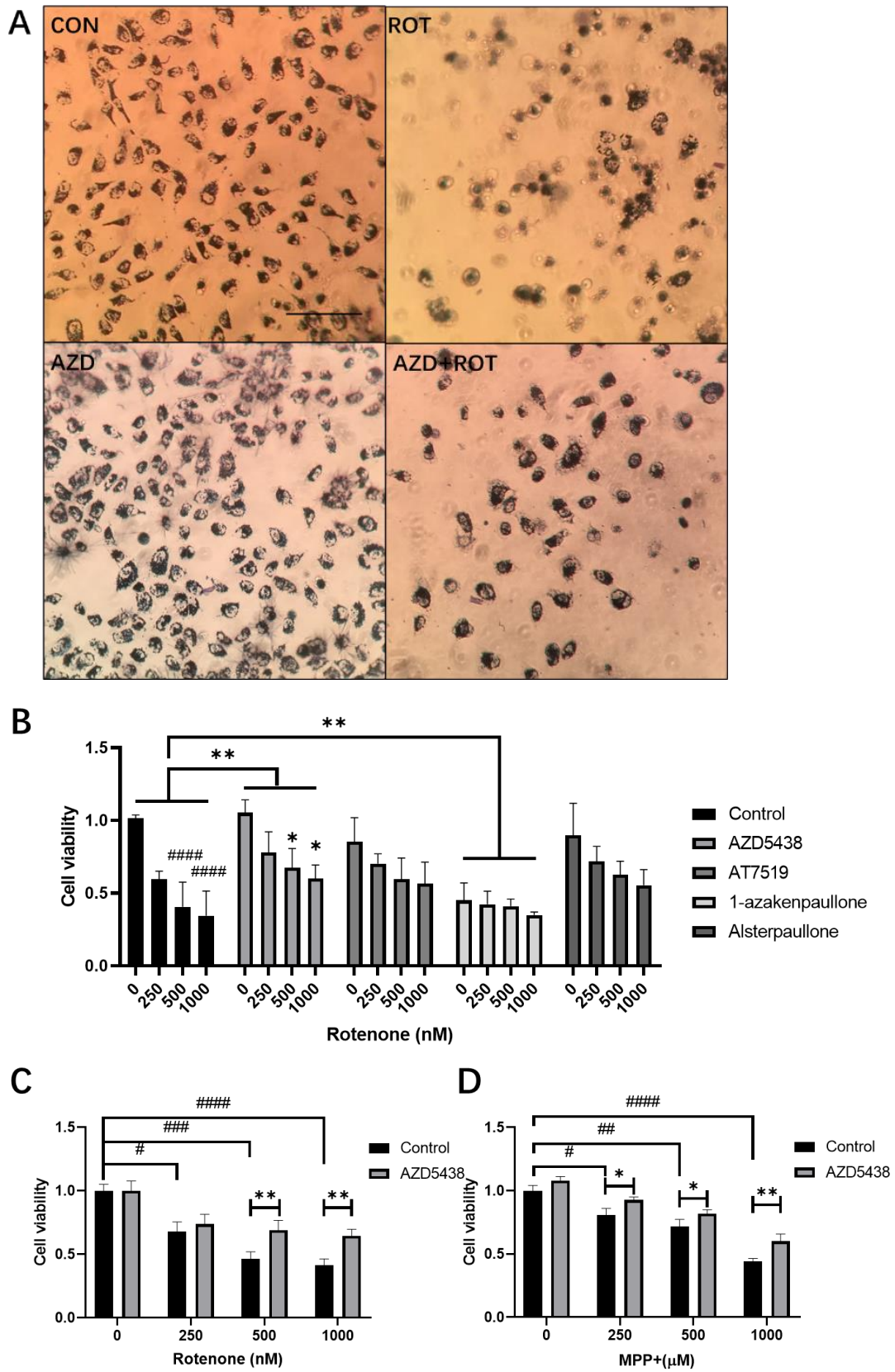
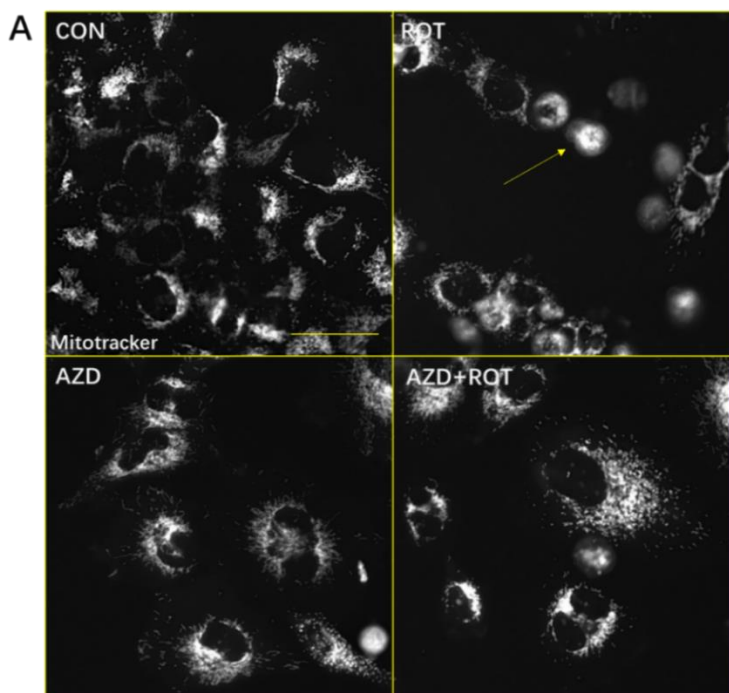


Figure 4-11 Assessing the protective effects of selected GSK/CDK inhibitory compounds following treatments with mitochondrial toxins associated with PD

A) Representative images taken under a brightfield microscope show the insoluble dark formazan appeared in cells with treatment of control (DMSO), 250nM AZD5438, 500nM Rotenone and 250nM AZD5438+500nM Rotenone, respectively. It shows less formazan in rotenone than CON, while more formazan with AZD5438+rotenone than rotenone alone. In addition, more round-up cells in rotenone than in CON, while there are fewer such cells in AZD5438+rotenone than rotenone. Scale bar=100 μ m. Scale bar=100 μ m. **B)** Bar graph shows the general performance of group one compounds through MTT-Rotenone assay. Rotenone doses were given at 0, 250, 500 and 1000nM, compounds doses were 500nM AZD5438, 500nM AT7519, 5 μ M 1-azakenpaullone and 250nM Alsterpaullone. It shows significant cell viability loss at rotenone treatment of 500nm and 1000nM alone($p<0.0001$), both of which were rescued by AZD5438, with significance as $p=0.0338$ and $p=0.0469$ respectively. The groups' significant differences are also marked between control and AZD5438($p=0.0047$) with a positive direction, 1-azakenpaullone ($p=0.0062$) with a negative direction. **C)** Bar graph shows the performance of 250nM AZD5438 through the MTT-Rotenone assay. It shows significant cell viability loss at rotenone treatment of 250 μ M ($p= 0.0188$), 500 μ M ($p= 0.0002$) and 1000 μ M ($p<0.0001$), the latter two of which were significantly rescued by 250nM AZD5438, $p= 0.0037$ and $p= 0.0032$, respectively. **D)** Bar graph shows the performance of 250nM AZD5438 through the MTT-MPP+ assay. It shows significant cell viability loss at MPP+ treatment of 250 μ M ($p=0.0137$), 500 μ M ($p=0.0018$) and 1000 μ M ($p<0.0001$), all were rescued by 250nM AZD5438 significantly ($p= 0.0147$, $p= 0.0352$ and $p= 0.0022$). Statistical analysis was carried out by two-way ANOVA test with Dunnett's multiple comparisons test (B) and Tukey's multiple comparisons test (B, C, D) and. N=3 plates, data is displayed as mean \pm SEM. * $p<0.05$, ** $p<0.01$, *** $p<0.001$, **** $p<0.0001$. Asterisks denote comparisons between no compound control and compound treatment, hashes denote comparisons between no stressor control and stressor treatment.

AZD5438 prevents the mitochondrial network damage associated with rotenone, a cellular model of PD

Mitochondrial network assays were performed with 500nM rotenone as the stressor. The images in **Figure 4-12 A** show that treatment with 500nM rotenone for 24hrs induced damage, indicated by the presence of many round cells and fewer cells in relatively healthy conditions. The measured mitochondrial network was damaged by rotenone; treatment with AZD5438 prevented the damage (**Figure 4-12 C**). As previously reported, AZD5438 alone also increased the total mitochondrial area (**Figure 4-12 C**). The results in **Figure 4-12 E** show single mitochondrial shape was altered by AZD5438 as the mitochondrial elongation value dropped, pointing to that the mitochondria had longer shape following AZD5438 treatment



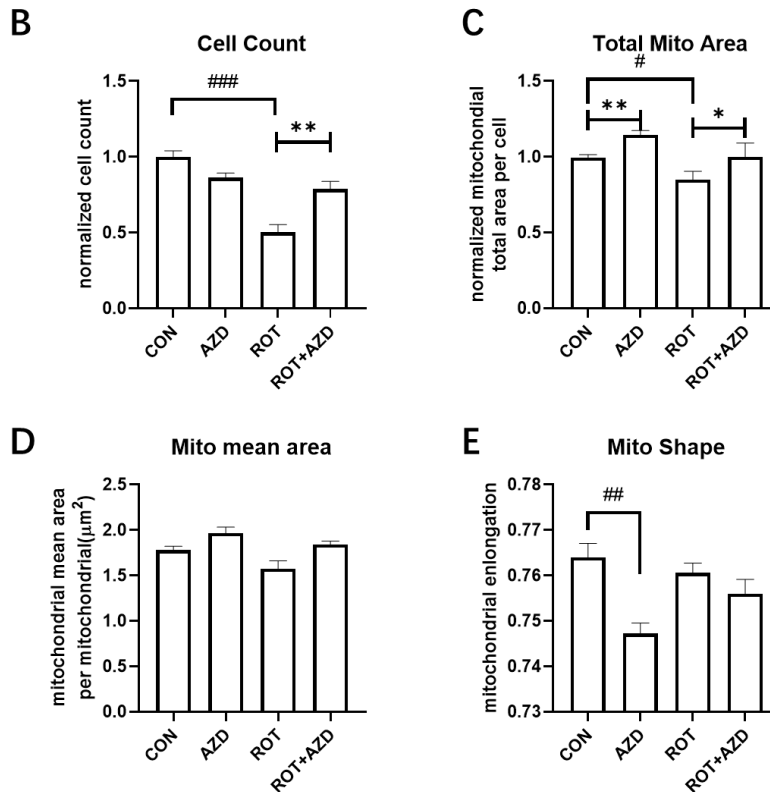


Figure 4-12 Assessing the protective effect of AZD5438 on mitochondrial morphology and network following treatments with rotenone

A) Representative images taken by INCell 2200 in greyscale showing Mitotracker stained mitochondria network change; AZD5438 alone spreads the mitochondrial network, rotenone alone shrinks it, AZD5438+rotenone increases mitochondrial network compared to rotenone alone. Arrow points to the ball-like cell with intensive staining, widely distributed in the rotenone group but barely seen in other groups. Scale bar=50 μm . **B-E)** are analysed data of images from INCell analyser. **B)** Cell count data normalised to CON shows rotenone significantly ($p=0.0002$) reduced the cell count while AZD5438+rotenone significantly ($p=0.0098$) prevented it. No significant difference between AZD5438 and CON. **C)** The total area of mitochondria per cell was significantly ($p=0.0058$) increased when cells were treated with AZD5438 compared to CON (DMSO vehicle). rotenone treatment significantly ($p=0.0387$) reduced mitochondrial total area compared to CON. AZD5438+rotenone significantly ($p=0.0228$) rescued mitochondrial total area compared to rotenone. **D)** The trend shows AZD5438 increased mitochondrial mean area and rotenone decreased it. No significant difference was marked. **E)** Mitochondrial shape became more elongated as elongation value dropped significantly ($p=0.0014$) by AZD5438 alone. Statistical analysis was carried out by two-way ANOVA test with Tukey's multiple comparisons test. $N=3$; data is displayed as mean \pm SEM, significance is displayed as * $p<0.05$, ** $p<0.01$, **** $p<0.0001$. Asterisks denote comparisons between AZD5438 and AZD5438+rotenone treatment, hashes denote comparisons between CON and treatment groups.

Rotenone has no effect on relative mtDNA content in eGFP-Parkin H4 cells

To further check AZD5438 protective effects mtDNA assays were conducted on H4 cells following treatment with rotenone. It was assumed that treatment with rotenone would lead to mtDNA damage due to DNA fragmentation or degradation. However, the results showed (**Figure 4-13**) there are no significant differences in mtDNA between rotenone and CON, nor between AZD5438+rotenone and rotenone.

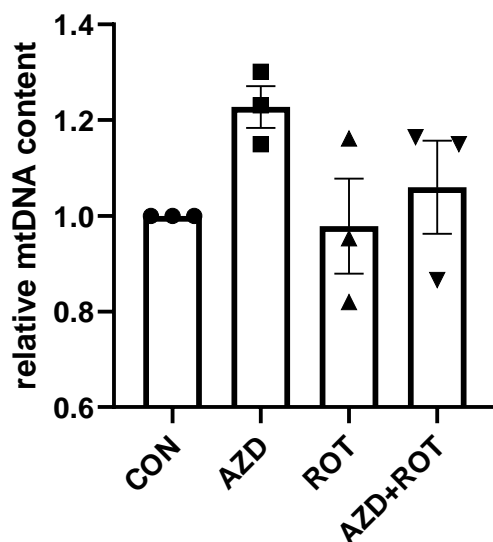


Figure 4-13 The relative mtDNA content following treatment with 250nM AZD5438 and 500nM rotenone for 24h assessed via qPCR mtDNA assay
rotenone treatment did not change the relative mtDNA content. AZD5438 increased the relative mtDNA with or without rotenone, but no significance was marked across the groups. Statistical analysis was carried out by two-way ANOVA test with Tukey's multiple comparisons test. N= 3 independent experiments; data is displayed as mean ± SEM.

AZD5438 inhibits cell death and apoptosis

To assess the mechanisms by which AZD5438 may protect cells, apoptosis assays were carried out using a flow cytometry-based assay. The live and dead cells were distinguished based on the intensity of Zombie NIR™ dye.

As shown in **Figure 4-14 A**, the density plots show that most live cells distribute in the square gate (CON), while a large population of rotenone-treated dead cells are outside the gate. Treatment with AZD5438 brings back the population into the square, while AZD5438 alone has fewer cells out of the square compared to CON. Statistical analyses of the results shown in **Figure 4-14 B** confirmed that rotenone significantly decreased the ratio of the live cells while AZD5438+rotenone significantly increased the ratio of the live cells compared to rotenone alone. AZD5438 alone did not show a significant effect on the ratio of the live cells.

The next step was to evaluate the levels of apoptosis; hence, the quadrant gate was set to show the apoptotic cell ratio based on the extremely high nuclear dye intensity in the single live cells. As shown in **Figure 4-15 A**, the density plots show that most cells distribute in the second quadrant as relatively healthy cells in CON, while a large population moves into the first quadrant as apoptotic cells in rotenone. Treated with AZD5438 brings back the population shift, while AZD5438 alone has no dramatic effect compared to CON. The statistical analysis shown in **Figure**

4-15 B confirmed that rotenone significantly decreased the ratio of the apoptotic cells while AZD5438+rotenone significantly increased the ratio of the apoptotic cells compared to rotenone alone. AZD5438 alone did not show an effect.

A Live cells ratio

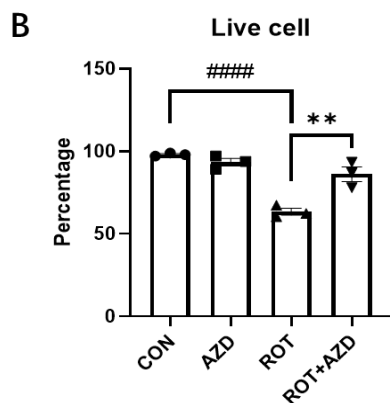
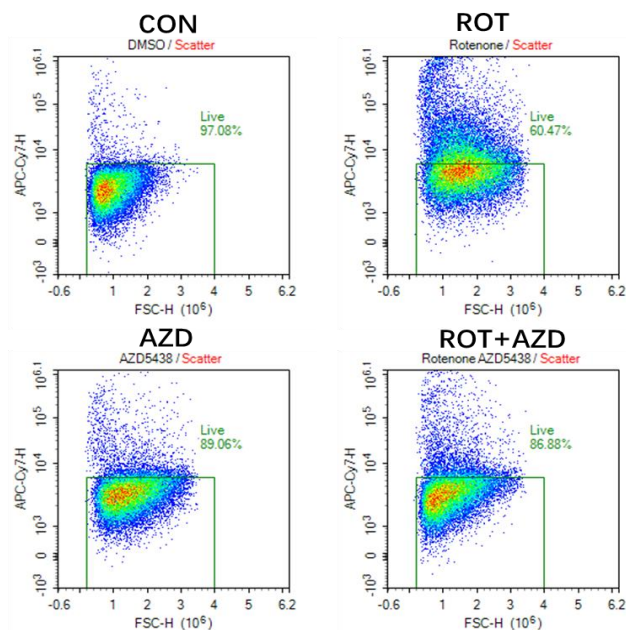
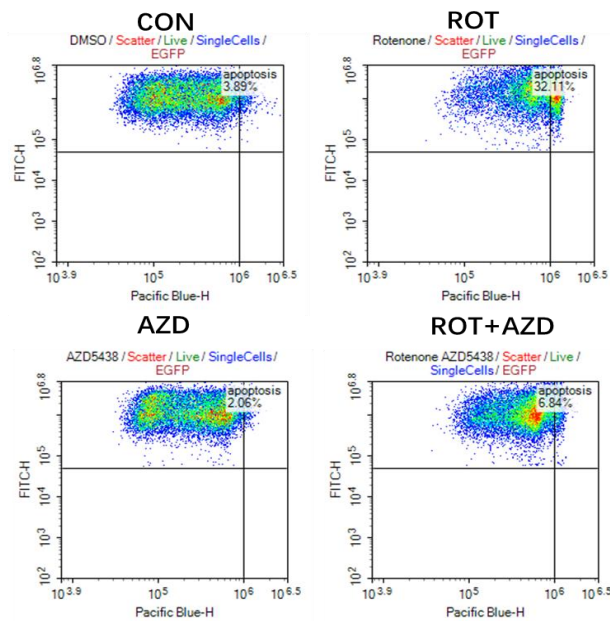


Figure 4-14 Flow cytometry assessed the ratio of the live cell following treatments with 250nM AZD5438 and 500nM rotenone for 24h.

A) The representative gating set-up and results from NovoExpress after the flow cytometry experiment shows that rotenone treatment dramatically increased the proportion of dead cells, which were prevented by AZD5438 treatment. B) The data analysis shows the significant ($p < 0.0001$) loss of live cells by rotenone treatment, while AZD5438+rotenone significantly ($p = 0.0017$) reduced that loss. No significant change by AZD5438 treatment alone was marked. Statistical analysis was carried out by two-way ANOVA test with Tukey's multiple comparisons test. $N = 3$ independent experiments; data is displayed as mean \pm SEM; significance is displayed as

** p<0.01, **** p<0.0001. Asterisks denote comparisons between AZD5438 and AZD5438+rotenone treatment, hashes denote comparisons between CON and treatment groups.

A Apoptotic cells ratio



B Apoptosis level

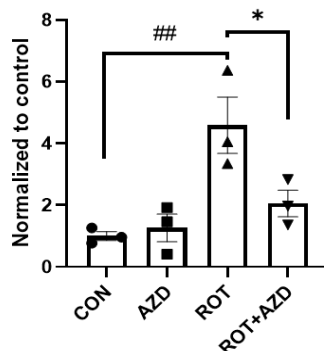


Figure 4-15 The apoptotic cell ratio following treatment with 250nM AZD5438 and 500nM rotenone for 24h was assessed by flow cytometry.

A) The representative quadrant set up as the first quadrant shows apoptotic cells and the results from NovoExpress after the flow cytometry experiment. It shows that rotenone treatment dramatically (almost 4X) increased the proportion of apoptotic cells, which were prevented by AZD5438 treatment. B) The data analysis result shows a significant (p= 0.0079) increase of apoptotic cells by rotenone treatment, while AZD5438+rotenone significantly (p= 0.0482) against that effect. No significant change by AZD5438 treatment alone was marked. Statistical analysis was carried out by two-way ANOVA test with Tukey's multiple comparisons test. N= 3 independent experiments; data is displayed as mean \pm SEM; significance is displayed as* p<0.05, ** p<0.01. Asterisks denote comparisons between AZD5438 and AZD5438+rotenone treatment, hashes denote comparisons between CON and treatment groups.

AZD5438 prevents the formation of ROS in the cellular PD model

It has been suggested that the generation of mitochondrial reactive oxygen species (ROS) plays a crucial role in rotenone-induced apoptosis [199]. To test the possibility that AZD5438 may also act at this level, assays measuring mitochondrial ROS were performed.

Mitochondrial-generated ROS was visualised by MitoSOX™ Red staining (**Figure 4-16 A**). rotenone treatment alone dramatically increased staining suggesting an increase in ROS, while this increase was prevented by treatment with AZD5438. AZD5438 alone had no noticeable effect on the ROS population. The merged images show ROS appeared alongside the corresponding unhealthy cells. The data presented in **Figure 4-16 B** confirmed that rotenone increased ROS levels in a dose-dependent manner. Compared to rotenone treatment alone up to 500nM, AZD5438 treatment significantly reduced the ROS induced by rotenone, while AZD5438 treatment alone did not affect ROS level.

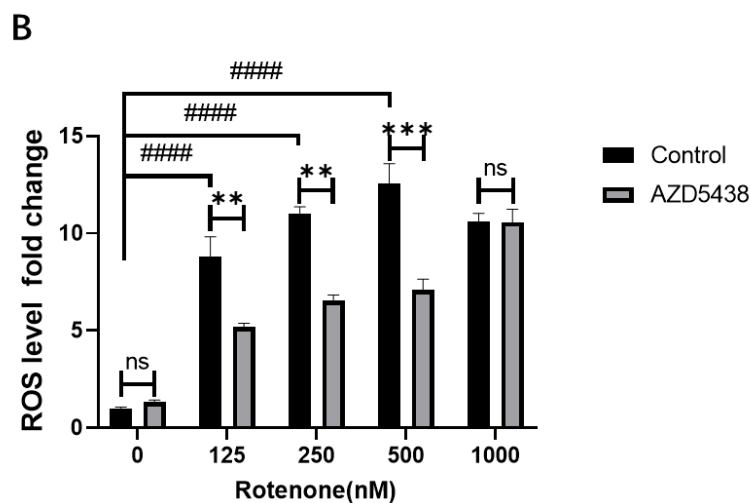
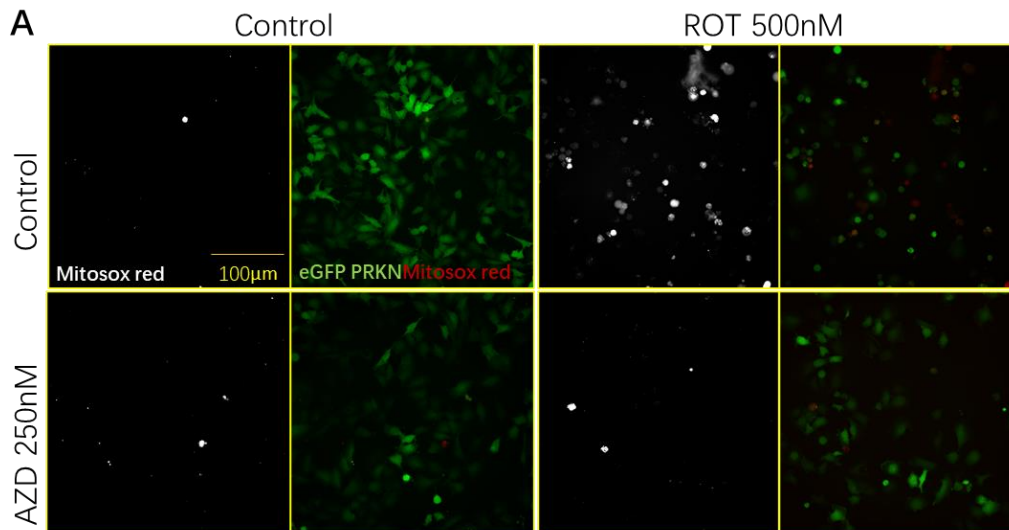


Figure 4-16 Mitochondrial reactive oxygen species (ROS) levels following treatments with 250nM AZD5438 and a series of concentrations of rotenone for 24h assessed by ROS assay.

A) Representative images taken by INCell 2200 in greyscale (Mitosox red) and merged (eGFP+Mitosox red) showing ROS condition and cells condition together after treatment. rotenone treatment alone dramatically enlarged the Mitosox staining positive population of cells suggesting increasing ROS, while it was prevented by together treated with AZD5438, AZD5438 alone showed no noticeable effect on the ROS. **B)** Bar graph shows rotenone started to trigger ROS significantly at the minimal given dose of 125nM and increased the ROS level following the dose-dependent manner from 125-500nM (all $p < 0.0001$). 250nM AZD5438 significantly reduced that ROS triggered by rotenone with p value of 0.0015, 0.0011 and 0.0004. Statistical analysis was carried out by two-way ANOVA test with Tukey's multiple comparisons test. $N = 3$ independent experiments; data is displayed as mean \pm SEM; significance is displayed as * $p < 0.05$, ** $p < 0.01$, *** $p < 0.001$, **** $p < 0.0001$. Asterisks denote comparisons between AZD5438 and AZD5438 + rotenone treatment, hashes denote comparisons between control and rotenone treatment groups.

AZD5438 inhibits the activation of caspase-3 and prevents the downregulation of mitochondrial proteins in the cellular PD model

Three key proteins were chosen to investigate the protective effect of AZD5438 in the rotenone-induced PD model. They were two mitochondrial proteins, TOMM20 and PGC1- α , to check mitochondrial activity and cleaved-caspase 3 to monitor apoptosis. Western blots were used to check their change following treatments of AZD5438 and rotenone. rotenone treatment dramatically and significantly increased the levels of cleaved-caspase 3, and this action was significantly inhibited by treatment with AZD5438. Treatment with AZD5438 alone had no effect when compared to control (**Figure 4-17 B**). These results show that caspase 3, the primary signal for apoptosis, was widely activated in the rotenone-induced PD model. Second, it indicated that AZD5438 prevents apoptosis via inhibiting the activation of caspase 3. As shown in **Figure 4-17 C and D**, rotenone significantly downregulated TOMM20 and PGC1- α protein levels. This action of rotenone was inhibited significantly by treatment with AZD5438, while AZD5438 treatment alone had no significant effect compared to control.

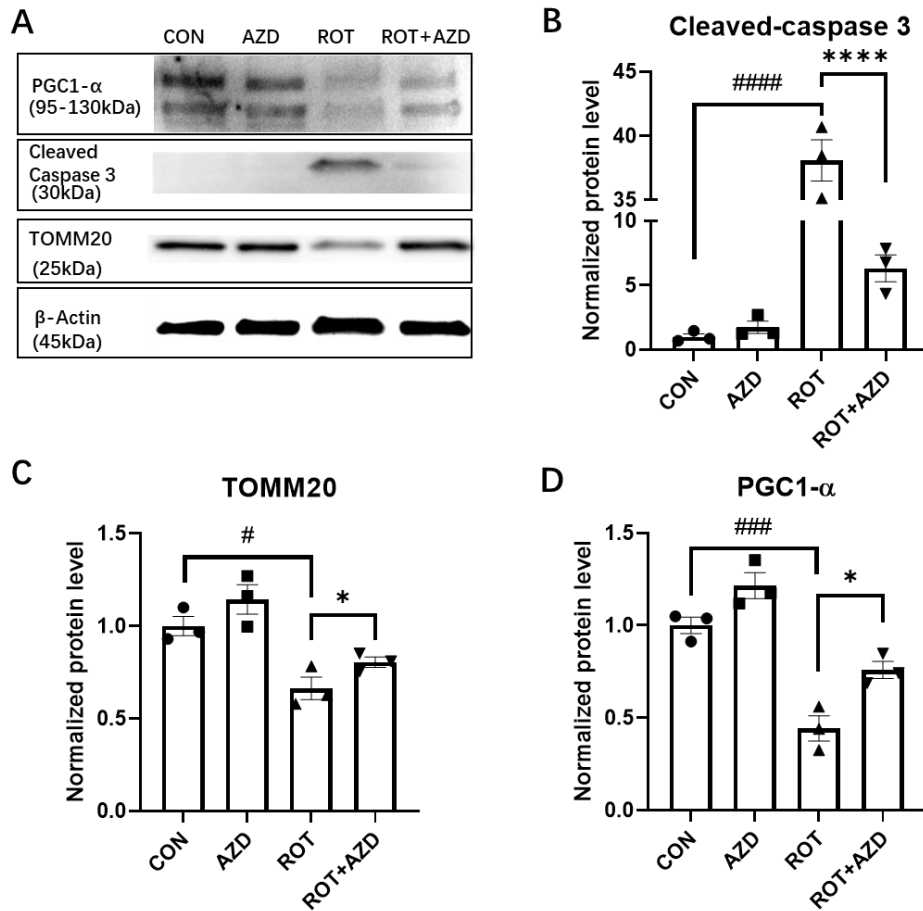


Figure 4-17 Cleaved-caspase 3, TOMM20 and PGC1- α protein levels change following treatments with 250nM AZD5438 and 500nM rotenone for 24h assessed by Weston blots.

A) The representative images of Western blots of protein samples from experiments probed for anti-PGC1- α , Cleaved-caspase 3 and TOMM20; β - Actin as the loading control. Protein bands corresponding to the approximate molecular weight are presented. Analysed data is presented in B, C and D. **B)** rotenone significantly ($p < 0.0001$) increased the Cleaved-caspase 3 level, which was significantly ($p < 0.0001$) prevented by AZD5438. **C)** rotenone significantly ($p = 0.0208$) decreased the TOMM20 level while it was significantly ($p = 0.0023$) prevented by AZD5438. **D)** rotenone significantly ($p = 0.0004$) decreased the PGC1- α level while it was significantly ($p = 0.0149$) prevented by AZD5438. Statistical analysis was carried out by two-way ANOVA test with Tukey's multiple comparisons test. $N = 3$ independent experiments; data is displayed as mean \pm SEM; significance is displayed as * $p < 0.05$, *** $p < 0.001$, **** $p < 0.0001$. Asterisks denote comparisons between AZD5438 and AZD5438+rotenone treatment, hashes denote comparisons between CON and treatment groups.

Measuring AZD5438's action on cell metabolism using the Seahorse analyser

An action of AZD5438 on mitochondrial/cellular metabolism may be involved in mediating its protective effects. Therefore, the Seahorse XF was used and the Cell Mito Stress Test protocol was performed to analyse mitochondrial respiration via oxygen consumption rate (OCR) and glycolysis condition via extracellular acidification rate (ECAR).

The results in **Figure 4-18 A** and **B** show the OCAR and ECR change after each drug injection. Based on the analysis of the OCAR data, the results in **Figure 4-18 C-E**, show rotenone treatment significantly reduced the mitochondrial basal respiration rate and ATP production rate. AZD5438 treatment did not reverse the action of rotenone on OXPHOS. Instead, the non-mitochondrial oxygen consumption rate was significantly increased by AZD5438 alone compared to CON, shown in **Figure 4-18 F**. Based on the analysis of the ECR data, the results in **Figure 4-18 G** and **H** show AZD5438 treatment significantly upregulated the glycolysis rate compared to CON. rotenone treatment was also shown to increase the glycolysis rate, and the treatment of AZD5438 further upregulated it. Moreover, rotenone treatment significantly decreased the glycolysis reserve level, while no significant effect was shown by AZD5438 treatment, alone or with rotenone.

The cells' basal energy map was drawn by plotting OCR against ECAR at baseline before oligomycin injection. **Figure 4-18 I** shows AZD5438-treated cells were more energetic (both more aerobic and more glycolytic), and rotenone-treated cells were more glycolytic but less aerobic, both compared to CON, while AZD5438+rotenone treated cells were more energetic compared to rotenone. These results suggest AZD5438 upregulated the metabolic status of cells. The energy potential of the cells following treatment was revealed by plotting the respiration reserve (Maximal respiration- Basal respiration) against the glycolytic reserve. **Figure 4-18 J** shows that AZD5438 treatment upregulated the glycolytic potential of cells at both the control level and in the cellular PD model.

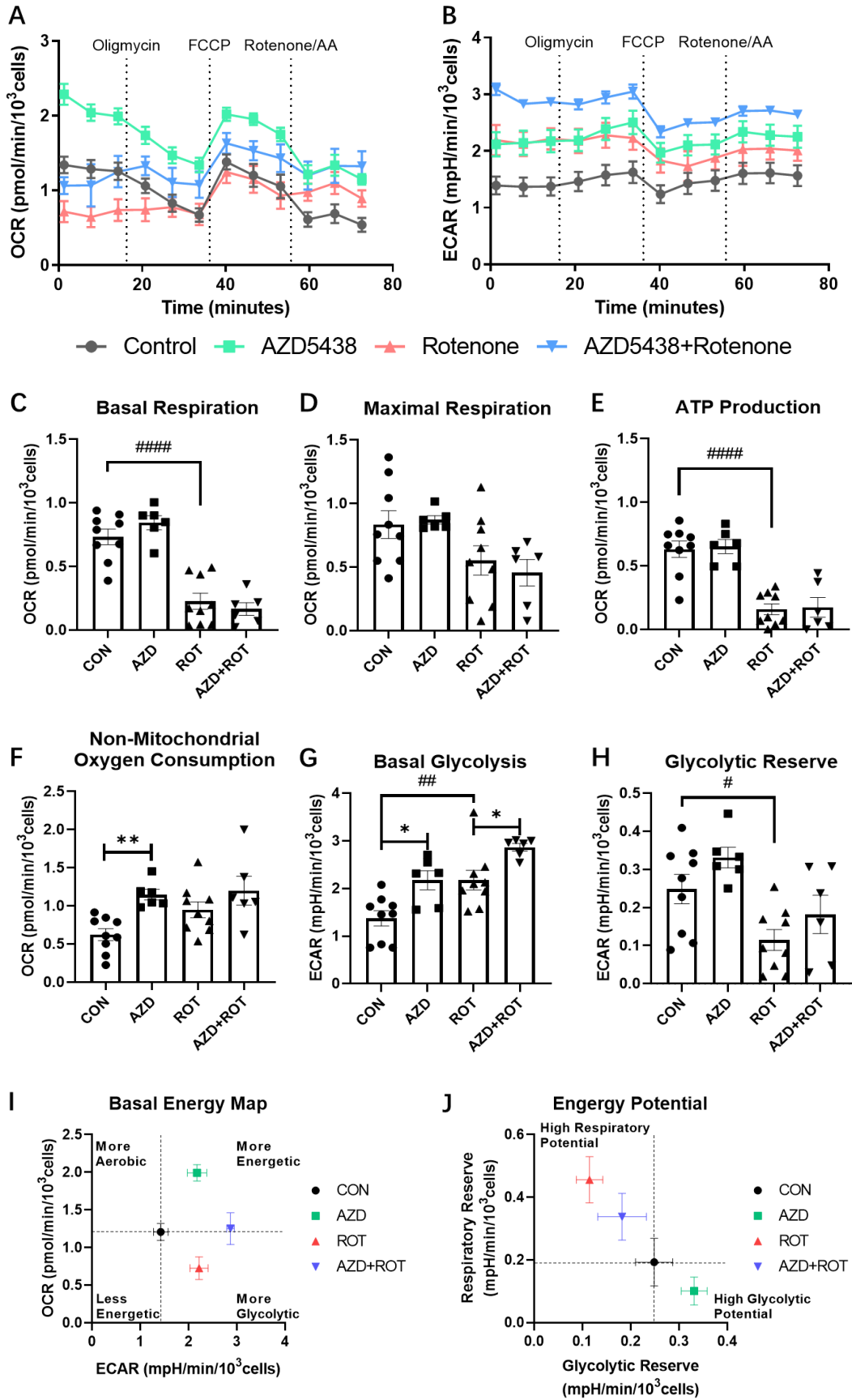


Figure 4-18 Assessing the action of AZD5438 on cellular energy metabolism using the Seahorse

analyser.

A) Oxygen consumption rate (OCR) during the experiments over time, C-F were based on these data. **B)** Extracellular acidification rate (ECAR) during the experiments over time, G-H were based on these data. **C)** rotenone significantly ($p < 0.0001$) reduced the mitochondrial basal respiration rate compared to CON. **D)** No significant change in maximal respiration rate across groups but the data distribution of AZD5438 was more concentrated than others. **E)** rotenone significantly ($p < 0.0001$) reduced the cellular ATP production rate compared to CON. **F)** AZD5438 significantly ($p = 0.0099$) increased the non-mitochondrial oxygen consumption rate compared to CON. **G)** AZD5438 significantly ($p = 0.0143$) increased the cellular basal glycolysis rate compared to CON, so did rotenone ($p = 0.0056$), together with treated with AZD5438+rotenone further significantly ($p = 0.0383$) increased that rate compared to rotenone alone. **H)** rotenone significantly ($p = 0.0256$) decreased the cellular glycolytic reserve. No significant change by AZD5438 either with or without rotenone. **I)** The basal energy map was drawn by plotting OCR with ECAR at the basal level, showing AZD5438 was more energetic, and rotenone was more glycolytic both compared to CON, while AZD5438+rotenone was more energetic compared to rotenone. **J)** The energy potential map was drawn by plotting respiratory reserve with glycolytic reserve, showing AZD5438 had higher glycolytic potential and rotenone had the higher respiratory potential both compared to CON, while AZD5438+rotenone had higher glycolytic potential compared to rotenone. Statistical analysis was carried out by two-way ANOVA test with Tukey's multiple comparisons test. Data from 3-4 biological replicates; data is displayed as mean \pm SEM; significance is displayed as * $p < 0.05$, ** $p < 0.01$, *** $p < 0.001$, **** $p < 0.0001$. Asterisks denote comparisons between AZD5438 and CON or AZD5438+rotenone with rotenone, hashes denote comparisons between CON and rotenone.

AZD5438's protective effects against stressors are dependent on glucose

The Seahorse study of metabolic activity suggested that treatment with AZD5438 resulted in a shift to glycolysis. It could therefore be hypothesised that this metabolic regulation might be associated with AZD5438's protective effects. To test this hypothesis, a low glucose (1500 mg/L glucose) culture medium was used to reduce the glycolysis activity and potential compared to cells with the standard medium (high glucose with 4500 mg/L glucose).

The results (**Figure 4-19 A**) show that rotenone treatment significantly reduced cell viability in the low and high glucose groups. AZD5438 significantly inhibited the loss in viability associated with rotenone treatment in the high glucose group. However, AZD5438 did not counter the actions of rotenone in the low glucose group. **Figure 4-19 B** shows that AZD5438 did not affect Parkin recruitment in the low glucose group. 15 μ M CCCP induced Parkin recruitment in the low glucose and high glucose groups. In contrast, AZD5438 did not inhibit Parkin recruitment activity in the low glucose group, while it significantly inhibited Parkin recruitment in the high glucose group. Moreover, 5 μ M CCCP triggered significant Parkin recruitment activity in the low glucose group but not in the high glucose group.

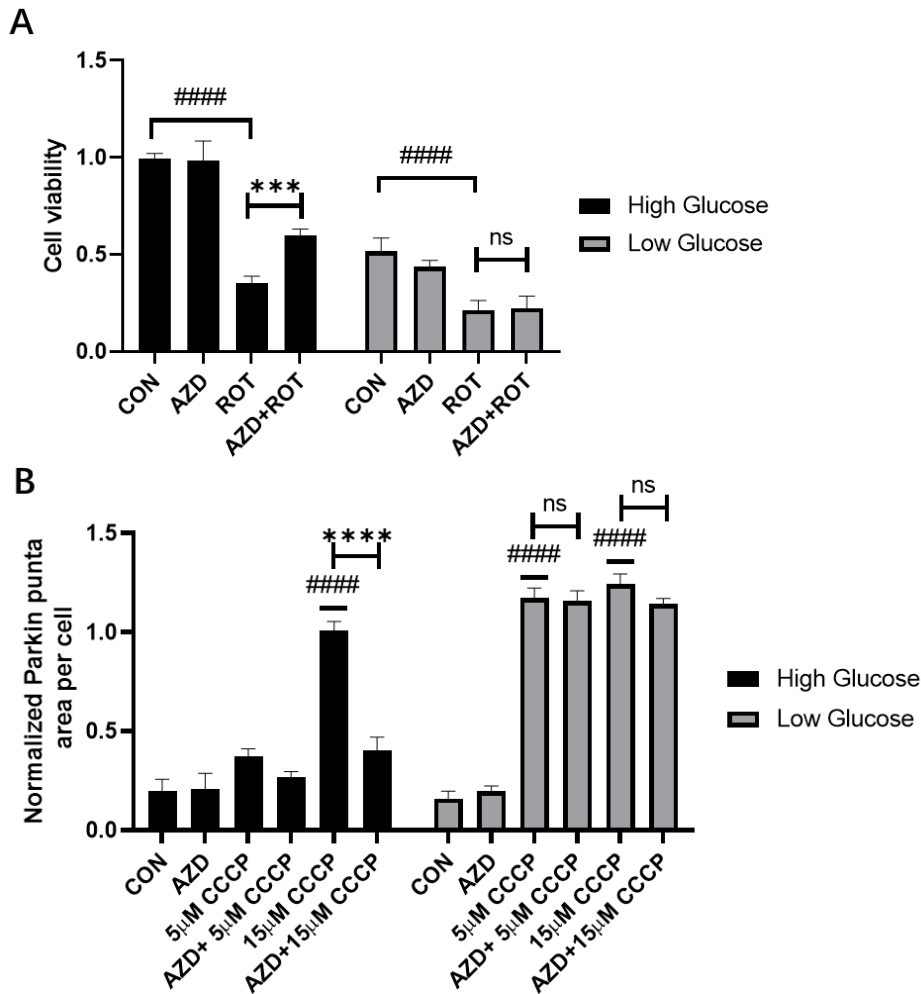


Figure 4-19 Effect of glucose concentration on the actions of AZD5438

A) The cell viability condition after treatment with 250nM AZD5438 and 500nM rotenone for 24h with low glucose medium and high glucose medium was assessed by MTT assay; cells were pre-treated with the same low glucose and high glucose culture medium, respectively, for 24h before applied compound and stressor treatment. Within the high glucose group, rotenone significantly ($p < 0.0001$) reduced the cell viability while which were protected by AZD5438+rotenone significantly ($p = 0.0003$). Within the low glucose group, similarly, rotenone significantly ($p < 0.0001$) reduced the cell viability, in contrast to the high glucose group, AZD5438+rotenone did not protect the cell viability. B) The mitochondrial mitophagy activity was indirectly assessed by Parkin recruitment assay after cells were pre-treated with the low and high glucose culture medium for 24h, separately. It shows the 15µM CCCP significantly induced the Parkin total area raise dropped by AZD5438 significantly in the high glucose group, but such effect was not recorded in the glucose group. More interestingly, 5µM CCCP had no effect in the high glucose group but significantly triggered strong Parkin recruitment activity as Parkin total area increased in the low glucose group, which had not been affected by AZD5438. Statistical analysis was carried out by two-way ANOVA test with Tukey's multiple comparisons test. $N = 3$; data is displayed as mean \pm SEM; significance is displayed as * $p < 0.05$, ** $p < 0.01$, *** $p < 0.001$, **** $p < 0.0001$. Asterisks

denote comparisons between stressor (rotenone or CCCP) and AZD5438 + stressor in the same glucose group, hashes denote comparisons between CON and stressor in the same glucose group.

Investigating whether AZD5438 acts via a specific CDK

CDK9 knockdown reproduced the regulation of Parkin recruitment by AZD5438

AZD5438 is a potent multi-cyclin-dependent kinase (CDK) inhibitor, with reported IC₅₀ values are 6 - 45, 14, 16 and 20 nM for CDK2, CDK5, CDK1 and CDK9, respectively. In addition, AZD5438 also inhibits CDK4 and CDK7 in the sub-micromolar range (IC₅₀ 449 nM and 821 nM). To investigate the main pathways that mediate AZD5438's actions, siRNAs were used to inhibit CDK1, CDK2, CDK5 and CDK9, and parkin recruitment was measured.

The data in **Figure 4-20 A** shows Parkin recruitment assays performed following siRNA knockdown. NTC served as negative control showing CCCP induces Parkin recruitment, and PINK1 served as positive control showing lack of PINK1 prevents the Parkin recruitment, indicating both Parkin recruitment assay and transfection worked. The results in **Figure 4-20 B** show that only combinations of siRNAs containing anti-CDK9 have a significant inhibitory effect on the Parkin puncta area compared to CCCP induced values in NTC. Experiments with anti-CDK5 siRNAs also showed a trend towards lower parkin recruitment though this did not reach significance.

The ability of the knockdown of an individual CDK (1,2, 5 and 9) to mimic

AZD5438's effect was next investigated. The results in **Figure 4-21 B**, showed that only the knockdown of CDK9 mediated an effect on Parkin recruitment following treatment with CCCP.

The possibility that CDK9 mainly mediates the effect of AZD5438 on Parkin recruitment was investigated by measuring the effects of AZD5438 on parkin recruitment in the presence of an anti-CDK9 siRNA. The data presented in **Figure 4-21 C** shows AZD5438 treatment does not mediate an effect on parkin recruitment if CDK9 has been knocked down. These results suggested that CDK9 may be involved in mediating AZD5438's effect on Parkin recruitment.

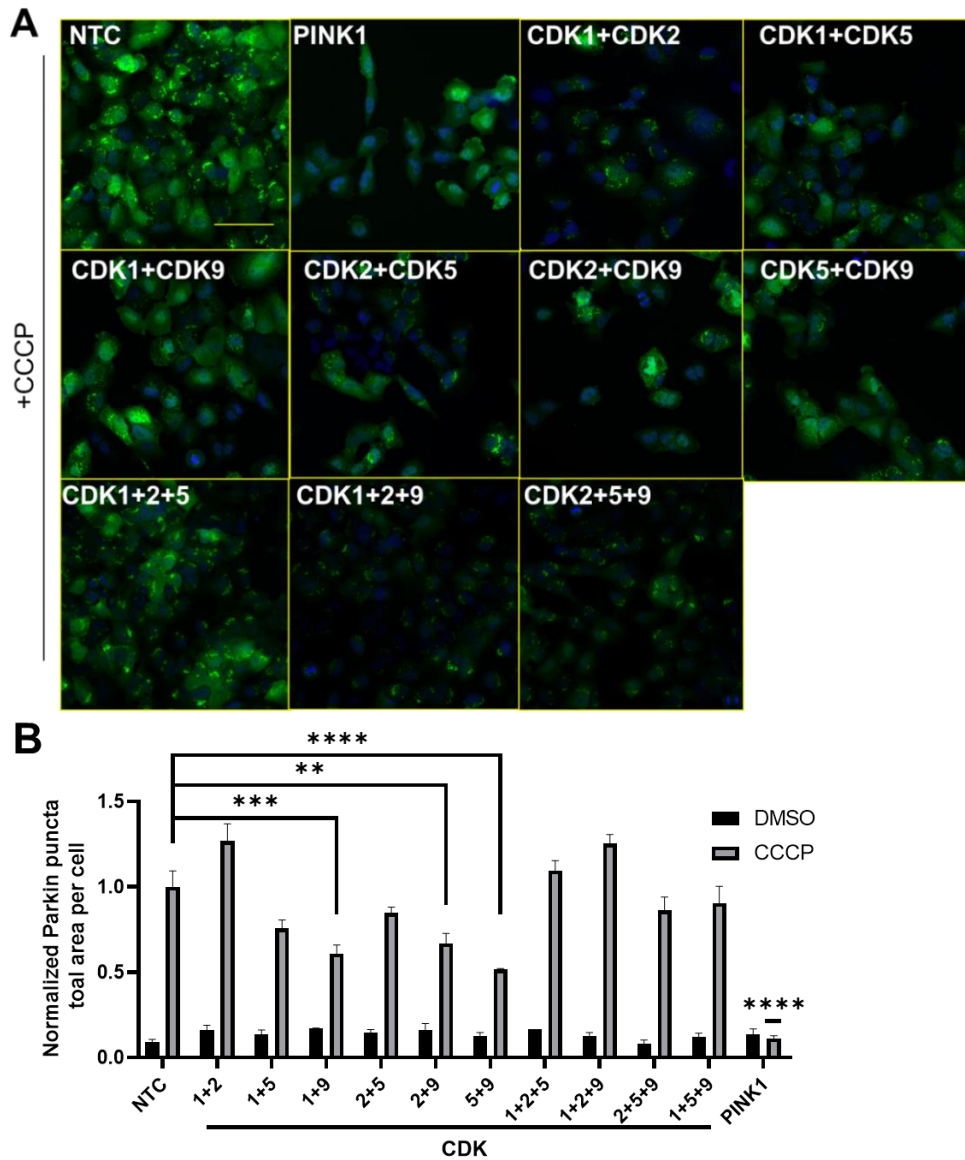


Figure 4-20 Combinations of siRNA-mediated knockdown of CDKs reproduce AZD5438's effect on Parkin recruitment

A) Representative images taken by INCell 2200 show the effects of multi CDKs knockdown on Parkin recruitment after 10 μ M CCCP treatment for 2.5h. Images were merged from green showing eGFP-Parkin and blue showing Hoechst stained nuclear. Scale bar=100 μ m. NTC served as the negative control, showing that CCCP induces Parkin recruitment, while PINK1 served as the positive control, showing that lack of PINK1 prevents Parkin recruitment, indicating that CCCP and transfection worked. Images show there are differences between each combination of CDKs knockdown. B) It shows that 3 of the CDKs combinations knockdown significantly decreased the Parkin total area induced by CCCP compared to NTC. They are CDK1+9 (p=0.0002), CDK2+9 (p=0.035) and CDK5+9 (p<0.0001). Statistical analysis was carried out by two-way ANOVA test with Tukey's multiple comparisons test. N=3; data is displayed as mean \pm SEM, significance is displayed as * p<0.05, ** p<0.01, ***p<0.001, **** p<0.0001.

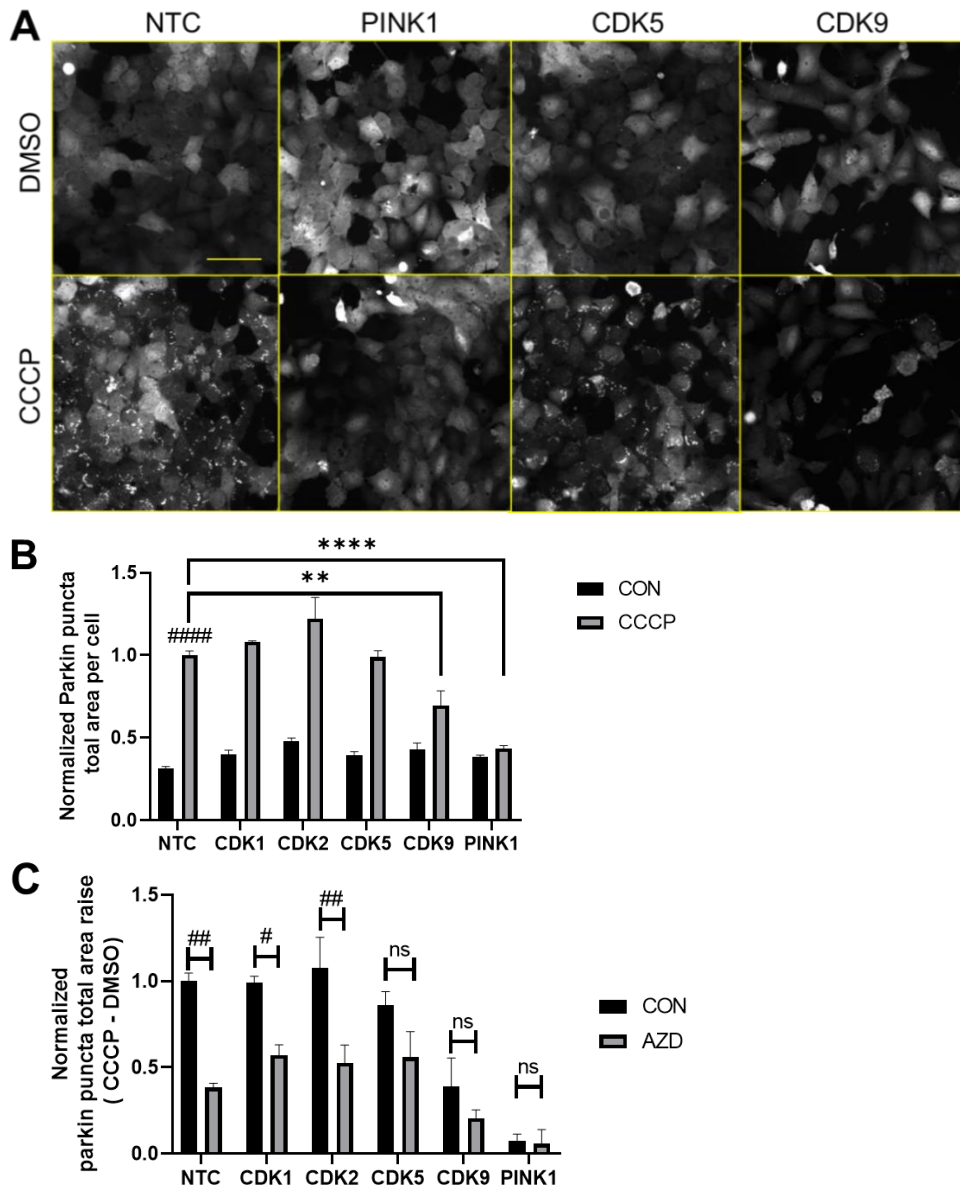


Figure 4-21 Knockdown of CDK9 reproduces AZD5438's effect on Parkin recruitment

A) Representative images taken by INCell 2200 show the effects of multi CDKs knockdown on Parkin recruitment after CCCP treatment for 2.5h. Greyscale images show many eGFP-Parkin puncta induced by CCCP in NTC and CDK5 but not in the CDK9 group. Scale bar=100µm. B) CCCP significantly increases Parkin puncta total area value in NTC, but this value is significantly ($p=0.0099$) decreased in the CDK9 group. C) AZD5438 significantly reduces Parkin puncta total area raise (CCCP-DMSO) in NTC($p=0.011$) and knockdown of CDK1 ($p=0.0373$) and CDK2($p=0.0038$) but not CDK5 or CDK9. Statistical analysis was carried out by two-way ANOVA test with Tukey's multiple comparisons test. $N=3$; data is displayed as mean \pm SEM, significance is displayed as * $p<0.05$, ** $p<0.01$, *** $p<0.001$, **** $p<0.0001$. Asterisks denote comparisons between NTC and knockdown groups with CCCP treatment, hashes denote comparisons between CCCP and DMSO in each group.

CDK9 knockdown reproduces the regulation of mitochondrial activities by AZD5438

The results suggested that AZD5438 may mediate its action of parkin recruitment via the inhibition of CDK9. Therefore, the possibility that AZD5438 also mediated its actions on mitochondrial network via the inhibition of CDK9 was also investigated.

To achieve this aim, CDK9 siRNA was transfected into the eGFP-Parkin H4 cells, CCCP was used to challenge the mitochondrial network, and Mitotracker red visualised mitochondria. The results in **Figure 4-22 A** show that in the NTC group, CCCP treatment mediated an increase in Parkin puncta formation and shrinkage of the mitochondrial network. In contrast, with CDK9 knockdown, the Parkin puncta amount is less than that in NTC, and the mitochondrial distribution spreads with higher intensity. **Figure 4-22 B** confirmed that CDK9 knockdown protects the mitochondrial network as the total mitochondrial area increased compared to NTC. **Figure 4-22 C** confirmed that CDK9 knockdown protects mitochondrial membrane potential as total mitochondrial area increased compared to NTC.

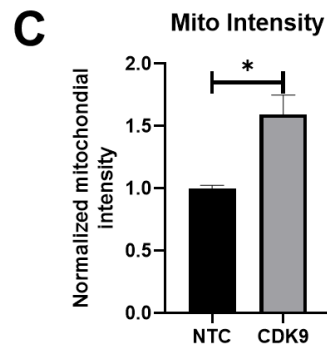
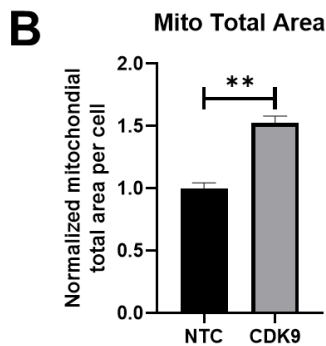
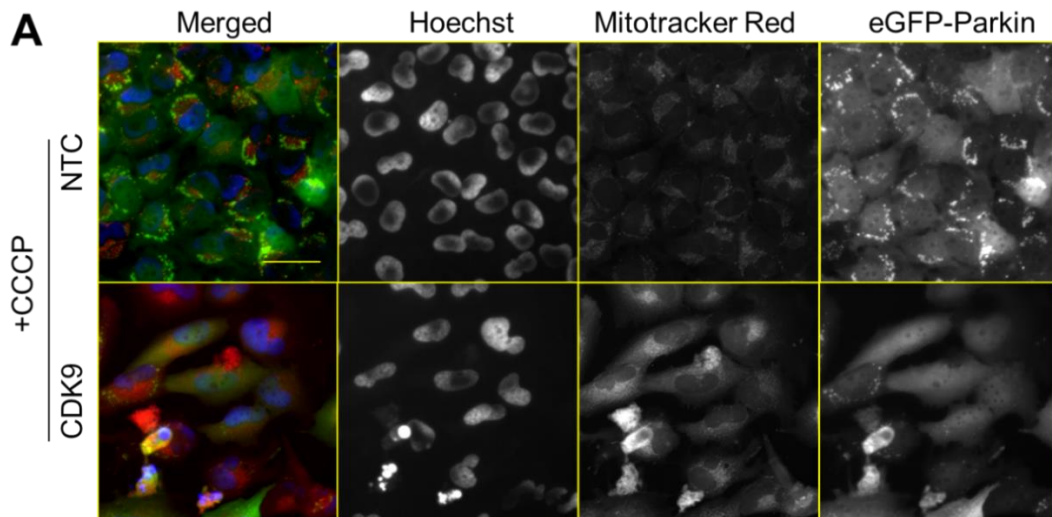


Figure 4-22 CDK9 knockdown reproduces AZD5438's effect on mitochondrial activity

A) Representative images taken by INCell 2200 show the effects of CDK9 knockdown on mitochondrial activities after 10µM CCCP treatment for 2.5h. Images show Hoechst stained nuclear, Mitotracker stained mitochondria, GFP labelled Parkin and merged images. Scale bar=50µm. Images show that CCCP triggers Parkin puncta formation in the NTC group and makes the mitochondrial network shrink and show less intensity. In the CDK9 knockdown group, Parkin puncta are less than NTC while the mitochondrial distribution is spreading, with higher intensity than NTC. B) CDK9 significantly ($p=0.0018$) increases the value of Parkin puncta total area per cell after CCCP treatment compared to NTC. C) CDK9 significantly ($p=0.0193$) increases the value of mitochondrial intensity after CCCP treatment compared to NTC. Statistical analysis was carried out by unpaired t-test. $N=3$; data is displayed as mean \pm SEM, significance is displayed as * $p<0.05$, ** $p<0.01$.

Inhibition of GSK-3 β alone does not alter Parkin recruitment

AZD5438 also inhibits glycogen synthase kinase 3 β (GSK3 β) (IC₅₀ = 17nM). To check the possibility that GSK3 β may also be involved in mediating AZD5438's actions on parkin recruitment, siRNA knockdown of GSK3 β was performed, followed by a Parkin recruitment assay.

As shown in **Figure 4-23**, GSK3 β knockdown did not inhibit parkin recruitment following CCCP treatment. PINK1 knockdown inhibited parkin recruitment indicating the assay was functional.

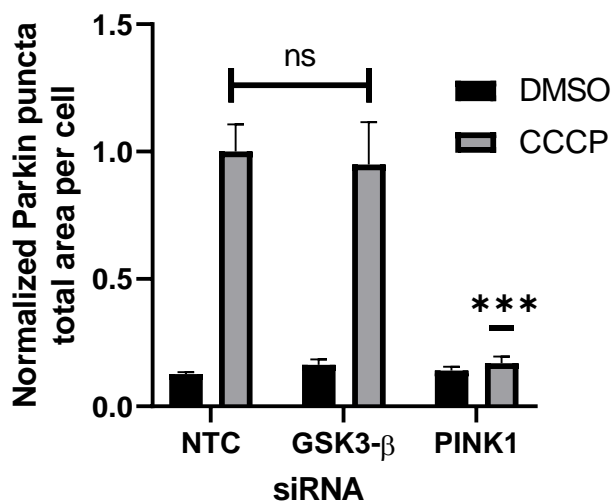


Figure 4-23 GSK3 β does not regulate Parkin recruitment

Analysed data from the INCell analyser workstation shows no significant difference between NTC and GSK3 β knockdown with CCCP treatment, while PINK1 significantly ($p=0.001$) reduces the Parkin puncta area compared to NTC with CCCP treatment. Statistical analysis was carried out by two-way ANOVA test with Tukey's multiple comparisons test. N=3; data is displayed as mean \pm SEM, significance is displayed as *** $p<0.001$.

Professor Richard Coward, Bristol Renal Group, generously provided a GSK3 β floxed podocyte cell line which was used to study the effect of GSK3 β knockout on Parkin recruitment. This was to add more evidence to evaluate that whether down regulating GSK3 β could affect parkin recruitment with a ready to use model published recently[200].

An EGFP-Parkin plasmid was kindly donated by Dr Helen Scott, and a lentivirus was made and used to transduce the GSK3 β floxed podocytes. A cre lentivirus was also used to knock down GSK expression. Western blots were used to confirm the GSK3 β knockout, as seen in **Figure 4-24 B**. Parkin recruitment assay was performed and images in **Figure 4-24 A** show that CCCP triggered the Parkin recruitment. **Figure 4-24 C** confirmed no difference between GSK3 β knockout and CON regarding CCCP-induced Parkin puncta total area raise.

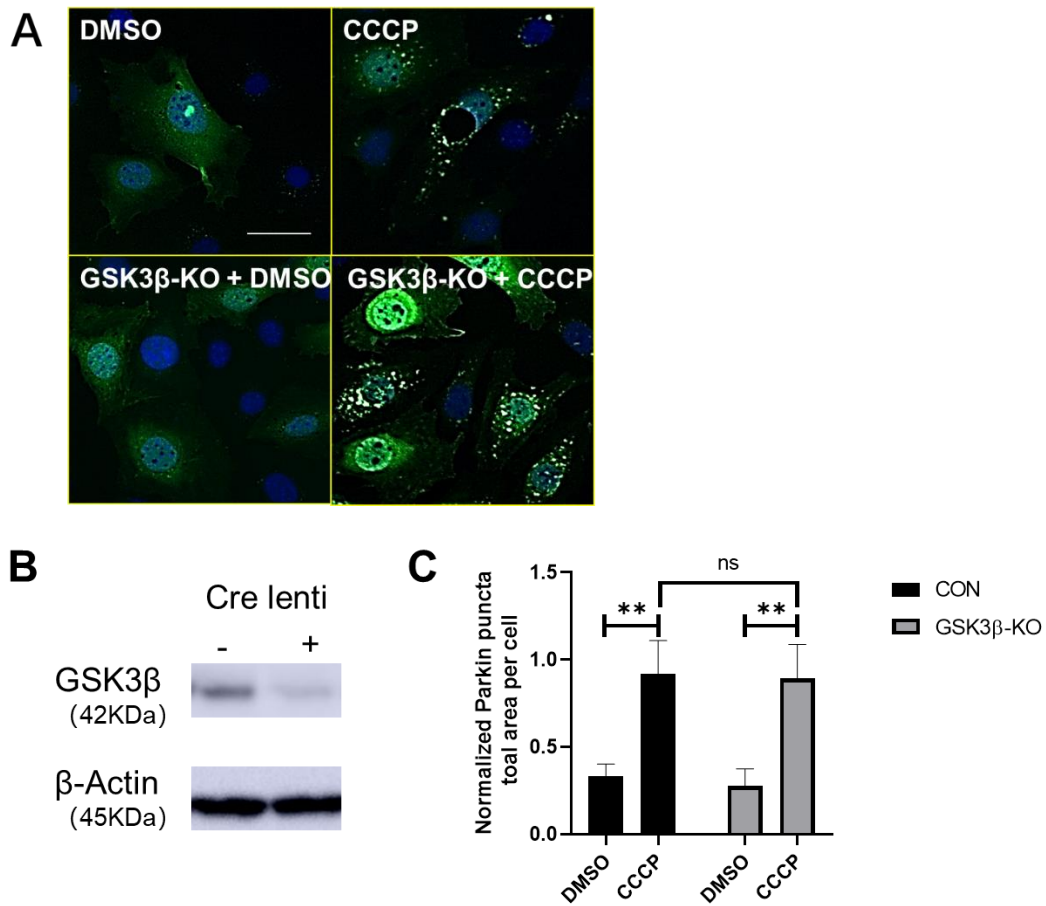


Figure 4-24 GSK3β knockout did not alter Parkin recruitment

A) Representative images were taken by INCell 2200, showing GSK3β knockout/CON via cre lentivirus transduction on GSK3β floxed podocyte cells following expression of eGFP-Parkin, and their effects on Parkin recruitment after 10μM CCCP treatment for 2.5h. Images were merged from green showing eGFP-Parkin and blue showing Hoechst stained nuclear. Scale bar=100μm. CCCP induced Parkin puncta formation both in the knockout and control cells. **B)** Weston blots confirmed GSK3β was knocked out by cre lentivirus. **C)** Bar graph from images data analysis shows that both GSK3β knockout ($p=0.0081$) and control ($p=0.0058$) cells significantly increase the Parkin puncta total area ($p=0.0081$, 0.0058), and they have no significant difference between each other. Statistical analysis was carried out by two-way ANOVA test with Tukey's multiple comparisons test. $N=3$; data is displayed as mean \pm SEM, and significance is displayed as $**p<0.01$.

Validating the protective effects of AZD5438 in SH-SY5Y cells

AZD5438 inhibits rotenone toxicity in SHSY-5Y cells

MTT assays were used to assess the viability of SHSY-5Y cells following exposure to rotenone. Prior to this assessment, dose-response experiments for AZD5438 and rotenone were performed to optimise the dose for SHSY-5Y cells.

Figure 4-25 A suggested that the IC₂₅ for AZD5438 in SH-SY5Y is between 100nM and 500nM. **Figure 4-25 B** suggested that the IC₅₀ for rotenone in SH-SY5Y is between 250nM and 500nM. Two doses within the IC₅₀ range of both AZD5438 and rotenone were used for the MTT-rotenone assay. The data shown in **Figure 4-25 C** indicates rotenone treatment significantly lowered cell viability at doses of 500nM and 1000nM. 100nM and 250nM AZD5438 treatment prevented the reduction in cell viability associated with treatment with 1000nM rotenone. It also shows that 250nM AZD5438 treatment decreased MTT activity in SH-SY5Y cells.

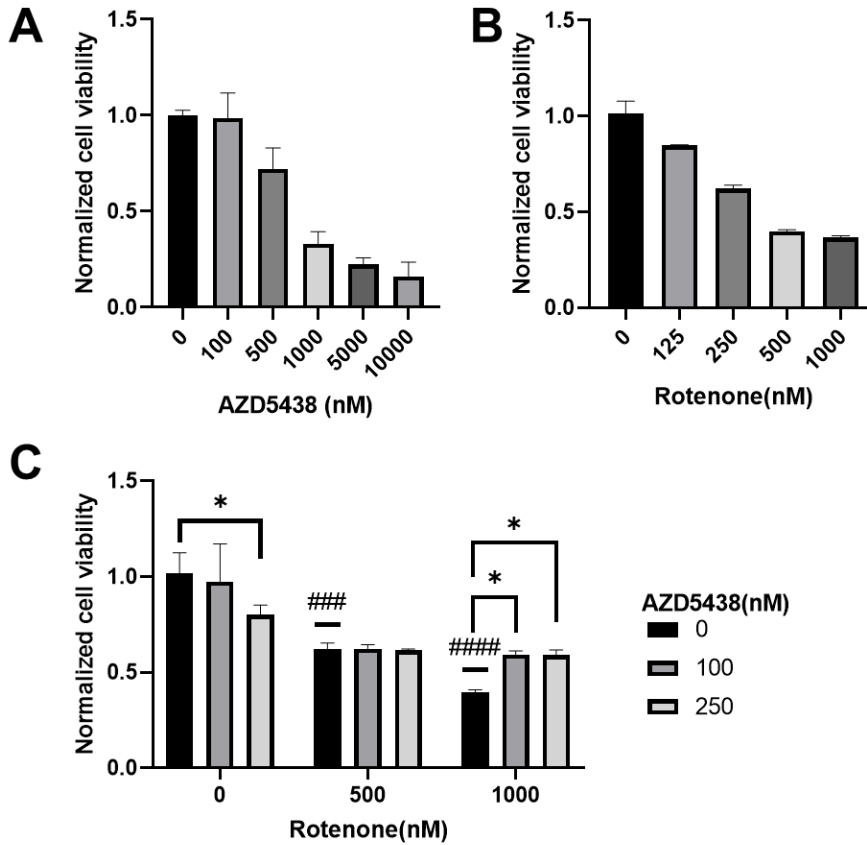


Figure 4-25 AZD5438 prevents rotenone induced toxicity in SH-SY5Y cells

A) Bar graph shows the dose-response of AZD5438 in SH-SY5Y cells. Data were collected after 24h AZD5438 treatment followed by 3h MTT assay. B) Dose-response of rotenone in SH-SY5Y cells. Data were collected after 24h rotenone treatment followed by 3h MTT assay. C) Bar graph shows AZD5438's performance in MTT-rotenone assay after 24h treatment. Doses of rotenone and AZD5438 are shown in the figure. It shows that 250nM AZD5438 alone significantly ($p=0.0105$) decreased the cell viability. Rotenone significantly reduced the cell viability at 500nM ($P=0.0002$) and 1000nM ($p<0.0001$). The viability loss by rotenone was significantly increased with 100nM ($P=0.0179$) and 250nM ($P=0.0205$) AZD5438. Statistical analysis for C was carried out by two-way ANOVA test with Tukey's multiple comparisons test. $N=3$; data is displayed as mean \pm SEM, significance is displayed as * $p<0.05$, ** $p<0.01$, *** $p<0.001$, **** $p<0.0001$. Asterisks denote comparisons between no rotenone control and rotenone treatment, hashes denote comparisons between no AZD5438 treatment and AZD5438 treatment.

AZD5438 inhibits Parkin recruitment in eGFP-Parkin SH-SY5Y cells

To validate another key effect of AZD5438, Parkin recruitment was measured in SHSY-5Y cells.

The results (**Figure 4-26 A-C**) show that Parkin puncta are formed in eGFP-Parkin SH-SY5Y cells following treatment with CCCP. The results also show that the formation of parkin puncta has been significantly inhibited by both doses (250nM and 500nM) of AZD5438. At the higher (500nm) dose of AZD5438, there was a significant reduction in cell viability as assessed by cell count (**Figure 4-26B**).

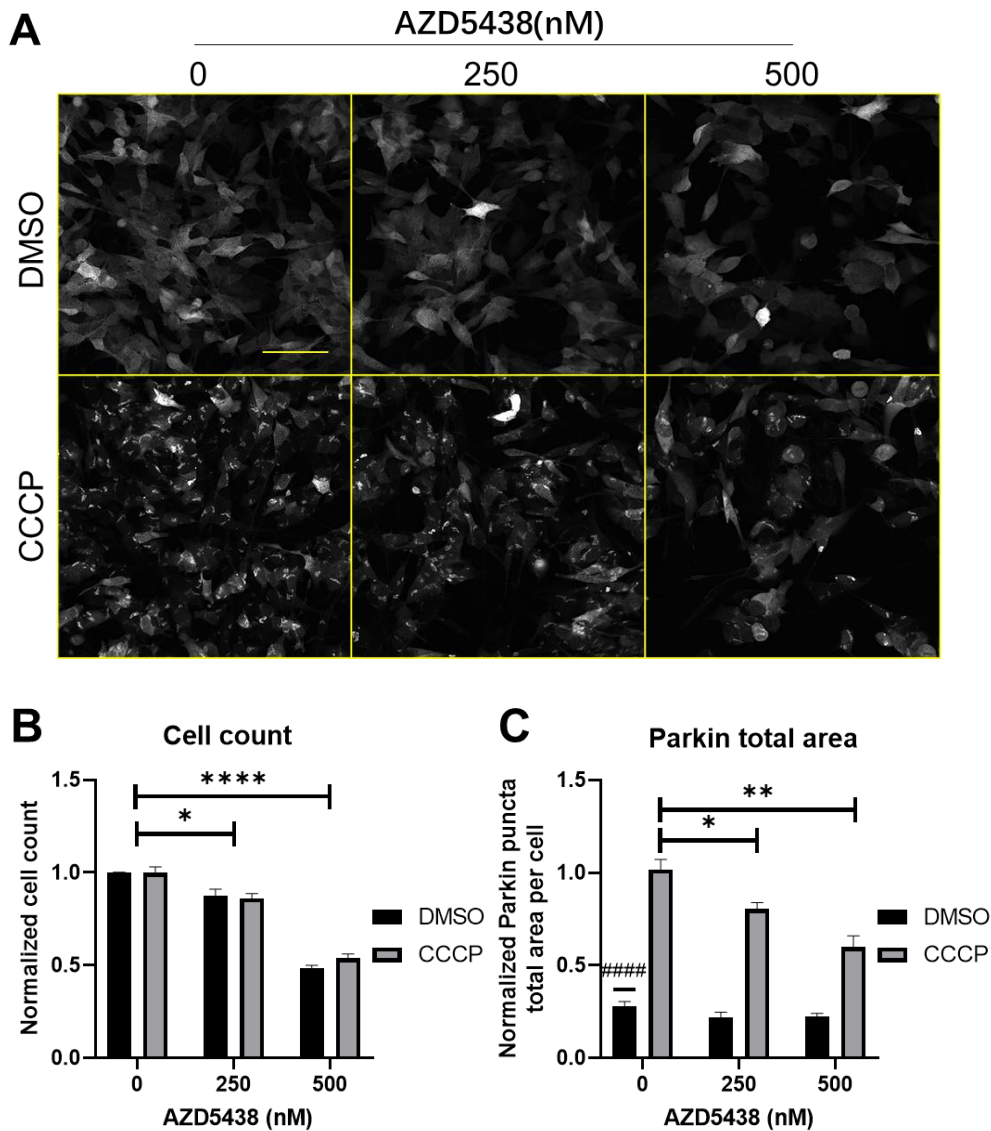


Figure 4-26 AZD5438 prevents Parkin recruitment in eGFP-Parkin SHSY-5Y cells

A) Images from INCell 2000 show the Parkin puncta formation in eGFP-Parkin SH-SY5Y cells after 10 μ M CCCP treatment for 6h. AZD5438 pre-treatment decreased the Parkin puncta content compared to no AZD5438. AZD5438 pre-treatment decreased the cell amount with or without CCCP. Bar Scale =100 μ m. **B** and **C** Bar graph shows data analysed by INCell analyser. **B**) The cell count was significantly decreased by AZD5438 at 250nM($p=0.0356$) and 500nM($p<0.0001$) with or without CCCP. **C**) CCCP significantly($p<0.0001$) induced the Parkin puncta formation without AZD5438. Both 250nM($p=0.0388$) AZD5438 and 500nM($p=0.001$) AZD5438 significantly decreased the CCCP induced Parkin puncta total area value. Statistical analysis was carried out by two-way ANOVA test with Tukey's multiple comparisons test. N=3; data is displayed as mean \pm SEM, significance is displayed as * $p<0.05$, ** $p<0.01$, *** $p<0.001$, **** $p<0.0001$. Asterisks denote comparisons between no rotenone control and rotenone treatment, hashes denote comparisons between no AZD5438 treatment and AZD5438 treatment.

AZD5438 regulates the mitochondrial network in eGFP-Parkin SH-SY5Y cells

The mitochondrial network was measured using the InCell analyser following the treatment of cells with 500nM rotenone. The data in **Figure 4-27 A-C** shows rotenone treatment induced cell loss. The distribution of mitochondria was also altered by rotenone, with them being closer to the nucleus and showing more vigorous Mitotracker staining. Treatment with 250nM AZD5438 alone did not change cell morphology, but there appeared to be more mitochondrial compared to CON. AZD5438 significantly reduced the cell loss caused by treatment with rotenone. rotenone did not mediate a significant decrease in the total mitochondrial area (though there was a trend. Notably, there was a significant difference between AZD5438 and rotenone treatments suggesting they have the opposite effect on cell viability.

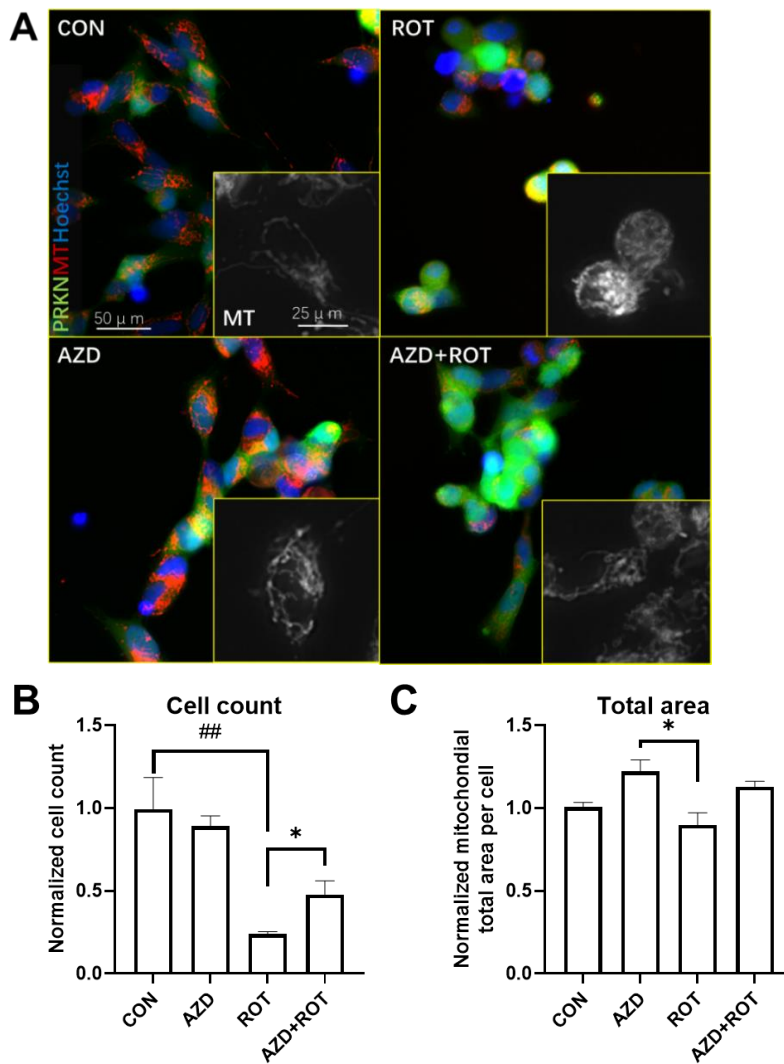


Figure 4-27 AZD5438 protects EGFP-Parkin SH-SY5Y cells from rotenone

A) Images from INCell 2200 show the merged channel of green-Parkin, red-mitotracker and blue-Hoechst, and the zoomed-in image of mitotracker in greyscale. Cells were treated with or without 250nM AZD5438 and 500nM rotenone for 24h before staining and imaging. rotenone treated cells were loss in amount and had rounder shape compared to CON. Mitochondria network shirked in rotenone. AZD5438 did not show clear change alone but rescued cell amount and mitochondrial network against rotenone. B) rotenone significantly($p=0.0070$) reduced the cell count, and which was significantly ($p=0.0173$) rescued by AZD5438. C) Although no significance, AZD5438 alone increased the mitochondrial total area and rotenone alone decreased it compared to CON. AZD5438+rotenone increased the total area compared to rotenone. AZD5438 alone significantly (0.0134) increased total area compared to rotenone alone. Statistical analysis was carried out by two-way ANOVA test with Tukey's multiple comparisons test. N=3; data is displayed as mean \pm SEM, significance is displayed as * $p<0.05$, ** $p<0.01$, *** $p<0.001$, **** $p<0.0001$. Asterisks denote comparisons between no rotenone control and rotenone treatment, hashes denote comparisons between no AZD5438 treatment and AZD5438 treatment.

The effect of AZD5438 on mitochondrial DNA levels following treatment with rotenone was also measured. 250nM AZD5438 and 500nM rotenone were used in this assay. The results in **Figure 4-28** show that AZD5438 treatment alone significantly increased the mtDNA content compared to CON. However, rotenone did not affect mtDNA levels, and therefore no protective effect of AZD5438 could be assessed.

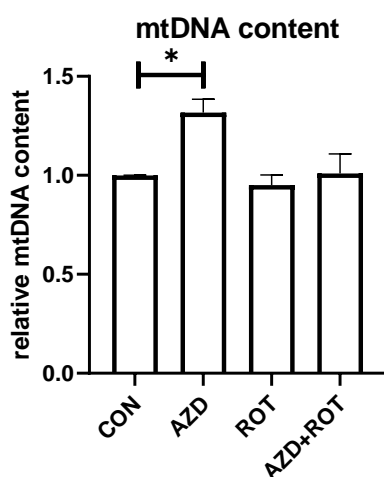


Figure 4-28 AZD5438 regulates relative mitochondrial DNA content in eGFP-Parkin SH-SY5Y Cells were treated with or without 250nM AZD5438 and 500nM rotenone for 24h before harvest and DNA extraction. mtDNA assay was used to check the relative mtDNA content compared to nuclei DNA. AZD5438 significantly increased the relative mtDNA content compared to CON($p=0.0261$). No significant difference between the other groups. Statistical analysis was carried out by two-way ANOVA test with Tukey's multiple comparisons test. $N=3$; data is displayed as mean \pm SEM, significance is displayed as * $p<0.05$, ** $p<0.01$, *** $p<0.001$, **** $p<0.0001$.

Alpha-Synuclein affects the cell viability protection by AZD5438

α -Synuclein is a presynaptic protein known to be linked to PD pathogenesis in many ways. It is mainly accepted that the misfolding and aggregation of this protein leads to cytotoxicity and eventually neuronal death[201]. Research has shown that rotenone induces α -synuclein upregulation in SH-SY5Y cells, making the association between α -synuclein and rotenone-induced cellular PD model even tighter[202] [203]. As a gift from Dr Fella Hammachi, multi α -synuclein mutant overexpression SH-SY5Y cell lines provided an excellent opportunity to study the AZD5438's effect in the cellular PD model with WT α -synuclein and the mutants. The mutants are C terminal truncated(CT) α -synuclein (110A), G51D mutant and CT α -synuclein (G51D) and A53T mutant and CT (A53T). They are all based on the dox inducible system, which means doxycycline (dox) treatment would allow the genes to express; otherwise, they were taken as the control without expressing the target genes.

Figure 4-29 A shows that the Weston blots result from Dr Fella confirmed that the 1.5ug/ml dox treatment for 2 days induced the expression of the target genes.

Figure 4-29 B shows that AZD5438 protected the cell viability loss caused by rotenone in the no dox and plus dox groups. In addition, cells with WT α -Synuclein overexpression by dox treatment were more resistant to rotenone-induced cell viability loss than no dox. Moreover, in the WT α -Synuclein overexpression group,

AZD5438 had a more significant cell viability protecting effect. **Figure 4-29 C** and **D** confirm that the mutant expression affected AZD5438 to protect cell viability as their value of viability of AZD5438+rotenone in the dox plus group was significantly higher than those in the no dox group. **Figure 4-29 E** shows a slightly different result than C and D. In both no dox and plus dox groups, AZD5438 had no significant protective effect. rotenone lost its significant cell viability damage effect in the plus dox group, although the trend still suggested it had the effect. **Figure 4-29 F** includes the images of the MTT formazan condition of each treatment in the dox inducible WT α -Synuclein cells, showing the plus dox groups had more MTT formazan observed compared to the no dox group.

Figure 4-29 Alpha-Synuclein might help AZD5438 protect cells in the cellular PD model

A) Western blot results show the α -Synuclein was expressed in each mutant cell line, plus dox changed those expression conditions. **B)** MTT-rotenone assay results of dox-inducible WT α -Synuclein SH-SY5Y cells. In no dox group(control), rotenone significantly ($p=0.0001$) decreased the cell viability, and AZD5438 significantly($p=0.0248$) rescued it. In the plus dox group (gene expression), rotenone significantly ($p=0.0235$) decreased the cell viability, and AZD5438 significantly($p=0.0076$) rescued it. Between no dox and the plus dox groups, the viability of both rotenone($p=0.0003$) and AZD5438+rotenone ($p<0.0001$) significantly increased in the plus dox group. **C)** MTT-rotenone assay results of dox-inducible 110a α -Synuclein SH-SY5Y cells. In no dox group(control), rotenone significantly ($p<0.0001$) decreased the cell viability, and AZD5438 significantly($p=0.0003$) rescued it. In the plus dox group, rotenone significantly ($p<0.0001$) decreased the cell viability, and AZD5438 significantly($p<0.0001$) rescued it. Between the no dox and the plus dox group, the viability of AZD5438+rotenone ($p=0.0157$) significantly increased in the plus dox group. **D)** MTT-rotenone assay results of dox-inducible G51D α -Synuclein SH-SY5Y cells. In the no dox group(control), rotenone significantly ($p<0.0001$) decreased the cell viability, and AZD5438 significantly($P=0.0005$) rescued it. In the plus dox group, rotenone significantly ($p<0.0001$) decreased the cell viability, and AZD5438 significantly($p=0.0005$) rescued it. Between the no dox and the plus dox group, the viability of AZD5438+rotenone ($p=0.0439$) significantly increased in the plus dox group. **E)** MTT-rotenone assay results of dox-inducible A53T α -Synuclein SH-SY5Y cells. In the no dox group(control), rotenone significantly ($p=0.0001$) decreased the cell viability. No significance was marked between other groups' comparisons. Statistical analysis was carried out by two-way ANOVA test with Tukey's multiple comparisons test. $N=3$; data is displayed as mean \pm SEM, significance is displayed as * $p<0.05$, ** $p<0.01$, *** $p<0.001$, **** $p<0.0001$. Asterisks denote comparisons between a combination of rotenone and AZD5438 treatment, hashes denote comparisons between the no dox treatment and the plus dox treatment.

Discussion

Graphic summary

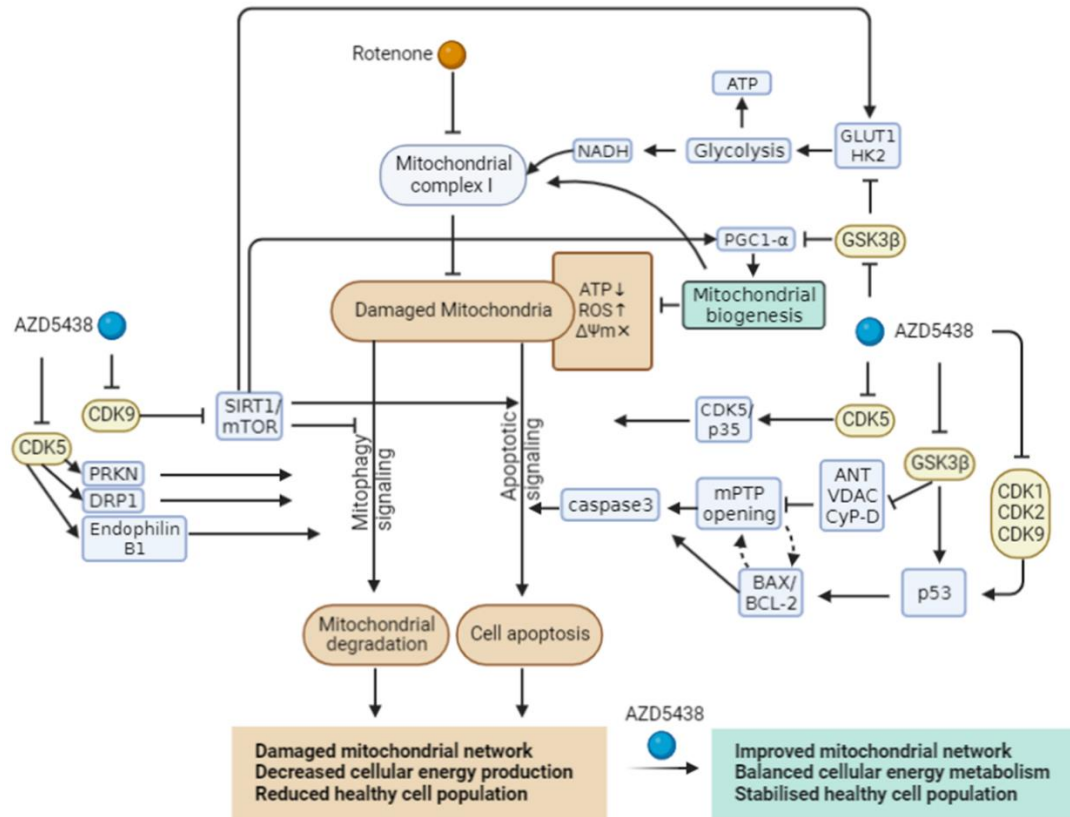


Figure 4-30 A graphic summary of the protection effects of AZD5438

AZD5438 helps improve the mitochondrial network and balance cellular energy homeostasis and thus preventing damage to cells from rotenone exposure.

The results described in chapter 3 and this chapter indicate that inhibitors of GSK3 α/β and CDKs, such as kenpaullone, modulate mitochondrial activity and protect cells from toxins associated with the aetiology of Parkinson's disease (PD). Evidence shows that GSK3 inhibitors are neuroprotective, however, kenpaullone, which inhibits both GSK3 and CDKs, was shown to protect and promote the

survival of motor neurons more efficiently than equivalent GSK3 inhibitors alone [111]. Furthermore, AZD5438 and AT7519, which have similar GSK3 inhibitory profiles to kenpaullone but distinct CDK inhibitory profiles, were shown to be more efficient inhibitors of cisplatin-mediated mitochondrial toxicity and apoptosis than kenpaullone [101, 204]. Experiments in this chapter examined the effectiveness of GSK3 and CDK inhibitors and drugs that target the mitochondrial permeability transition pore (mPTP) to alter mitochondrial function, compared with that of kenpaullone. The results demonstrated that AZD5438 pre-treatment restored mitochondrial membrane potential following CCCP exposure and prevented parkin recruitment and mitochondrial network fragmentation, which were linked with CCCP exposure. Furthermore, CCCP-mediated parkin recruitment and mitochondrial fragmentation were also suppressed by AT7519, kenpaullone and its analogues, alsterpaullone, and 1-azakenapauillone, though not as effectively as AZD5438. These findings indicate that the effects mediated on parkin recruitment and the mitochondrial network are facilitated at least to some extent via an action on CDKs, as these compounds have comparable inhibitory actions of GSK3 α/β but differ in their anti-CDK profiles. Dexamipexole (KNS-760704) and olesoxime (TR019622), compounds reported to target the mPTP [205] and assessed in phase II ALS trials [206], showed no effect on parkin recruitment or mitochondrial form in this study. Kenpaullone which is a GSK3 inhibitor, that also inhibits the formation of the mPTP [207], was previously found to protect motor neurons more effectively than Dexamipexole (KNS-760704) and

olesoxime (TR019622) [111]. Therefore, the findings further support the suggestion that drugs that target both GSK3 and CDKs are effective modulators of mitochondrial function with therapeutic promise.

Further experiments in this chapter assessed the protective properties of AZD5438 against the complex I inhibitors rotenone and MPP+, both of which are used to model the pathophysiology of Parkinson's disease. The findings showed that AZD5438 mediated significant protection against complex I inhibitors. Studies have shown the link between the use of pesticides with mitochondrial complex I inhibitory properties and the development of PD [199, 208, 209]. Rotenone, a widely used pesticide, is employed in models that reproduce PD's clinical and biochemical characteristics. Dopaminergic cell loss, Lewy body formation, and altered mitochondrial activity are seen in nigral-striatal pathways utilising rotenone in vivo models. Rotenone disrupts mitochondrial complex I in rat and human primary neurons in vitro, resulting in free radical production and apoptosis, partly due to activation of the mPTP[199, 208, 210]. Dopaminergic neurons were shown to be especially vulnerable to rotenone toxicity in a recent RNA-seq investigation of 215 iPSC lines differentiated towards a midbrain neural fate[210]. AZD5438 was found to inhibit both GSK3 and CDKs, promote the mitochondrial network's expansion, encourage glycolytic metabolism, and prevent the cytotoxicity associated with mitochondrial complex I inhibitors. This robust protective profile points to AZD5438 as a therapeutic candidate for PD.

Treatment with AZD5438 alone enhanced the mitochondrial network's complexity as mitochondria showed an elongated shape. This could be due to the mitochondrial fission-fusion balance shifting to the more fusion side. This shift could be potentially protective for mitochondrial as it was suggested that mitochondrial fusion could enhance their energy capacity in response to stress[211]. Because fusion promotes mitochondria exchange of protein components or lipids with other mitochondria to repair mtDNA damage, further overcome environmental stress[212, 213]. This shift to increased fusion might be due to the inhibition of fission, an activity required for mitophagy[214]. The results showing that AZD5438 treatment inhibited the initiation of Parkin-mediate mitophagy of the cells supports this idea. The inhibition of fission and/or mitophagy by AZD5438 is also supported by findings in this thesis that show mtDNA is increased, but PGC-1 α protein levels remain unchanged following AZD5438 treatment. As discussed in chapter 3, p25-activated CDK5 can mediate the phosphorylation of DRP1[188] [189] [190] [191]. Thus, inhibition of CDK5/p25 by AZD5438 could reduce DRP1 activation, thus preventing DRP1-dependent fission, contributing to the actions on mitochondrial activities in this chapter. A future investigation on the essential fission protein, Drp1 level, could further confirm the fact[215].

The findings suggest that AZD5438 inhibits parkin recruitment via an inhibition

of CDK-9 and not the inhibition of GSK3. However, the pro-survival effects of AZD5438 could be mediated via the inhibition of GSK3 β and/or CDK pathways. These conclusions are supported by studies that have linked CDK pathways in the aetiology of neurodegenerative illness and demonstrated that inhibiting them is neuroprotective [216, 217]. As discussed in chapter 3, CDK5, a protein that controls glucose metabolism, endocytosis, and neurite development, has been linked to Parkinson's and Alzheimer's diseases [217, 218]. Significantly, kenpaullone and AZD5438 have previously been shown to inhibit CDK2 and reduce the cisplatin-induced production of ROS by mitochondria [101, 204]. Furthermore, CDK-9 inhibition was recently shown to inhibit autophagy via PINK1/PRKN-dependent pathways in a hepatocellular carcinoma cell line [219], which is consistent with the findings in this study that cells showed less parkin recruitment activity when pre-treated with AZD5438.

GSK3 α/β inhibitors have previously been found to modulate mitochondrial quality control and apoptotic pathways, suggesting that the protective effects of AZD5438 might also be mediated by GSK3 β inhibition (discussed in chapter 3). In addition, PGC1 α , a critical regulator of mitochondrial respiration and quality control, has been demonstrated to be regulated by GSK3 β . GSK3 β was shown to target PGC1 α to proteasome degradation, and the inhibition of GSK3 β was shown to upregulate PGC1 α and increase mitochondrial activity. This is consistent with the findings that AZD5438 prevented the decrease of PGC1 α and TOMM20 protein levels

following rotenone treatment. Furthermore, GSK3 β has been shown to interact with VDAC2 and Bax, thereby increasing the mPTP and Bax-mediated apoptosis, respectively. Therefore, the inhibition of GSK3 β could inhibit apoptosis following mPTP disruption. Indeed, AZD5438 mediated powerful anti-apoptosis action as indicated by the inhibition of the executioner caspase, caspase 3. Moreover, the findings showed that AZD5438 encouraged glycolytic metabolism in cells. This result is also in line with the action of GSK3 β , which has been suggested to negatively regulate glucose metabolism [164] [166] [167] [168]. In addition, preclinical studies, have shown GSK inhibitors to be effective at inhibiting the onset of neurodegenerative illnesses in models of AD, ALS and PD (reviewed in [207]. These findings have encouraged the development of several classes of GSK3 inhibitors, some of which have been evaluated in phase I clinical trials [220].

AZD5438 protective effects may also be mediated via a differential inhibitory effect on CDKs influencing cellular energy metabolism. It is known that cells can shift between mitochondrial respiration and glycolytic metabolism to adapt to environmental stress and energy demand. In addition, it was shown that inhibiting CDK9 activity by AT7519 drives cells to be less dependent on mitochondria for ATP production [221]. Mitochondria are the major suppliers of energy in the brain, and their dysregulation is linked to the aetiology of PD and HD. However, recent research suggests that energy from glycolysis plays an important role in maintaining synaptic transmission [222], providing energy during periods of

intense neuronal activity[223] and may protect against Parkinson's disease[224]. Therefore, the increased glycolysis mediated by AZD5438 could provide an immediate source of energy to protect cells under conditions of high energy demand and compromised mitochondrial function.

Apart from ATP generation, one of the major reasons cancer cells employ the upregulated glycolytic pathway is to supply glycolytic intermediates, which are required for the production of nucleic acids, proteins, and lipids, as well as lactate to maintain the redox balance of NAD⁺/NADH [225]. The upregulation of glycolysis is beneficial as the cells usually show lower mitochondrial stress with less ROS generation, another key factor mediating apoptosis. This healthier condition of cells has been seen with AZD5438 treatment than the untreated ones following rotenone exposure, that both rotenone-induced mitochondrial ROS generation and caspase-3-activated apoptosis induction were prevented by AZD5438 treatment. These actions from AZD5438 treatment could mediate protective effects to cells facing mitochondrial stress, especially to the highly mitochondrial function-dependent cells, neurons.

In addition, one report showed that activation of cardiac CDK9 represses PGC-1, which accounts for mitochondrial dysfunction [226]. This evidence is consistent with the findings in this study and further supports the hypothesis that inhibition of CDK9 by AZD5438 stabilises the PGC-1 protein activity and prevents damage

to the mitochondrial population. These findings suggest that drugs like AZD5438, inhibiting both GSK3 and multi CDKs, have powerful protective actions against mitochondrial stressors. Hence, they would be promising candidates for the treatment of PD.

The validation study using SH-SY5Y cells confirmed that the actions of AZD5438 are reproducible in the other cell line, bringing the confidence that the AZD5438 might protect human neurons, which serves as the starting aim to investigate in the next chapter. Different types of α -synuclein mutants were selected to be investigated based on the purpose of comparing the protective effects of AZD5438 on preventing damage to cells from different toxic strengths according to their different protein aggregation levels. Interestingly, the findings from the mutant SH-SY5Y study suggest that the WT α -synuclein overexpression but not the CT mutant ones might be involved in eliminating rotenone-induced cellular damage as it protected the cell viability loss caused by rotenone as AZD5438. Although broad evidence suggests that α -synuclein aggregation contributes to Lewy body formation as a crucial event in PD, some studies point out its neuronal protective role in preventing cytochrome c release and caspase-activated apoptosis [227] [228] [229]. The findings suggest that treating the cells with AZD5438 and upregulating WT α -synuclein together might mediate a stronger anti-apoptosis effect. Further investigations are encouraged to validate this suggestion.

Limitations and concerns

There is a concern that the knockdown mediated by the targeted siRNA transfection was not further confirmed in this chapter. This could lead to insufficient evidence to conclude whether the negative results were due to no effects from the targets or because the targets knocked down were not reached. And this is the reason why this study does not exclude the possibility that the AZD5438's effects seen could be due to targeting CDK1, CDK2, CDK5, and GSK3b. A further study confirming the knockdown via checking mRNA expression levels or investigating the protein levels could add more crucial evidence to this research and is therefore recommended.

It needs to be noted that the mtDNA assay in this chapter investigated the change of relative mitochondrial DNA content to the nuclear DNA. Assuming that a single cell is in the non-dividing stage, mitochondrial genesis and degradation will increase and decrease the value from the assay, respectively. As the nature of dynamic mitochondria, the data of mtDNA assay indicates the balance shift of their genesis and degradation activities. In the case that AZD5438 treatment increased the relative mtDNA content, it suggests the balance of mitochondrial genesis and degradation shifted to a more genesis stage, which could be due to the prevention of mitochondrial degradation. Although it is suggested that this assay could identify the fragmentation level of mitochondrial DNA, the rotenone treatment did not mediate a significant effect on it. This could be because the cells

used are parkin overexpressed cells, which have a healthier nature in preventing mtDNA damage, or the nuclear DNA was damaged at the same time by rotenone exposure. Therefore, it is recommended to apply this assay to further investigate cells with no mitochondrial positive alterations or introduce a positive control (specific mitochondrial DNA damage inducer), which could give the assay window to evaluate the treatment effects in protecting against rotenone exposure or other stress.

Chapter5 Investigating the effects of AZD5438 in rodent primary neurons and human iPSC derived midbrain neurons.

Introduction

AZD5438 was confirmed as a potential PD protective drug in the previous chapter. However, the findings were based on experiments conducted in the H4 neuroglioma and SH-SY5Y neuroblastoma cells. In tumour cell lines, energy metabolism, cell cycle regulation, and the stress response differ to that found in non- carcinogenic cells. Furthermore, neurons are post-mitotic and there will therefore be further differences in the metabolic and signaling pathways compared to cancer cell lines.

Thus, the main aim of the experiments performed in this chapter was to investigate whether AZD5438 mediated similar effects on mitochondrial function and neuroprotection in primary rat and human neurons. The main reason for using rat primary cortical neuron culture is that this culture is well established to reach a relatively high population of neuronal cells, and therefore, suits the purpose that investigating AZD5438's actions on neurons. In addition, the mechanism by which AZD5438 acted was also investigated using cellular and electrophysiological assays. Importantly, to thoroughly investigate the potential as AZD5438 as a

treatment for PD its neuroprotective potential in cultures of midbrain dopaminergic neurons was investigated.

Results

Evaluation of AZD5438's action in rat primary cortical neurons

AZD5438 protects rat primary cortical neurons from rotenone-induced toxicity

To assess AZD5438's protective effects in neurons, cells isolated from E18 rat embryos were seeded and maintained in a 96-well plate as described in the method chapter. After ten days of culture in vitro (DIV 10), AZD5438 and rotenone were added for 24hrs, and MTT assays were performed.

The data shows (**Figure 5-1**) that AZD5438 alone at a concentration of 2 μ M did not affect the cell viability of primary cortical neurons. Treatment with rotenone at doses of 250nM and 500nM significantly reduced cell viability as assessed by MTT assays. AZD5438 was found to significantly protect the neurons from rotenone toxicity when applied at a dose of 2 μ M.

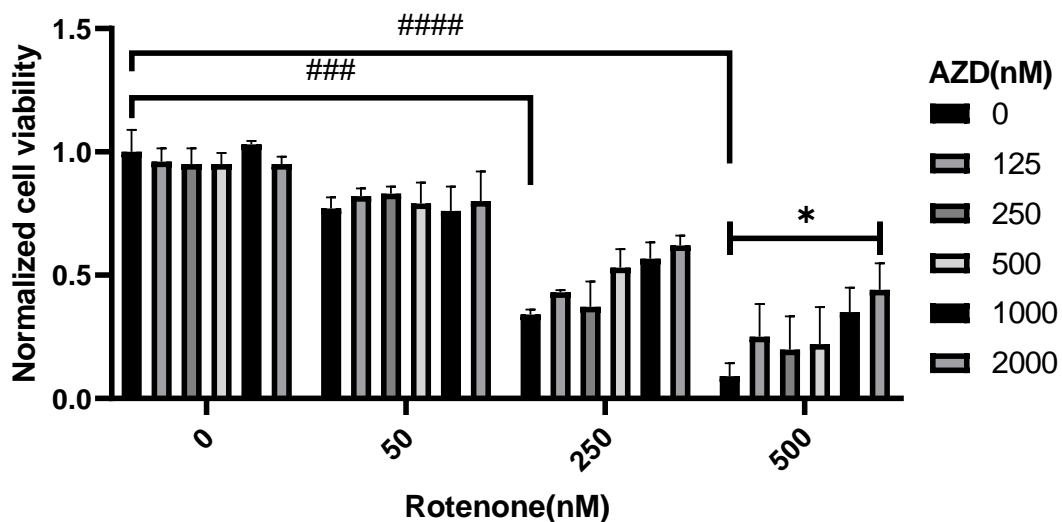


Figure 5-1 AZD5438 protects rat primary cortical neurons from rotenone toxicity

Cell viability was measured in E18 primary neuronal cultures by MTT assays following treatment with AZD5438 and rotenone. 250nM($p=0.0002$) and 500nm($p<0.0001$) rotenone significantly reduced neuronal viability when compared to CON. AZD5438 mediated significant protective effects ($p=0.0421$) compared to the no AZD5438 control in the 500nM rotenone group. Statistical analysis was carried out by two-way ANOVA test with Tukey's multiple comparisons test. $N=3$; data is displayed as mean \pm SEM, significance is displayed as * $p<0.05$, ** $p<0.01$, *** $p<0.001$, **** $p<0.0001$. Asterisks denote comparisons between no rotenone control and rotenone treatment, and hashes denote comparisons between no AZD5438 treatment and AZD5438 treatment.

AZD5438 protects the neuronal network of primary cortical neurons

The next step was to test the effects of AZD5438 on neuronal morphology and mitochondrial form using the INCell analyser to conduct image analysis. Combinations of AZD5438 and rotenone were added to rat cortical cultures (DIV 10) for 24h, Mitotracker Red was used to visualise mitochondria, Tuj1 was used to label neurons, and Hoechst was used to stain nuclei.

The results showed that 1000nM AZD5438 protected neurons from 250nM rotenone (**Figure 5-2 A**). Analyses showed that rotenone mediated the disruption of the neuronal mitochondrial population and decreased Tuj1 staining of neurones. Tuj1 staining in the rotenone group showed severe neuronal damage compared to Tuj1 staining in the control groups, which showed healthy neuronal cell bodies and neurites. Treatment with AZD5438 prevented damage to the neuronal mitochondrial population, and neuronal network caused by rotenone. Treatment with AZD5438 alone did not mediate damage to the neuronal cultures(**Figure 5-2 B**). The results also confirm that rotenone mediated a decrease in the neuronal population and reduced the total neurite length and mitochondrial population (**Figure 5-2 B**) and that this was reversed by treatment with AZD5438.

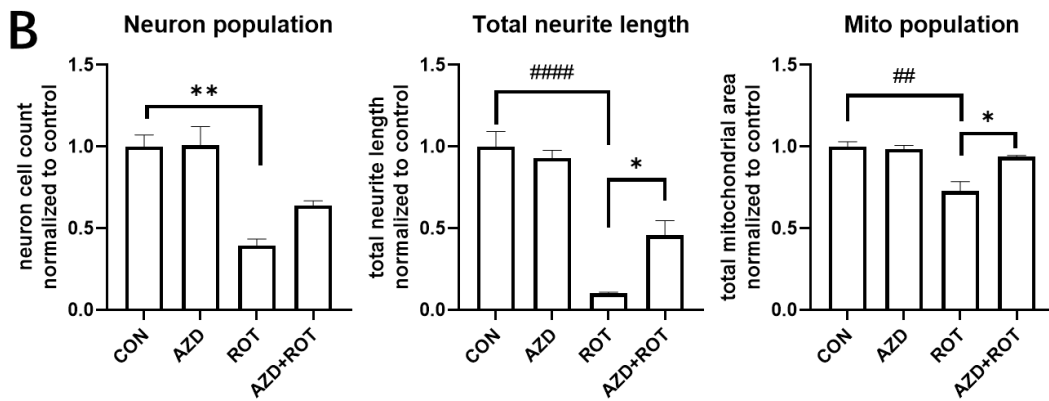
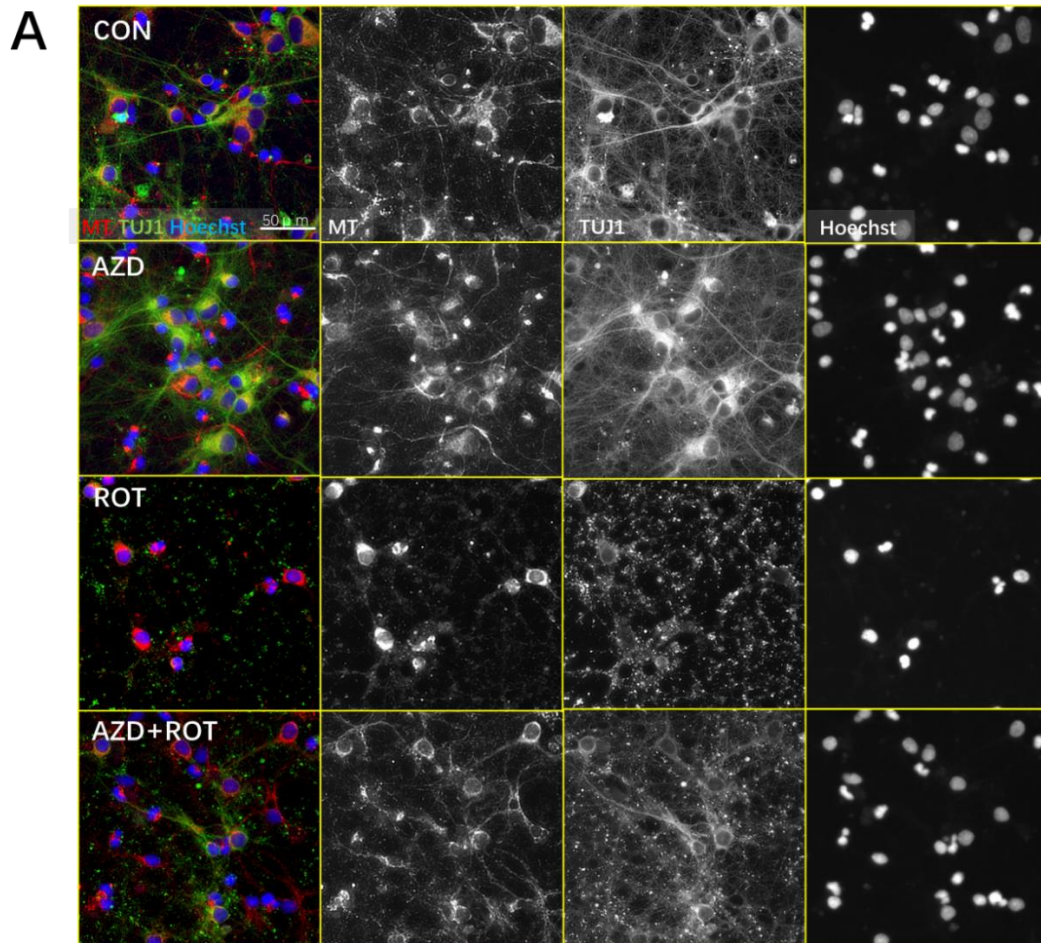


Figure 5-2 AZD5438 protects the neuronal network of primary cortical neurons from rotenone toxicity

E18 primary cortical cultures were treated with rotenone and AZD5438 for 24h before being stained with Mitotracker (mitochondria), Tuj1 (general neuron) and Hoechst (nuclei). Images were taken using the INCell Analyzer 2200 high-content imaging system. The corresponding data output was processed using the INCell Workstation software, and statistical analysis was performed using GraphPad Prism. A) Figure shows the merged images of 3 single channels (mitotracker-red, Tuj1-

green and Hoechst-blue) and the images of these individual channels in grey-scale. It shows that rotenone significantly reduces the complexity of the neuronal network and the mitochondrial network within neurites. AZD5438+rotenone improved these damaged conditions compared to rotenone. **B)** Neuron population characterised by neuron cell count was significantly ($p=0.0014$) reduced by rotenone. There was a trend for AZD5438 to be protective but this did not reach significance. Total neurite length was significantly ($p<0.0001$) decreased by rotenone compared to CON, and AZD5438 mediated a significant protective effect ($p= 0.0384$). The mitochondrial population indicated by total mitochondrial area was significantly ($p= 0.0027$) reduced by rotenone, and this effect was reversed by AZD5438 ($p= 0.0128$). Statistical analysis was carried out by two-way ANOVA test with Tukey's multiple comparisons test. $N=3$; data is displayed as mean \pm SEM, significance is displayed as * $p<0.05$, ** $p<0.01$, *** $p<0.001$, **** $p<0.0001$. Asterisks denote comparisons between no rotenone control and rotenone treatment, and hashes denote comparisons between no AZD5438 treatment and AZD5438 treatment.

AZD5438 regulates the mitochondrial network of primary cortical neurons

Image analysis using the INCell analyser's high magnification and data processing capabilities were used. The results showed (**Figure 5-3 A**) that treatment with 1000nM AZD5438 mediated an increase of the mitochondrial network (appearing as stronger staining) compared to control in which mitochondria appear as individual dots and dotted lines. Analysis of mitochondrial form (**Figure 5-3 B**) confirmed the shape change ($1/(\text{form factor})$), and the mean area of mitochondria was increased by AZD5438, which suggested the mitochondria were generally longer following AZD5438 treatment. $1/(\text{form factor})$ is the alternative shape indicator to the previously used 'elongation' factor. The form factor better differentiates mitochondrial form in primary neurons; hence, it was used in preference to the elongation factor used in the analysis of cell lines.

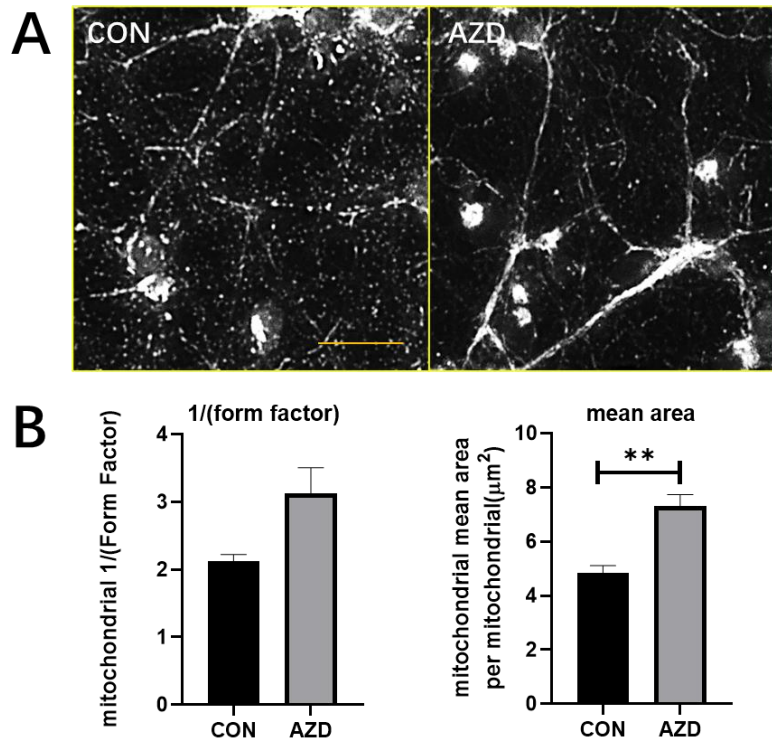


Figure 5-3 AZD5438 regulates the mitochondrial network of primary cortical neurons

E18 primary cortical neurons were treated with rotenone and AZD5438 for 24h before being stained with Mitotracker. Images were taken with the INCell Analyser 2200 high-content imaging system; corresponding data output was processed using INCell Workstation software, and statistical analysis was performed using GraphPad Prism. A) Grey-scale images of Mitotracker staining indicate mitochondrial network changed by AZD5438 treatment. Instead of a single dot-like distribution of mitochondrial network in CON, mitotracker staining became more in line shape with a stronger uninterrupted signal in AZD5438. Scale bar= 25 μM . B) AZD5438 treatment increased mitochondrial 1/(form factor) and significantly(0.0085) increased the mean mitochondrial area compared to CON. Statistical analysis was carried out by unpaired t-test. N=3; data is displayed as mean \pm SEM, and significance is displayed as ** p<0.01.

AZD5438 prevents the induction of ROS by rotenone in primary cortical neurons

Rotenone is known to mediate neuronal toxicity by inducing the production of ROS and the experiments in cell lines (chapter 4) showed AZD5438 protected against this effect. Experiments were therefore carried out to assess the ability of AZD5438 to prevent ROS induction in primary rat neurons.

Cortical neurons were incubated with 1000nM AZD5438 and 250nM rotenone for 24h (at DIV 10), and MitoSox was used to visualise ROS produced by mitochondria. There was a higher level of mitosox staining in primary neuronal cultures compared to that previously observed in H4 cells (Chapter 4). The results show (**Figure 5-4 A and B**) that treatment with rotenone increased the intensity of MitoSox staining when compared to CON. Treatment with AZD5438 significantly protected against the effects of rotenone.

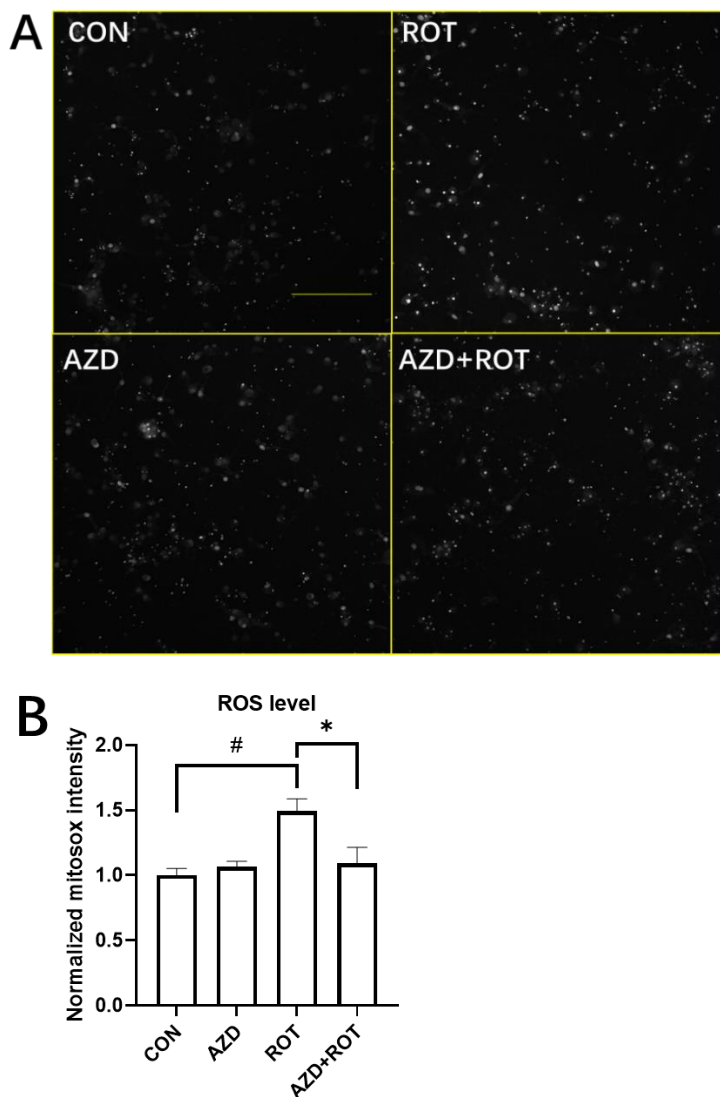


Figure 5-4 AZD5438 prevents ROS induction by rotenone in primary cortical neurons

E18 primary cortical cultures were treated with rotenone and AZD5438 for 24h before being stained with Mitosox to detect mitochondrial ROS. Images were from INCell Analyzer 2200 high-content imaging system; corresponding data output was processed using INCell Workstation software, and statistical analysis was performed using GraphPad Prism. A) Grey-scale images of Mitosox staining showed higher intensity of rotenone treatment than CON. No clear changes from the images in the other groups. Scale bar= 200 μ M. B) rotenone increased mitochondrial ROS level significantly (0.0134). AZD5438 weakened the rotenone-induced the ROS level up significantly (p= 0.0378). AZD5438 had no effect shown on its own. Statistical analysis was carried out by two-way ANOVA test with Tukey's multiple comparisons test. N=3; data is displayed as mean \pm SEM, significance is displayed as * p<0.05. Asterisks denote comparisons between no rotenone control and rotenone treatment, and hashes denote comparisons between no AZD5438 treatment and AZD5438 treatment

Assessing AZD5438's protective effects in hiPSC derived midbrain neuronal cells

Midbrain neuronal cultures were generated from hiPSCs

NAS2 hiPSCs with smooth edges of colonies and high dividing speed (approximately doubling every 24hrs) were cultured and expanded carefully with daily medium changes. The cells were then differentiated into midbrain neurons following the protocol described in the methods chapter. Confirmation of cell viability and morphology under a brightfield microscope during the differentiation stages (at certain stages/ days, as shown in **Figure 5-5 A**) was carried out. Following this quality control step, the expression of Tuj1 and TH was measured. Tuj1 is the main component of microtubules primarily expressed in neurons; thus, the positive staining indicates successfully differentiated neuron cells. TH is the enzyme needed to synthesise dopamine and is therefore used as a marker for dopaminergic neurons.

Cells were differentiated into midbrain neurons, as shown in **Figure 5-5 B**, with neuronal neurites marked by Tuj1(Green) and a healthy population of dopaminergic neurons marked by TH(Red). The calculation for cells count was conducted by ImageJ, showing general neuron/nuclei at $33.5\pm 7.5\%$ and $25.4\pm 10.3\%$ of which were dopaminergic neurons.

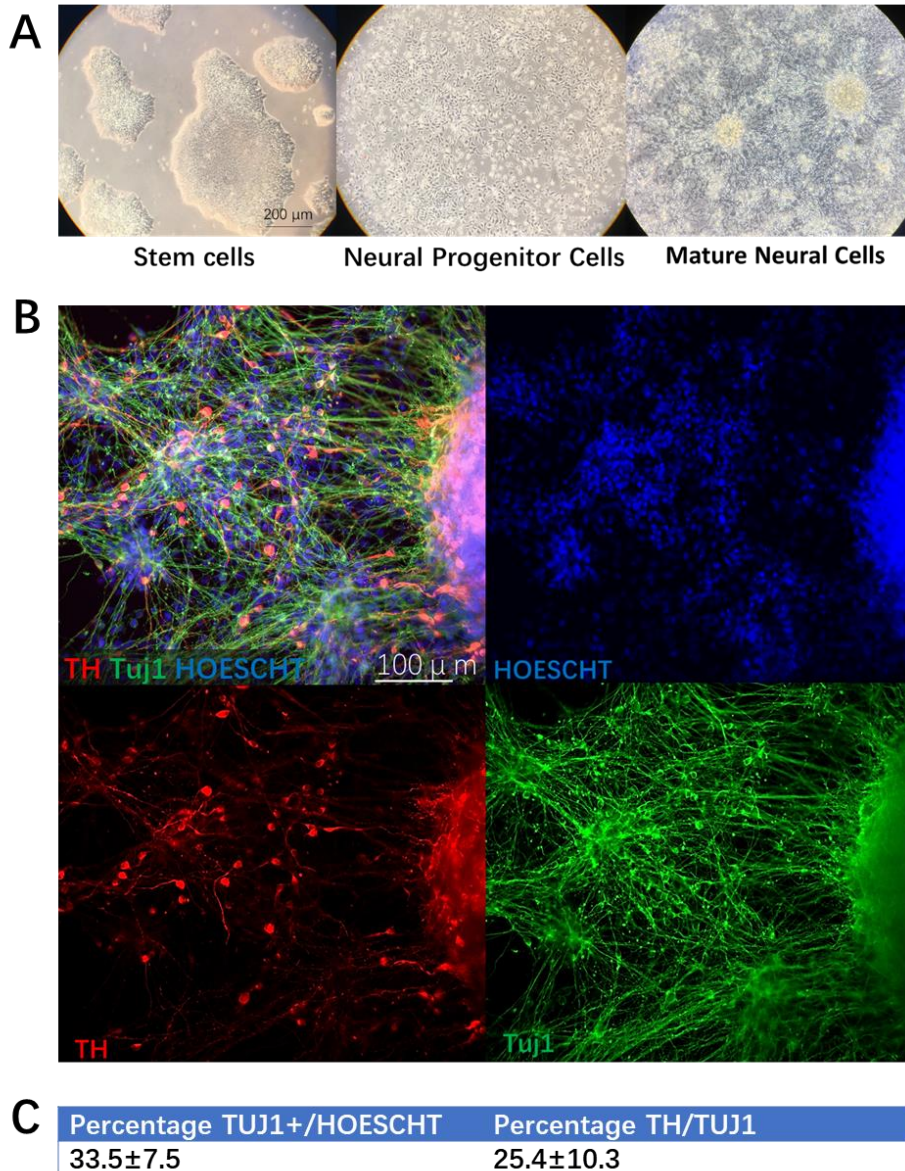


Figure 5-5 Midbrain neuronal cell culture was generated from hiPSCs

A) Brightfield images showing the morphology of the cells at specific stages of the differentiation process as 1. stem cells, 2. neural progenitors, 3. mature neurons. Scale bars =200 μm . B) Images of differentiated NAS2 iPSCs into midbrain dopaminergic neurons at day 45. Midbrain neuronal cell culture differentiation was characterised by visualising the expression of both general neuronal marker TUJ1 and dopaminergic neuronal marker TH. Images show the merged images followed by single-channel images individually. A large general population of TUJ1 positive cells can be seen as neurons, while among them, a small population of TH positive cells can be seen as dopaminergic neurons. C) Table graph shows the average percentage ($\pm\text{SD}$) of cells expressing TUJ1 and the percentage of which expressing TH(n=3).

AZD5438 protects human midbrain neurons from rotenone-induced stress

Since promising results with the MTT assay were obtained in cell lines and rat primary neurons, it was considered that a corresponding experiment should be applied to human midbrain neurons. To achieve this, MTT assays were optimized in human neurons. The same concentration of MTT was used, however, a shorter incubation period of 2 hours was used as this gave clear results without affecting cell morphology (no obvious collapsed cell bodies or damaged axons were observed compared to incubation for 3.5 hours). A dose-response experiment was conducted to find the dose range suited and was based on a previous study in primary neurons [230]. From the dose-response graph (**Figure 5-6**) the trend was:

- 1) With 0 AZD5438, bars showed decreasing trend along rotenone concentration increasing; 500nM rotenone had the most potent effect.
- 2) With 0 rotenone, bars showed an increasing trend along AZD5438 increasing in the range of 0 to 500nM.

The results suggested AZD5438 could be used below 1000nM without damaging the viability of human midbrain neurons. Based on this trend summary and the criteria mentioned earlier, 500nM AZD5438 and 500nM rotenone were chosen as the experimental dose for human neurons for further study.

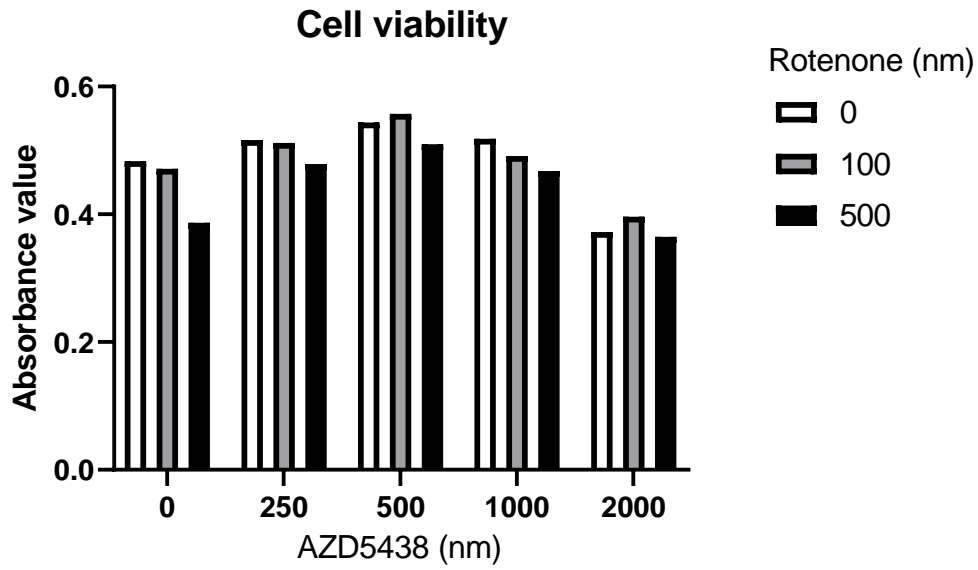


Figure 5-6 Dose-response of rotenone and AZD5438 assessed by MTT assay.

Groups were formed from 3 doses of rotenone and 5 doses of AZD5438 to optimise the assay for iPSC midbrain neuron cells. Bar value was shown by the mean value of absorbance of 6 wells in one experiment; hence no statistical analysis was performed. The graph shows that either rotenone or AZD5438 alone treatment at 500nM had the most potent effect on cell viability than control.

As described previously, more dark dots reflect more MTT formazan generated with more robust mitochondrial activity. There was a general level of MTT formazan across the wells examined in the control group, with similar levels in the AZD5438 group. In contrast, there was a decreased level of MTT formazan in the rotenone group, which was partially reversed by treatment with AZD5438 (**Figure 5-7 A**). Those initial observations from the images were supported by the statistically analysed data collected after absorbances of formazan from 3 independent experiments were examined. rotenone significantly reduced the cell viability of human neurons by approximately 40%. In line with previous findings, AZD5438 prevented the loss of viability due to treatment with rotenone(**Figure 5-7 B**).

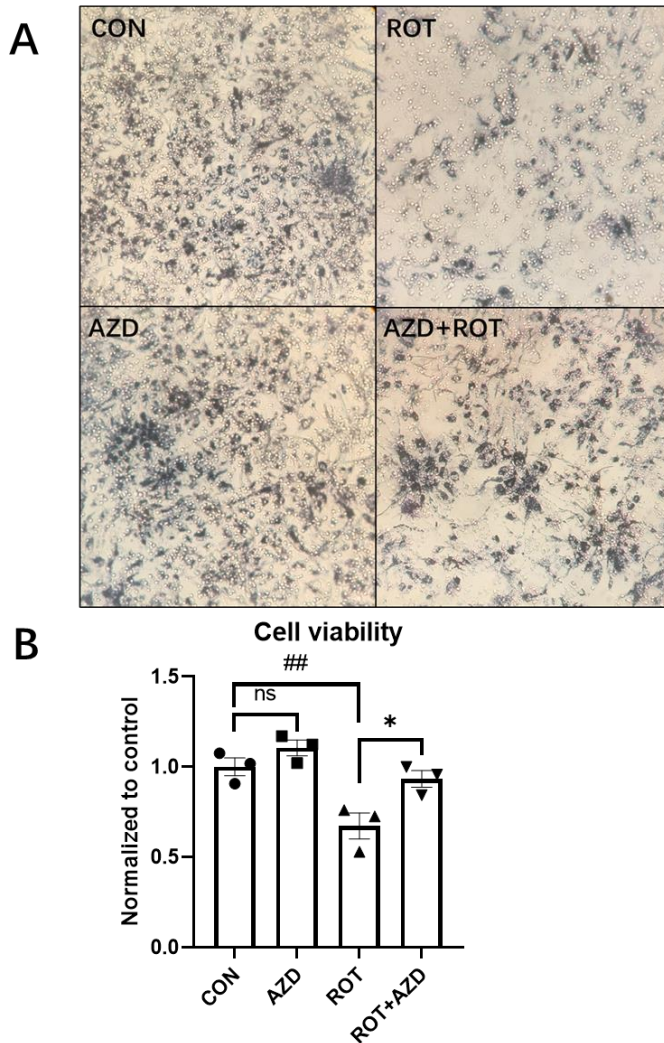


Figure 5-7 AZD5438 protects human midbrain cells against rotenone-induced stress

(A) Bright-field images show MTT formazan formation as dark spots in each group after 24h treatment of vehicle treatment, 500nM AZD5438, 500nM rotenone, 500nM AZD5438+500nM rotenone, respectively. rotenone significantly reduced the appearance of the formazan product compared to control, while AZD5438+rotenone enhanced the formation compared to rotenone alone. AZD5438 treated alone mediated no visible change compared to control. (B) The bar graph shows the data normalised to control and statistically analysed after triplication of experiments (each symbol indicates the mean value from an individual experiment). It shows the significant loss of cell viability induced by rotenone ($p=0.0081$) and the significant rescue effect of AZD5438 ($p=0.0277$). Statistical analysis was carried out by two-way ANOVA test with Tukey's multiple comparisons test. $n=3$ plates, data is displayed as mean \pm SEM. * $p<0.05$, ** $p<0.01$. A symbol stands for the mean value of data from one individual experiment. Hashes denote comparisons between control and experimental group, asterisks denote comparisons between experimental groups (rotenone and AZD5438+rotenone)

AZD5438 protects the neuronal network formed by human midbrain cells from rotenone-induced stress

Immunocytochemical images (**Figure 5-8 A**), showed there was no difference in TuJ1 staining in neuronal cultures treated with AZD5438 compared to controls. Treatment with rotenone for 24hrs mediated damage to the neuronal cell population, and this was visible as decreased TuJ1 staining. Neurites were also evidently damaged as they were less dense and fragmented. Images of TH staining showed similar effects on dopaminergic neurons.

The data showed that AZD5438 protected the neurons as the decreases in the neuron population mediated by rotenone were reversed by AZD5438 (54.26% to 83.52%) (**Figure 5-8 B**). However, AZD5438 did not prevent the neurite loss mediated by rotenone (**Figure 5-8 C**).

Analyses of dopaminergic neurons were conducted using the INCell analyser and by ImageJ analysis of cells on coverslips. Although the percentage of TH positive cells in 96-well plates shown in the images from INCell (**Figure 5-8**) was considered relatively low compared to those on coverslips (**Figure 5-9**), the data analysis of both(**Figure 5-8 D and E, Figure 5-9 B and C**) supported the same findings. 1. 500nM rotenone treatment for 24 hours damaged dopaminergic neurons in terms of cell population and neurite number. 2. 500nM AZD5438

treatment for 24 hours did not affect dopaminergic neurons in terms of morphology.

3. Incubation with AZD5438 did not attenuate the effects of rotenone on dopaminergic neuron morphology. When a higher percentage of dopaminergic neurons were present, the protection trend was stronger but did not reach significance.

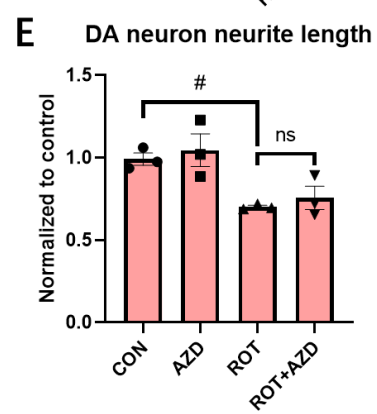
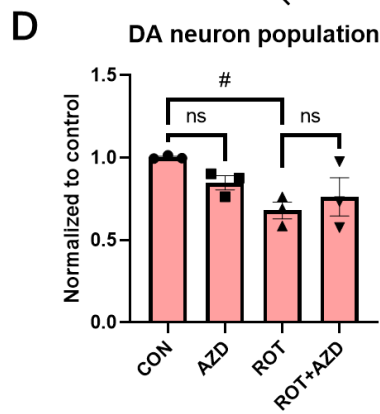
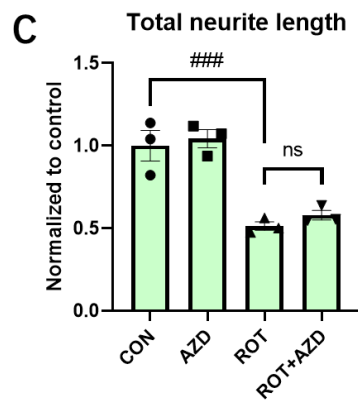
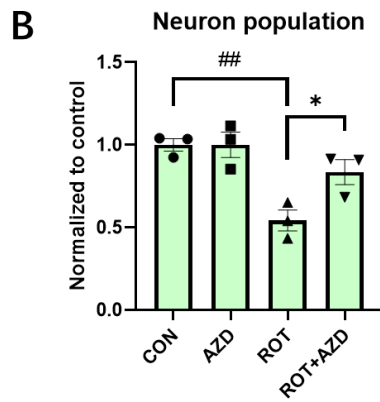
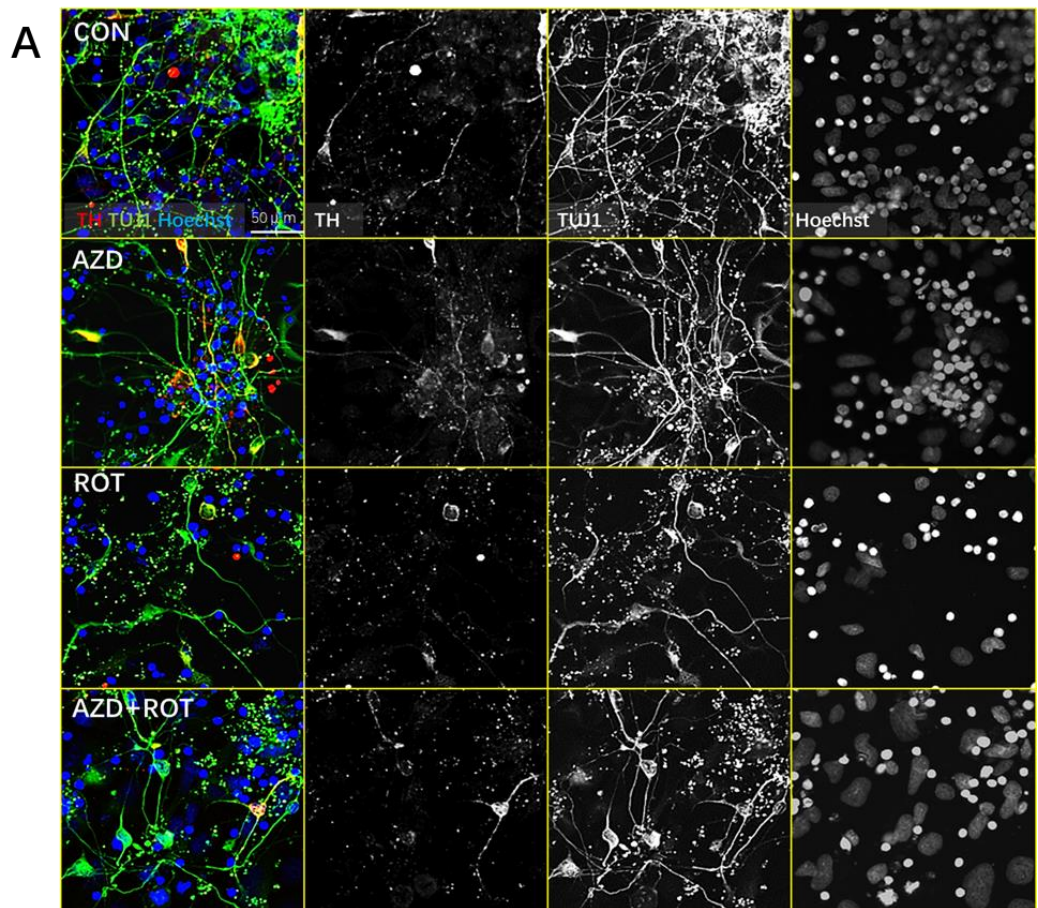


Figure 5-8 AZD5438 protects the neuronal network of human midbrain neurons.

Human-induced pluripotent stem cells (hiPCs) were differentiated towards a midbrain fate for 45-55 days, and immunostained for tyrosine hydroxylase (dopaminergic neurons) Tuj1 (general neurons) and Hoechst (nuclei). Images were taken with the INCell Analyzer 2200 high-content imaging system, corresponding data output was processed using INCell Workstation software, statistical analysis was performed using GraphPad Prism 8. A) The immunofluorescent staining images show midbrain neurons cells culture treated with AZD5438/rotenone in each group. Samples were stained for each marker and processed as described in methods showing TH (red), Tuj-1(Green) and Hoechst (blue), followed by the greyscale single-channel images used as original images for analysis accordingly. The group of bar charts show statistically analysed data, each graph has its title indicating the content correspondingly. B) neuron population bar graph shows rotenone decreased neuron population significantly ($p=0.0034$) while AZD5438+rotenone attenuated it significantly ($p=0.0397$). C) Total neurite length graph shows rotenone decreased neuron neurite length significantly ($p=0.0010$) while no effect was shown with AZD5438 alone or together with rotenone. D) DA neuron population graph shows rotenone decreased DA neuron population significantly ($p=0.0277$) while no effect shown with AZD5438 alone or together with rotenone, E) DA neuron neurite length graph shows rotenone decreased DA neuron neurite length significantly ($p=0.0495$) while no effect shown with AZD5438 alone or together with rotenone. Statistical analysis was carried out by two-way ANOVA test with Tukey's multiple comparisons test. $n=3$ plates, data is displayed as mean \pm SEM. * $p<0.05$, ** $p<0.01$, *** $p<0.001$. One symbol stands for the mean value of 6 wells from one individual experiment. Hashes denote comparisons between control and experimental group, asterisks denote comparisons between experimental groups (rotenone and AZD5438+rotenone).

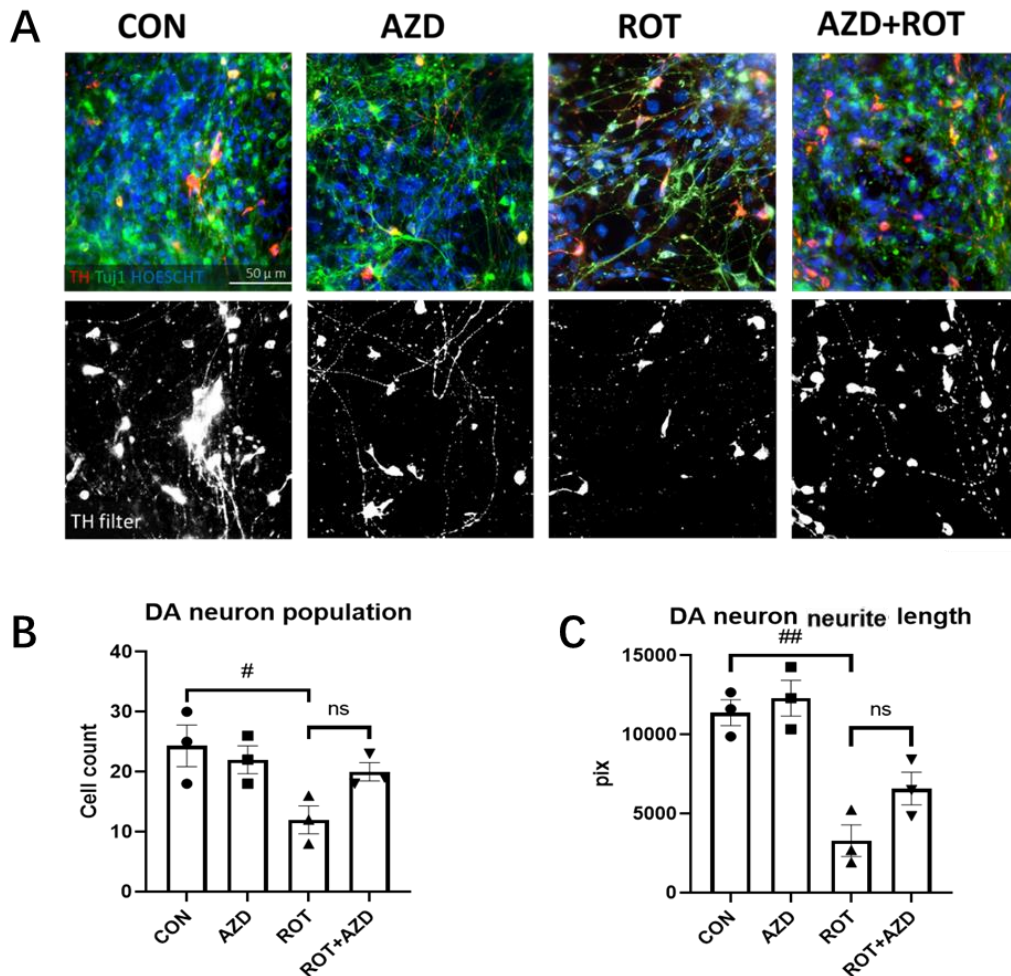


Figure 5-9 AZD5438 potentially protects the human dopaminergic neuronal network

Images were from cells on coverslips taken by a conventional fluorescent microscope, corresponding data were processed using ImageJ with NeuronJ plugins. Merged images show TH (red), Tuj-1 (Green) and Hoechst (blue), followed by the greyscale single TH channel images below used as images for analysis accordingly. A) The representative images show changes of TH positive cells among midbrain neurons cells culture treated with AZD5438/rotenone in each group. rotenone treatment damaged the visible TH positive cells network in terms of reduced cell count and reduced length of neurites compared to the control group, while AZD5438+rotenone rescued them compared to the rotenone group. B) DA neuron population graph shows rotenone decreased DA neuron count significantly ($p = 0.0247$) while no effect shown with AZD5438 alone or together with rotenone, C) DA neuron neurite length graph shows rotenone decreased DA neuron neurite length significantly ($p = 0.0013$) while no effect shown with AZD5438 alone or together with rotenone. Statistical analysis was carried out by two-way ANOVA test with Tukey's multiple comparisons test. $n = 3$, data is displayed as mean \pm SEM. * $p < 0.05$, ** $p < 0.01$.

AZD5438 regulates the mitochondrial network of human midbrain cells

Mitotracker-red was used to visualise the mitochondria network across the culture. The samples were also stained for Tuj1 and Hoechst to localise neurons and nuclei accordingly. As shown in, **Figure 5-10 B** and **C**, the mitochondrial network was slightly different between non-neuronal cells and neurons. In a non-neuronal cell, mitochondria are distributed around the nuclei and evenly across the cell body, while in neurons, mitochondria do not only localise around the nuclei but also spread along the neurites. Healthy non-neuronal and neuronal cells contained evenly distributed rodlike mitochondria.

When cultures were treated with rotenone, the cell death could cause the loss of neuronal markers, which would interfere with the interpretation of the results. Therefore, rather than attempt to measure mitochondria number in neurons alone the effect of AZD5438 on total mitochondrial number was measured. The results in (**Figure 5-11 A**) showed that rotenone treatment changed the mitochondrial morphology and they distributed much closer to the nuclei than in the control group, as they no longer appeared to be evenly distributed in the cells. AZD5438 treatment alone did not change the distribution but treatment did overcome the collapsed distribution observed in the rotenone alone group, and the mitochondria were elongated as also seen when treated with AZD5438 alone. Data

(**Figure 5-11**) supported the observational findings as total mitochondrial area per cell reduced significantly when treated by rotenone, which was rescued by treatment with AZD5438. Interestingly, AZD5438 significantly altered the mitochondrial elongation with or without the presence of rotenone.

Results (**Figure 5-12**) obtained from TOMM20 stained coverslips showed the presence of a large number of red intensive ball-like inclusions in cells following treatment with rotenone treatment, which was reduced with AZD5438 treatment. Cells with increased TOMM20 staining were considered to be the membrane damaged cells by rotenone as they would be more permeable to the TOMM20 antibody, thus increasing the fluorescence intensity by binding to secondary antibody [231]. Taken this into consideration, the results suggested AZD5438 was protecting against rotenone induced cellular damage as fewer intensively staining red cells were present.

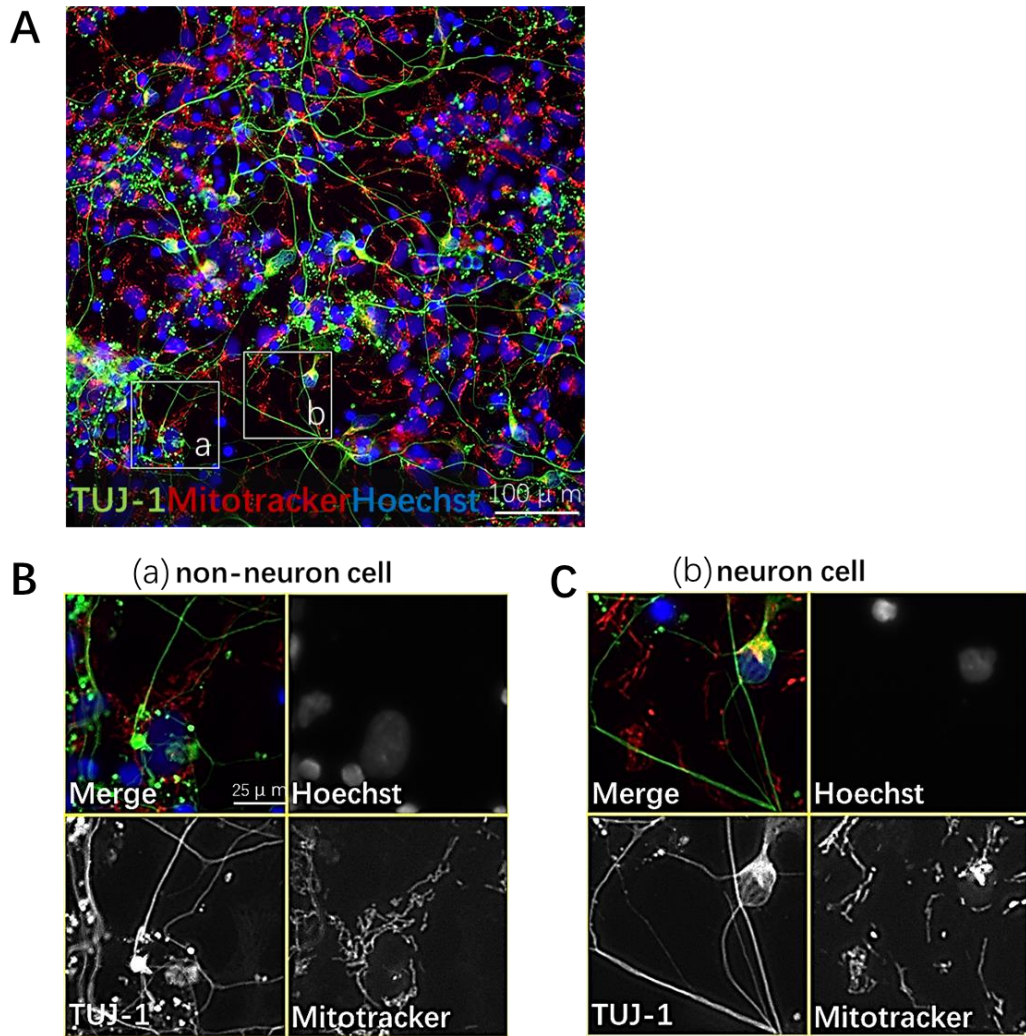


Figure 5-10 Mitochondrial visualisation in hiPSC derived midbrain neuronal cultures.

A) The representative merged immunofluorescent image shows human midbrain cells and the mitochondrial network (INCell 2200). Samples were stained for each marker and processed as described in the methods section showing Mitotracker (red), Tuj-1 (Green) and Hoechst (blue), followed by zoomed-in images from 2 areas as shown in a-B (non-neuron cell) and b-C (neuron cell). The group images show merged channels, visualise nuclei (Hoechst), neurons (Tuj-1) and mitochondria (Mitotracker) individually. B) It shows Tuj-1 negative cell which was considered non-neuronal cell with big nuclei and its mitochondrial distribution was around its cell body. C) It shows Tuj-1 positive cell which was considered as a neuronal cell with small nuclei and its mitochondrial distribution was around its neurites.

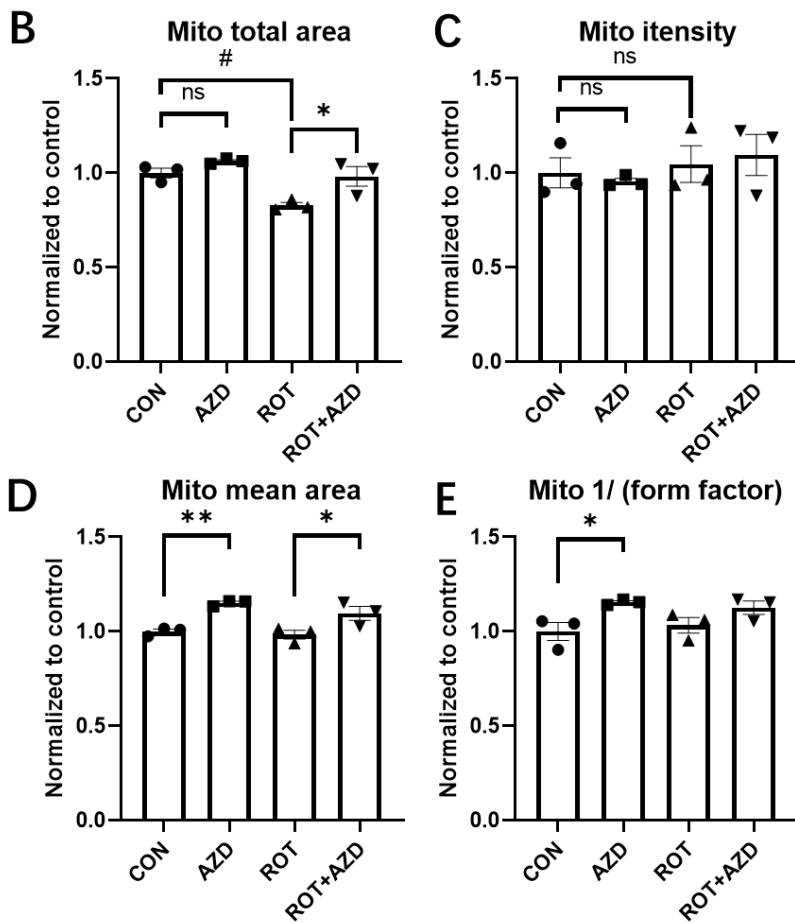
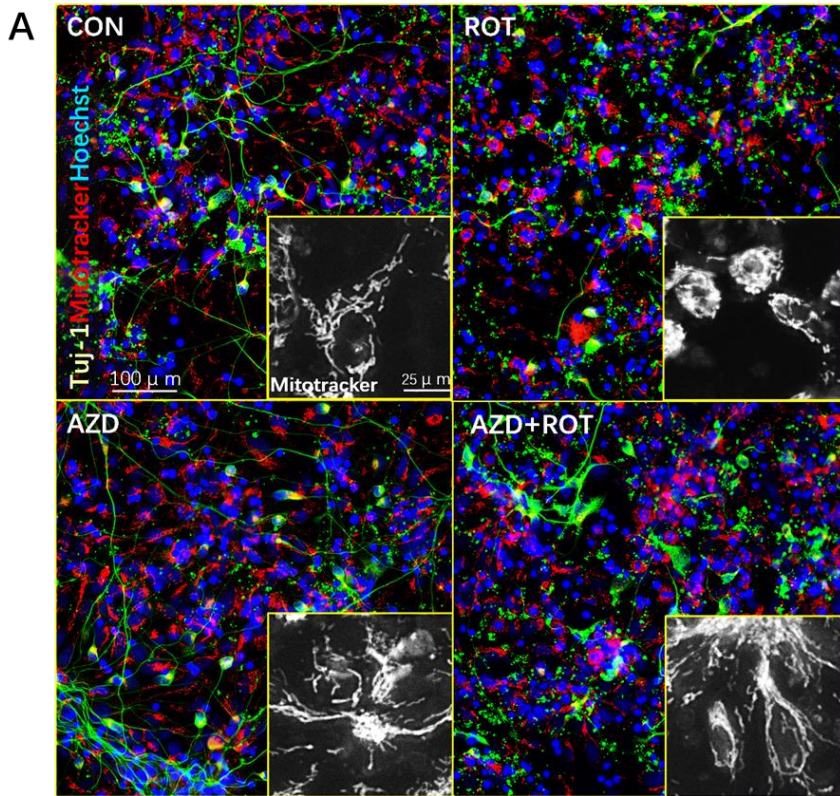


Figure 5-11 Mitochondrial network in hiPSC derived midbrain neuron cultures following treatment with rotenone and AZD5438

AZD5438 modulates the mitochondrial network of human induced pluripotent stem cells (hiPCs) differentiated towards a midbrain fate for 45-55 days, stained for Mitotracker (mitochondria), Tuj1 (general neurons) and Hoechst (nuclei). Images were from INCell Analyzer 2200 high-content imaging system, corresponding data output were processed using INCell Workstation software, statistical analysis was performed using GraphPad Prism 8. The immunofluorescent staining images show mid brain neurons cells and mitochondria network change treated with AZD5438/rotenone in each group. Samples were stained for each marker and processed as described in methods showing mitochondria (red), Tuj-1(Green) and Hoechst (blue), followed by the grey scale single channel images showing mitochondria used as original images for analysis accordingly. The group of bar charts show statistically analysed data, each graph has its title indicating the content correspondingly. A) rotenone damaged the mitochondrial network as shown to have reduced mitochondrial area across the image, while AZD5438 appeared to reduce that damage. AZD5438 treatment alone was observed to have more mitochondria in longer shape. B) Mito total area bar graph shows rotenone decreased neuron population significantly ($p=0.0117$) while AZD5438+rotenone attenuated it significantly ($p=0.0212$). C) Mito intensity shows not mitochondrial intensity change recorded with the treatments. D) Mito mean area graph shows AZD5438 increased mitochondrial mean area significantly with ($p=0.0269$) or without rotenone ($p=0.0053$) challenge while no effect shown with rotenone alone, E) Mito 1/ (form factor) graph shows AZD5438 increased mitochondrial 1/ (form factor) significantly ($p=0.0489$) while rotenone seems to weaken which. Statistical analysis carried out by two-way ANOVA test with Tukey's multiple comparisons test. $n=3$ plates, data is displayed as mean \pm SEM. * $p<0.05$, ** $p<0.01$, *** $p<0.001$. Symbol stands for the mean value of data from one individual experiment. Hashes denote comparisons between control and experimental group, asterisks denote comparisons between experimental groups (rotenone and AZD5438+rotenone).

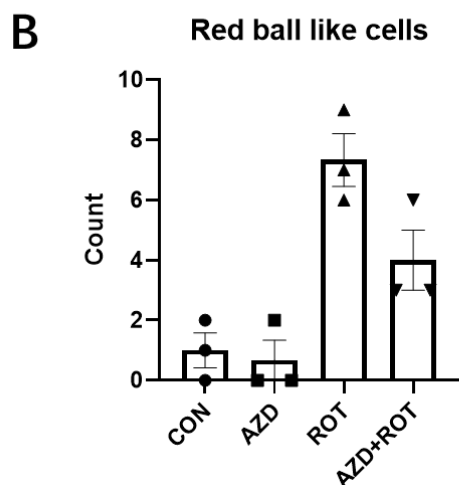
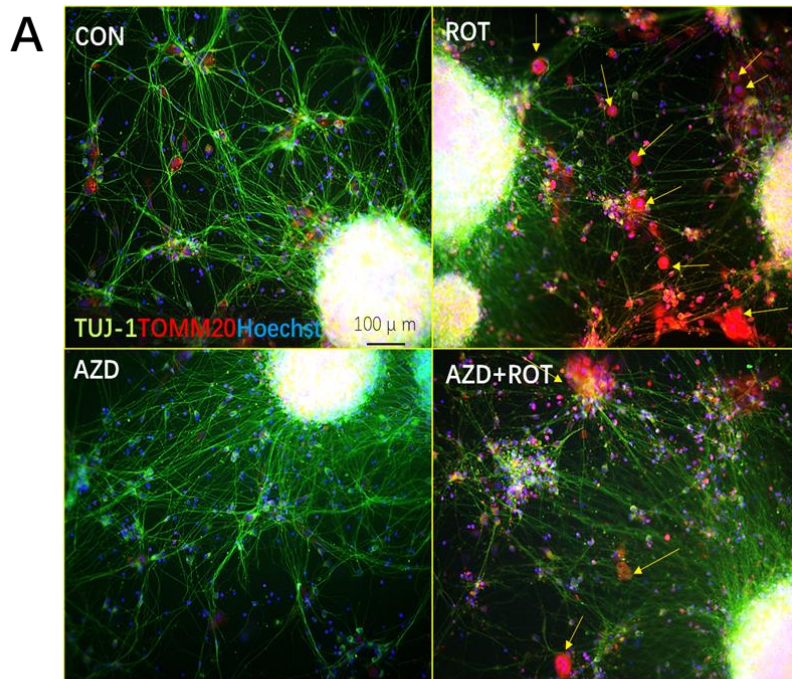


Figure 5-12 Mitochondria in hiPSC derived midbrain neuronal cultures stained for TOMM20 following treatment with rotenone and AZD5438.

hiPCs derived midbrain cells at day 48 on coverslips, stained for TOMM20 (mitochondria), Tuj1 (general neurons) and Hoechst (nuclei). Images were from fluorescent microscope; objectives were manually count and presented using GraphPad Prism 8. A) General Red positive staining was distributed evenly across the images in CON group and AZD5438 group, while rotenone triggered the highly intensive red ball like objectives to appear in a denser way. Treat with AZD5438+rotenone together was observed to have reduced the intensity and the amount of the red ball like cells compared to rotenone alone. B) In the bar graph, rotenone dramatically increased the red ball like cells count while AZD5438+rotenone weaken that count. AZD5438 alone was shown no effect on the red ball like cells count compared to control. Samples were from 3 fields of 3 coverslips in each treatment. No statistical analysis was performed as it lacks sufficient individual

experiment samples.

AZD5438 potentially stabilises PGC-1 α in human midbrain cells following rotenone-induced stress

Immunostaining for PGC-1 α was performed and **Figure 5-13 B** shows the expression of PGC-1 α in control cells, while **Figure 5-13 C** shows rotenone treatment mediates cell apoptosis characterised by collapsed nuclei, which are stained with a higher red intensity.

Staining intensity was calculated (**Figure 5-14**) and showed that rotenone treatment significantly decreased the PGC-1 cell population and increased apoptosis. Treatment with AZD5438 reduced the cell loss and number of apoptotic cells (mediated by rotenone treatment) but this effect did not reach significance. These results confirmed that rotenone served as a toxic insult that altered PGC-1 α expression in hiPSC derived midbrain cultures. A high level of PGC-1 α was associated with rotenone induced apoptosis and there was a trend for AZD5438 to protect cells from changes in PGC-1 α expression due to rotenone.

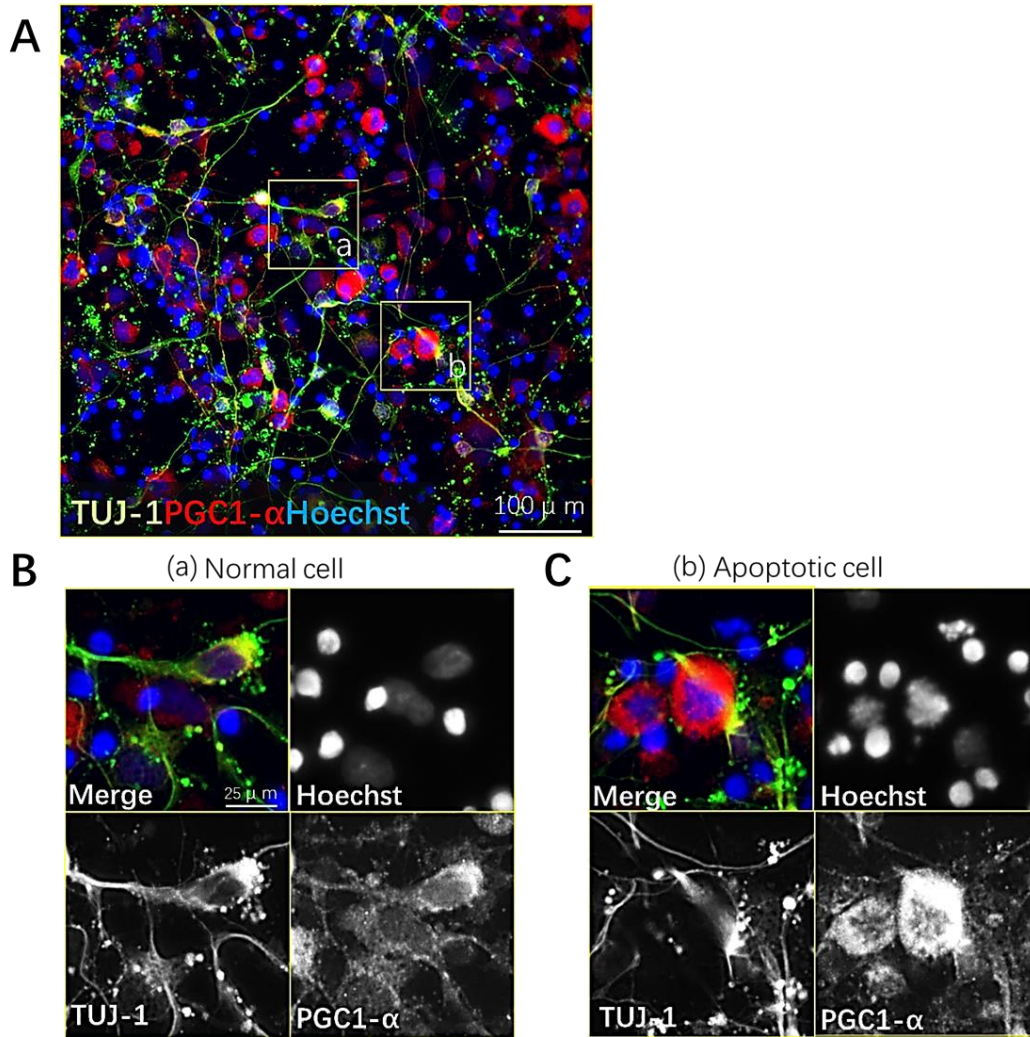


Figure 5-13 PGC-1 α expression in human midbrain cells following rotenone-induced stress

The immunofluorescent staining images show mid brain cells culture and PGC-1 α expression condition treated with rotenone for 24h. Samples were stained for each marker and processed as described in methods showing PGC-1 α (red), Tuj-1(Green) and Hoechst (blue), followed by zoomed-in images from 2 areas as shown in the square a(normal cell) and b(apoptotic cell). Individual single-channel images are shown for closer and more detailed examination. a) It shows PGC-1 α positive cells with general red intensity with round nuclei, which were considered as normal cells. Those cells either had neuronal marker expression or not. b) It shows extremely intense red fluorescent cells with damaged nuclei shape, which were considered as apoptotic cells, and those cells had no visible neuronal marker around cell bodies.

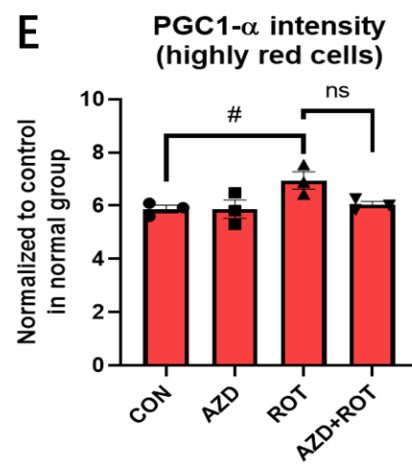
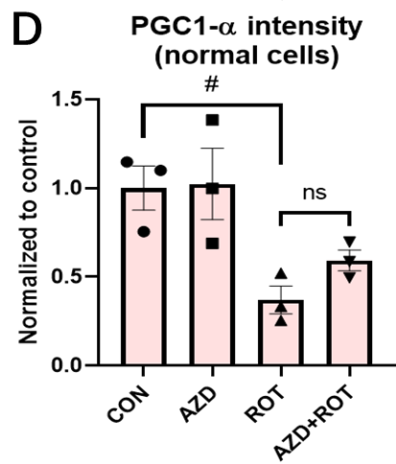
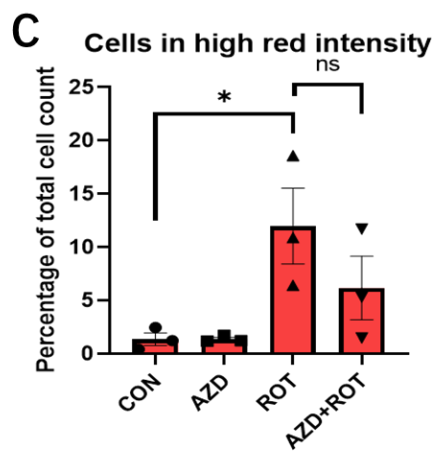
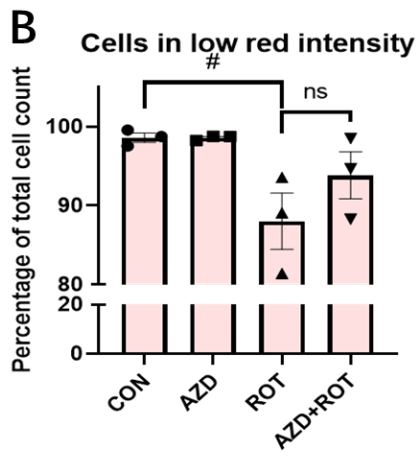
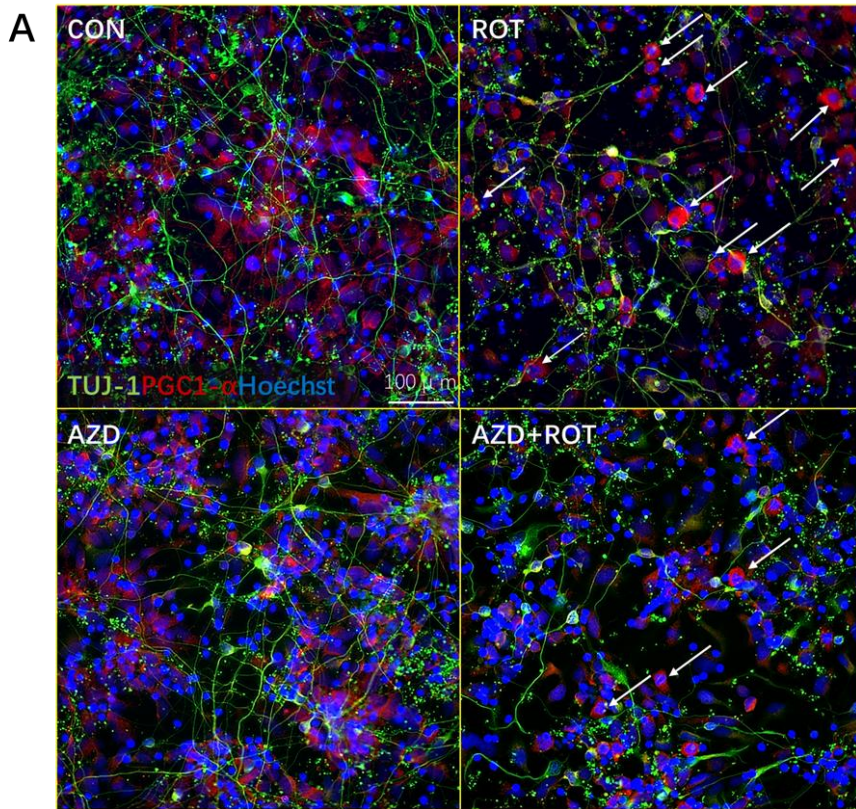


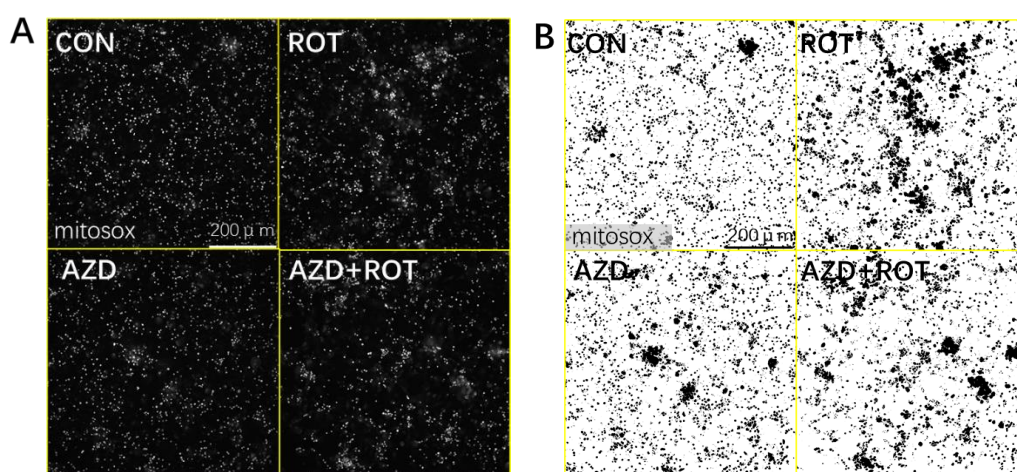
Figure 5-14 AZD5438 mediates a non-significant protective trend against changes in PGC-1 α expression following rotenone treatment in human midbrain cells

Investigation of AZD5438's effect on modulating PGC1- α expression in human induced pluripotent stem cells (hiPCs) differentiated towards a midbrain fate for 45-55 days. Images were taken by INCell Analyzer 2200 high-content imaging system; corresponding data output was processed using INCell Workstation software, and statistical analysis was performed using GraphPad Prism 8. The immunofluorescent staining images show mid brain neuron cells and PGC- α expression change after each group is treated with AZD5438/rotenone. Samples were stained for each marker and processed as described in methods showing PGC- α (red), Tuj-1(Green) and Hoechst (blue). The bar charts show statistically analysed data; each graph has its title indicating the content correspondingly. A) General Red positive cells were distributed evenly across the images in the CON and AZD5438 groups, while rotenone triggered the highly intensive red cells to appear, and reduced general red staining can be observed. Treat with AZD5438+rotenone together was observed to have reduced the size and amount of the highly intensive red cells from the image. B) Percentage of cells with general PGC1- α expression was significantly reduced with rotenone treatment ($p=0.0471$). C) Percentage of cells with intensive PGC1- α red fluorescent signal was significantly increased with rotenone treatment ($p=0.0471$). D) rotenone significantly reduced the general PGC- α expression within the normal PGC- α positive cells($p=0.0245$). E) rotenone significantly increased the intensity of the PGC- α marker within the highly red cells($p=0.0497$). Across all groups, AZD5438 alone did not show an effect on PGC- α expression, although some trends show it was protecting against rotenone induced change. Statistical analysis was carried out by Kruskal-Wallis test with Dunn's multiple comparisons test (B and C); two-way ANOVA test with Tukey's multiple comparisons test (D and E). $n=3$ plates, data is displayed as mean \pm SEM. * $p<0.05$, ** $p<0.01$, *** $p<0.001$. A symbol stands for the mean value of data from one individual experiment. Hashes denote comparisons between control and experimental group, asterisks denote comparisons between experimental groups (rotenone and AZD5438+rotenone)

AZD5438 prevents ROS formation and Caspase-3 mediated apoptosis in human midbrain cells following rotenone-induced stress

The results shown in **Figure 5-15 A and B** show rotenone increased the intensity of ROS staining while treatment with AZD5438 reversed this effect. The analysis of the results shown as bargraphs in **Figure 5-15 C** shows AZD5438 significantly reduced the formation of ROS due to rotenone.

Analysis of active caspase-3 expression (**Figure 5-16**) showed that treatment with rotenone increased the number of active caspase-3 positive cells, while treatment with AZD5438 inhibited this effect. Together with the results described in chapters 3 and 4, it is possible to suggest AZD5438 downregulates the activity of caspase-3 related pathways.



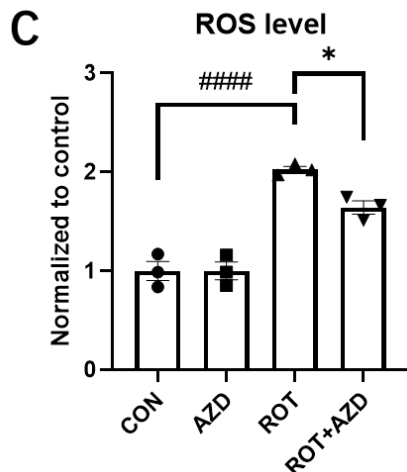
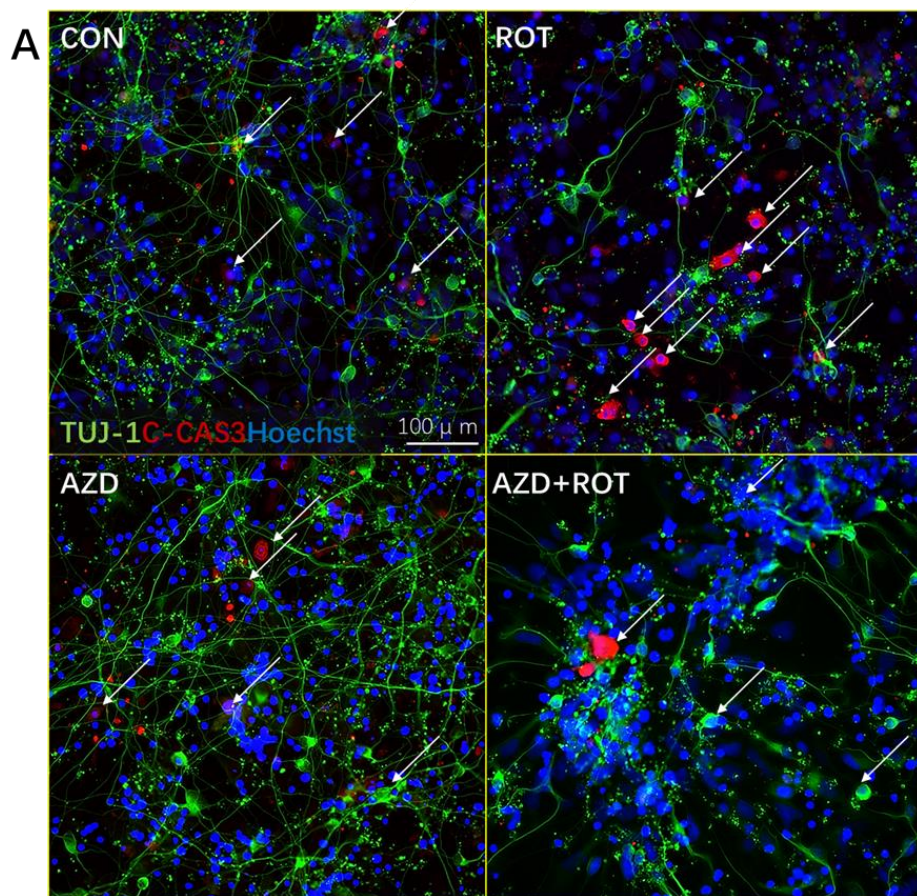


Figure 5-15 AZD5438 prevents ROS formation in human midbrain cells following rotenone-induced stress

Investigation of AZD5438' effect on modulating ROS level change induced by rotenone treatment in human induced pluripotent stem cells (hiPCs) differentiated for midbrain fate for 45-55 days. Live cell images in greyscale from red channel were taken by INCell Analyzer 2200 high-content imaging system, corresponding data output were processed using INCell Workstation software, statistical analysis was performed using GraphPad Prism 8. ROS were visualised using Mitosox-red dye in live cells. A) Small dots were background as dead cells nuclei in the culture. Large intensive clusters show the ROS level change. rotenone increased the level of ROS while AZD5438+rotenone weaken the change compared to rotenone alone. AZD5438 alone has no effect. B) Images were processed by ImageJ to show better contrast to support the observation findings. C) The bar chart shows statistically analysed data on ROS levels in each treatment. rotenone dramatically and significantly increased the ROS level as it almost doubled the level compared to control ($p < 0.0001$), while AZD5438+rotenone significantly prevented it ($p = 0.0208$). AZD5438 alone had no effect. The data value shown has been normalised to control. Statistical analysis was carried out by two-way ANOVA test with Tukey's multiple comparisons test. $n = 3$ plates, data is displayed as mean \pm SEM. * $p < 0.05$, ** $p < 0.01$, *** $p < 0.001$, **** $p < 0.0001$. A symbol stands for the mean value of data from one individual experiment. Hashes denote comparisons between control and experimental group, asterisks denote comparisons between experimental groups (rotenone and AZD5438+rotenone)



B Cleaved-caspase 3 level

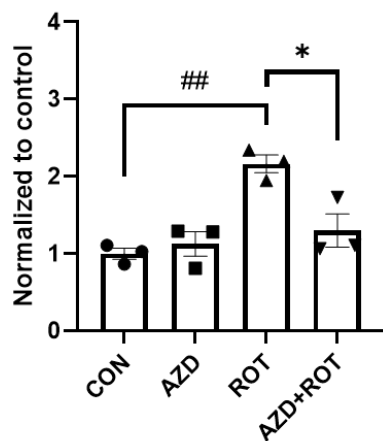


Figure 5-16 AZD5438 prevents Caspase-3 activation in human midbrain cells following rotenone-induced stress

Investigation of AZD5438's effect on modulating caspase-3 activity change induced by rotenone treatment in human induced pluripotent stem cells (hiPCs) differentiated for midbrain fate for 45-55 days. Images were taken by INCell Analyzer 2200 high-content imaging system, and corresponding data output was processed using INCell Workstation software; statistical analysis

was performed using GraphPad Prism 8. The immunofluorescent staining images show cleaved caspase-3 expression change when each group is treated with AZD5438/rotenone. Samples were stained for each marker and processed as described in methods showing cleaved caspase 3 (red), Tuj-1(Green) and Hoechst (blue). A) General Red positive cells were distributed sparsely across the images in the CON group and AZD5438 group, while rotenone triggered the highly intensive red objective to appear more densely. Treat with AZD5438+rotenone together was observed to have reduced the intensity and the amount of the highly intensive red cells compared to rotenone alone. B) The bar chart shows statistically analysed data according to the single red channel for cleaved caspase 3 level calculation. rotenone significantly increased the cleaved caspase 3 level ($p=0.0023$), while AZD5438+rotenone significantly prevented it ($p=0.0141$). AZD5438 alone did not affect cleaved caspase-3 levels. The data shown have been normalised to control. Statistical analysis was carried out by two-way ANOVA test with Tukey's multiple comparisons test. $n=3$ plates, data is displayed as mean \pm SEM. * $p<0.05$, ** $p<0.01$, *** $p<0.001$. A symbol stands for the mean value of data from one individual experiment. Hashes denote comparisons between control and experimental group, asterisks denote comparisons between experimental groups (rotenone and AZD5438+rotenone).

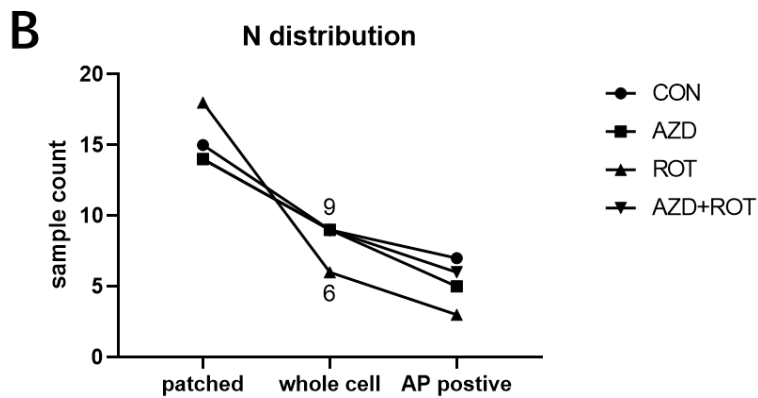
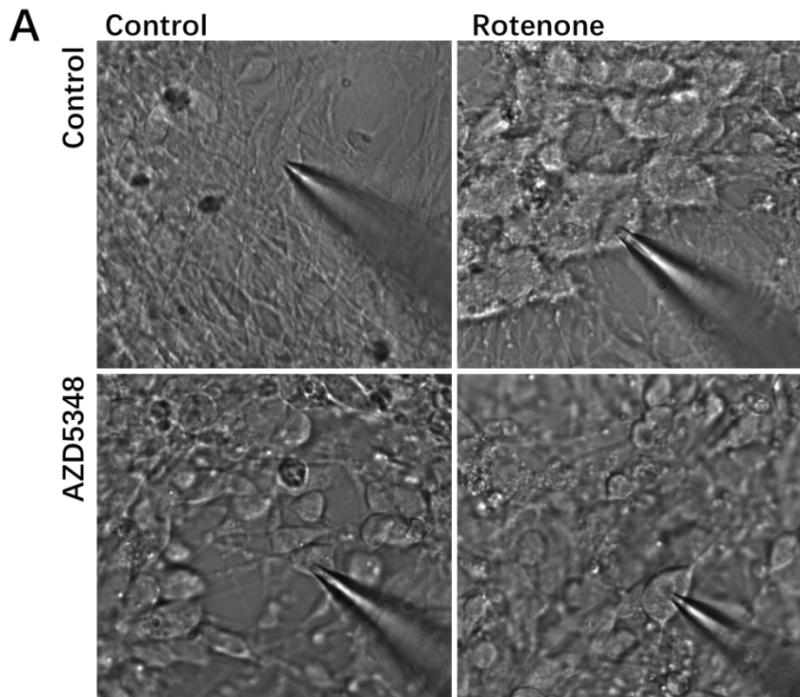
Investigating the mechanism of AZD5438 actions using an electrophysiology approach

Statistically significant data showed that AZD5438 protected neuronal cells from damage by altering mitochondrial activity and activating anti-apoptosis pathways. To evaluate the effect of AZD5438 on electrophysiological properties of neurons, these midbrain neurons were patch-clamped following rotenone and AZD5438 treatment.

Patch-clamp experiments (**Figure 5-17 A**) in the non-drug/compound treated group showed cells were had a smooth and regular shape, and there was no evidence of apoptotic membrane blebbing. When treated with AZD5438 for 24 hours, the cells became slightly more spherical. Notably, following treatment with rotenone the cells showed uneven blebbing membranes, and cell fragmentation around axons and dendrites was observed. In addition, rotenone treated cells were unstable and difficult to patch. In **Figure 5-17 B** show the distribution of successfully 'patched cells' and refers to the cells that were patched with a giga-seal (a seal with electrical resistance above a giga-ohm). 'Whole cell' refers to the cells that entered whole-cell mode (the mode after suction is applied to open the membrane but still sealed) and were stable for recording, 'AP positive' are cells that had an action potential triggered and recorded during the experiment. The whole-cell rate of patched cells and the AP positive rate of whole-cell cells in

separate groups are listed in **Figure 5-17 C**.

The table in **Figure 5-17** indicates that a low patch success rate is associated with unhealthy cells and more attempts are needed to make an N of 9 recordings. The Control group had a general whole-cell rate of 60%, while rotenone dramatically reduced this rate to 33.33%, which was about half the rate of the control. AZD5438 did not dramatically alter this rate compared to control, but it prevented rotenone's reducing effect and brought the rate back to the control level. AP positive rate indicates the general electrophysiologic-active neuronal cell population among the samples. About 77% of cells patched were active neurons in control, and the compound and drug did not dramatically altered this rate. However, the N number is low and further experiments need to be conducted to increase the robustness of the findings.



C

	Whole-cell rate (%)	AP positive rate (%)
CON	60	77.78
AZD	64.29	55.56
ROT	33.33	60
ROT+ AZD	64.29	66.67

Figure 5-17 Patch clamping of midbrain neurons with treatments.

(A) Shows that brightfield photomicrographs of midbrain neurons derived from human iPSCs were treated in groups with rotenone and AZD5348. (B) The graph shows the number of cells patched and subsequent numbers which were whole-cell and AP positive. (C) Table shows the percentages of the whole-cell and AP positive cells from (B).

The data in **Figure 5-18** shows the resting membrane potential (RMP) was evenly distributed across each of the various experimental groups. The RMP of control was recorded from 0mv to -38mv with the mean of -20mv. By treatment of AZD5438, a slight RMP shift to more negative was recorded with a mean of -24mv from -10 to -47mv. After being treated with rotenone for 24h, the RMP shifted more positive with a mean of -10 mv from -4mv to -30mv. When treated with AZD5438+rotenone, the RMP mean shifted back from -10mv to -16mv as a sign of preventing the membrane potential loss caused by rotenone.

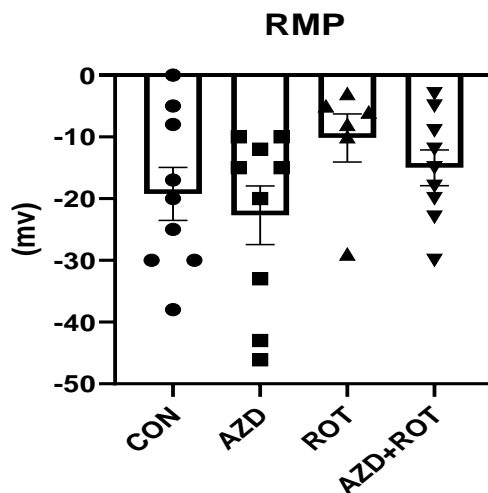


Figure 5-18. Resting membrane potential of midbrain neurons following treatment with rotenone and AZD5438.

The resting membrane potential was measured in midbrain neurons derived from hiPSCs. Symbols represent individual measurements.

For neuronal cells, the ability to fire an action potential (AP) is one of the most important electrophysiologic properties. To investigate the effects of AZD5438 and rotenone's on the AP of the hiPSC derived midbrain neuronal cells, APs were measured in response to step current injections of 25 pA (upper panel) in the current-clamp mode were performed by holding voltage at -60mv. **Figure 5-19 A** shows each group's single representative AP trace when 100pA current was injected. The trace In the control group showed the standard action potential lacked a clear hyperpolarisation stage, while the AZD5438 group had a full action potentials at a faster pace. When treated with rotenone, the firings became slow and weak, while treated together with AZD5438+rotenone, APs returned to the fast and robust pattern. For the amplitude measurements (**Figure 5-19 B**), there was no difference between the control and AZD5438 groups for the AP peak. Although not significant, the AP peak was lower in the rotenone group than in the control when treated with AZD5438+rotenone. For the speed analysis (**Figure 5-19 C**), the time needed to reach the first peak in the AZD5438 group was significantly shorter than in the control group. Although not significant, the trend that rotenone slowed the speed down while AZD5438+rotenone again boosted it can be observed.

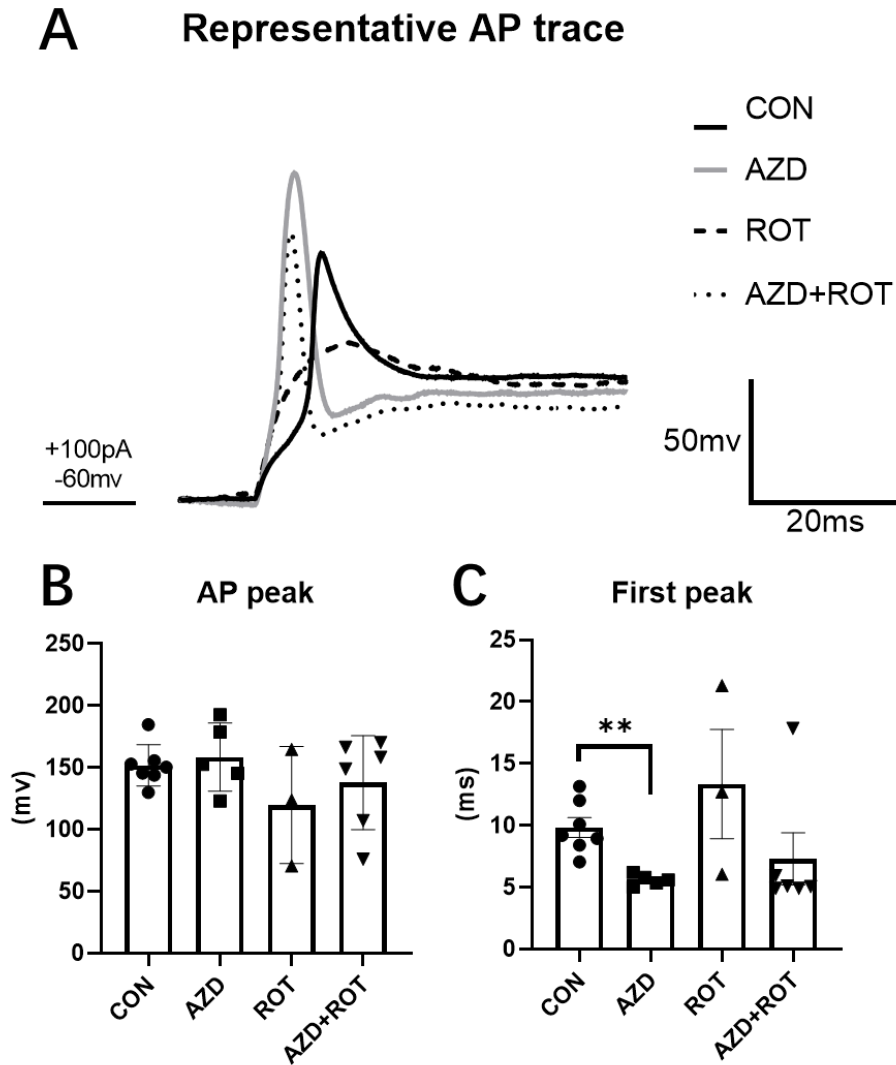


Figure 5-19 Action potential properties of midbrain neurons following treatment with AZD5438 and rotenone

A) shows the representative action potential traces from each treatment, labelled as the right-side legend. B) shows action potential peak voltage value, shows the time to reach the first action potential peak in each group. AZD5438 reduced the time to reach the first AP peak significantly ($p=0.0048$), while no significant effect was shown with rotenone alone or together with AZD5438. Statistical analysis was carried out by Welch's ANOVA test with Dunnett's T3 multiple comparisons test. $N=7$ (CON), 5 (AZD5438), 3 (rotenone) and 6 (AZD5438+rotenone), data is displayed as mean \pm SEM. ** $p<0.01$.

When treated by AZD5438/rotenone, three passive electrical membrane properties, the membrane resistance R_m , membrane capacity C_m and the membrane time constant τ , changed accordingly (**Figure 5-20**). There was no significant change due to AZD5438 after analysis. However, more samples showed lower R_m and τ in the AZD5438 group. Cells in control showed high R_m and τ values, both of which decreased significantly in the rotenone group. However, when treated with AZD5438+rotenone, that change was inhibited though this did not reach significance (**Figure 5-20 B and D**). Together, the results suggest that the membrane of the cells treated with rotenone had been either damaged or in high sensitivity to current injection, and AZD5438 had a protective effect against this. C_m remained in the same range, which is supportive evidence that the cells patched were in matching size in terms of the double-layer lipid membrane, which had not been affected by treatment (**Figure 5-20 C**).

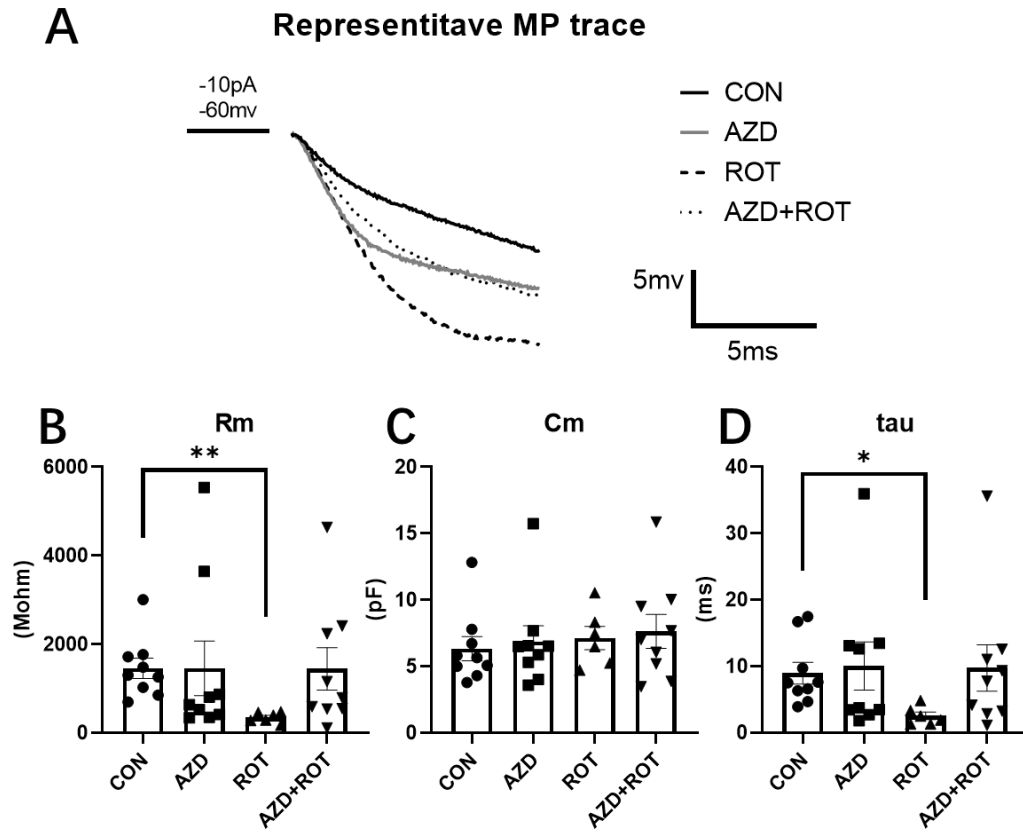


Figure 5-20 Membrane potential properties of midbrain neurons following treatment with AZD5438 and rotenone

(A) shows the representative passive potential trace triggered by -10pA, (B) shows membrane input resistance (Rm) value, (C) shows membrane capacitance (Cm) value, (D) shows the time constant of the membrane voltage (Tau) value in each treatment group. rotenone decreased cells' Rm($p=0.0057$) and Tau($p=0.0222$) significantly while no effect was shown with AZD5438 alone or together with rotenone. Statistical analysis was carried out by Welch's ANOVA test with Dunnett's T3 multiple comparisons test. N=9 in all groups except n=6 in the rotenone group, data is displayed as mean \pm SEM. * $p<0.05$, ** $p<0.01$.

Summary and discussion

Study on primary neurons

AZD5438 had similar protective effects on primary neurons as on cell lines

In this section, rat primary cortical neurons were used to investigate the neuroprotective effects of AZD5438. The results confirmed the findings obtained in Chapter 4 and showed that AZD5438 mediated effects on mitochondrial form and prevented the toxic and apoptotic effects of rotenone on neurons.

MTT cell viability assay in neurons

MTT assays are widely used to measure cell viability change, and the assays are based on the measurement of NAD-dependent oxidoreductases in the whole cell population. It is known that two main factors contribute to MTT cell viability assay values. One is the cells' population, and the other is the cells' metabolic activity. In cancerous cells, with the relatively high contribution from fast-dividing cells with population change and relatively low contribution from single cells' metabolism change, the MTT measurement indicates cell viability. It should be noticed that in neuronal cells, with a limited dividing rate of the cells, the MTT results also reflect the activity of mitochondria, specifically, complex I [232]. Thus, the cells' population and morphology were also examined and provided a supportive

interpretation of the result. A later imaging study using neuronal cell count further supported the MTT assay's result that AZD5438 protected the cell viability against rotenone, which is consistent with the previous findings. The assay's performance showed that the well-established MTT assay is suitable for neuron viability study with its reliable advantages of high efficiency and consistency, just as it is suitable for cell lines.

AZD5438 protected primary neurons from rotenone toxicity

The first finding from the cell viability results is that the protective effect of AZD5438 was observed against rotenone-induced cell viability damage in the primary neuron culture. This observation confirmed that AZD5438 could protect neurons, as previously discussed. Besides, neuron culture showed higher tolerance to AZD5438 as 2000nM did not reduce cell viability. In contrast, 250nM AZD5438 induced a significant cell viability decrease in H4 and SH-SY5Y cells. The high compound dose tolerance of primary neurons could be because the culture at DIV10 had a lower level of cell proliferation activity [233]. Thus, the inhibitory effect of CDKs from high doses of AZD5438 on the cell cycle did not significantly impact the cell population after 24h in primary neuron culture as it did in cell lines. The cell count results in the imaging assay further supported this assumption. It is suggested that AZD5438 might be safer to use in neurons than in cell lines, even at higher doses, which might maximise its protecting effects. Notably, the primary

neuron culture might contain a small population of other cells other than pure neurons. However, it is unlikely that the results from the small number of other cells could largely interfere with the results from neurons. The imaging assay was performed further to confirm the effect of AZD5438 on neuron viability.

AZD5438 protected the neuronal network of primary neurons

The study in primary neurons confirmed that AZD5438 protected neurons, the neurite network, and mitochondrial networks from rotenone-induced stress. Healthy neurites are essential for neuronal function, and the degradation of neurites are often resulted from dysfunctional mitochondria with reduced ATP levels and increased ROS levels[234]. AZD5438 protected mitochondria, thus securing the ATP generation and preventing the ROS formation, resulting in the neurites protection in the primary neurons. It is then suggested that AZD5438 could be an up-and-coming candidate to prevent neurodegenerative disease mediated pathogenesis.

AZD5438 protected the mitochondria of primary neurons

Imaging analysis of mitochondria in the primary neurons indicated that AZD5438 altered the neurons' mitochondrial activities and potentially protected the neurons. This effect is evidenced by mitochondria having a greater area after AZD5438 treatment. A potential explanation for this phenomenon is that more mitochondria

were present in neurites after AZD5438 treatment. As the mitochondria spread along the neurites, they followed the neurites' shape and network. Thus, they were shown as longer in shape and more in area than distributed around cell bodies. Therefore, it is assumed that AZD5438 increased the ratio of mitochondrial on the neurites to the cell body. This potentially increased mitochondrial amount on neurites would benefit the neuron network with increased energy and functional Ca²⁺ homeostasis, preventing stress-induced damage, thus protecting the neuronal network. Another explanation for the mitochondrial shape is that the mitochondrial activities shifted to more fusion following AZD5438 treatment, which increases ATP production. The mitochondrial conditions could be further evaluated by checking the fission and fusion protein level change and mtDNA level.

AZD5438 protected the primary neurons by preventing ROS formation

Mitochondrial ROS assay confirmed that AZD5438 prevented intensive ROS formation induced by rotenone, potentially protecting neurons. The primary neuron cell culture generally showed higher mitochondrial ROS levels when untreated with AZD5438 or rotenone than H4 cells. This ROS level difference is known between cancerous cells and neurons. The relatively high mitochondrial ROS level in untreated neurons reflected the extensive mitochondrial activities in

the healthy functioning neuronal cells[235]. Notably, AZD5438 did not reduce the base level of the mitochondrial ROS in the primary neuron cells, suggesting AZD5438 did not affect the general health and function of the neurons. Besides, neurons are suggested to be more sensitive to mitochondrial stressors because their activities are highly dependent on mitochondrial ATP production. Therefore, neurons are more easily triggered into a higher level of ROS from the dysfunction of the mitochondrial electron transport chain when they face mitochondrial stressors [236]. From this point of view, the effect of AZD5438 on protecting mitochondria with less ROS generation could be the protective effect that benefits neurons more than the cell lines.

Study on hiPSC derived midbrain neurons

AZD5438 had similar protective effects on human midbrain neurons as on rat primary neurons

In this section, the previous findings on H4 cells, SH-SY5Y cells (Chapter 4), and rat primary neurons were compared with hiPSC derived midbrain neuron cultures. First, NAS2 lines were cultured and expanded carefully and successfully differentiated to midbrain neurons following the established protocol and characterised by a dopaminergic neuronal marker, TH. Research using midbrain cultures of dopaminergic neurons are also highly relevant to PD. AZD5438 protected against the effects of rotenone on cell viability, neuronal and

mitochondrial network, ROS formation and Caspase-3 activation, and electrophysiologic activity. Again, these protective profiles of AZD5438 in the human midbrain neurons could make it a great candidate for PD treatment.

AZD5438 protected the human midbrain neurons against rotenone

In this study, the cell viability conditions affected by the candidate compound AZD5438 and damage inducer rotenone were thoroughly examined using multi-dose and single-dose focused experiments. As a result, rotenone, a well-known mitochondrial stressor, severely damaged the viability of these human iPSC induced midbrain cells in cell morphology and activity, consistent with another study [237]. This result indicated that the assay effectively detected the damage from rotenone on human neurons and, thus, can credibly indicate the AZD5438 treatment's effect. As the main result, the severe damage from rotenone was remarkably prevented by the treatment of AZD5438. This result is consistent with the previous findings of studies in cell lines and primary neurons, thus, suggesting AZD5438's protective effect is highly translational. It is also suggested that the mechanism underlying AZD5438's cell protection could be similar to the previously discussed effects that were linked to stabilising mitochondrial activity and upregulating glycolysis, thus securing ATP and preventing ROS and apoptosis (discussed in Chapter 3 and 4).

Neuronal Tuj-1 positive cells were protected from rotenone by AZD5438. However, Tuj-1 expressing neurite loss was not prevented by AZD5438. Evidence suggests that rotenone strongly destabilises microtubules by perturbing the secondary structure of tubulin, and this is not dependent on ATP generated by mitochondria [238] [239]. Thus, AZD5438 may not protect neurites as the damage is caused by a pathway not altered by the improved mitochondrial function. However, it may be that a larger number of experiments need to be completed to see the significance or that the dose of rotenone (500nM), used is too high to allow the protective effect to be seen. Hence, chronic treatment with a lower dose may better reflect AZD5438's protective effects against rotenone. Although further evaluation is needed before an accurate conclusion can be reached, it is highly promising that AZD5438 could prevent human midbrain neuronal death from acute and severe mitochondrial damage, as findings in this study suggest.

For dopaminergic neurons marked by TH staining, the protection trend of AZD5438 became more clearly noticed with the cells grown on the coverslips than when they were grown on 96-well plates. This trend suggests that AZD5438 might protect the dopaminergic neurons just as it did for the general neurons when the culture is rich in detectable dopaminergic neurons for analysis. Thus, further investigation on dopaminergic neuron rich cultures should be conducted to confirm AZD5438's protective effect before reaching an accurate conclusion.

AZD5438 protected the mitochondria network in human midbrain neurons against rotenone

Neurons have a damaged mitochondrial network following rotenone treatment. AZD5438 protects the mitochondrial network against rotenone-induced damage, which could restore ATP generation and prevent mitochondrial ROS formation, and these action of the drug may be efficacious in PD treatment.

In addition, AZD5438 was found to mediate mitochondrial elongation. This result could be the effect of more mitochondria presented along the neurites. Considering the previous finding that AZD5438 prevented CCCP induced Parkin recruitment in H4 and SH-SY5Y cells, this increased mitochondrial elongation could result from halted mitophagy. Research suggested that mitochondrial elongation protects mitochondria from autophagic degradation [240] and as a result, the remaining part of functioning mitochondria optimise ATP production. The mitochondrial protein level study confirmed 1) rotenone reduced the general PGC-1 α expression across the culture. 2) rotenone triggered a small population(11.33 \pm 4.9%) of cells showing highly intensive PGC-1 α expression with apoptosis progress. 3) AZD5438 potentially stabilised the alteration of PGC-1 α activities against rotenone induced change. The reduction in PGC-1 α protein levels due to rotenone treatment might be linked to stress-induced Parkin-mediate mitophagy activity,

where Parkin Interacting Substrate (PARIS) was released from Parkin, suppressing PGC-1 α gene expression (detailed explanation in the next chapter) [241]. This reduced PGC-1 α expression might contribute to the downregulated mitochondrial population as PGC-1 α regulates the mitochondrial transcription factor A (TFAM), which regulates mitochondrial biogenesis [242]. AZD5438 prevented the PGC-1 α alteration from rotenone, thus, protecting the mitochondrial network. AZD5438 alone did not mediate detectable changes in PGC-1 α levels, suggesting the hypothesis that AZD5438 enhances mitochondrial biogenesis by upregulating PGC-1 α expression might not hold true.

Unlike the general PGC-1 α level, this study identified that the high level of PGC-1 α protein expression might be associated with rotenone induced apoptosis as they were found to colocalise with the apoptotic morphology of nuclei. This was consistent with findings that suggest the downstream actions of PGC-1 α buffer oxidative stress, mediating the ROS associated apoptosis where mitophagy is induced but insufficient to hold the healthy condition of the cells [243, 244]. AZD5438 potentially stabilised the alteration of PGC-1 α activities against rotenone. This suggested AZD5438 potentially inhibited rotenone-induced mitochondrial biogenesis disruption, mitophagy and apoptosis induction, which could benefit from a healthier mitochondrial network achieved from glycolysis upregulation, as previously discussed in Chapter 4. It is also recommended that a focused study of PGC-1 α upstream and downstream pathways be further

performed, which could add more evidence to reveal the mechanism of the alterations involved.

Moreover, the results confirmed that AZD5438 prevented the mitochondrial ROS formation and caspase-3 activated apoptosis induced by rotenone in hiPSC derived midbrain neuron culture. Caspase-3 activation, the direct signalling for apoptosis has been identified to be dependent on cytochrome c released from mitochondria following high ROS levels[3][19][4]. This ROS-prevention effect of AZD5438 may be mediated as mitochondria are healthier (as previously discussed). The findings suggest that maintaining of the healthy mitochondrial network by AZD5438 is a promising treatment for PD.

AZD5438 and the electrophysiological measurement of neuronal function

The actions of AZD5438 on regulating the electrophysiologic activities of the hiPSC derived midbrain neurons against rotenone-induced stress were investigated. rotenone disrupted neuron membrane properties and there was a trend for AZD5438 to be protective. Interestingly, moreover, AZD5438 enhanced the neuronal firing speed.

Rm and tau usually indicate the level of activity of ion channels on the cell's

membrane; the lower they are, the more active the cell is. Research also shows that R_m and τ decrease over time as neurons mature and have more active channels [245]. However, a massive loss in R_m might suggest a relatively high degree of disruption of the function of the cell's membrane. This disruption could be due to specific ion channels on the membrane being disrupted and unable to maintain ion gradients, or it could be due to physical damage to the cell membrane, leading to leakage of ions [237]. It is unclear to what degree rotenone physically damaged the membrane structure, but the damaging effect was suggested to be associated with microtubule degradation [246]; thus, loss of essential R_m and τ by rotenone treatment was observed. More importantly, evidence highly suggests that rotenone disrupts ion channels by rapidly disrupting ATP production due to complex I inhibition, leading to a decreased Na^+/K^+ ATPase function and further contributing to Na^+ inward current overload [247]. This view is supported by the results showing more positive RMPs in the rotenone group. Consequently, the resting potential is highly depolarised, and the neurons can barely meet the requirements to fire action potentials [248], consistent with the weak AP curve shown in this study. Interestingly, AZD5438 seemed to play the opposite role as it decreased the RMP, enhanced the AP, and restored the failure caused by rotenone, confirming its protective role in the PD model and generally implying its neuronal properties enhancing role.

The spread of RMP values in each group indicates that the cells patched had

different membrane conditions. This could be because 1) they were different types of neuron/cell (neuron or Gila cells), 2) they were in different ageing conditions (mature neurons or young ones), 3) they were in different health conditions (fragmented membrane). Thus, the RMP In the control group indicated the general condition of the RMP in this culture. Compared to the significantly server damage caused by rotenone, AZD5438's effect on RMP and membrane properties alone was not dramatic, but the trends could be discussed. The mechanism underlying AZD5438's contribution to negatively (more functional) regulating RMP of human midbrain neurons is unclear, but the leading hypotheses are the following. 1) Enhancement of the Na/K pump activity by AZD5438 maintained the gradients. 2) Enhancement of K⁺ channel by AZD5438 mediated more outward K⁺ current. 3) Enhancement of Na⁺ channel by AZD5438 inhibited the inward Na⁺ current. These three hypotheses are independent; each or all of them might contribute to the more negative RMP observed by AZD5438 treatment. The first hypothesis is possible as the Na/K pump activity is closely supported by ATP, where AZD5438 might strengthen ATP generation by upregulating glycolysis and protecting mitochondria to enhance the pump. This hypothesis explains the mechanism of rotenone-induced damage on RMP and the protective effect of AZD5438. Hypotheses 2 and 3, in theory, could be the results of GSK3/CDKs-inhibition leaded alteration of ion channel protein assembly or interacting activation [249]. However, the arguments under the kinases' contribution to ion channels make it difficult to analyse the hypotheses without additional targeted evidence. For

example, many studies suggest that GSK3 inhibition positively regulates Na⁺ channels [250] [251] [252] [253], while a recent one suggests GSK3 activation is required for FGF14-Na⁺ channel complex interaction mediated Na⁺ channel function [254]. Therefore, those hypotheses should be further investigated by individually blocking Na⁺/K⁺ ATPase with its inhibitor ouabain, blocking the Na⁺ channel with a blocker such as TTX, blocking the K⁺ channel with class III antiarrhythmic compounds or using other methods selectively to verify the compound's effect on RMP first, and then to perform a more focused analysis [255].

Furthermore, AZD5438 drove the neurons to appear more excited and energetic with fast and robust firings than the control observed. The main explanation for the AP alteration could be the enhanced RMP (more negative) by AZD5438, facilitating the cells with a relatively lower (more negative) threshold potential. In this way, the cells with a lower threshold potential fired more frequently when triggered by the same stimulus current from the same voltage held (pass the threshold), consistent with the observation that firings were faster when cells were treated with AZD5438. Besides RMP, Na⁺ channels and Ca²⁺ channels were considered to be closely linked to the alteration of AP by AZD5438. The voltage-gated Na⁺ channels are the main channels mediating the firing of APs, which occurs after the depolarised neurons meet the voltage threshold. Therefore, it was suggested that the observation of AZD5438-modified AP properties might be due to the voltage-gated Na⁺ channels being activated by a lower voltage after

AZD5438 treatment. This effect might be facilitated by the activation gates of a Na^+ channel that were charged faster to be activated after AZD5438 treatment[256]. This possibility suggested that the individual functional domains of the Na^+ channel could be affected by AZD5438, probably through post-translational modification effects from the kinases it inhibits.

In addition, Ca^{2+} flux and Ca^{2+} channel activities are essential for neurons and are highly likely to be altered by AZD5438 but should be further investigated. Ca^{2+} flux via Ca^{2+} channels modulates presynaptic neurotransmitter release, signal transduction, and synaptic plasticity [257] [258] [259] [260]. There is a long-known relationship between Ca^{2+} and mitochondria, as Ca^{2+} affects mitochondrial functions, while mitochondria contribute to Ca^{2+} dynamics, further building the link between all evidence in this chapter and former chapters [261]. It is suggested that AZD5438 maintained the Ca^{2+} homeostasis through its mitochondrial protective role and thus secured Ca^{2+} flux for AP generation and modulated both pre/post-synaptic functions of neurons [262]. Furthermore, AZD5438 might help improve the activities of Ca^{2+} channels by inhibiting the phosphorylation inhibition of their protein interaction sites, which ensures neuronal activities. The specific phosphorylation inhibitions of synprint sites which are dependent on GSK-3 beta, Cdk5/p25 were seen from N-type and P/Q-type Ca^{2+} channels deactivation[263] [264, 265]. Thus, the inhibition of those kinases could mediate AZD5438's neuron functional enhancing effects. Future studies are highly recommended to validate

the relationship between AZD5438 and Ca²⁺ flux and channels. Specifically and individually inhibiting AZD5438's targets could further reveal the underlying mechanisms of neuronal alteration by AZD5438.

Although the number of samples in this study is considered relatively low to convince the effect of rotenone on AP, research evidence supports that rotenone causes AP failure, which is strongly linked to the loss of ATP production to meet the energy demand in maintaining the resting membrane potential[266]. Furthermore, the evidence presented in the former chapter supports the conclusion that the cell decreases ATP production following rotenone treatment. Therefore, the observation that rotenone disrupted AP in this study is reliable. From the traces recorded, AZD5438 prevented rotenone induced AP failure, which is a good sign that AZD5438 could functionally rescue neuron activity. Admittedly, more study is needed to fully evaluate the risks and benefits of the neuronal activity change mediated by AZD5438 in a broader aspect of view.

Limitations and concerns

It needs to be noted that the term of 'midbrain' was only used for the purpose of brief illustration of the cells fate in expectation, as the culture were carefully generated by following the well-established protocol for midbrain dopaminergic cells. However, the main limitation in this study is that the lack of full

characterisation of the human iPSC derived culture. It is important and highly recommended that at least one of the midbrain markers, such as FOXA2 or Corin expression levels to be checked at the stage of both progenitors and neurons to ensure the culture was growing towards the midbrain fate. Co-staining with TH and FOXA2 should be applied to further confirm the cell are midbrain dopaminergic neurons. This is crucial as the aim of this thesis is to evaluate the potential drugs to treat PD, which is characterised by the loss of midbrain dopaminergic neurons. It is well known that midbrain dopaminergic neurons are generally more vulnerable than others, so it is possible that AZD5438 may not be effective in protecting this type of cells even it could protect the others. Thus, considering the nature of the culture with uncharacterised neuronal fate and a low percentage of TH-positive cells, it is hard to reach a direct conclusion that AZD5348 can treat PD. Therefore, a further study with full characterisation is needed, and single-cell study (Single-cell RNA sequencing, targeted electrophysiology) of midbrain dopaminergic neurons is specifically recommended. However, given the results that AZD5438 protects neurons and non-neuronal cells against PD-related toxins, and the view that PD pathology involves multiple types of cells loss in different regions, the suggestion from this thesis remains solid that AZD5438 could be a potential candidate for PD, but admittedly, further research is required to get a comprehensive view.

It can be noticed from the electrophysiology study that the iPSC-derived neurons'

properties and activities remain unnatural. This is one of the disadvantages when using iPSC as specific developmental or functional proteins may not express sufficiently compared to the real human brain regions, although iPSC-derived cell culture reproduces the developmental procedures by similar signals exposure in vivo in different differentiation stages. This problem may result in failures in specific disease models or assays which highly require the correct expression of effective target genes, and thus the methods of study may need to adjust accordingly to reach the research aim. For example, the study of action potential frequency is based on triggering multiple action potentials of cells with correct threshold and functional ion gates which accounts for the activities such as depolarisation. In this study, most of the ‘unmatured’ neurons can only be triggered by one action potential, thus the study was designed to investigate the effects of a single action potential rather than its frequency. It is also recommended that the models and assays which are built on certain developmental or functional bases should be evaluated first for their reliability, effectiveness, and efficiency. For instance, the confirmation of the target gene expression and the function to reach a clear assay window are required. Ideally, the specific functions of dopaminergic neurons should be investigated to add more evidence to this study, including levels of dopamine generate marker DDC, and dopamine release assays should be evaluated.

After plating hiPSC derived neuron culture onto a 96-well plate, some small

transparent dots under a bright field microscope and highly bright dots with Hoechst staining under a fluorescent microscope were observed. They were identified as dead cell debris after seeding. It might be because the coating condition was not optimal for these plates or cell density failed to match the environment provided in these plates. However, the dots were considered to be background and were excluded from the results. Because the dots' distribution was even across all groups, the rest of the cells grew healthily without a sign of being affected. Further study using iPSC derived neurons should consider this potential disadvantage and perform an optimisation when designing such experiments on 96-well plates.

Interestingly, from the imaging study, the general nuclei area was slightly larger after being treated with AZD5438 in the 2D images, although this had not been quantified. A review study suggests that the changes in nuclear size are closely associated with development, differentiation, and disease [267]. In many cases, the structural components of nuclear envelope assembly and modification can affect the nuclear size. This link between AZD5438 and nuclei size should be further investigated to reveal the potential regulatory mechanisms of AZD5438 on nuclear signalling pathways.

Chapter summary

This chapter confirmed that AZD5438 protected the human midbrain neurons in the PD model and provided the optimised doses of chemicals, assay conditions and objectives for future studies. Using hiPSCs carrying PD related mutations affecting mitochondrial function would be a highly desirable means to evaluate AZD5438's effect on preventing PD pathogenesis. Animal work should also be done testing this compound in vivo to provide dose tolerance and protection evidence for evaluation before taking into clinical study. Although more study is needed from other aspects to investigate the effects of AZD5438 on hiPSCs derived neurons to reach a more comprehensive understanding of the pathways underlying the protective mechanism, it is highly suggested that AZD5438 could be a therapeutic candidate for PD as it protects the cells against the strong PD-like stressors.

Chapter6 Study of genes that regulate Parkin-mediated mitophagy

Introduction

UBE2N

In the past twenty years, drug companies have unfortunately had little success finding drugs to combat neurodegenerative diseases such as Parkinson's and Alzheimer's. Therefore, new approaches to drug screening have been employed to discover potential disease-modifying drugs. One very promising approach is phenotypic screening, where a cell-based assay is used to screen a library of 1000s of drugs to identify the ones that elicit a specific response (such as protection from a toxic insult). In collaboration with Takeda, the Uney laboratory developed a high-throughput phenotypic based on parkin recruitment that can identify agents that modify mitochondrial function. Using this assay, a siRNA library that targets 7500 genes (considered druggable, i.e. can be targeted by pharmaceutical agents) was screened to identify genes that modulated parkin recruitment and, therefore, may have therapeutic potential. Following this screen and a second confirmatory screen using new siRNAs, we identified 80 genes that when 'knocked down' significantly altered parkin recruitment. These genes fell into three broad classes, those that regulate: 1) protein degradation pathways; 2) free radical levels; 3) DNA repair and transcription. Three of these hit genes were chosen for further

evaluation in this chapter. Experiments were conducted to assess their role in regulating parkin recruitment and mitochondrial function.

One of the top hits, ubiquitin-conjugating enzyme E2 N (UBE2N), was a regulator of protein degradation, and it was found to be a positive modulator of Parkin recruitment along with UBE2L6, ubiquitin-conjugating enzyme E2 J2 [108]. UBE2N is required to activate E3 ubiquitin ligases (UBE3s) like Parkin. Other research also reported UBE2N as a mitophagy modulator, which mediates the formation of K63-linked ubiquitin chains, interacts with Parkin, and is responsible for the autophagic degradation of mutant DJ-1. These findings suggest that UBE2N may modulate mitophagy and thus may play an important role in mitochondrial homeostasis.

In eukaryotic cells, ubiquitination occurs following a sequential series of reactions governed by the E1 activation enzymes, E2 conjugation enzymes, and E3 ligation enzymes that attach ubiquitin to substrate proteins. The downstream effects of ubiquitination may lead to protein substrate degradation and/or alter protein activity by affecting its localisation or interaction with other proteins [268]. In the human genome, two E1 enzymes have been identified as being responsible for an ATP-dependent activation that transfers the ubiquitin to the E2 enzymes [269]. 30-50 E2 enzymes have been identified, and their interaction with E3 enzymes dictates the type of inter-ubiquitin link and fate of the substrate. For example,

UBE2N (Ubc13)-mediated K63-linked ubiquitin chains are involved in degradation signalling [270]. 600-700 E3 enzymes have been discovered as three different types of catalytic domains: Homologous to E6-AP Carboxyl Terminus (HECT), Really Interesting New Gene (RING), and Ring-Between-Ring (RBR) [271]. The altered function/mutations in E3 ligases have also been linked to neurological disorders [272].

UBR5, GBP2 and HECTD2

Apart from UBE2N, based on the effective score being high within the initial screen results[108] and evidence showing their links with PD from literature research, three more genes, UBR5, GBP2 and HECTD2, were chosen for further validation and they are independent of UBE2N. UBR5 and GBP2 were located very close to PINK1 in the primary screen results (**Table 6-1**), indicating they positively regulate the mitophagy pathway (as PINK1 does). In contrast, HECTD2 was one of the most statistically significant negative regulators of parkin recruitment according to the previous screen.

SSMD.new	genes
- 8.532050092	UBR5
- 8.252922726	PINK1
- 7.441368447	GBP2

Table 6-1. Genes were found to significantly affect parkin recruitment, as indicated by the strictly standardised mean difference (SSMD) score. The complete list should refer to the publication[108].

UBR5 is an E3 ubiquitin-protein ligase that is highly conserved and essential for mammalian development; it was also identified as a progestin-regulated gene in breast cancer [273]. UBR5 has been shown to be expressed in various regions, including the human brain [274]. E3 ubiquitin-protein ligases are known to be involved in protein degradation in the ubiquitin-proteasome system, mediating important cell regulations, such as DNA damage response and transcription regulations, thus, it could have a link with mitochondrial protein degradation by mitophagy associated with DNA damage signaling. One recent study showed that DNA damage triggered p53 expression affects Spata18 levels and its function on mitophagy activity[275]. Additionally, UBR5 was found to regulate proteostasis in iPSCs and prevents the aggregation of polyQ-expanded huntingtin (HTT) misfolded proteins[276] which counts for Huntingtin Disease, another neurodegenerative diseases associated with mitochondrial dysfunction.

GBP2, Guanylate-binding protein 2, is a GTPase that is strongly induced by interferon- γ (IFN- γ). It is reported that GBP2 inhibits mitochondrial fission and cell metastasis in breast cancer cells, both in vitro and in vivo. A recent study found that GBP2 interacted with Dynamin-related protein 1(Drp1), a key regulator of mitochondrial fission, and blocks Drp1 from translocating from the cytoplasm to mitochondria, potentially reducing mitochondrial fission[277]. It is known that mitochondrial fission is important for mitophagy process, hence, GBP2 is highly possible to be linked with mitophagy alteration. Although not widely studied, there

are numerous research which previously revealed the relationship between GBP2 and PD. From a study focusing on α -synuclein, the most well known risk gene in PD, GBP2 was identified as its induce gene [278]. In a risk genes' study of PD and alcohol, it shows the correlation of GBP2/PI3K/AKT pathway with PD[279]. Given this evidence, it is suggested that altering GBP2 could alter parkin recruitment, and therefore alter mitochondrial quality control in response to stress.

HECTD2, HECT domain E3 ubiquitin-protein ligase 2, was reported to mediate and ubiquitinate PIAS1 resulting in inflammation [280]. PIAS1 is an E3 SUMO-protein ligase which regulates key inflammatory pathways including NF- κ B, targeting PIAS1 for degradation by HECTD2 is required for activation of NF- κ B for innate immune response. It has been reviewed that mitophagy and mitochondrial stress have strong relationship with innate immune response[281], thus, HECTD2 may be involved in mitochondrial activities during immune processes. HECTD2 was also found to mediate proteasomal degradation in cancer cells [282]. Additionally, HECTD2 overexpression was reported to inhibit apoptosis [283], which is well linked with mitochondrial activity as mitochondria are the core players of apoptosis (introduced in chapter one). HECTD2 was recently identified to drive proliferation of melanoma cells [284]. Mitochondria play important roles in proliferation, especially in tumor cells, as they provide not only ATP, but also metabolites and support NAD⁺ regeneration, which are crucial to maintain the homeostasis of cells [285]. This may indicate there is a link

between mitochondria and HECTD2. HECTD2 was therefore chosen as it might be involved in activities including the protein degradation process of mitochondria and the alteration of HECTD2 may alter mitochondrial stress response activities.

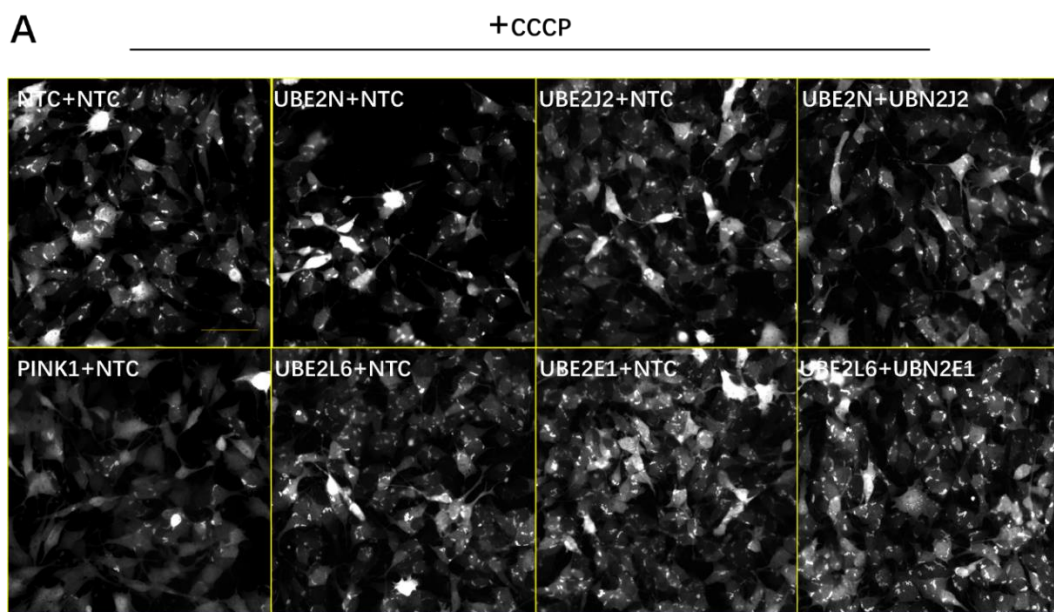
Result

Validation: UBE2N is a positive modular of Parkin-mediated mitophagy in SH-SY5Y cells

In previously published work from our laboratory[108], Dr Helen Scott et al. reported that a group of regulators of Parkin recruitment in H4 cells were members of the E2 ubiquitin-conjugating enzymes (UBE2s). Of the four UBE2s reported, UBE2N and UBE2J1 were positive modulators, and ubiquitin-conjugating enzyme E2 L6 (UBE2L6) ubiquitin-conjugating enzyme E2 E1 (UBE2E1) were negative regulators.

To validate these findings, siRNAs targeting the selected combinations of UBE2s were transfected into eGFP-Parkin SH-SY5Y cells, and 48 hours later, Parkin recruitment assays were carried out in 96-well plates in the presence of 10 μ M CCCP (for 4hrs). NTC+NTC was the negative control, while PINK1 siRNA+NTC was the positive control (known to regulate Parkin recruitment negatively). The results shown in Figure 6-1 B confirmed that co-transfection with UBE2L6+UBE2E2 upregulated Parkin recruitment as the Parkin puncta total area increased significantly compared to the negative control. UBE2L6 knockdown alone also showed the trend of increasing the Parkin total puncta area. This result is in line with the previous findings in H4 cells. Nevertheless, the previous study found that co-transfection with UBE2N+UBE2J2 did not significantly

downregulate Parkin recruitment activity. While in this study, UBE2N knockdown mediated a (with NTC) significant inhibition of Parkin recruitment. It should be noted that some Parkin puncta were observed following PINK1 knockdown in SH-SY5Y cells. However, in H4 cells, following PINK1 knockdown, Parkin puncta were absent. To ensure the siRNAs were knocking down the expression of their targets, SHSY-5Y cells were transfected with the selected siRNAs and incubated for 48 hours. RNA was extracted, and RT-qPCR was used to quantify the expression of the target gene. The results shown in **Figure 6-1 C** confirmed that all siRNAs mediated the effective knockdown of their targets in SH-SY5Y cells.



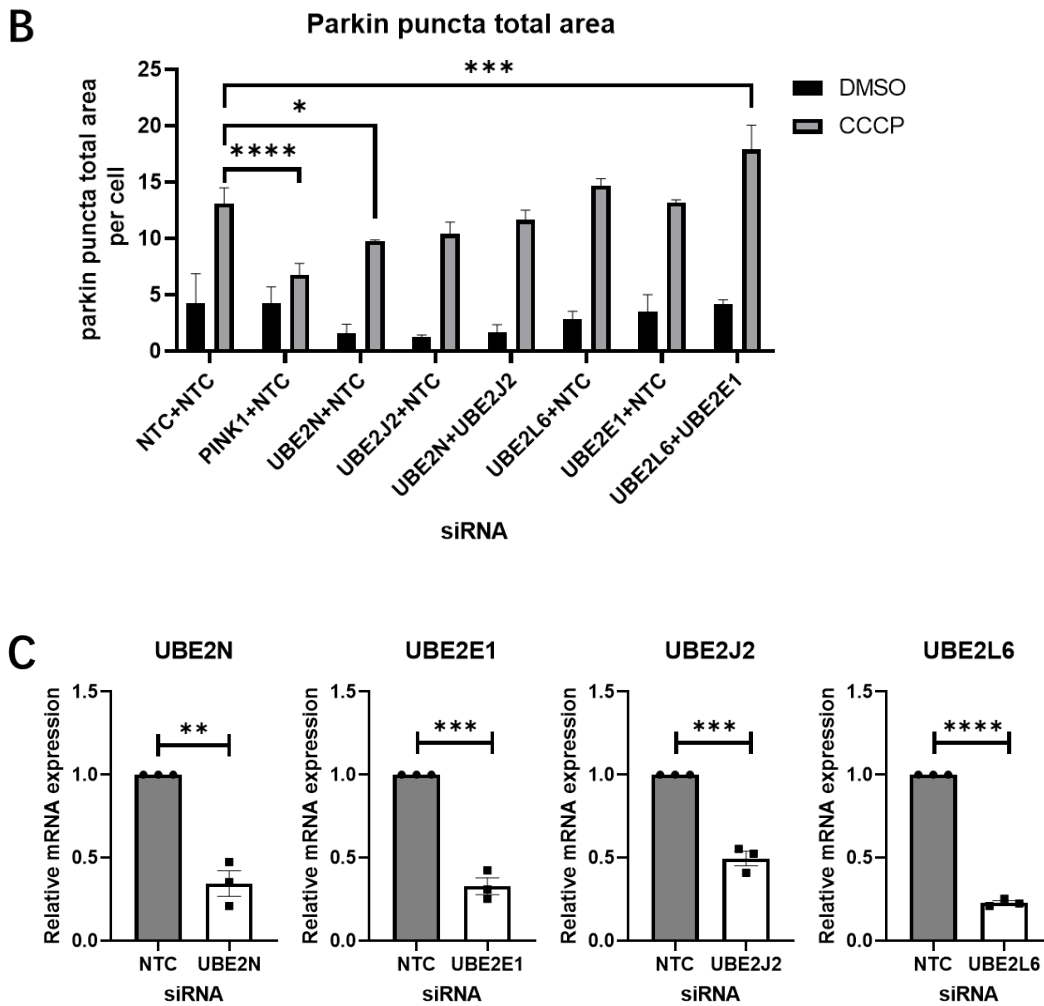


Figure 6-1 UBE2N is a positive modulator of Parkin-recruitment in SH-SY5Y cells

A) Images taken by INCell 2000 show the Parkin puncta formation with CCCP after cells were transfected with the indicated combination of siRNAs. Only GFP channel images are shown. PINK1 knockdown inhibits the formation of Parkin puncta. B) Analysis results from INCell Workstation by the optimised protocol for SH-SY5Y cells. PINK1+NTC ($p < 0.0001$), UBE2N+NTC ($p = 0.0366$) significantly reduced the Parkin puncta total area compared to NTC+NTC, while UBE2L6+UBE2E1 (0.0009) significantly increased it. C) The pre-selected siRNAs effectively reduced the mRNA expression of the target genes with high significance: UBE2N ($p = 0.0010$), UBE2E1 ($p = 0.0002$), UBE2J2 ($p = 0.0003$) and UBE2L6 ($p < 0.0001$). Statistical analysis was carried out by two-way ANOVA test with Tukey's multiple comparisons test (B) and unpaired t-test (C). $N = 3$; data is displayed as mean \pm SEM, significance is displayed as * $p < 0.05$, ** $p < 0.01$, *** $p < 0.001$, **** $p < 0.0001$.

UBE2N is a potent modular of Parkin-mediated mitophagy

A higher concentration of UBE2N siRNA that used in previous experiments was used to transfect H4 cells. The results showed that cells transfected with UBE2N siRNA had fewer Parkin puncta than NTC control (**Figure 6-2 A**). The results in **Figure 6-2 B** confirmed the observation showing a significant decrease of Parkin puncta total area per cell in UBE2N compared to NTC control. Its value decreased to approximately 50% of control, indicating the effect of UBE2N knockdown on Parkin-mediated mitophagy is strong. Given the robust effect of UBE2N siRNAs on Parkin recruitment, it was hypothesised that the upregulation of UBE2N may have the opposite effect and was therefore cloned into a lentiviral vector.

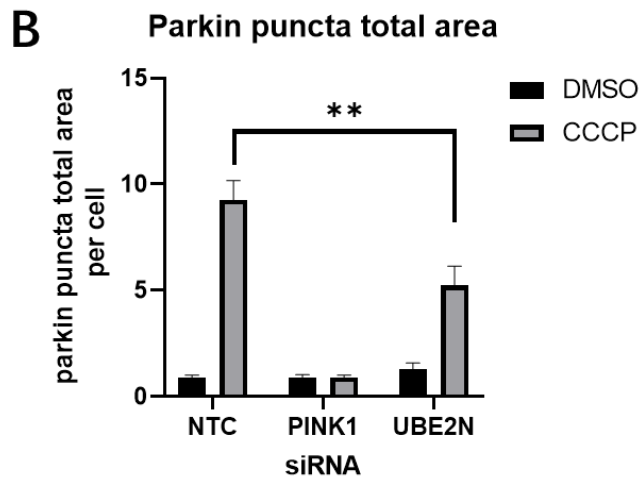
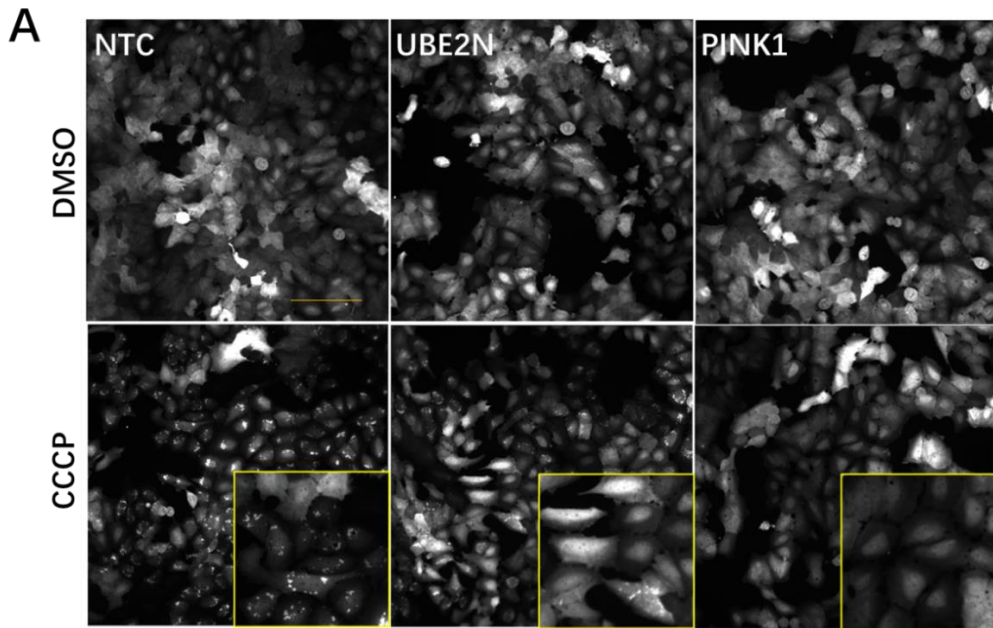


Figure 6-2 UBE2N is a potent modular of Parkin recruitment

A) Images taken by INCell 2200 show cells and the Parkin puncta formed after transfection with the indicated siRNAs. Only GFP channel images were shown. In the NTC group, CCCP triggered a large amount of Parkin puncta formation. In UBE2N and PINK1 knockdown groups, CCCP did not induce many Parkin puncta. Knockdown shows less amount of observed Parkin puncta. Scale bar=100, B) Analysis results from INCell Workstation by the optimised protocol for H4 cells. Positive control PINK1 effectively reduced the Parkin puncta ($p < 0.0001$, not shown in graph). UBE2N ($p = 0.0022$) significantly reduced the Parkin puncta total area compared to NTC with the presence of CCCP. Statistical analysis was carried out by two-way ANOVA test with Tukey's multiple comparisons test. $N = 3$; data is displayed as mean \pm SEM, significance is displayed as ** $p < 0.01$

UBE2N lentiviral construction

The HA-UBE2N coding sequence was cloned into the pRRL backbone, and this plasmid was used to transfect HEK293 cells, and further, a lentiviral vector can be produced for more stable overexpression of the target gene in cell lines and neuron cultures.

PcDNA3.0-HA-UbcH13 was purchased from Addgene (plasmid #12461). The plasmid was mini-prepped, and the insert was sequenced for preparation. There were no suitable restriction enzyme sites to allow direct cloning into the pRRL plasmid, so PCR primers with XbaI and SalI sites were designed to clone into these sites in the pRRL.sin.cppt.CMV.EGFP.WPRE plasmid (cutting out the EGFP).

Forward primer requires a 5' leader sequence and XbaI site (*TCTAGA*), which was designed as

GS001 5' TCAGTCTAGAATGTACCCATACGACGTCCCAGA.

Reverse primer needs a SalI (GTC GAC) site and leader sequence, which was designed as

GS002 5' TACGGTCGACGGATCGCGGCCGCTTAAAT.

PCR was performed with the two primers, as shown in **Figure 6-3**, with those two sites for the subsequent step used.

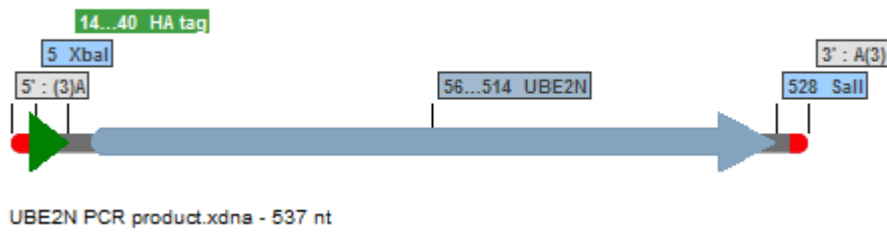


Figure 6-3 The map of PCR product with XbaI and Sall sites.

The PCR product was purified and then digested with XbaI and Sall at 37°C for 2 hours to confirm the right product with the active sites for the subsequent ligation. The pRRL.sin.cppt.CMV.EGFP.WPRE plasmid, shown in **Figure 6-4**, was digested with the same enzymes simultaneously. This process was to open the circle plasmid at the designed sites hoping to get the backbone ready for ligation.

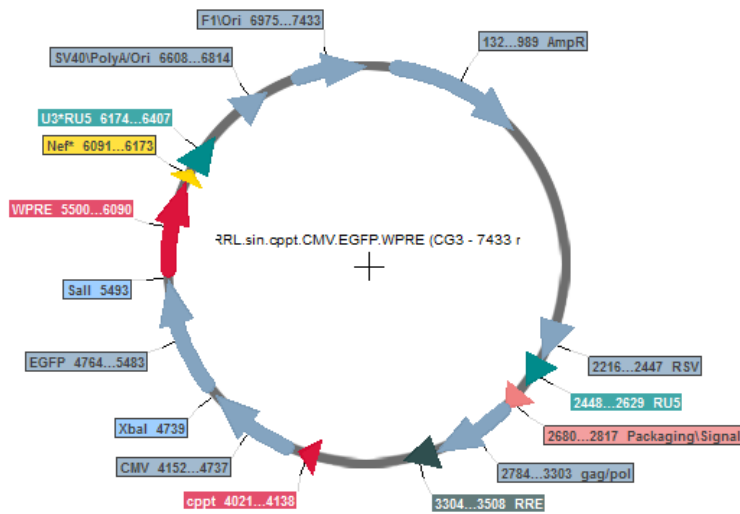


Figure 6-4 The map of pRRL.sin.cppt.CMV.EGFP.WPRE plasmid, showing the two aim digestion sites(Sall and XbaI) marked by blue boxes.

The cut plasmid was predicted to have two fragments after the restriction digestion,

as shown in Figure 6-5, one at 7kbp and the other at 800bp.

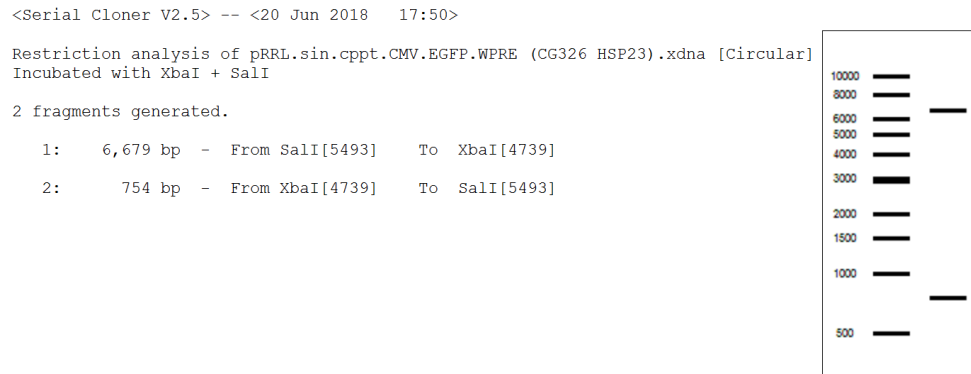


Figure 6-5 Virtual cut result of Xba I +Sal I on pRRL.sin.cppt.CMV.EGFP.WPRE plasmid, showing two fragments generated.

After the digestion, the predicted product was observed (**Figure 6-6**) and collected for ligation.

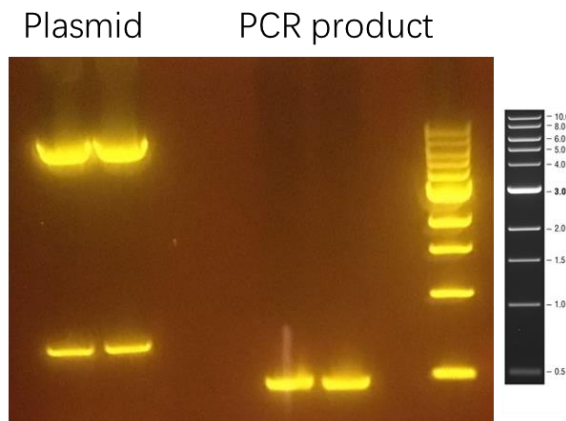


Figure 6-6 Figure 22. Gel running image showing ppl plasmid in the left was cut into 2 pieces and the digested PCR product was in the right.

After the ligation, transformation, and growth in bacteria, the plasmid was amplified by mini-prep and checked by restriction digestion to ensure the correct plasmid. The predicted plasmid map is shown in **Figure 6-7**. Virtual cutting was used to choose the suitable enzymes, which cut the old backbone into one band

but cut the aimed plasmid into two bands, as shown in **Figure 6-8**.

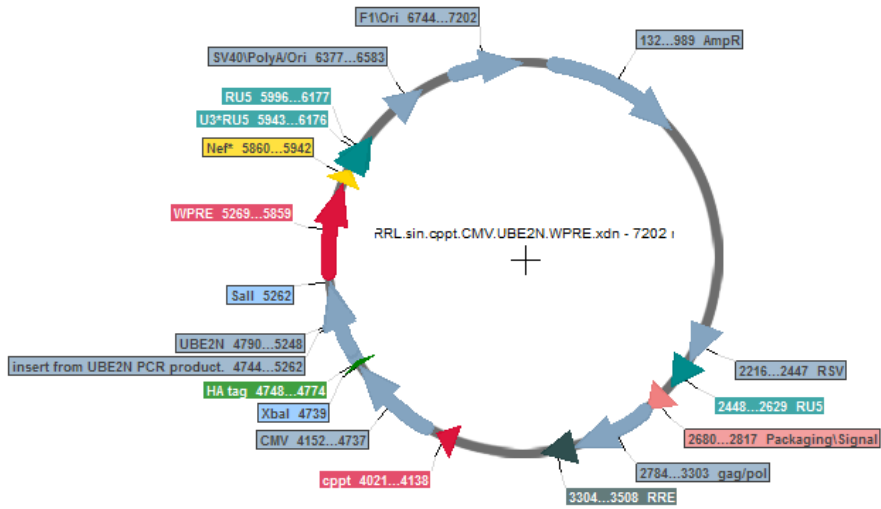


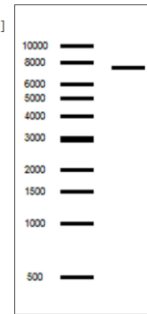
Figure 6-7 The map of virtual ligation results of insert a gene of interest into the backbone.

<Serial Cloner V2.5> -- <20 Jun 2018 17:46>

Restriction analysis of pRRL.sin.cppt.CMV.EGFP.WPRE (CG326 HSP23).xdna [Circular]
Incubated with Acc65I

1 fragment generated.

1: 7,433 bp - Linearized by Acc65I[6103]



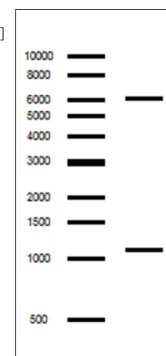
<Serial Cloner V2.5> -- <20 Jun 2018 17:46>

Restriction analysis of pRRL.sin.cppt.CMV.UBE2N.WPRE.xdna [Circular]
Incubated with Acc65I

2 fragments generated.

1: 6,113 bp - From Acc65I[5872] To Acc65I[4783]

2: 1,089 bp - From Acc65I[4783] To Acc65I[5872]

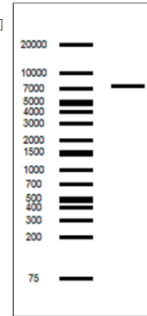


<Serial Cloner V2.5> -- <23 Nov 2018 11:11>

Restriction analysis of pRRL.sin.cppt.CMV.EGFP.WPRE (CG326 HSP23).xdna [Circular]
Incubated with KpnI

1 fragment generated.

1: 7,433 bp - Linearized by KpnI[6103]



<Serial Cloner V2.5> -- <23 Nov 2018 11:09>

Restriction analysis of pRRL.sin.cppt.CMV.UBE2N.WPRE.xdna [Circular]
Incubated with KpnI

2 fragments generated.

1: 6,113 bp - From KpnI[5872] To KpnI[4783]

2: 1,089 bp - From KpnI[4783] To KpnI[5872]

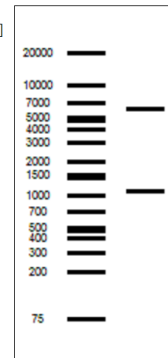


Figure 6-8 Virtual cut results for restriction digestion check. Acc65I, KpnI and StuI cut the backbone and the cloned product, respectively, showing a single band for the backbone and double bands for the cloned product.

After restriction digestion with KpnI, sample X was shown to have the predicted bands and is shown in **Figure 6-9**.

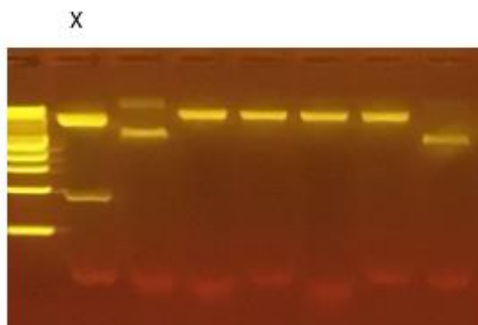


Figure 6-9 The X sample showed two bands with the correct position, indicating the insert was correctly cloned into the backbone.

The product was then used for maxiprep to harvest a large amount of DNA and then was double confirmed with KpnI and Acc65 digestion, shown in **Figure 6-10**.

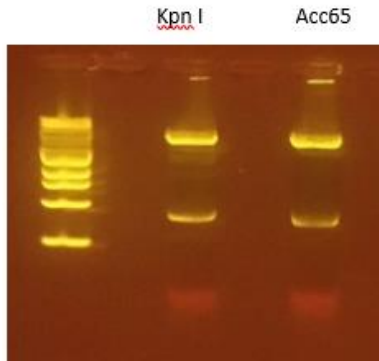
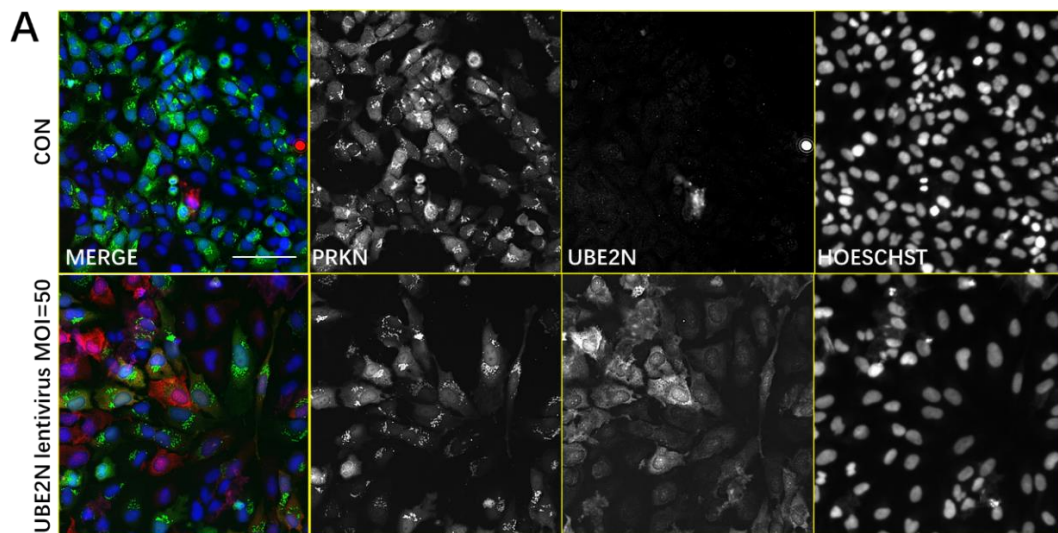


Figure 6-10 Restriction digestion check results after maxiprep of the cloned DNA, cut by KpnI, Acc65 respectively. Kpn I and Acc65 results showed correct bands.

Further sequencing results confirmed that the insert was cloned into the vector correctly. The plasmid was first used for direct plasmid transfection to overexpress UBE2N in eGFP-Parkin H4 cells. Unfortunately, no positive results were seen due to high cell loss after transfection. Additionally, no UBE2N staining was observed after transfection. The plasmid was also used for lentivirus construction (described in the method chapter). After harvesting the virus, the titre was calculated as 3×10^9 vg/mL by applying the TaqMan titre strategy with a reference virus with the same CMV promoter.

Overexpression of UBE2N upregulates Parkin recruitment activity

The lentiviral mediated expression of UBE2N was confirmed by immunostaining (**Figure 6-11 A**). Lentiviral-UBE2N was used to transduce H4 cells, and Parkin recruitment assays were performed 48hrs later. There was a trend indicating Parkin recruitment (puncta total area per cell after CCCP treatment) increased with increasing viral MOI. At an MOI of 10, the cell count did not change, while Parkin puncta were not significantly different to that of control (**Figure 6-11 B**). However, at a MOI=100, there was a significant difference in Parkin puncta total area per cell compared to control after CCCP treatment (**Figure 6-11 C**).



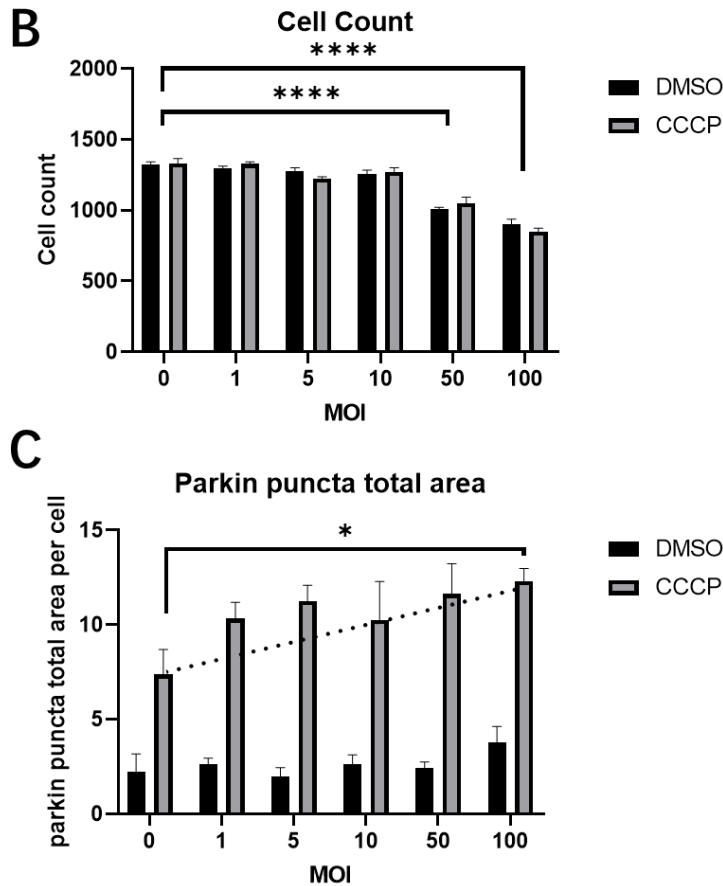


Figure 6-11. Overexpression of UBE2N upregulates Parkin recruitment activity

A) The merged images from INCell 2000 show the condition of H4 cells with eGFP-labeled Parkin (green), immunostained UBE2N (red) and Hoechst-stained nuclei (blue). Cells were incubated with series doses of UBE2N-virus, and Parkin recruitment assays were performed. Representative images only show the control and the virus dose MOI=50 with the presence of CCCP. Intensive UBE2N staining confirmed the overexpression was achieved by the UBN2N virus. B) Analysis results from INCell Workstation by optimised protocol for H4 cells. It shows cell count reduced significantly ($p < 0.0001$) from MOI>50. C) Graph shows MOI=100 significantly ($p = 0.0252$) increased the Parkin puncta total area per cell compared to no virus with CCCP. There is a trend of increasing Parkin puncta total area per cell with virus dose increased with CCCP. Statistical analysis was carried out by two-way ANOVA test with Tukey's multiple comparisons test. N=3; data is displayed as mean \pm SEM, significance is displayed as ** $p < 0.01$

Overexpression of UBE2N alters PGC-1 α activity

The results in **Figure 6-12 B** show that UBE2N was expressed by the lentivirus. And that (**Figure 6-12 C**) the PGC-1 α protein level was significantly decreased with CCCP treatment following the lentiviral mediated expression of UBE2N. However, no significant change in another mitochondrial protein, TOM20, was detected by Weston blots in these experiments.

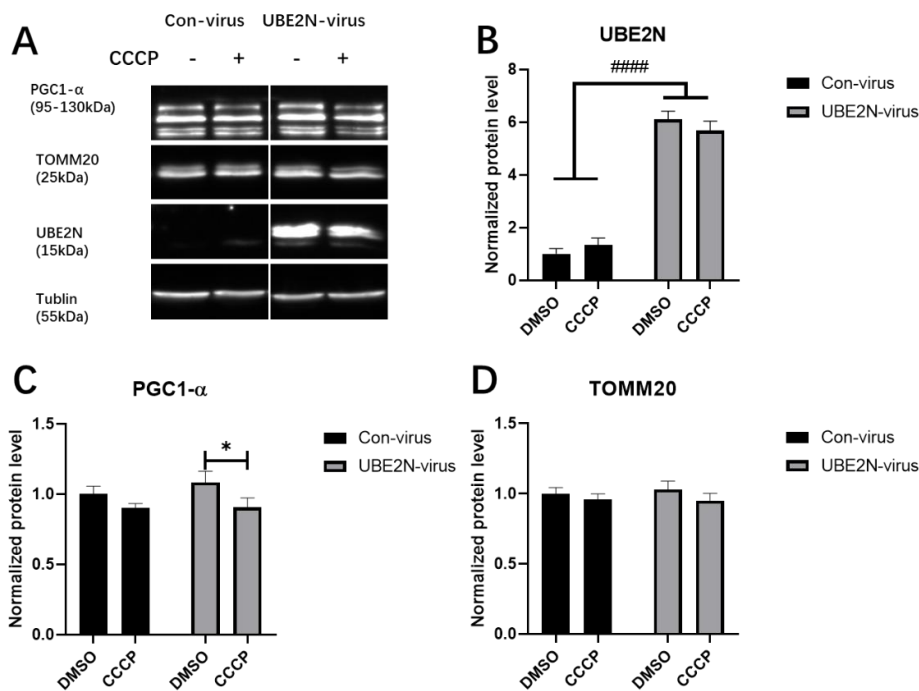


Figure 6-12 Overexpression of UBE2N alters PGC-1 α gene expression

A) The representative images of Western blots of protein samples from experiments probed for anti-PGC1- α , anti-TOM20, and anti-UBE2N; α - tubulin as the loading control. Protein bands corresponding to the approximate molecular weight are presented. Analysed data is presented in B, C and D. B) UBE2N-virus transduction significantly ($p < 0.0001$) increased the UBE2N band intensity compared to Con-virus. C) UBE2N-virus transduction significantly ($p = 0.0156$) decreased the PGC-1 α band intensity compared to Con-virus with the presence of CCCP. D) No significant change with TOM20 expression was observed with the WB bands. Statistical analysis was carried out by two-way ANOVA test with Tukey's multiple comparisons test. $N = 3$ independent experiments; data is displayed as mean \pm SEM; significance is displayed as * $p < 0.05$, *** $p < 0.001$, **** $p < 0.0001$. Hashes denote comparisons between UBE-virus and Con-virus; asterisks denote comparisons between DMSO and CCCP groups.

Overexpression of UBE2N does not protect cells in a cellular model of PD

The overexpression of UBE2N upregulated Parkin recruitment activity and altered PGC-1 α protein levels. Thus, it was assumed that the overexpression of UBE2N may protect cells against mitochondrial-targeted stressors. To validate this assumption, an MTT-rotenone assay was performed. After 48h lentivirus transduction of H4 cells (MOI=50), 250nM rotenone was loaded for another 24h before measuring cell viability by MTT assays. However, the results showed that the overexpression of UBE2N does not protect cells from rotenone (**Figure 6-13**).

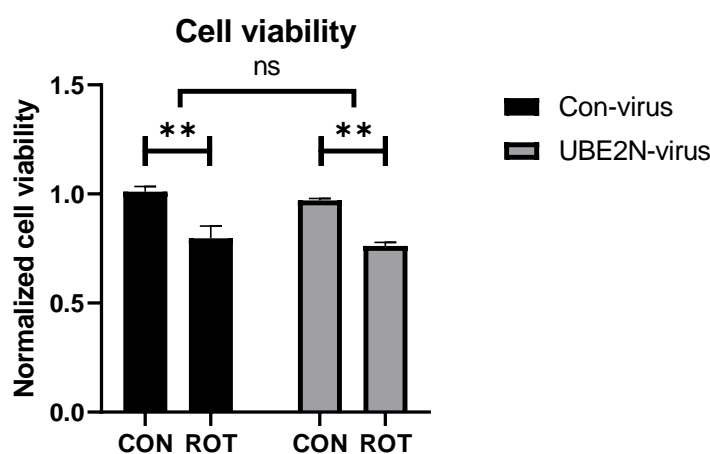


Figure 6-13 Overexpression of UBE2N does not protect cells against rotenone

After 48h lentivirus transduction in H4 cells (MOI=50), 250nM rotenone was loaded for another 24h before checking the cell viability through MTT assay. rotenone significantly reduced the cell viability in both Con-virus group ($p=0.0065$) and UBE2N-virus transduction group ($p=0.0075$). Data were normalised to CON in Con-virus group. Statistical analysis was carried out by two-way ANOVA test with Tukey's multiple comparisons test. $N=3$ independent experiments; data is displayed as mean \pm SEM; significance is displayed as * $p<0.05$, *** $p<0.001$, **** $p<0.0001$. Asterisks denote comparisons between CON and rotenone; no significant difference between Con-virus and UBE2N-virus groups.

Actions of UBR5, GBP2 and HECTD2 knockdown on Parkin recruitment

In addition to UBE2N, the action of UBR5, GBP2 and HECTD2 on Parkin recruitment were also investigated. Knockdown efficiency using three siRNAs against each target gene was first evaluated. To achieve this, H4 cells were transfected with the selected siRNAs individually and incubated for 48 hours. RNA was then extracted, and RT-qPCR was performed to quantify the expression of the target gene. The results shown in Figure 6-12 C confirmed that at least two siRNAs of each target gene mediated the significant mRNA level reduction compared to NTC.

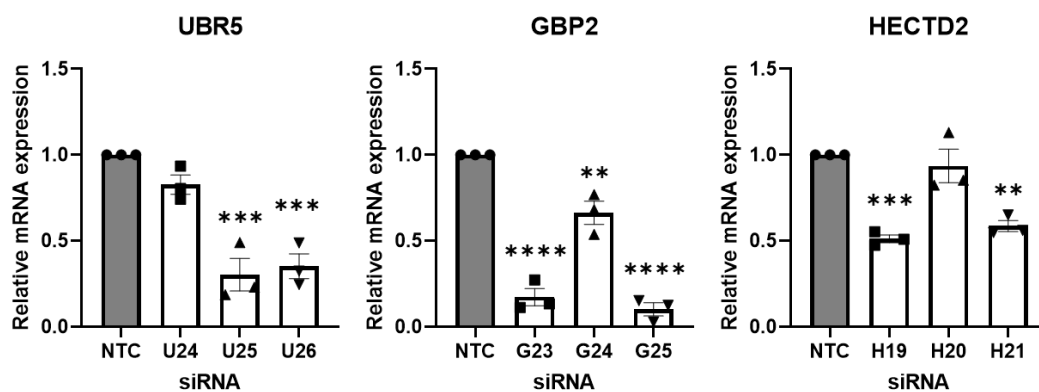


Figure 6-14 Validation of target knockdown by siRNAs.

EGFP-Parkin H4 cells were transfected with selected siRNAs and incubated for 48 hours. RNA was extracted, and expression of the target gene was quantified by RT-qPCR. Statistical analysis was carried out by one-way ANOVA test with Bonferroni post hoc tests between the NTC and target siRNAs. N=3; data is displayed as mean \pm SEM, significance is displayed as * $p < 0.05$, ** $p < 0.01$, *** $p < 0.001$, **** $p < 0.0001$.

The two siRNAs mediating the most effective knockdown of each gene were used for transfection of eGFP-Parkin H4 cells. 48h after transfection, the Parkin recruitment assay was performed with 10 μ M CCCP treatment for 2h. As shown in Figure 6-15, the positive control PINK1 knockdown blocked Parkin puncta formation, confirming that the transfection and assay worked. However, no other siRNAs mediated an effect on the formation of Parkin puncta.

To further confirm that these genes do not affect Parkin recruitment, the selected siRNAs were then used to transfect eGFP-Parkin SH-SY5Y cells, and the performance in the Parkin recruitment assay was tested. 10 μ M CCCP treatment for 4h was applied in SH-SY5Y cells. Unlike H4 cells, the results (**Figure 6-16**) showed that only the siRNA against HECTD2 significantly increased the Parkin puncta total area per cell compared to the NTC in SH-SY5Y cells. No other siRNAs mediated an effect on Parkin recruitment, which is consistent with the findings in H4 cells.

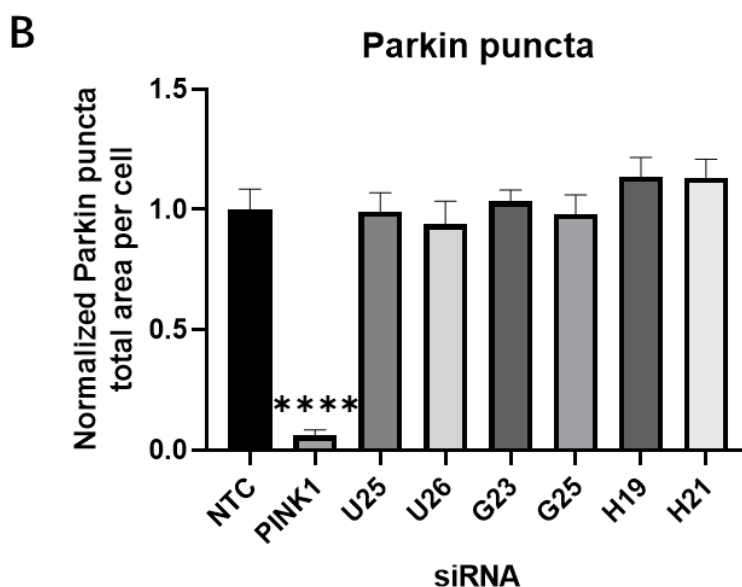
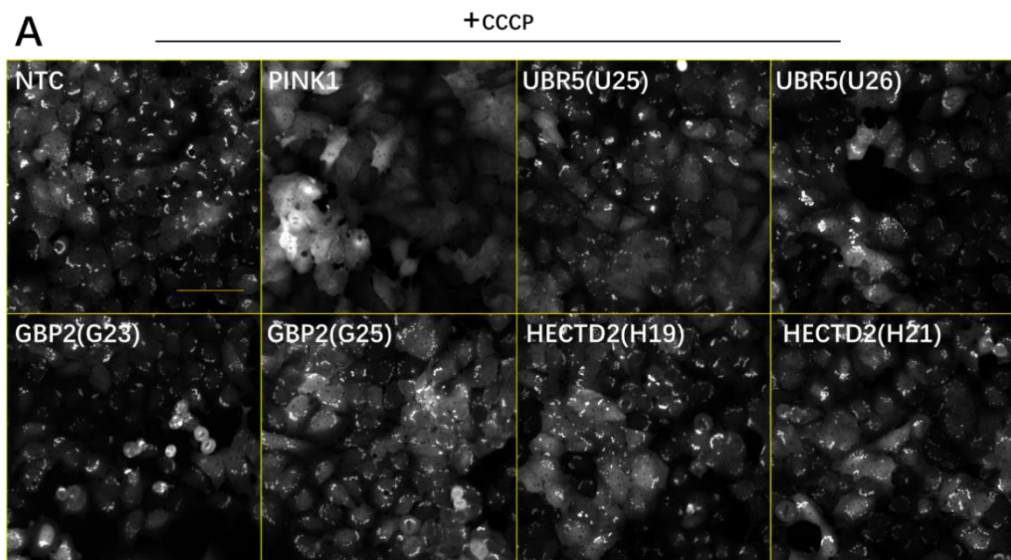


Figure 6-15 Effect of siRNA knockdown of UBR5, GBP2 and HECTD2 on Parkin recruitment in H4 cells

A) Images taken by INCell 2200 show the Parkin puncta formation with CCCP after transfected cells with selected siRNAs. Only GFP channel images were shown. PINK1 knockdown shows less amount of observed Parkin puncta. There is no dramatic change with other siRNA compared to NTC from observation B) Analysis results from INCell Workstation by the optimised protocol for H4 cells. PINK1 ($p < 0.0001$) significantly reduced the Parkin puncta total area compared to NTC. Statistical analysis was carried out by one-way ANOVA test with Dunnett's multiple comparisons test, compared to NTC. $N=3$; data is displayed as mean \pm SEM, and significance is displayed as **** $p < 0.0001$. U=UBR5, G=GBP2, H=HECTD2

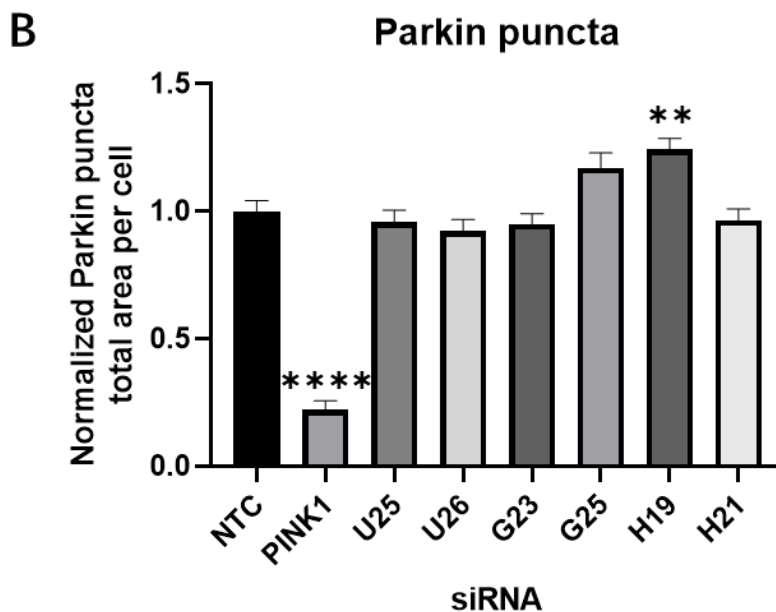
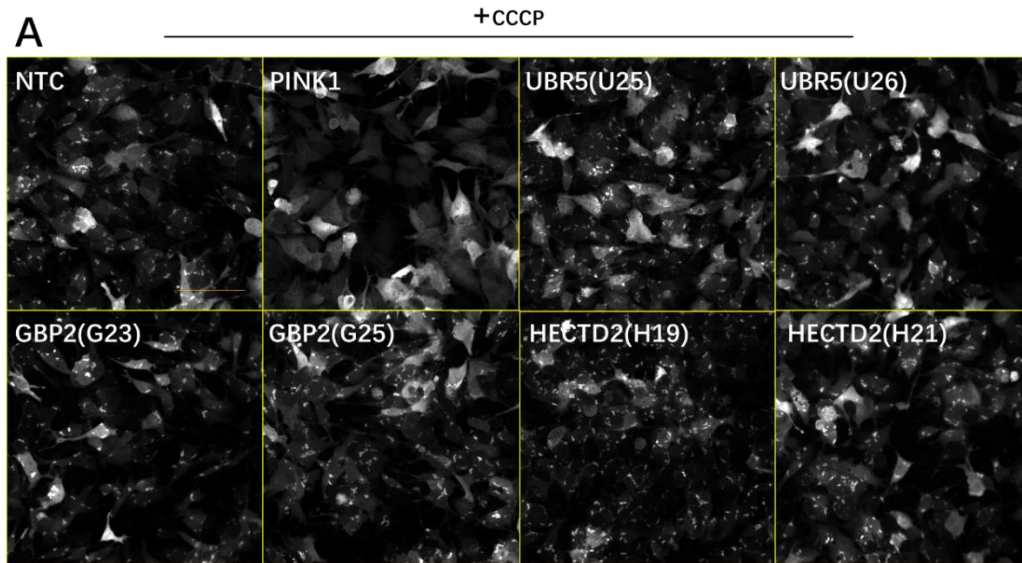


Figure 6-16 Effect of siRNA knockdown of UBR5, GBP2 and HECTD2 on Parkin recruitment in SH-SY5Y cells

A) Images taken by INCell 2200 show the Parkin puncta formation with CCCP after transfected cells with selected siRNAs. Only GFP channel images were shown. PINK1 knockdown shows less amount of observed Parkin puncta. H19 slightly increased the Parkin puncta observation compared to NTC. There is no dramatic change with other siRNA compared to NTC from observation B) Analysis results from INCell Workstation by the optimised protocol for SH-SY5Y cells. PINK1 ($p < 0.0001$) significantly reduced the Parkin puncta total area compared to NTC. H19 significantly ($p = 0.0084$) increased the Parkin puncta area per cell compared to NTC. Statistical analysis was carried out by one-way ANOVA test with Dunnett's multiple comparisons test, compared to NTC. $N = 3$; data is displayed as mean \pm SEM, significance is displayed as ** $p < 0.01$, **** $p < 0.0001$. U=UBR5, G=GBP2, H=HECTD2

Summary and discussion

Results summary

The results showed that siRNA-mediated UBE2N knockdown negatively regulates Parkin recruitment, and the lentiviral mediated overexpression of UBE2N mediated upregulated Parkin recruitment. This suggests the upregulation of UBE2N may enhance Parkin mediate mitophagy, thus enhancing the clearance of damaged mitochondria following stress. Notably, overexpression of UBE2N also altered the expression of PGC1- α protein level and mediated its downregulation in the presence of CCCP. This suggests that UBE2N might directly or indirectly alter the PGC1- α -related pathways, which will be discussed further. However, the overexpression of UBE2N did not show a protective effect against rotenone-induced cell viability damage. This suggests that UBE2N overexpression might not lead to enhanced mitophagy/ an improvement in mitochondrial health or that increasing mitophagy is insufficient to mediate protection against toxic stressors. The knockdown of UBR5, and GBP2 were found to have no effect on parkin recruitment. However, the knockdown of HECTD2 was found to significantly increase parkin recruitment in SH-SY5Y cells. Further investigation of HECTD2 actions on parkin recruitment and the induction of mitophagy are therefore needed.

Discussion

UBE2N and Parkin recruitment study

In this study, the knockdown of UBE2N was shown to inhibit Parkin recruitment. Thus, this reduced Parkin signalling might lead to impaired substrate ubiquitylation and degradation of mitochondria, which would disrupt the function of the mitochondrial clearance system. Thus, UBE2N is a positive regulator of Parkin recruitment, suggesting that its impairment could lead to dysfunction of the mitochondrial clearance system and mediate related disease pathogenesis. However, it can be noticed that the knockdown of UBE2N did not mediate a substantial block of Parkin recruitment like the knockdown of PINK1 did. This could be due to a number of reasons.

First, the knockdown of UBE2N may not be sufficient to mediate a notable effect. The UBE2N knockdown in this study, characterised by the relative mRNA level, was only about 40% of the NTC control (in SH-SY5Y cells). This also suggests that UBE2N is a relatively stable protein. In addition, the single knockdown of UBE2N with a relatively high dose of siRNA in H4 cells showed a more substantial reduction of Parkin recruitment activity. Second, considering the dynamic association of E2s and E3s, the reduced UBE2N expression by knockdown might be compensated for by closely related E2s and E3s. This assumption is based on the evidence that the knockdown of multiple E2 enzymes

and E3enzymes typically gives a more substantial effect than a single knockdown [286] [287]. It is suggested that a further study by blocking UBE2N with its paired patterners might have a more potent effect beyond what has been shown in this study.

Evidence suggests that UBE2N is primarily responsible for K63-linked ubiquitylation [288], and the knockdown of UBE2N reduced K63-ubiquitin level and inhibited mitochondrial clustering by CCCP. However, it was recently reported that Parkin binds to K63-linked chains, sufficient to induce Parkin recruitment when PINK1 is overexpressed [289]. Moreover, a study reported that UBE2N does not affect the ubiquitin charging of Parkin, which works differently from other E2s [288]. Therefore, it is conceivable that the UBE2N is involved but might not be indispensable for Parkin recruitment. In other words, UBE2N might work more like an efficiency enhancer rather than the core player in the Parkin-mediated mitophagy process. Given this assumption, the negative effect on Parkin puncta formation in this study shown by UBE2N knockdown might delay but not block the effect on Parkin recruitment. More prolonged treatment of CCCP could be applied to evaluate this assumption.

Conversely, that UBE2N as an efficiency enhancer of Parkin recruitment is supported by the result that overexpression of UBE2N enhanced the Parkin puncta formation. Thus, the Parkin recruitment efficiency may depend more on other

related players in this pathway. When overexpressed, UBE2N serves as the accelerator, speeding up the K63-ubiquitin chain building process, and then the ubiquitin chain binds to Parkin. This accelerated binding process recruits more Parkin in a positive feedback manner faster. As a result, this UBE2N-Parkin enhanced Parkin recruitment was shown with more Parkin puncta than control under the same time of CCCP treatment. However, enhanced Parkin recruitment does not necessarily lead to an enhanced clearance effect of damaged mitochondria, as the latter is dependent more on lysosome capacity. Thus, a protein levels investigation to confirm that UBE2N regulates mitophagy, not just Parkin recruitment, is needed prior to reaching any conclusion.

UBE2N and the mitochondria-related proteins

TOM20, the mitochondrial content indicator, was not significantly altered by the overexpression of UBE2N. However, this does not necessarily confirm that overexpression of UBE2N regulates mitochondrial protein degradation as CCCP treatment did not trigger a significant degradation of TOM20 in the experiments. Although the selected CCCP treatment time, 2h, was shown to significantly induce the early signalling of mitophagy, Parkin recruitment, from the imaging assay, this duration might be too short to record the change levels of mitochondrial proteins, which happens at the later stage of mitophagy process. The unchanged relative mtDNA content following 2h CCCP treatment shown in chapter 4 supports this

view. Moreover, the trend towards a reduced PGC1- α protein level was observed in the same pattern as TOM20 when treated with CCCP, suggesting the change of TOM20 expression might be associated with the downregulated mitochondrial biogenesis through PGC1- α alteration. Therefore, a longer duration of CCCP treatment to trigger the degradation of TOM20 should be used in future experiments to investigate the actual effect of UBE2N on the degradation of mitochondrial protein.

However, a significant change in the level of PGC1- α following UBE2N overexpression under CCCP treatment was observed. This change suggests that UBE2N might directly or indirectly alter the PGC1- α -related pathways. PGC1- α , the master regulator of mitochondria, was recently reported to be associated with the representative receptor-mediated mitophagy, FUN14 domain containing 1 (FUNDC1)-mediated mitophagy but not the Parkin mediated mitophagy[290]. A report suggests overexpression of PGC1- α upregulated FUNDC1-mediated mitophagy by enhancing FUNDC1 expression under hypoxic conditions [32]. This evidence might be closely linked to the observation that the PGC1- α protein level was lower in the CCCP group than in the DMSO group. It suggests the downregulation of PGC1- α leads to the downregulation of FUNDC1 and, further, a negatively regulated FUNDC1-mediated mitophagy activity when CCCP was applied to trigger Parkin-mediated mitophagy. This suggestion is consistent with many reports. FUNDC1 seems not to be present in starvation-induced mitophagy

or CCCP-induced mitophagy, where Parkin-mediated mitophagy is active, while hypoxia-induced mitophagy mainly relies on FUNDC1 but not Parkin [31] [291]. It is not well-known that whether these two systems could coordinate to protect cells; however, recently, a study [292] showed that rotenone could induce both these types of mitophagy, suggesting they might work together in response to stress.

This thesis study further suggested that FUNDC1-mediated mitophagy is negatively associated with Parkin-mediated mitophagy, and upregulation of one leads to a compensatory inhibition of the other. On one hand, the overexpression of UBE2N downregulated the PGC1- α protein levels following CCCP treatment, where the imaging assay confirmed the enhanced Parkin recruitment by UBE2N overexpression. These findings suggests that the upregulation of Parkin-mediated mitophagy might lead to the downregulation of FUNDC1-mediated mitophagy. On the other hand, when FUNDC1-mediated mitophagy is activated during hypoxia, the increased binding ability for LC3 [293] and enhanced interaction with DRP1 [294] of FUNDC1 might allow FUNDC1-mediated mitophagy to compete with Parkin-mediated mitophagy. FUNDC1-mediated mitophagy might be more competitive as its LC3 binding does not conflict with the hydrophobic pocket of LC3, while Parkin inhibits the binding affinity [295] [295]. This analysis suggests that upregulation of FUNDC1-mediated mitophagy might lead to the downregulation of Parkin-mediated mitophagy.

Together, it is suggested that Parkin-mediated mitophagy and FUNDC1-mediated mitophagy are likely to be linked by PGC1- α activity; and they might be on a compensatory balance to maintain the efficiency of the mitochondrial clearance system. Parkin-mediated mitophagy is more competitive when facing CCCP-mediated mitochondrial membrane potential disruption, while FUNDC1-mediated mitophagy is more competitive under hypoxic conditions.

Another supportive interpretation of the result is that overexpression of UBE2N enhanced Parkin recruitment to mitochondria and thus reduced the Parkin available for its other roles. Parkin mediates the proteasomal degradation of PARIS (ZNF746). In the absence of Parkin, PARIS is bound to the upstream promoter of the PGC-1 α gene, which suppresses PGC-1 α gene expression [241]. Additionally, the PGC1- α protein level change appeared simultaneously when Parkin activity changed as Parkin recruitment was recorded, which indirectly supports the assumption that Parkin affects PGC1- α activity. Thus, the significantly reduced PGC-1 α protein level seen with UBE2N overexpression under treatment with CCCP suggests the significantly increased presence of PARIS, which could be the consequence of significantly less available Parkin for the degradation of PARIS, as UBE2N drives more Parkin to translocate to mitochondria. If the compensatory balance hypothesis is true, the above process further suggests that overexpression of UBE2N might enhance the Parkin-mediated mitophagy as it might

downregulate the PGC1- α altered FUNDC1-mediated mitophagy.

UBE2N might also regulate PGC1- α through other pathways. Although no evidence supports a direct link between UBE2N and PGC1- α under unchallenged conditions, the activated ubiquitin-proteasome system (UPS) might mediate the link under stress conditions. The UPS and autophagy are two major clearance systems in the cell, and they are suggested to work under compensatory balance in most scenarios to keep the cell healthy [296] [297]. It is suggested that the overexpression of UBE2N might enhance UPS, and evidence suggests the positive association of UBE2N and proteasome activity [298]. It is known that the activated UPS mediates PGC1- α degradation under stress [299]. Thus, the enhanced reduction of the PGC1- α protein level might result from the enhanced degradation effect of enhanced UPS by overexpression of UBE2N under CCCP treatment.

Furthermore, in this way, the FUNDC1-mediated mitophagy is downregulated by the lack of PGC1- α signalling under UPS upregulation, which is consistent with another report showing that downregulation of FUNDC1 is associated with UPS activation following hypoxia-induced mitochondrial damage [300]. By indirectly altering PGC1- α , UBE2N might mediate the UPS and mitophagy activities shifting, which is consistent with the report that autophagy negatively correlates with UPS activation [297]. Thus, the enhanced UPS by UBE2N overexpression might lead to downregulated mitophagy. In this study, however, no Parkin

recruitment was negatively affected, which might benefit from overexpression of Parkin and UBE2N together. As a result, this dual overexpression might enhance the clearance system activity in the scenarios when the UPS or Parkin-mediated mitophagy is dominantly required, thus protecting the cells.

UBE2N overexpression and rotenone-induced damage

Mitophagy coupled with fission is widely accepted as a protective activity that maintains healthy cell populations by clearing damaged and non-functional mitochondria. This process may also reduce mitochondrial ROS formation and damage-induced apoptosis, thus keeping cells healthy [301]. It is therefore hypothesised that the enhancement of Parkin-mediated mitophagy by UBE2N overexpression could improve the protective effect, especially against mitochondrial-targeted stress inducers. In this study, rotenone was used to trigger the PD-like mitochondrial stress, and the evaluation of the protective effect from overexpression of UBE2N was performed through the MTT cell viability assay. However, the result did not support the hypothesis, as there was no protective effect on cell viability following the upregulation of UBE2N. This result indicates that enhancing Parkin recruitment is insufficient to protect against the rotenone-induced damage to mitochondria. This may be due to mitophagy not being induced, thus not leading to enhanced clearance of the damaged mitochondria.

The other possible explanation is that high levels of rotenone-induced stress may

prevent mitophagy induction. Evidence reported that mitophagy is only induced by mild and transient oxidative stress [290]. The low dose of rotenone with a short treatment period initiates a ROS signalling cascade, leading to mitophagy induction to clear countable partially damaged mitochondria. In contrast, high dose rotenone might drive apoptosis to clear the damaged cells instead of mitophagy. To reach a more comprehensive conclusion, further studies with lower oxidative stress conditions should be performed to verify the effect of enhanced Parkin recruitment by upregulation of UBE2N on the potential of protecting the cells from stress.

UBR5, GBP2 and HECTD2

The study of UBR5, GBP2 and HECTD2 showed that knockdown of HECTD2 increased Parkin puncta formation. This effect could be because the HECTD2 mediates the proteasomal degradation of cleaved PINK1 [282]. With the downregulation of HECTD2, the degradation of PINK1 was impaired, leading to its accumulation on the mitochondrial membrane when incubated with CCCP, which further recruited more Parkin to be observed. However, that effect of HECTD2 was only seen in SH-SY5Y cells (and not in H4 cells). The reason for this discrepancy is uncertain it may again be due to the relative expression levels of HECTD2 combined with transfection efficiency or the relative abundance of accessory proteins involved in regulating this process.

Chapter7 General discussion

Thesis results summary and broader context

The incidence of neurodegenerative diseases is increasing globally, and the associated severe reduction in quality of life for an individual with the disease and the economic impact on society is considerable. Thus, treatments for neurodegenerative diseases are urgently needed. Emerging evidence shows ageing is the most significant risk factor for diseases such as Parkinson's disease, where mitochondrial dysfunction is closely linked to the aetiology of the condition. (Reviewed in [302] [303, 304]). Neurons, especially dopaminergic neurons whose degeneration causes PD, are highly vulnerable to disrupted energy homeostasis caused by dysfunctional mitochondria during ageing and stress [305]. Therefore, improving mitochondrial function may improve neuronal health and delay or prevent the onset of the degenerative condition. This thesis focused on investigating mechanisms by which mitochondrial function can be improved and thus could be used as potential treatments for PD. The findings suggested that the drug compound AZD5438, a GSK3 and CDKs inhibitor that positively regulates mitochondrial activity, might be a therapeutic solution for neurodegenerative diseases like PD.

In chapter 3, pharmacological compounds that targeted GSK3 and CDKs and the

mPTP were investigated. Kenpaullone was shown to negatively regulate Parkin recruitment to mitochondria following treatment with CCCP in two human neurological cell lines. A follow-up study showed kenpaullone enhanced the mitochondrial network and prevented changes to the network caused by treatment with CCCP. Kenpaullone also upregulated the glycolytic potential of cells, and its protective actions may be due to it differentially inhibiting GSK3 and CDKs.

In chapter 4, studies comparing the effectiveness of GSK3 and CDKs inhibitors were evaluated. AZD5438, AT7519, alsterpaullone and 1-azakenapaullone were found to mediate similar effects to kenpaullone. AZD5438 was shown to have the strongest effects on mitochondrial morphology and parkin recruitment, and it was also shown to protect cells from mitochondrial stressors, rotenone and MPP+ induced damage. AZD5438 was also observed to inhibit the upregulation of mitochondrial ROS and apoptosis and increase glycolysis. Further investigation showed that AZD5438's protective effects were dependent on glucose availability, which suggested the pro-glycolytic metabolic influence on cells may be essential to mediate AZD5438's protective actions. Moreover, CDK9 inhibition was shown to mediate AZD5438's inhibitory effect on Parkin recruitment, while its protective effects are likely to be mediated via the differential inhibition of GSK3 and CDKs.

In chapter 5, the protective effect of AZD5438 was investigated in rodent primary cortical neuron cells and human midbrain dopaminergic neurons. AZD5438 was

shown to protect rodent and human neurons from rotenone-induced PD-like stress, and cells treated with AZD5438 alone had a healthier mitochondrial and neuronal network with less ROS and apoptotic levels.

In chapter 6, genetic modulators of Parkin recruitment were investigated, and the cellular protective potential of UBE2N was evaluated. UBE2N is a mediator of Parkin-mediated mitophagy by binding to Parkin, subsequently activating the positive feedback of Parkin recruitment. This study confirmed that the inhibition of UBE2N impaired Parkin recruitment while overexpressing UBE2N enhanced Parkin recruitment. However, the results showed that increased Parkin recruitment due to the overexpression of UBE2N did not protect cells from rotenone. This suggests that improving the initiation of mitophagy (Parkin recruitment) may not be sufficient to protect cells. Another gene of interest, HECTD2, was shown to negatively regulate Parkin recruitment. HECTD2 mediates the degradation of PINK1, thus, the modification of HECTD2 expression may potentially improve the induction of mitophagy.

Mitophagy alteration for PD treatment: Upregulation or downregulation?

Mitophagy is widely accepted as a critical protective process that clears damaged and dysfunctional mitochondria in order to maintain healthy cell populations.

Functional mitophagy coupled with mitochondrial fission and fusion reduces dysfunctional mitochondrial protein aggregation, restores ATP generation, and prevents mitochondrial ROS formation and stress-induced apoptosis, thus protecting the cells. Given the positive role of mitophagy in maintaining cells' health, it is suggested that the upregulation of mitophagy and fission could protect cells from mitochondrial-targeted stress inducers. On the contrary, the downregulation of mitophagy may prevent the clearance of damaged mitochondria, resulting in cell death.

UBE2N was overexpressed and found to upregulate Parkin recruitment, though this did not protect cells from rotenone-induced cell damage. This indicates that enhancing Parkin recruitment is insufficient to protect cells from mitochondrial stress. Conversely, this study found that AZD5438, downregulated Parkin recruitment and yet had a cell-protective effect. However, this association does not necessarily suggest that downregulation of mitophagy will protect cells. In fact, the downregulation of mitophagy might result from improved mitochondrial homeostasis by AZD5438 treatment. Therefore, dynamic mitophagy activity might not be induced as it is not required. This study does not contradict the theory that enhanced mitophagy benefits cells but adds a novel view that the downregulation of mitophagy may indicate a healthier mitochondrial network with less stress. Hence, cells with a healthier mitochondrial network may be more tolerant of stress damage.

The cellular metabolic balance and PD treatment: Mitochondrial activity and glycolysis

Mitochondrial respiration and glycolysis are the two main processes that generate cellular energy. Glycolysis is not an efficient process for ATP production, with only 2 ATP molecules generated compared to the 36 ATP molecules per glucose molecule that mitochondrial respiration produces. However, glycolysis also generates NADH, and glycolysis-generated pyruvate (from glucose) is essential for mitochondrial to generate NADH. Mitochondria require NADH to proceed with oxidative phosphorylation and generate ATP[306]. Moreover, glycolytic production of lactate is another energy source driving the TCA cycle for oxidative phosphorylation [307]. Thus, when there is a lack of such sources in the cells, mitochondria will be prompted to recycle these sources for reuse. This suggests mitochondrial activity is relatively dependent on glycolytic activity and improving glycolysis might benefit mitochondrial function.

Mitochondrial activity and glycolysis are kept in balance to meet the energy demand of cells. Evidence shows that the balance can shift under proliferation and stress conditions [308, 309] [310]. For example, when a large amount of energy is required by the cells, mitochondria will produce more ATP, and this puts them under stress. This is also why neurons generally have higher mitochondrial ROS levels and are more vulnerable to mitochondrial stress. Stress-damaged

mitochondria reduce ATP generation and induce apoptosis, leading to neuronal degeneration. Therefore, the decrease in mitochondrial stress mediated by a shift to glycolytic pathways might help protect neurons. Recent research supports this assumption and shows that energy from glycolysis plays an important role in maintaining synaptic transmission[222], providing energy during periods of intense neuronal activity[223], and glycolysis may protect against Parkinson's disease[224]. The above evidence and findings in this thesis (AZD5438 enhanced glycolysis and protected cells from mitochondrial stress) support the theory that enhanced glycolysis might protect against PD.

Recommendations for future work

Findings in this study reported that a pharmacologic compound, AZD5438, protected the cells against PD-like stress. This could be investigated further using dopaminergic neurons from human iPSCs carrying PD-related mutations. Animal models of PD could also be used to investigate the actions of AZD5438 and provide further evidence to carry the drug toward human trials.

This study suggested that the upregulation of glycolysis may be protective. Thus, a thorough study of glycolytic pathways and their influence on cells with or without PD stress is recommended for future work. That study should be performed in neuronal cells as their metabolism is different from cell lines'.

Besides the cell-protective actions, genetic and pharmacological tools altering glycolysis should also be evaluated for their effects contributing to altering the electrophysiological function of neuronal cells. This further study would provide a comprehensive insight into the alteration of glycolysis with its potential actions in treating neurodegenerative diseases.

This study found that the inhibition of CDK9 mediated an inhibitory effect on Parkin recruitment., However, whether the inhibition of CDK9 alone would protect cells was not investigated. Future experiments should be carefully designed to investigate the pathways and factors between CDK9, glycolysis and mitophagy, building the evidential link that CDK9 alteration may affect cells' stress response. Apart from CDK9, CDK1 and CDK2 are also potentially effective anti-apoptosis targets of AZD5438. Future work should investigate their protective actions with the confirmation of the knockdown delivered by a single or combination of siRNA transfection (alone and with AZD5438) and compare their cell protection to those with AZD5438 treatment.

Reference

1. Sorbo, M.D., et al., [*The prevalence of the Wolff-Parkinson-White syndrome in a population of 116,542 young males*]. *G Ital Cardiol*, 1995. **25**(6): p. 681-7.
2. Alexander, G.E., *Biology of Parkinson's disease: pathogenesis and pathophysiology of a multisystem neurodegenerative disorder*. *Dialogues Clin Neurosci*, 2004. **6**(3): p. 259-80.
3. Gan-Or, Z., P.A. Dion, and G.A. Rouleau, *Genetic perspective on the role of the autophagy-lysosome pathway in Parkinson disease*. *Autophagy*, 2015. **11**(9): p. 1443-57.
4. Liu, J., et al., *Mitophagy in Parkinson's Disease: From Pathogenesis to Treatment*. *Cells*, 2019. **8**(7).
5. Dauer, W. and S. Przedborski, *Parkinson's disease: mechanisms and models*. *Neuron*, 2003. **39**(6): p. 889-909.
6. Gao, F., et al., *Mitophagy in Parkinson's Disease: Pathogenic and Therapeutic Implications*. *Front Neurol*, 2017. **8**: p. 527.
7. Valente, E.M., et al., *Hereditary early-onset Parkinson's disease caused by mutations in PINK1*. *Science*, 2004. **304**(5674): p. 1158-60.
8. Dehay, B., et al., *Loss of P-type ATPase ATP13A2/PARK9 function induces general lysosomal deficiency and leads to Parkinson disease neurodegeneration*. *Proc Natl Acad Sci U S A*, 2012. **109**(24): p. 9611-6.
9. Zimprich, A., et al., *Mutations in LRRK2 cause autosomal-dominant parkinsonism with pleomorphic pathology*. *Neuron*, 2004. **44**(4): p. 601-7.
10. Chu, C.T., *Multiple pathways for mitophagy: A neurodegenerative conundrum for Parkinson's disease*. *Neurosci Lett*, 2018.
11. Chang, J.Y., et al., *Studies of the neural mechanisms of deep brain stimulation in rodent models of Parkinson's disease*. *Neurosci Biobehav Rev*, 2008. **32**(3): p. 352-66.
12. Isacson, O., *Models of repair mechanisms for future treatment modalities of Parkinson's disease*. *Brain Res Bull*, 2002. **57**(6): p. 839-46.
13. Bulthuis, E.P., et al., *Mitochondrial Morphofunction in Mammalian Cells*. *Antioxid Redox Signal*, 2019. **30**(18): p. 2066-2109.
14. Giorgi, C., et al., *Mitochondrial calcium homeostasis as potential target for mitochondrial medicine*. *Mitochondrion*, 2012. **12**(1): p. 77-85.
15. Anderson, S., et al., *Sequence and organization of the human mitochondrial genome*. *Nature*, 1981. **290**(5806): p. 457-65.
16. Ventura-Clapier, R., A. Garnier, and V. Veksler, *Transcriptional control of mitochondrial biogenesis: the central role of PGC-1alpha*. *Cardiovasc Res*, 2008. **79**(2): p. 208-17.
17. Zheng, B., et al., *PGC-1alpha, a potential therapeutic target for early*

- intervention in Parkinson's disease. Sci Transl Med, 2010. 2(52): p. 52ra73.*
18. Jiang, H., et al., *Adult Conditional Knockout of PGC-1alpha Leads to Loss of Dopamine Neurons. eNeuro, 2016. 3(4).*
 19. Burman, J.L., et al., *Mitochondrial fission facilitates the selective mitophagy of protein aggregates. J Cell Biol, 2017. 216(10): p. 3231-3247.*
 20. Fox, T.D., *An MBoC favorite: mitochondrial transmission during mating in Saccharomyces cerevisiae is determined by mitochondrial fusion and fission and the intramitochondrial segregation of mitochondrial DNA. Mol Biol Cell, 2012. 23(21): p. 4144.*
 21. Westermann, B., *Merging mitochondria matters: cellular role and molecular machinery of mitochondrial fusion. EMBO Rep, 2002. 3(6): p. 527-31.*
 22. Eura, Y., et al., *Two mitofusin proteins, mammalian homologues of FZO, with distinct functions are both required for mitochondrial fusion. J Biochem, 2003. 134(3): p. 333-44.*
 23. Smirnova, E., et al., *A human dynamin-related protein controls the distribution of mitochondria. J Cell Biol, 1998. 143(2): p. 351-8.*
 24. Parone, P.A., et al., *Preventing mitochondrial fission impairs mitochondrial function and leads to loss of mitochondrial DNA. PLoS One, 2008. 3(9): p. e3257.*
 25. Tatsuta, T. and T. Langer, *Quality control of mitochondria: protection against neurodegeneration and ageing. EMBO J, 2008. 27(2): p. 306-14.*
 26. Qureshi, M.A., C.M. Haynes, and M.W. Pellegrino, *The mitochondrial unfolded protein response: Signaling from the powerhouse. J Biol Chem, 2017. 292(33): p. 13500-13506.*
 27. Galluzzi, L., et al., *Molecular definitions of autophagy and related processes. EMBO J, 2017. 36(13): p. 1811-1836.*
 28. Youle, R.J. and D.P. Narendra, *Mechanisms of mitophagy. Nat Rev Mol Cell Biol, 2011. 12(1): p. 9-14.*
 29. Goudarzi, S., et al., *Insights Into Parkin-Mediated Mitophagy in Alzheimer's Disease: A Systematic Review. Front Aging Neurosci, 2021. 13: p. 674071.*
 30. Zhuang, N., et al., *PINK1-dependent phosphorylation of PINK1 and Parkin is essential for mitochondrial quality control. Cell Death Dis, 2016. 7(12): p. e2501.*
 31. Liu, L., et al., *Mitochondrial outer-membrane protein FUNDC1 mediates hypoxia-induced mitophagy in mammalian cells. Nat Cell Biol, 2012. 14(2): p. 177-85.*
 32. Liu, L., et al., *Mitophagy receptor FUNDC1 is regulated by PGC-1alpha/NRF1 to fine tune mitochondrial homeostasis. EMBO Rep, 2021. 22(3): p. e50629.*

33. Zhang, J. and P.A. Ney, *Role of BNIP3 and NIX in cell death, autophagy, and mitophagy*. *Cell Death Differ*, 2009. **16**(7): p. 939-46.
34. Okamoto, K., N. Kondo-Okamoto, and Y. Ohsumi, *Mitochondria-anchored receptor Atg32 mediates degradation of mitochondria via selective autophagy*. *Dev Cell*, 2009. **17**(1): p. 87-97.
35. Brentnall, M., et al., *Caspase-9, caspase-3 and caspase-7 have distinct roles during intrinsic apoptosis*. *BMC Cell Biol*, 2013. **14**: p. 32.
36. Rasmusson, A.G., et al., *Mitochondrial NAD(P)H oxidation pathways and nitrate/ammonium redox balancing in plants*. *Mitochondrion*, 2020. **53**: p. 158-165.
37. Li, P., et al., *Cytochrome c and dATP-dependent formation of Apaf-1/caspase-9 complex initiates an apoptotic protease cascade*. *Cell*, 1997. **91**(4): p. 479-89.
38. Shi, Y., *Mechanisms of caspase activation and inhibition during apoptosis*. *Mol Cell*, 2002. **9**(3): p. 459-70.
39. Redza-Dutordoir, M. and D.A. Averill-Bates, *Activation of apoptosis signalling pathways by reactive oxygen species*. *Biochim Biophys Acta*, 2016. **1863**(12): p. 2977-2992.
40. Hekimi, S., Y. Wang, and A. Noe, *Mitochondrial ROS and the Effectors of the Intrinsic Apoptotic Pathway in Aging Cells: The Discerning Killers!* *Front Genet*, 2016. **7**: p. 161.
41. Rolfe, D.F. and G.C. Brown, *Cellular energy utilization and molecular origin of standard metabolic rate in mammals*. *Physiol Rev*, 1997. **77**(3): p. 731-58.
42. Harris, J.J., R. Jolivet, and D. Attwell, *Synaptic energy use and supply*. *Neuron*, 2012. **75**(5): p. 762-77.
43. Yamano, K., N. Matsuda, and K. Tanaka, *The ubiquitin signal and autophagy: an orchestrated dance leading to mitochondrial degradation*. *EMBO Rep*, 2016. **17**(3): p. 300-16.
44. Rangaraju, V., N. Calloway, and T.A. Ryan, *Activity-driven local ATP synthesis is required for synaptic function*. *Cell*, 2014. **156**(4): p. 825-35.
45. Mandal, A. and C.M. Drerup, *Axonal Transport and Mitochondrial Function in Neurons*. *Front Cell Neurosci*, 2019. **13**: p. 373.
46. Corti, O., *Neuronal Mitophagy: Lessons from a Pathway Linked to Parkinson's Disease*. *Neurotox Res*, 2019. **36**(2): p. 292-305.
47. Li, Z., et al., *The importance of dendritic mitochondria in the morphogenesis and plasticity of spines and synapses*. *Cell*, 2004. **119**(6): p. 873-87.
48. Ly, C.V. and P. Verstreken, *Mitochondria at the synapse*. *Neuroscientist*, 2006. **12**(4): p. 291-9.
49. Arun, S., L. Liu, and G. Donmez, *Mitochondrial Biology and Neurological Diseases*. *Curr Neuropharmacol*, 2016. **14**(2): p. 143-54.
50. Luce, K., A.C. Weil, and H.D. Osiewacz, *Mitochondrial protein quality*

- control systems in aging and disease*. Adv Exp Med Biol, 2010. **694**: p. 108-25.
51. Fivenson, E.M., et al., *Mitophagy in neurodegeneration and aging*. Neurochem Int, 2017. **109**: p. 202-209.
 52. Levytsky, R.M., E.M. Germany, and O. Khalimonchuk, *Mitochondrial Quality Control Proteases in Neuronal Welfare*. J Neuroimmune Pharmacol, 2016. **11**(4): p. 629-644.
 53. Coleman, M., *Axon degeneration mechanisms: commonality amid diversity*. Nat Rev Neurosci, 2005. **6**(11): p. 889-98.
 54. Rugarli, E.I. and T. Langer, *Mitochondrial quality control: a matter of life and death for neurons*. EMBO J, 2012. **31**(6): p. 1336-49.
 55. Lopez-Otin, C., et al., *The hallmarks of aging*. Cell, 2013. **153**(6): p. 1194-217.
 56. Bossy-Wetzell, E., A. Petrilli, and A.B. Knott, *Mutant huntingtin and mitochondrial dysfunction*. Trends Neurosci, 2008. **31**(12): p. 609-16.
 57. Kerr, J.S., et al., *Mitophagy and Alzheimer's Disease: Cellular and Molecular Mechanisms*. Trends Neurosci, 2017. **40**(3): p. 151-166.
 58. Palikaras, K. and N. Tavernarakis, *Mitophagy in neurodegeneration and aging*. Front Genet, 2012. **3**: p. 297.
 59. Arneric, S.P., V.D. Kern, and D.T. Stephenson, *Regulatory-accepted drug development tools are needed to accelerate innovative CNS disease treatments*. Biochem Pharmacol, 2018. **151**: p. 291-306.
 60. Dolmetsch, R. and D.H. Geschwind, *The human brain in a dish: the promise of iPSC-derived neurons*. Cell, 2011. **145**(6): p. 831-4.
 61. Arimura, N. and K. Kaibuchi, *Neuronal polarity: from extracellular signals to intracellular mechanisms*. Nat Rev Neurosci, 2007. **8**(3): p. 194-205.
 62. Lazarovici, P., et al., *Long-term, heterologous down-regulation of the epidermal growth factor receptor in PC12 cells by nerve growth factor*. J Cell Biol, 1987. **104**(6): p. 1611-21.
 63. Morooka, T. and E. Nishida, *Requirement of p38 mitogen-activated protein kinase for neuronal differentiation in PC12 cells*. J Biol Chem, 1998. **273**(38): p. 24285-8.
 64. Kuo, W.L., K.C. Chung, and M.R. Rosner, *Differentiation of central nervous system neuronal cells by fibroblast-derived growth factor requires at least two signaling pathways: roles for Ras and Src*. Mol Cell Biol, 1997. **17**(8): p. 4633-43.
 65. Huang, E.J. and L.F. Reichardt, *Trk receptors: roles in neuronal signal transduction*. Annu Rev Biochem, 2003. **72**: p. 609-42.
 66. Chen, Y.M., et al., *Microtubule affinity-regulating kinase 2 functions downstream of the PAR-3/PAR-6/atypical PKC complex in regulating hippocampal neuronal polarity*. Proc Natl Acad Sci U S A, 2006. **103**(22): p. 8534-9.
 67. Li, J., et al., *GSK-3beta Contributes to Parkinsonian Dopaminergic Neuron*

- Death: Evidence From Conditional Knockout Mice and Tideglusib*. Front Mol Neurosci, 2020. **13**: p. 81.
68. Reinhardt, L., et al., *Dual Inhibition of GSK3beta and CDK5 Protects the Cytoskeleton of Neurons from Neuroinflammatory-Mediated Degeneration In Vitro and In Vivo*. Stem Cell Reports, 2019. **12**(3): p. 502-517.
 69. Embi, N., D.B. Rylatt, and P. Cohen, *Glycogen synthase kinase-3 from rabbit skeletal muscle. Separation from cyclic-AMP-dependent protein kinase and phosphorylase kinase*. Eur J Biochem, 1980. **107**(2): p. 519-27.
 70. Plyte, S.E., et al., *Glycogen synthase kinase-3: functions in oncogenesis and development*. Biochim Biophys Acta, 1992. **1114**(2-3): p. 147-62.
 71. Kim, L. and A.R. Kimmel, *GSK3, a master switch regulating cell-fate specification and tumorigenesis*. Curr Opin Genet Dev, 2000. **10**(5): p. 508-14.
 72. Li, B., et al., *Overexpression of GSK3betaS9A resulted in tau hyperphosphorylation and morphology reminiscent of pretangle-like neurons in the brain of PDGSK3beta transgenic mice*. Transgenic Res, 2004. **13**(4): p. 385-96.
 73. Langston, J.W., et al., *Chronic Parkinsonism in humans due to a product of meperidine-analog synthesis*. Science, 1983. **219**(4587): p. 979-80.
 74. Schapira, A.H., *Mitochondrial complex I deficiency in Parkinson's disease*. Adv Neurol, 1993. **60**: p. 288-91.
 75. Yang, K., et al., *The Key Roles of GSK-3beta in Regulating Mitochondrial Activity*. Cell Physiol Biochem, 2017. **44**(4): p. 1445-1459.
 76. Obame, F.N., et al., *Cardioprotective effect of morphine and a blocker of glycogen synthase kinase 3 beta, SB216763 [3-(2,4-dichlorophenyl)-4(1-methyl-1H-indol-3-yl)-1H-pyrrole-2,5-dione], via inhibition of the mitochondrial permeability transition pore*. J Pharmacol Exp Ther, 2008. **326**(1): p. 252-8.
 77. Nishihara, M., et al., *Modulation of the mitochondrial permeability transition pore complex in GSK-3beta-mediated myocardial protection*. J Mol Cell Cardiol, 2007. **43**(5): p. 564-70.
 78. Yuskaitis, C.J. and R.S. Jope, *Glycogen synthase kinase-3 regulates microglial migration, inflammation, and inflammation-induced neurotoxicity*. Cell Signal, 2009. **21**(2): p. 264-73.
 79. Kozikowski, A.P., et al., *Highly potent and specific GSK-3beta inhibitors that block tau phosphorylation and decrease alpha-synuclein protein expression in a cellular model of Parkinson's disease*. ChemMedChem, 2006. **1**(2): p. 256-66.
 80. Malumbres, M. and M. Barbacid, *Mammalian cyclin-dependent kinases*. Trends Biochem Sci, 2005. **30**(11): p. 630-41.
 81. Dhavan, R. and L.H. Tsai, *A decade of CDK5*. Nat Rev Mol Cell Biol, 2001.

- 2(10): p. 749-59.
82. Anshabo, A.T., et al., *CDK9: A Comprehensive Review of Its Biology, and Its Role as a Potential Target for Anti-Cancer Agents*. Front Oncol, 2021. **11**: p. 678559.
 83. Leost, M., et al., *Paullones are potent inhibitors of glycogen synthase kinase-3beta and cyclin-dependent kinase 5/p25*. Eur J Biochem, 2000. **267**(19): p. 5983-94.
 84. Knockaert, M., P. Greengard, and L. Meijer, *Pharmacological inhibitors of cyclin-dependent kinases*. Trends Pharmacol Sci, 2002. **23**(9): p. 417-25.
 85. Wang, Z., et al., *Cyclin B1/Cdk1 coordinates mitochondrial respiration for cell-cycle G2/M progression*. Dev Cell, 2014. **29**(2): p. 217-32.
 86. Candas, D., et al., *CyclinB1/Cdk1 phosphorylates mitochondrial antioxidant MnSOD in cell adaptive response to radiation stress*. J Mol Cell Biol, 2013. **5**(3): p. 166-75.
 87. Taguchi, N., et al., *Mitotic phosphorylation of dynamin-related GTPase Drp1 participates in mitochondrial fission*. J Biol Chem, 2007. **282**(15): p. 11521-9.
 88. Harbauer, A.B., et al., *Mitochondria. Cell cycle-dependent regulation of mitochondrial preprotein translocase*. Science, 2014. **346**(6213): p. 1109-13.
 89. Chou, L.C., et al., *The synthesized 2-(2-fluorophenyl)-6,7-methylenedioxyquinolin-4-one (CHM-1) promoted G2/M arrest through inhibition of CDK1 and induced apoptosis through the mitochondrial-dependent pathway in CT-26 murine colorectal adenocarcinoma cells*. J Gastroenterol, 2009. **44**(10): p. 1055-63.
 90. Xie, B., et al., *Cyclin B1/CDK1-regulated mitochondrial bioenergetics in cell cycle progression and tumor resistance*. Cancer Lett, 2019. **443**: p. 56-66.
 91. Terrano, D.T., M. Upreti, and T.C. Chambers, *Cyclin-dependent kinase 1-mediated Bcl-xL/Bcl-2 phosphorylation acts as a functional link coupling mitotic arrest and apoptosis*. Mol Cell Biol, 2010. **30**(3): p. 640-56.
 92. Ozeki, M., et al., *Response of cyclin B1 to ionizing radiation: regulation by NF-kappaB and mitochondrial antioxidant enzyme MnSOD*. Anticancer Res, 2004. **24**(5A): p. 2657-63.
 93. Qin, L., et al., *CDK1 Enhances Mitochondrial Bioenergetics for Radiation-Induced DNA Repair*. Cell Rep, 2015. **13**(10): p. 2056-63.
 94. Milton, N.G., *Phosphorylation of amyloid-beta at the serine 26 residue by human cdc2 kinase*. Neuroreport, 2001. **12**(17): p. 3839-44.
 95. Bibb, J.A., et al., *Phosphorylation of DARPP-32 by Cdk5 modulates dopamine signalling in neurons*. Nature, 1999. **402**(6762): p. 669-71.
 96. Nguyen, M.D., R.C. Lariviere, and J.P. Julien, *Deregulation of Cdk5 in a mouse model of ALS: toxicity alleviated by perikaryal neurofilament inclusions*. Neuron, 2001. **30**(1): p. 135-47.

97. Kaminosono, S., et al., *Suppression of mutant Huntingtin aggregate formation by Cdk5/p35 through the effect on microtubule stability*. J Neurosci, 2008. **28**(35): p. 8747-55.
98. Luo, S., et al., *Cdk5 phosphorylation of huntingtin reduces its cleavage by caspases: implications for mutant huntingtin toxicity*. J Cell Biol, 2005. **169**(4): p. 647-56.
99. Katchanov, J., et al., *Mild cerebral ischemia induces loss of cyclin-dependent kinase inhibitors and activation of cell cycle machinery before delayed neuronal cell death*. J Neurosci, 2001. **21**(14): p. 5045-53.
100. Bordet, T., et al., *Identification and characterization of cholest-4-en-3-one, oxime (TRO19622), a novel drug candidate for amyotrophic lateral sclerosis*. J Pharmacol Exp Ther, 2007. **322**(2): p. 709-20.
101. Hazlitt, R.A., et al., *Development of Second-Generation CDK2 Inhibitors for the Prevention of Cisplatin-Induced Hearing Loss*. J Med Chem, 2018. **61**(17): p. 7700-7709.
102. Yin, P., et al., *Alsterpaullone induces apoptosis of HepG2 cells via a p38 mitogen-activated protein kinase signaling pathway*. Oncol Lett, 2019. **17**(1): p. 1177-1183.
103. Stathakos, P., et al., *A monolayer hiPSC culture system for autophagy/mitophagy studies in human dopaminergic neurons*. Autophagy, 2021. **17**(4): p. 855-871.
104. Rivera, T., et al., *Human-Induced Pluripotent Stem Cell Culture Methods Under cGMP Conditions*. Curr Protoc Stem Cell Biol, 2020. **54**(1): p. e117.
105. Yu, J., et al., *Induced pluripotent stem cell lines derived from human somatic cells*. Science, 2007. **318**(5858): p. 1917-20.
106. Hanna, J., et al., *Human embryonic stem cells with biological and epigenetic characteristics similar to those of mouse ESCs*. Proc Natl Acad Sci U S A, 2010. **107**(20): p. 9222-7.
107. Neganova, I., et al., *Expression and functional analysis of G1 to S regulatory components reveals an important role for CDK2 in cell cycle regulation in human embryonic stem cells*. Oncogene, 2009. **28**(1): p. 20-30.
108. Scott, H.L., et al., *A dual druggable genome-wide siRNA and compound library screening approach identifies modulators of parkin recruitment to mitochondria*. J Biol Chem, 2020. **295**(10): p. 3285-3300.
109. Petit-Paitel, A., et al., *Involvement of cytosolic and mitochondrial GSK-3beta in mitochondrial dysfunction and neuronal cell death of MPTP/MPP-treated neurons*. PLoS One, 2009. **4**(5): p. e5491.
110. Joo, H.C., et al., *Protective effects of kenpaullone on cardiomyocytes following H2O2-induced oxidative stress are attributed to inhibition of connexin 43 degradation by SGSM3*. Biochem Biophys Res Commun, 2018. **499**(2): p. 368-373.
111. Yang, Y.M., et al., *A small molecule screen in stem-cell-derived motor*

- neurons identifies a kinase inhibitor as a candidate therapeutic for ALS.* Cell Stem Cell, 2013. **12**(6): p. 713-26.
112. Liu, M.L., T. Zang, and C.L. Zhang, *Direct Lineage Reprogramming Reveals Disease-Specific Phenotypes of Motor Neurons from Human ALS Patients.* Cell Rep, 2016. **14**(1): p. 115-128.
 113. Hilton, J.B., et al., *Cu(II)(atsm) improves the neurological phenotype and survival of SOD1(G93A) mice and selectively increases enzymatically active SOD1 in the spinal cord.* Sci Rep, 2017. **7**: p. 42292.
 114. Lee, H.W., et al., *High-content screening assay-based discovery of paullones as novel podocyte-protective agents.* Am J Physiol Renal Physiol, 2018. **314**(2): p. F280-F292.
 115. Kovalevich, J., M. Santerre, and D. Langford, *Considerations for the Use of SH-SY5Y Neuroblastoma Cells in Neurobiology.* Methods Mol Biol, 2021. **2311**: p. 9-23.
 116. Jaishankar, J. and P. Srivastava, *Molecular Basis of Stationary Phase Survival and Applications.* Front Microbiol, 2017. **8**: p. 2000.
 117. Xicoy, H., B. Wieringa, and G.J. Martens, *The SH-SY5Y cell line in Parkinson's disease research: a systematic review.* Mol Neurodegener, 2017. **12**(1): p. 10.
 118. Xie, H.R., L.S. Hu, and G.Y. Li, *SH-SY5Y human neuroblastoma cell line: in vitro cell model of dopaminergic neurons in Parkinson's disease.* Chin Med J (Engl), 2010. **123**(8): p. 1086-92.
 119. Mei, Y., et al., *FOXO3a-dependent regulation of Pink1 (Park6) mediates survival signaling in response to cytokine deprivation.* Proc Natl Acad Sci U S A, 2009. **106**(13): p. 5153-8.
 120. Duan, X., et al., *Upregulation of human PINK1 gene expression by NFkappaB signalling.* Mol Brain, 2014. **7**: p. 57.
 121. Bueno, M., et al., *ATF3 represses PINK1 gene transcription in lung epithelial cells to control mitochondrial homeostasis.* Aging Cell, 2018. **17**(2).
 122. Shires, S.E., et al., *Nuclear Parkin Activates the ERRalpha Transcriptional Program and Drives Widespread Changes in Gene Expression Following Hypoxia.* Sci Rep, 2020. **10**(1): p. 8499.
 123. Chandrachud, U., et al., *Unbiased Cell-based Screening in a Neuronal Cell Model of Batten Disease Highlights an Interaction between Ca²⁺ Homeostasis, Autophagy, and CLN3 Protein Function.* J Biol Chem, 2015. **290**(23): p. 14361-80.
 124. Diot, A., et al., *A novel quantitative assay of mitophagy: Combining high content fluorescence microscopy and mitochondrial DNA load to quantify mitophagy and identify novel pharmacological tools against pathogenic heteroplasmic mtDNA.* Pharmacol Res, 2015. **100**: p. 24-35.
 125. Roberts, B.R., et al., *Oral treatment with Cu(II)(atsm) increases mutant SOD1 in vivo but protects motor neurons and improves the phenotype of*

- a transgenic mouse model of amyotrophic lateral sclerosis.* J Neurosci, 2014. **34**(23): p. 8021-31.
126. Hung, L.W., et al., *The hypoxia imaging agent Cull(at5m) is neuroprotective and improves motor and cognitive functions in multiple animal models of Parkinson's disease.* J Exp Med, 2012. **209**(4): p. 837-54.
 127. Przedborski, S., et al., *Free radical and nitric oxide toxicity in Parkinson's disease.* Adv Neurol, 2003. **91**: p. 83-94.
 128. Redmann, M., V. Darley-Usmar, and J. Zhang, *The Role of Autophagy, Mitophagy and Lysosomal Functions in Modulating Bioenergetics and Survival in the Context of Redox and Proteotoxic Damage: Implications for Neurodegenerative Diseases.* Aging Dis, 2016. **7**(2): p. 150-62.
 129. Schluter, O.M., et al., *Role of alpha-synuclein in 1-methyl-4-phenyl-1,2,3,6-tetrahydropyridine-induced parkinsonism in mice.* Neuroscience, 2003. **118**(4): p. 985-1002.
 130. Hantraye, P., et al., *Inhibition of neuronal nitric oxide synthase prevents MPTP-induced parkinsonism in baboons.* Nat Med, 1996. **2**(9): p. 1017-21.
 131. Duda, J.E., et al., *Widespread nitration of pathological inclusions in neurodegenerative synucleinopathies.* Am J Pathol, 2000. **157**(5): p. 1439-45.
 132. Donnelly, P.S., et al., *An impaired mitochondrial electron transport chain increases retention of the hypoxia imaging agent diacetylbis(4-methylthiosemicarbazonato)copperII.* Proc Natl Acad Sci U S A, 2012. **109**(1): p. 47-52.
 133. Yang, F., et al., *Exposure to copper induces mitochondria-mediated apoptosis by inhibiting mitophagy and the PINK1/parkin pathway in chicken (Gallus gallus) livers.* J Hazard Mater, 2021. **408**: p. 124888.
 134. Quinn, P.M.J., et al., *PINK1/PARKIN signalling in neurodegeneration and neuroinflammation.* Acta Neuropathol Commun, 2020. **8**(1): p. 189.
 135. Bonora, M., et al., *Role of the c subunit of the FO ATP synthase in mitochondrial permeability transition.* Cell Cycle, 2013. **12**(4): p. 674-83.
 136. Shanmughapriya, S., et al., *SPG7 Is an Essential and Conserved Component of the Mitochondrial Permeability Transition Pore.* Mol Cell, 2015. **60**(1): p. 47-62.
 137. Perez, M.J. and R.A. Quintanilla, *Development or disease: duality of the mitochondrial permeability transition pore.* Dev Biol, 2017. **426**(1): p. 1-7.
 138. Du, H. and S.S. Yan, *Mitochondrial permeability transition pore in Alzheimer's disease: cyclophilin D and amyloid beta.* Biochim Biophys Acta, 2010. **1802**(1): p. 198-204.
 139. Berman, S.B. and T.G. Hastings, *Dopamine oxidation alters mitochondrial respiration and induces permeability transition in brain mitochondria:*

- implications for Parkinson's disease.* J Neurochem, 1999. **73**(3): p. 1127-37.
140. Milakovic, T., R.A. Quintanilla, and G.V. Johnson, *Mutant huntingtin expression induces mitochondrial calcium handling defects in clonal striatal cells: functional consequences.* J Biol Chem, 2006. **281**(46): p. 34785-95.
 141. Javadov, S., M. Karmazyn, and N. Escobales, *Mitochondrial permeability transition pore opening as a promising therapeutic target in cardiac diseases.* J Pharmacol Exp Ther, 2009. **330**(3): p. 670-8.
 142. Bouchier-Hayes, L., L. Lartigue, and D.D. Newmeyer, *Mitochondria: pharmacological manipulation of cell death.* J Clin Invest, 2005. **115**(10): p. 2640-7.
 143. Reichman, N., C.M. Porteous, and M.P. Murphy, *Cyclosporin A blocks 6-hydroxydopamine-induced efflux of Ca²⁺ from mitochondria without inactivating the mitochondrial inner-membrane pore.* Biochem J, 1994. **297 (Pt 1)**: p. 151-5.
 144. Ganote, C.E. and S.C. Armstrong, *Effects of CCCP-induced mitochondrial uncoupling and cyclosporin A on cell volume, cell injury and preconditioning protection of isolated rabbit cardiomyocytes.* J Mol Cell Cardiol, 2003. **35**(7): p. 749-59.
 145. Miyazono, Y., et al., *Uncoupled mitochondria quickly shorten along their long axis to form indented spheroids, instead of rings, in a fission-independent manner.* Sci Rep, 2018. **8**(1): p. 350.
 146. Gao, Q.Y., et al., *Mitochondrial Fission and Mitophagy Reciprocally Orchestrate Cardiac Fibroblasts Activation.* Front Cell Dev Biol, 2020. **8**: p. 629397.
 147. Poole, A.C., et al., *The PINK1/Parkin pathway regulates mitochondrial morphology.* Proc Natl Acad Sci U S A, 2008. **105**(5): p. 1638-43.
 148. Brand, M.D. and D.G. Nicholls, *Assessing mitochondrial dysfunction in cells.* Biochem J, 2011. **435**(2): p. 297-312.
 149. Nogueira, V., et al., *Mitochondrial respiratory chain adjustment to cellular energy demand.* J Biol Chem, 2001. **276**(49): p. 46104-10.
 150. Depaoli, M.R., et al., *Real-Time Imaging of Mitochondrial ATP Dynamics Reveals the Metabolic Setting of Single Cells.* Cell Rep, 2018. **25**(2): p. 501-512 e3.
 151. Filosa, J.A., J.B. Dean, and R.W. Putnam, *Role of intracellular and extracellular pH in the chemosensitive response of rat locus coeruleus neurones.* J Physiol, 2002. **541**(Pt 2): p. 493-509.
 152. Wang, G.J., S.R. Richardson, and S.A. Thayer, *Intracellular acidification is not a prerequisite for glutamate-triggered death of cultured hippocampal neurons.* Neurosci Lett, 1995. **186**(2-3): p. 139-44.
 153. Humez, S., et al., *The role of intracellular pH in cell growth arrest induced by ATP.* Am J Physiol Cell Physiol, 2004. **287**(6): p. C1733-46.

154. Yambire, K.F., et al., *Impaired lysosomal acidification triggers iron deficiency and inflammation in vivo*. *Elife*, 2019. **8**.
155. Teixeira, J., et al., *Extracellular acidification induces ROS- and mPTP-mediated death in HEK293 cells*. *Redox Biol*, 2018. **15**: p. 394-404.
156. Chaudhry, R. and M. Varacallo, *Biochemistry, Glycolysis*, in *StatPearls*. 2022: Treasure Island (FL).
157. Naifeh, J., M. Dimri, and M. Varacallo, *Biochemistry, Aerobic Glycolysis*, in *StatPearls*. 2022: Treasure Island (FL).
158. Berezhnov, A.V., et al., *Intracellular pH Modulates Autophagy and Mitophagy*. *J Biol Chem*, 2016. **291**(16): p. 8701-8.
159. Lee, M. and J.H. Yoon, *Metabolic interplay between glycolysis and mitochondrial oxidation: The reverse Warburg effect and its therapeutic implication*. *World J Biol Chem*, 2015. **6**(3): p. 148-61.
160. Zaharevitz, D.W., et al., *Discovery and initial characterization of the paullones, a novel class of small-molecule inhibitors of cyclin-dependent kinases*. *Cancer Res*, 1999. **59**(11): p. 2566-9.
161. Arrazola, M.S., et al., *Wnt Signaling Prevents the Abeta Oligomer-Induced Mitochondrial Permeability Transition Pore Opening Preserving Mitochondrial Structure in Hippocampal Neurons*. *PLoS One*, 2017. **12**(1): p. e0168840.
162. Juhaszova, M., et al., *Glycogen synthase kinase-3beta mediates convergence of protection signaling to inhibit the mitochondrial permeability transition pore*. *J Clin Invest*, 2004. **113**(11): p. 1535-49.
163. Ruiz-Meana, M., et al., *Mitochondrial Ca²⁺ uptake during simulated ischemia does not affect permeability transition pore opening upon simulated reperfusion*. *Cardiovasc Res*, 2006. **71**(4): p. 715-24.
164. Papadopoli, D., M. Pollak, and I. Topisirovic, *The role of GSK3 in metabolic pathway perturbations in cancer*. *Biochim Biophys Acta Mol Cell Res*, 2021. **1868**(8): p. 119059.
165. He, L., et al., *mTORC1 Promotes Metabolic Reprogramming by the Suppression of GSK3-Dependent Foxk1 Phosphorylation*. *Mol Cell*, 2018. **70**(5): p. 949-960 e4.
166. Buller, C.L., et al., *A GSK-3/TSC2/mTOR pathway regulates glucose uptake and GLUT1 glucose transporter expression*. *Am J Physiol Cell Physiol*, 2008. **295**(3): p. C836-43.
167. Momcilovic, M., et al., *The GSK3 Signaling Axis Regulates Adaptive Glutamine Metabolism in Lung Squamous Cell Carcinoma*. *Cancer Cell*, 2018. **33**(5): p. 905-921 e5.
168. Kim, D.J., et al., *Tristetraprolin-mediated hexokinase 2 expression regulation contributes to glycolysis in cancer cells*. *Mol Biol Cell*, 2019. **30**(5): p. 542-553.
169. Mueckler, M. and B. Thorens, *The SLC2 (GLUT) family of membrane transporters*. *Mol Aspects Med*, 2013. **34**(2-3): p. 121-38.

170. Bijur, G.N. and R.S. Jope, *Glycogen synthase kinase-3 beta is highly activated in nuclei and mitochondria*. Neuroreport, 2003. **14**(18): p. 2415-9.
171. Yamashita, S.I., et al., *Mitochondrial division occurs concurrently with autophagosome formation but independently of Drp1 during mitophagy*. J Cell Biol, 2016. **215**(5): p. 649-665.
172. Solesio, M.E., et al., *Characterization of mitophagy in the 6-hydroxydopamine Parkinson's disease model*. Toxicol Sci, 2012. **129**(2): p. 411-20.
173. Tanaka, A., et al., *Proteasome and p97 mediate mitophagy and degradation of mitofusins induced by Parkin*. J Cell Biol, 2010. **191**(7): p. 1367-80.
174. Gelmetti, V., et al., *PINK1 and BECN1 relocalize at mitochondria-associated membranes during mitophagy and promote ER-mitochondria tethering and autophagosome formation*. Autophagy, 2017. **13**(4): p. 654-669.
175. Rodriguez-Arribas, M., et al., *Mitochondria-Associated Membranes (MAMs): Overview and Its Role in Parkinson's Disease*. Mol Neurobiol, 2017. **54**(8): p. 6287-6303.
176. Barazzuol, L., et al., *PINK1/Parkin Mediated Mitophagy, Ca(2+) Signalling, and ER-Mitochondria Contacts in Parkinson's Disease*. Int J Mol Sci, 2020. **21**(5).
177. Stoica, R., et al., *ER-mitochondria associations are regulated by the VAPB-PTPIP51 interaction and are disrupted by ALS/FTD-associated TDP-43*. Nat Commun, 2014. **5**: p. 3996.
178. Peggion, C., et al., *Regulation of Endoplasmic Reticulum-Mitochondria Tethering and Ca(2+) Fluxes by TDP-43 via GSK3beta*. Int J Mol Sci, 2021. **22**(21).
179. Icard, P., et al., *Interconnection between Metabolism and Cell Cycle in Cancer*. Trends Biochem Sci, 2019. **44**(6): p. 490-501.
180. Hu, J.W., et al., *Hexokinase 2 regulates G1/S checkpoint through CDK2 in cancer-associated fibroblasts*. Cell Signal, 2014. **26**(10): p. 2210-6.
181. Gao, L., et al., *6-phosphofructo-2-kinase/fructose-2,6-bisphosphatase Suppresses Neuronal Apoptosis by Increasing Glycolysis and "cyclin-dependent kinase 1-Mediated Phosphorylation of p27 After Traumatic Spinal Cord Injury in Rats*. Cell Transplant, 2020. **29**: p. 963689720950226.
182. Chang, J.G., et al., *Oxidative Stress-Induced Unscheduled CDK1-Cyclin B1 Activity Impairs ER-Mitochondria-Mediated Bioenergetic Metabolism*. Cells, 2021. **10**(6).
183. Avraham, E., et al., *Phosphorylation of Parkin by the cyclin-dependent kinase 5 at the linker region modulates its ubiquitin-ligase activity and aggregation*. J Biol Chem, 2007. **282**(17): p. 12842-50.

184. Nandi, N., et al., *Stress-induced Cdk5 activity enhances cytoprotective basal autophagy in Drosophila melanogaster by phosphorylating acinus at serine(437)*. Elife, 2017. **6**.
185. Wong, A.S., et al., *Cdk5-mediated phosphorylation of endophilin B1 is required for induced autophagy in models of Parkinson's disease*. Nat Cell Biol, 2011. **13**(5): p. 568-79.
186. Karbowski, M., S.Y. Jeong, and R.J. Youle, *Endophilin B1 is required for the maintenance of mitochondrial morphology*. J Cell Biol, 2004. **166**(7): p. 1027-39.
187. Wang, Y.H., et al., *Endophilin B2 promotes inner mitochondrial membrane degradation by forming heterodimers with Endophilin B1 during mitophagy*. Sci Rep, 2016. **6**: p. 25153.
188. Park, J., et al., *Abnormal Mitochondria in a Non-human Primate Model of MPTP-induced Parkinson's Disease: Drp1 and CDK5/p25 Signaling*. Exp Neurobiol, 2019. **28**(3): p. 414-424.
189. Cherubini, M., et al., *Cdk5-mediated mitochondrial fission: A key player in dopaminergic toxicity in Huntington's disease*. Biochim Biophys Acta, 2015. **1852**(10 Pt A): p. 2145-60.
190. Rong, R., et al., *Cdk5-mediated Drp1 phosphorylation drives mitochondrial defects and neuronal apoptosis in radiation-induced optic neuropathy*. Cell Death Dis, 2020. **11**(9): p. 720.
191. Sun, K.H., et al., *Deregulated Cdk5 promotes oxidative stress and mitochondrial dysfunction*. J Neurochem, 2008. **107**(1): p. 265-78.
192. Meuer, K., et al., *Cyclin-dependent kinase 5 is an upstream regulator of mitochondrial fission during neuronal apoptosis*. Cell Death Differ, 2007. **14**(4): p. 651-61.
193. Boss, D.S., et al., *Safety, tolerability, pharmacokinetics and pharmacodynamics of the oral cyclin-dependent kinase inhibitor AZD5438 when administered at intermittent and continuous dosing schedules in patients with advanced solid tumours*. Ann Oncol, 2010. **21**(4): p. 884-894.
194. Sorf, A., et al., *Cyclin-dependent kinase inhibitors AZD5438 and R547 show potential for enhancing efficacy of daunorubicin-based anticancer therapy: Interaction with carbonyl-reducing enzymes and ABC transporters*. Biochem Pharmacol, 2019. **163**: p. 290-298.
195. Bozik, M.E., et al., *A post hoc analysis of subgroup outcomes and creatinine in the phase III clinical trial (EMPOWER) of dextramipexole in ALS*. Amyotroph Lateral Scler Frontotemporal Degener, 2014. **15**(5-6): p. 406-13.
196. Alavian, K.N., et al., *Effects of dextramipexole on brain mitochondrial conductances and cellular bioenergetic efficiency*. Brain Res, 2012. **1446**: p. 1-11.
197. Jayashankar, V. and S.M. Rafelski, *Integrating mitochondrial organization*

- and dynamics with cellular architecture.* Curr Opin Cell Biol, 2014. **26**: p. 34-40.
198. Rooney, J.P., et al., *PCR based determination of mitochondrial DNA copy number in multiple species.* Methods Mol Biol, 2015. **1241**: p. 23-38.
 199. Li, N., et al., *Mitochondrial complex I inhibitor rotenone induces apoptosis through enhancing mitochondrial reactive oxygen species production.* J Biol Chem, 2003. **278**(10): p. 8516-25.
 200. Hurcombe, J.A., et al., *Podocyte GSK3 is an evolutionarily conserved critical regulator of kidney function.* Nat Commun, 2019. **10**(1): p. 403.
 201. Ozansoy, M. and A.N. Basak, *The central theme of Parkinson's disease: alpha-synuclein.* Mol Neurobiol, 2013. **47**(2): p. 460-5.
 202. Sala, G., et al., *Rotenone upregulates alpha-synuclein and myocyte enhancer factor 2D independently from lysosomal degradation inhibition.* Biomed Res Int, 2013. **2013**: p. 846725.
 203. Wang, Y., et al., *The novel mechanism of rotenone-induced alpha-synuclein phosphorylation via reduced protein phosphatase 2A activity.* Int J Biochem Cell Biol, 2016. **75**: p. 34-44.
 204. Teitz, T., et al., *CDK2 inhibitors as candidate therapeutics for cisplatin- and noise-induced hearing loss.* J Exp Med, 2018. **215**(4): p. 1187-1203.
 205. Bordet, T., et al., *Identification and characterization of cholest-4-en-3-one, oxime (TRO19622), a novel drug candidate for amyotrophic lateral sclerosis.* Journal of Pharmacology and Experimental Therapeutics, 2007. **322**(2): p. 709-720.
 206. Cudkowicz, M., et al., *The effects of dextramipexole (KNS-760704) in individuals with amyotrophic lateral sclerosis.* Nature Medicine, 2011. **17**(12): p. 1652-U169.
 207. Rippin, I. and H. Eldar-Finkelman, *Mechanisms and Therapeutic Implications of GSK-3 in Treating Neurodegeneration.* Cells, 2021. **10**(2).
 208. Xiong, N., et al., *Mitochondrial complex I inhibitor rotenone-induced toxicity and its potential mechanisms in Parkinson's disease models.* Crit Rev Toxicol, 2012. **42**(7): p. 613-32.
 209. Tanner, C.M., et al., *Rotenone, paraquat, and Parkinson's disease.* Environ Health Perspect, 2011. **119**(6): p. 866-72.
 210. Jerber, J., et al., *Population-scale single-cell RNA-seq profiling across dopaminergic neuron differentiation.* Nat Genet, 2021. **53**(3): p. 304-312.
 211. Youle, R.J. and A.M. van der Bliek, *Mitochondrial fission, fusion, and stress.* Science, 2012. **337**(6098): p. 1062-5.
 212. Nakada, K., et al., *Inter-mitochondrial complementation: Mitochondria-specific system preventing mice from expression of disease phenotypes by mutant mtDNA.* Nat Med, 2001. **7**(8): p. 934-40.
 213. Schon, E.A. and R.W. Gilkerson, *Functional complementation of mitochondrial DNAs: mobilizing mitochondrial genetics against dysfunction.* Biochim Biophys Acta, 2010. **1800**(3): p. 245-9.

214. Twig, G., et al., *Fission and selective fusion govern mitochondrial segregation and elimination by autophagy*. EMBO J, 2008. **27**(2): p. 433-46.
215. Friedman, J.R., et al., *ER tubules mark sites of mitochondrial division*. Science, 2011. **334**(6054): p. 358-62.
216. Lukasik, P., M. Zaluski, and I. Gutowska, *Cyclin-Dependent Kinases (CDK) and Their Role in Diseases Development-Review*. Int J Mol Sci, 2021. **22**(6).
217. Mushtaq, G., et al., *Neuroprotective Mechanisms Mediated by CDK5 Inhibition*. Curr Pharm Des, 2016. **22**(5): p. 527-34.
218. Smith, P.D., et al., *Cyclin-dependent kinase 5 is a mediator of dopaminergic neuron loss in a mouse model of Parkinson's disease*. Proceedings of the National Academy of Sciences, 2003. **100**(23): p. 13650.
219. Yao, J., et al., *CDK9 inhibition blocks the initiation of PINK1-PRKN-mediated mitophagy by regulating the SIRT1-FOXO3-BNIP3 axis and enhances the therapeutic effects involving mitochondrial dysfunction in hepatocellular carcinoma*. Autophagy, 2021: p. 1-19.
220. Eldar-Finkelman, H. and A. Martinez, *GSK-3 Inhibitors: Preclinical and Clinical Focus on CNS*. Front Mol Neurosci, 2011. **4**: p. 32.
221. Itkonen, H.M., et al., *CDK9 Inhibition Induces a Metabolic Switch that Renders Prostate Cancer Cells Dependent on Fatty Acid Oxidation*. Neoplasia, 2019. **21**(7): p. 713-720.
222. Lujan, B., et al., *Glycolysis selectively shapes the presynaptic action potential waveform*. J Neurophysiol, 2016. **116**(6): p. 2523-2540.
223. Diaz-Garcia, C.M., et al., *Neuronal Stimulation Triggers Neuronal Glycolysis and Not Lactate Uptake*. Cell Metab, 2017. **26**(2): p. 361-374 e4.
224. Cai, R., et al., *Enhancing glycolysis attenuates Parkinson's disease progression in models and clinical databases*. J Clin Invest, 2019. **129**(10): p. 4539-4549.
225. Lunt, S.Y. and M.G. Vander Heiden, *Aerobic glycolysis: meeting the metabolic requirements of cell proliferation*. Annu Rev Cell Dev Biol, 2011. **27**: p. 441-64.
226. Sano, M., et al., *Activation of cardiac Cdk9 represses PGC-1 and confers a predisposition to heart failure*. EMBO J, 2004. **23**(17): p. 3559-69.
227. Alves Da Costa, C., et al., *Alpha-synuclein lowers p53-dependent apoptotic response of neuronal cells. Abolishment by 6-hydroxydopamine and implication for Parkinson's disease*. J Biol Chem, 2002. **277**(52): p. 50980-4.
228. Hashimoto, M., et al., *alpha-Synuclein protects against oxidative stress via inactivation of the c-Jun N-terminal kinase stress-signaling pathway in neuronal cells*. J Biol Chem, 2002. **277**(13): p. 11465-72.

229. Musgrove, R.E., A.E. King, and T.C. Dickson, *alpha-Synuclein protects neurons from apoptosis downstream of free-radical production through modulation of the MAPK signalling pathway*. Neurotox Res, 2013. **23**(4): p. 358-69.
230. Pamies, D., et al., *Rotenone exerts developmental neurotoxicity in a human brain spheroid model*. Toxicol Appl Pharmacol, 2018. **354**: p. 101-114.
231. Reardon, A.J., J.A. Elliott, and L.E. McGann, *Fluorescence as an alternative to light-scatter gating strategies to identify frozen-thawed cells with flow cytometry*. Cryobiology, 2014. **69**(1): p. 91-9.
232. Surin, A.M., et al., *Disruption of Functional Activity of Mitochondria during MTT Assay of Viability of Cultured Neurons*. Biochemistry (Mosc), 2017. **82**(6): p. 737-749.
233. Shabanipour, S., et al., *Primary Culture of Neurons Isolated from Embryonic Mouse Cerebellum*. J Vis Exp, 2019(152).
234. Persson, A.K., et al., *Sodium channels contribute to degeneration of dorsal root ganglion neurites induced by mitochondrial dysfunction in an in vitro model of axonal injury*. J Neurosci, 2013. **33**(49): p. 19250-61.
235. Oswald, M.C.W., et al., *Regulation of neuronal development and function by ROS*. FEBS Lett, 2018. **592**(5): p. 679-691.
236. Auten, R.L. and J.M. Davis, *Oxygen toxicity and reactive oxygen species: the devil is in the details*. Pediatr Res, 2009. **66**(2): p. 121-7.
237. Harris, G., et al., *Toxicity, recovery, and resilience in a 3D dopaminergic neuronal in vitro model exposed to rotenone*. Arch Toxicol, 2018. **92**(8): p. 2587-2606.
238. Srivastava, P. and D. Panda, *Rotenone inhibits mammalian cell proliferation by inhibiting microtubule assembly through tubulin binding*. FEBS J, 2007. **274**(18): p. 4788-801.
239. Passmore, J.B., et al., *The respiratory chain inhibitor rotenone affects peroxisomal dynamics via its microtubule-destabilising activity*. Histochem Cell Biol, 2017. **148**(3): p. 331-341.
240. Gomes, L.C. and L. Scorrano, *Mitochondrial elongation during autophagy: a stereotypical response to survive in difficult times*. Autophagy, 2011. **7**(10): p. 1251-3.
241. Shin, J.H., et al., *PARIS (ZNF746) repression of PGC-1alpha contributes to neurodegeneration in Parkinson's disease*. Cell, 2011. **144**(5): p. 689-702.
242. Onishi, Y., et al., *Regulation of mitochondrial proliferation by PGC-1alpha induces cellular apoptosis in musculoskeletal malignancies*. Sci Rep, 2014. **4**: p. 3916.
243. Austin, S. and J. St-Pierre, *PGC1alpha and mitochondrial metabolism--emerging concepts and relevance in ageing and neurodegenerative disorders*. J Cell Sci, 2012. **125**(Pt 21): p. 4963-71.
244. Baldelli, S., K. Aquilano, and M.R. Ciriolo, *PGC-1alpha buffers ROS-*

- mediated removal of mitochondria during myogenesis. Cell Death Dis*, 2014. **5**: p. e1515.
245. Pre, D., et al., *A time course analysis of the electrophysiological properties of neurons differentiated from human induced pluripotent stem cells (iPSCs)*. PLoS One, 2014. **9**(7): p. e103418.
 246. Marshall, L.E. and R.H. Himes, *Rotenone inhibition of tubulin self-assembly*. Biochim Biophys Acta, 1978. **543**(4): p. 590-4.
 247. Bonsi, P., et al., *Early ionic and membrane potential changes caused by the pesticide rotenone in striatal cholinergic interneurons*. Exp Neurol, 2004. **185**(1): p. 169-81.
 248. Namba, H., T. Okubo, and H. Nawa, *Perinatal Exposure to Neuregulin-1 Results in Disinhibition of Adult Midbrain Dopaminergic Neurons: Implication in Schizophrenia Modeling*. Sci Rep, 2016. **6**: p. 22606.
 249. Shao, D., K. Okuse, and M.B. Djamgoz, *Protein-protein interactions involving voltage-gated sodium channels: Post-translational regulation, intracellular trafficking and functional expression*. Int J Biochem Cell Biol, 2009. **41**(7): p. 1471-81.
 250. Beaulieu, J.M., R.R. Gainetdinov, and M.G. Caron, *Akt/GSK3 signaling in the action of psychotropic drugs*. Annu Rev Pharmacol Toxicol, 2009. **49**: p. 327-47.
 251. Hernandez, F., et al., *GSK3 inhibitors and disease*. Mini Rev Med Chem, 2009. **9**(9): p. 1024-9.
 252. Coghlan, M.P., et al., *Selective small molecule inhibitors of glycogen synthase kinase-3 modulate glycogen metabolism and gene transcription*. Chem Biol, 2000. **7**(10): p. 793-803.
 253. Yanagita, T., et al., *Chronic lithium treatment up-regulates cell surface Na(V)1.7 sodium channels via inhibition of glycogen synthase kinase-3 in adrenal chromaffin cells: enhancement of Na(+) influx, Ca(2+) influx and catecholamine secretion after lithium withdrawal*. Neuropharmacology, 2009. **57**(3): p. 311-21.
 254. Shavkunov, A.S., et al., *The fibroblast growth factor 14.voltage-gated sodium channel complex is a new target of glycogen synthase kinase 3 (GSK3)*. J Biol Chem, 2013. **288**(27): p. 19370-85.
 255. Persson, A.-K., et al., *Sodium Channels Contribute to Degeneration of Dorsal Root Ganglion Neurites Induced by Mitochondrial Dysfunction in an *In Vitro* Model of Axonal Injury*. The Journal of Neuroscience, 2013. **33**(49): p. 19250-19261.
 256. Armstrong, C.M., *Na channel inactivation from open and closed states*. Proc Natl Acad Sci U S A, 2006. **103**(47): p. 17991-6.
 257. Catterall, W.A., *Voltage-gated calcium channels*. Cold Spring Harb Perspect Biol, 2011. **3**(8): p. a003947.
 258. Sudhof, T.C., *Calcium control of neurotransmitter release*. Cold Spring Harb Perspect Biol, 2012. **4**(1): p. a011353.

259. Xie, C.W., *Calcium-regulated signaling pathways: role in amyloid beta-induced synaptic dysfunction*. *Neuromolecular Med*, 2004. **6**(1): p. 53-64.
260. Kochlamazashvili, G., et al., *The extracellular matrix molecule hyaluronic acid regulates hippocampal synaptic plasticity by modulating postsynaptic L-type Ca(2+) channels*. *Neuron*, 2010. **67**(1): p. 116-28.
261. Bravo-Sagua, R., et al., *Calcium Transport and Signaling in Mitochondria*. *Compr Physiol*, 2017. **7**(2): p. 623-634.
262. Jaafari, N. and M. Canepari, *Functional coupling of diverse voltage-gated Ca(2+) channels underlies high fidelity of fast dendritic Ca(2+) signals during burst firing*. *J Physiol*, 2016. **594**(4): p. 967-83.
263. Yokoyama, C.T., Z.H. Sheng, and W.A. Catterall, *Phosphorylation of the synaptic protein interaction site on N-type calcium channels inhibits interactions with SNARE proteins*. *J Neurosci*, 1997. **17**(18): p. 6929-38.
264. Zhu, L.Q., et al., *GSK-3 beta inhibits presynaptic vesicle exocytosis by phosphorylating P/Q-type calcium channel and interrupting SNARE complex formation*. *J Neurosci*, 2010. **30**(10): p. 3624-33.
265. Tomizawa, K., et al., *Cdk5/p35 regulates neurotransmitter release through phosphorylation and downregulation of P/Q-type voltage-dependent calcium channel activity*. *J Neurosci*, 2002. **22**(7): p. 2590-7.
266. Rueda, C.B., et al., *Mitochondrial ATP-Mg/Pi carrier SCA₃/SLC25A23 counteracts PARP-1-dependent fall in mitochondrial ATP caused by excitotoxic insults in neurons*. *J Neurosci*, 2015. **35**(8): p. 3566-81.
267. Jevtic, P., et al., *Sizing and shaping the nucleus: mechanisms and significance*. *Curr Opin Cell Biol*, 2014. **28**: p. 16-27.
268. Haglund, K. and I. Dikic, *Ubiquitylation and cell signaling*. *EMBO J*, 2005. **24**(19): p. 3353-9.
269. Jin, J., et al., *Dual E1 activation systems for ubiquitin differentially regulate E2 enzyme charging*. *Nature*, 2007. **447**(7148): p. 1135-8.
270. Deng, L., et al., *Activation of the I κ B kinase complex by TRAF6 requires a dimeric ubiquitin-conjugating enzyme complex and a unique polyubiquitin chain*. *Cell*, 2000. **103**(2): p. 351-61.
271. Upadhyay, A., et al., *E3 Ubiquitin Ligases Neurobiological Mechanisms: Development to Degeneration*. *Front Mol Neurosci*, 2017. **10**: p. 151.
272. Hegde, A.N. and S.C. Upadhyaya, *Role of ubiquitin-proteasome-mediated proteolysis in nervous system disease*. *Biochim Biophys Acta*, 2011. **1809**(2): p. 128-40.
273. Shearer, R.F., et al., *Functional Roles of the E3 Ubiquitin Ligase UBR5 in Cancer*. *Mol Cancer Res*, 2015. **13**(12): p. 1523-32.
274. Callaghan, M.J., et al., *Identification of a human HECT family protein with homology to the Drosophila tumor suppressor gene hyperplastic discs*. *Oncogene*, 1998. **17**(26): p. 3479-91.
275. Dan, X., et al., *DNA damage invokes mitophagy through a pathway involving Spata18*. *Nucleic Acids Res*, 2020. **48**(12): p. 6611-6623.

276. Koyuncu, S., et al., *The ubiquitin ligase UBR5 suppresses proteostasis collapse in pluripotent stem cells from Huntington's disease patients*. Nat Commun, 2018. **9**(1): p. 2886.
277. Zhang, J., et al., *Correction: Guanylate-binding protein 2 regulates Drp1-mediated mitochondrial fission to suppress breast cancer cell invasion*. Cell Death Dis, 2018. **9**(11): p. 1127.
278. Qin, H., et al., *Inhibition of the JAK/STAT Pathway Protects Against alpha-Synuclein-Induced Neuroinflammation and Dopaminergic Neurodegeneration*. J Neurosci, 2016. **36**(18): p. 5144-59.
279. Shao, C., et al., *Parkinson's Disease Risk and Alcohol Intake: A Systematic Review and Dose-Response Meta-Analysis of Prospective Studies*. Front Nutr, 2021. **8**: p. 709846.
280. Coon, T.A., et al., *The proinflammatory role of HECTD2 in innate immunity and experimental lung injury*. Sci Transl Med, 2015. **7**(295): p. 295ra109.
281. Song, Y., Y. Zhou, and X. Zhou, *The role of mitophagy in innate immune responses triggered by mitochondrial stress*. Cell Commun Signal, 2020. **18**(1): p. 186.
282. Ryu, T.Y., et al., *Human gut-microbiome-derived propionate coordinates proteasomal degradation via HECTD2 upregulation to target EHMT2 in colorectal cancer*. ISME J, 2022.
283. Lv, D., et al., *HIF-1alpha Induces HECTD2 Up-Regulation and Aggravates the Malignant Progression of Renal Cell Cancer via Repressing miR-320a*. Front Cell Dev Biol, 2021. **9**: p. 775642.
284. Ottina, E., et al., *E3 ubiquitin ligase HECTD2 mediates melanoma progression and immune evasion*. Oncogene, 2021. **40**(37): p. 5567-5578.
285. Yan, X.J., et al., *Mitochondria play an important role in the cell proliferation suppressing activity of berberine*. Sci Rep, 2017. **7**: p. 41712.
286. Fiesel, F.C., et al., *A specific subset of E2 ubiquitin-conjugating enzymes regulate Parkin activation and mitophagy differently*. J Cell Sci, 2014. **127**(Pt 16): p. 3488-504.
287. Geisler, S., et al., *The ubiquitin-conjugating enzymes UBE2N, UBE2L3 and UBE2D2/3 are essential for Parkin-dependent mitophagy*. J Cell Sci, 2014. **127**(Pt 15): p. 3280-93.
288. Komander, D. and M. Rape, *The ubiquitin code*. Annu Rev Biochem, 2012. **81**: p. 203-29.
289. Zheng, X. and T. Hunter, *Parkin mitochondrial translocation is achieved through a novel catalytic activity coupled mechanism*. Cell Res, 2013. **23**(7): p. 886-97.
290. Kim, D., J. Song, and E.J. Jin, *BNIP3-Dependent Mitophagy via PGC1alpha Promotes Cartilage Degradation*. Cells, 2021. **10**(7).
291. Chen, Z., et al., *Mitochondrial E3 ligase MARCH5 regulates FUNDC1 to*

- fine-tune hypoxic mitophagy*. EMBO Rep, 2017. **18**(3): p. 495-509.
292. Park, S.Y. and H.C. Koh, *FUNDC1 regulates receptor-mediated mitophagy independently of the PINK1/Parkin-dependent pathway in rotenone-treated SH-SY5Y cells*. Food Chem Toxicol, 2020. **137**: p. 111163.
293. Zhou, H., et al., *Pathogenesis of cardiac ischemia reperfusion injury is associated with CK2alpha-disturbed mitochondrial homeostasis via suppression of FUNDC1-related mitophagy*. Cell Death Differ, 2018. **25**(6): p. 1080-1093.
294. Wu, W., et al., *FUNDC1 regulates mitochondrial dynamics at the ER-mitochondrial contact site under hypoxic conditions*. EMBO J, 2016. **35**(13): p. 1368-84.
295. Ney, P.A., *Mitochondrial autophagy: Origins, significance, and role of BNIP3 and NIX*. Biochim Biophys Acta, 2015. **1853**(10 Pt B): p. 2775-83.
296. Wang, Z.V. and J.A. Hill, *Protein quality control and metabolism: bidirectional control in the heart*. Cell Metab, 2015. **21**(2): p. 215-226.
297. Kocaturk, N.M. and D. Gozuacik, *Crosstalk Between Mammalian Autophagy and the Ubiquitin-Proteasome System*. Front Cell Dev Biol, 2018. **6**: p. 128.
298. Bailey, J., et al., *Tetrahydrobiopterin modulates ubiquitin conjugation to UBC13/UBE2N and proteasome activity by S-nitrosation*. Sci Rep, 2018. **8**(1): p. 14310.
299. Anderson, R.M., et al., *Dynamic regulation of PGC-1alpha localization and turnover implicates mitochondrial adaptation in calorie restriction and the stress response*. Aging Cell, 2008. **7**(1): p. 101-11.
300. Wu, W., et al., *FUNDC1 is a novel mitochondrial-associated-membrane (MAM) protein required for hypoxia-induced mitochondrial fission and mitophagy*. Autophagy, 2016. **12**(9): p. 1675-6.
301. Schofield, J.H. and Z.T. Schafer, *Mitochondrial Reactive Oxygen Species and Mitophagy: A Complex and Nuanced Relationship*. Antioxid Redox Signal, 2021. **34**(7): p. 517-530.
302. Collier, T.J., N.M. Kanaan, and J.H. Kordower, *Aging and Parkinson's disease: Different sides of the same coin?* Mov Disord, 2017. **32**(7): p. 983-990.
303. Kwong, J.Q., M.F. Beal, and G. Manfredi, *The role of mitochondria in inherited neurodegenerative diseases*. J Neurochem, 2006. **97**(6): p. 1659-75.
304. Reddy, P.H., *Role of mitochondria in neurodegenerative diseases: mitochondria as a therapeutic target in Alzheimer's disease*. CNS Spectr, 2009. **14**(8 Suppl 7): p. 8-13; discussion 16-8.
305. Liu, X.L., et al., *Mitochondria-mediated damage to dopaminergic neurons in Parkinson's disease (Review)*. Int J Mol Med, 2018. **41**(2): p. 615-623.
306. Granchi, C., et al., *Inhibitors of lactate dehydrogenase isoforms and their therapeutic potentials*. Curr Med Chem, 2010. **17**(7): p. 672-97.

307. Hui, S., et al., *Glucose feeds the TCA cycle via circulating lactate*. Nature, 2017. **551**(7678): p. 115-118.
308. Esteban-Martinez, L., et al., *Programmed mitophagy is essential for the glycolytic switch during cell differentiation*. EMBO J, 2017. **36**(12): p. 1688-1706.
309. Shiratori, R., et al., *Glycolytic suppression dramatically changes the intracellular metabolic profile of multiple cancer cell lines in a mitochondrial metabolism-dependent manner*. Sci Rep, 2019. **9**(1): p. 18699.
310. Requejo-Aguilar, R., et al., *PINK1 deficiency sustains cell proliferation by reprogramming glucose metabolism through HIF1*. Nat Commun, 2014. **5**: p. 4514.